SYNTHESIS, PHOTOPHYSICS, AND NONLINEAR ABSORPTION OF PLATINUM

(II) AND IRIDIUM (III) COMPLEXES

A Dissertation
Submitted to the Graduate Faculty
of the
North Dakota State University
of Agriculture and Applied Sciences

By

Zhongjing Li

In Partial Fulfillment of the Requirements
for the Degree of
DOCTOR OF PHILOSOPHY

Major Department:
Chemistry and Biochemistry

November 2013

Fargo, North Dakota

North Dakota State University
Graduate School

Title

**SYNTHESIS, PHOTOPHYSICS, AND NONLINEAR ABSORPTION
OF PLATINUM (II) AND IRIDIUM (III) COMPLEXES**

By

Zhongjing Li

The Supervisory Committee certifies that this ***disquisition*** complies with

North Dakota State University's regulations and meets the accepted

standards for the degree of

DOCTOR OF PHILOSOPHY

SUPERVISORY COMMITTEE:

Wenfang Sun
Chair

Gregory Cook

Pinjing Zhao

Sivaguru Jayaraman

Sanku Mallik

Approved:

November 12, 2013	Gregory Cook
Date	Department Chair

ABSTRACT

Square planar d^8 platinum(II) complexes and octahedral d^6 iridium(III) complexes were synthesized. Their photophysics were studied in detail. Structure-property relationship was studied by varying the substitution on the ligands or the π-conjugation extent of the ligands.

In Chapter 2, bipyridyl platinum(II) bisstilbenylacetylide complexes (**2-1** – **2-6**) with different auxiliary substituents on the stilbenylacetylide ligands were synthesized. While the substitution of H on the 4'-position of stilbene by Br and OMe groups does not alter the photophysical properties of the complexes eminently, the photophysical properties are significantly tuned by the CHO, NO$_2$ and NPh$_2$ substituents.

In Chapter 3, platinum(II) complexes (**3-1** – **3-6**) containing 6-[7-*R*-9,9-di(2-ethylhexyl)-9*H*-fluoren-2-yl]-2,2'-bipyridine (R = NO$_2$, CHO, benzothiazol-2-yl, *n*-Bu, carbazol-9-yl, NPh$_2$) ligands were synthesized. It is found that electron-withdrawing substituents (NO$_2$, CHO, BTZ) and electron-donating substituents (*n*-Bu, CBZ, NPh$_2$) exert distinct effects on the photophysics of the complexes.

In chapter 4, platinum(II) complexes (**4-1** – **4-6**) containing 6-[9,9-di(2-ethylhexyl)-7-*R*-9*H*-fluoren-2-yl]-2,2'-bipyridine ligands (*R* = 4-R'-phenylethynyl with R'= NO$_2$, BTZ, H and OCH$_3$ or *R* = 4'-BTZ-phen-1-yl or BTZ) were synthesized. The effects of terminal substituents and the different π-conjugated linkages between the BTZ component and the C^N^N core on the photophysics of these ligands and complexes were systematically investigated.

In Chapter 5, iridium(III) complexes (**5-1** – **5-5**) featuring 7-(benzothiazol-2-yl)-9,9-di(2-ethylhexyl)-9H-fluoren-2-yl attachment to the 2-phenylpyridine was synthesized and studied. The effects of the extent of the π conjugation was studied in by the comparison

between **5-1** and **5-2**, and the effect of the number of the 7-(benzothiazol-2-yl)-9,9-di(2-ethylhexyl)-9H-fluoren-2-yl unit was compared in **5-3 – 5-5**.

In Chapter 6, bypyridyl iridium(III) complexes (**6-1 – 6-7**) with different cylometallated arylpyridyl ligands were synthesized. The effects of π-conjugation extension and direction were systematically investigated.

Most complexes showed moderate to strong ns transient absorption from visible to near-IR region, indicating stronger excited-state absorption than ground-state absorption in the corresponding region and potential application as reverse saturable absorption materials. Thus, their application as nonlinear absorption materials was demonstrated by reverse saturable absorption (RSA) upon 532 nm ns laser. The RSA trend can be deciphered by the absorption cross section ratio between the excited states and ground states (σ_{ex}/σ_0).

TABLE OF CONTENT

x

LIST OF TABLES

LIST OF FIGURES

vii

LIST OF CHARTS

LIST OF SCHEMES

CHAPTER 1. INTRODUCTION

As the third row of transition metals, platinum and iridium are regarded as noble metals due to their stable chemical properties and their preciousness considering their rarity in the earth's crust. Photophysical and photochemical properties of platinum(II) and iridium(III) complexes have drawn intense interest for decades due to their unique structural and spectroscopic properties and potential applications in organic light emitting diodes (OLEDs),[1 – 4] dye-sensitized solar cells (DSSCs),[5] DNA intercalation,[6] and biological labeling.[7, 8] The research of our group has been focused on the nonlinear absorption of platinum(II) complexes based on their excited-state absorption (ESA) and/or two-photon absorption (TPA), which can significantly reduce the transmittance of high intensity lasers. To date, we have discovered many complexes that show excellent reverse saturable absorption (RSA, absorption of light increases with increasing light intensity) and/or TPA.[9,10] In order to enhance the RSA of complexes, the materials have to have large ratios of ESA cross section (σ_{ex}) relative to those of their ground-state (σ_0). This requires us to reduce the ground-state absorption but increase the ESA at the interested wavelengths. To reach this goal, understanding the structure-property correlation is the key. To fully understand and utilize these processes for photonic device applications, detailed photophysical studies are of vital importance in regard to targeted design and molecular engineering based on structure-property correlations and paradigms.

In this chapter, the basic concepts of photophysics, as well as the photophysics of selected platinum(II) and iridium complexes(III), will be introduced and discussed briefly. Four parts are introduced herein ranging from basic photophysical concepts to general photophysics of platinum and iridium complexes, and then to applications as nonlinear optical materials.

1.1. Basic Concepts in Photophysics

The interaction between light and materials is an important and interesting process, which shines light on important processes such as photosynthesis. The basic photophysical principles that govern these processes are introduced in this chapter.

1.1.1. Some Insights into Light and Molecular Electronic Structure

In 1860, Maxwell defined the concept of light based on his electromagnetism theory. In his theory, light was considered as eletromagnetic wave with the transmit speed of 3×10^8 m/s. However, since the beginning of last century, the particle character of light is discovered after Max Planck's black body radiation experiment, in which he found that the continuous wavelength reflection of the electromagnetic radiation in a confined cavity was not plausible. Notably, Einstein proposed and defined the dual wave-particle nature of light based on the combination of Maxwell wave equation and Planck's law.

Similarly, wave-particle duality of electron was also recognized, and it was described in Schrödinger's equation for atomic structures, in which the electrons resemble the behavior of classical wave equations for light. Based on the similar wave-particle characters of light and electron, we can expect strong interactions between light and electrons. In the viewpoint of chemist, who is seeking the principle governing the changes and transformations at the molecular level, the interaction between light and electrons could possibly shine light on the molecular electronic structure.

1.1.2. The Interaction between Light and Molecules

The interaction between light and materials is a broad topic and an intriguing research field. In this dissertation, this process is described and understood at the molecular level. As a result, the process will be limited to interaction between the light and the molecular electronic structures. The light absorption behaviors of a molecule can be described by Frank-Condon

principle as illustrated in Figure 1.1. The excited-state properties can be described by Jablonski Diagram shown in Figure 1.2. The Lambert-Beer's Law describes the absorption behavior of massive molecules in solutions. These three theories/principles will be discussed briefly in the following part, aiming to provide necessary theoretical understanding of the light-material interaction discussed in this dissertation.
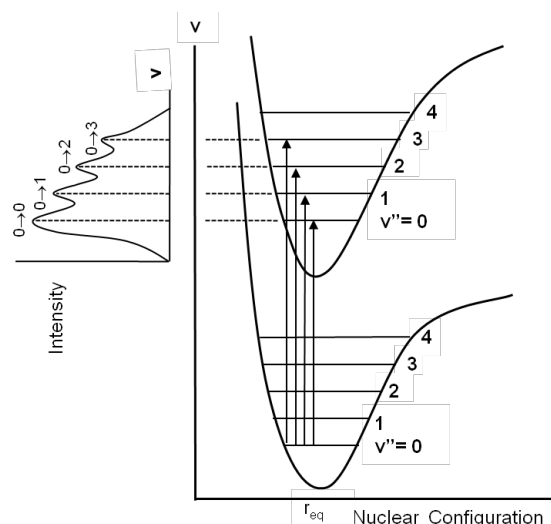
Figure 1.1. Frank-Condon principle. Reprinted with the permission from Ref. 11.

The behavior of the absorption of light by a molecule can be described by Franck-Condon principle shown in Figure 1.1. The potential energy of a molecule is the function of the bond length, and a certain distance between nuclei gives the minimum energy of a molecule. Either elongation or shortening of the distance will increase the potential energy and result in higher vibrational levels. A molecule is promoted to its excited-states by absorbing a photon, during which an electron is excited to a higher energy level. According to Frank-Condon principle, this transition from a lower potential energy level to a higher one is "vertical" to the nuclear geometry of the molecule, illustrated by the vertical arrows in Figure 1.1. However, after the molecule is promoted to higher energy levels, the initial nuclear geometry is not always at the potential energy minimum position of the higher energy level because electron redistribution happens after the "vertical" transition. Meanwhile, to fully understand this mark point, it has to be pointed out that the re-equilibration process is

3

much slower (in the time scale of 10^{-13} s) than the absorption of a photon (in the time scale of 10^{-15} s). The frequency of the light absorbed during such a transition reveals the energy difference between the beginning and the final states.

Lambert-Beers law expresses the relationship between the absorption of the light and the properties of the absorbing materials. In liquid phase, the principle can be expressed in the following equations:

$$T = \frac{I}{I_0} = 10^{-\varepsilon lc} \tag{1.1}$$

$$A = -\log_{10} T = \varepsilon lc \tag{1.2}$$

In equation 1.1, the transmittance of the light, donated as T, is expressed by the ratio between I (intensity of the transmitted light) and I_0 (intensity of the incident light). This ratio can be further expressed by the power function of 10 with the monomial of $(-\varepsilon lc)$, in which ε is the molar extinction coefficient representing the electronic transition probability in mol^{-1} L cm^{-1}, l is the path length of the light in the medium in cm, and c is the concentration of solute in the solution in mol/L. The relationship between the transmittance and absorbance in liquid can be defined by equation 1.2.

The initial process after the light absorption can be illustrated by Jablonski diagram shown in Figure 1.2. According to Frank-Condon's principle discussed above, absorption of light leads the molecule to a higher vibrational level of the singlet excited-states (S_n).[12] Then the molecule relaxed to the lowest vibrational level of the singlet excited-state (S_n) after the dissipation of excess vibrational energy through thermal process such as collision with other molecules in the matrix. Triplet excited-states (T_n) lies at lower energy levels in comparison to the corresponding singlet excited-states due to the absence of the Coulomb repulsion in the paired electrons.[13] The spin of the excited electron is no longer paired with the ground-state electron and the total spin quantum number of the system becomes three. As a result, the population of a triplet excited-state from the singlet ground-state involves changing of the

spin of the excited electron, and this process is a spin "forbidden" process according to selection rule. Generally, triplet excited-state can be populated through intersystem crossing (ISC, as shown in Figure 1.2), during which the spin of the excited electron is reversed. ISC involves the coupling of the singlet and triplet vibrational levels at the isoenergetic point to produce a higher energy triplet excited-state (T_n), which evolves to the lowest triplet excited-state (T_1) through vibrational relaxation. Deactivation pathway of the excited-states can be summarized as radiative and nonradiative decay pathways. The lowest excited singlet and triplet excited-states can undergo radiative decay to ground-state with emission of photons. Radiative decay from a singlet excited-state is called fluorescence, while the radiative decay from a triplet excited-state is referred to as phosphorescence. Radiationless transition between two electronic states can occur if there is an intersection (isoenergetic point) of their potential energy surfaces. The radiationless transition will occur at the isoenergetic point to produce a molecule at a higher vibratinal level of the ground-state, which will further rapidly loose excess of energy by vibrational deactivation. Nonradiative deactivation includes internal conversion (IC), electron transfer, and intersystem crossing (ISC). In internal conversion process, the energy difference between the two states with the same spin is dissipated in the form of heat. Nonradiative processs IC and ISC are shown as curve arrows in Figure 1.2. Energy or electron transfer processes could occur in the presence of acceptor.
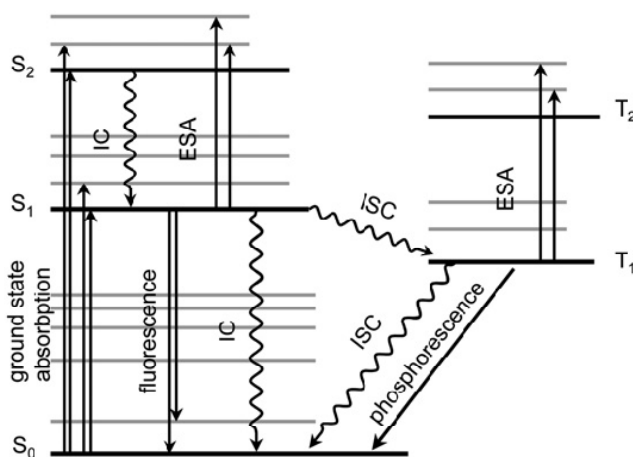
Figure 1.2. Jablonski diagram. Reprinted with permission from Ref. 14.

1.1.3. Radiative Decay (Fluorescence and Phosphorescence)

Radiative decay involves deactivation of an excited-state with the emission of a photon, and the energy of the emitted photon corresponds to the energy difference between the excited and ground-states. As shown in Figure 1.2, the energy of the singlet excited-state is higher than the energy of the analogous triplet excited-state. As a result, fluorescence will always occur at a higher energy than phosphorescence from the corresponding triplet excited-state. Meanwhile, since fluorescence is an allowed process, the radiative decay rate for the singlet excited-state is large ($k \approx 10^9$ s^{-1}, $\tau \approx 1$ ns). In contrast, the radiative decay rate of phosphorescence, which involves a spin forbidden transition between states of different spin multiplicities (triplet excited-state to singlet ground-state), is small ($k_r \approx 10^2 - 10^4$ s^{-1}). Thus the lifetime of phosphorescence is relatively long ($\tau \approx 10^{-3} - 10^{-6}$ s).

The emission energy is generally lower than the excitation energy, because a fraction of the absorbed energy is dissipated by vibrational relaxation. The energy difference between absorption and fluorescence/phosphorescence is defined as the Stokes shift and it describes the extent of distortion of the excited state with respect to the ground state. In many cases, a vibrational progression is observed in both fluorescence and phosphorescence spectra.

The lifetime of radiative decay can be measured by time-resolved spectroscopy, in which the emitting radiation is a function of time. By fitting of the decay curve the radiative decay lifetime can be obtained. However, the measured radiative transition lifetime is shorter than their natural lifetime, due to the competition with ISC and IC. The natural lifetime of S_1 and T_1 can be expressed as:[15]

$$\tau_{S_1} = \frac{1}{k_r^f + k_{nr}^{S_1}} \tag{1.3}$$

$$\tau_{T_1} = \frac{1}{k_r^p + k_{nr}^{T_1}} \tag{1.4}$$

In equations 1.3 and 1.4, k_r^f is the rate constant of fluorescence, k_r^p is the rate constant of phosphorescence, and $k_{nr}^{S_1}$ and $k_{nr}^{T_1}$ are the rate constants of non-radiative decay of S_1 and T_1 respectively.

The radiative lifetime is subject to emission quencher Q in the solution. Self-quenching of the radiation can happen if the excimer formation is feasible, by reaction between one excited-state molecule and one ground-state molecule of the same species in concentrated solutions. In other words, the interaction of the excited-state molecule and quencher Q leads to the increase of radiative decay. This behavior can be depicted by Stern-Volmer relationship:

$$\frac{I_0}{I} = \frac{\tau_0}{\tau} = 1 + k_{SV}[Q] \qquad (1.5)$$

$$\frac{1}{\tau} = \frac{1}{\tau_0} + k_{SQ}[Q] \qquad (1.6)$$

In equations 1.5 and 1.6, I_0 and I denote for the emission intensity without and with quencher, respectively; τ_0 and τ denote for the emission lifetimes without and with quenchers, respectively; k_{SV} and k_{SQ} denote for the Stern-Volmer constant or self-quenching rate constant; and $[Q]$ is the concentration of the quencher. As a result, a linear relationship is expected for $1/\tau$ vs $[Q]$, and intrinsic lifetime of the emission can be deduced from the inception of the function.

The quantum yield of radiative transition is the ratio of the emitted photons with respect to the absorbed photons. The fluorescence quantum yield is expressed as:[16]

$$\Phi_f = \frac{k_f}{k_f + k_{nr}} \qquad (1.7)$$

This equation shows that the emission quantum yield decreases when nonradiative decay process competes with the radiative decay process.

The phosphorescence yield is expressed as:[17]

$$\Phi_p = \frac{k_{ISC} k_p}{k_p + \sum k_d + \sum k_q} \qquad (1.8)$$

In equation 1.8, k_{ISC} is the rate constant of ISC, k_p is the rate constant of phosphorescence, $\sum k_d$ and $\sum k_q$ are the de-activation and quenching pathways except for fluorescence and phosphorescence, respectively.

The radiative quantum yield in this dissertation is measured by comparative method using standard materials with similar structure and absorbance at the excitation wavelength and by applying the following equation:

$$\Phi_S = \Phi_R * \frac{F_S}{F_R} * \frac{A_R}{A_S} * \left(\frac{n_S}{n_R}\right)^2 \qquad (1.9)$$

In equation 1.9, Φ_S and Φ_R are the quantum yields of the sample and reference respectively. A_S and A_R are the absorbance of the sample and reference at the excitation wavelength. F_S and F_R are the integrated area of the emission spectra of sample and reference, respectively. n_S and n_R are the refractive indexes of the solvents for the sample solution and reference solution, respectively.

1.1.4. Heavy Atom Effect and Spin-orbit Coupling

Due to the separated coupling and quantization of spin angular momentum and orbital angular momentum, the transition involving the change of electron's spin is forbidden by selection rule. As a result, the ISC yields in small organic molecules are typically low. However, when heavy atoms are present in the system, the spin angular momentum and orbital angular momentum of the same electron interact significantly. This effect is defined as heavy atom effect. As a result of heavy atom effect, spin-orbit coupling is observed, in which the spin angular momentum and orbital angular momentum are no longer separately conserved but the total angular momentum is conserved. ISC yields can be greatly enhanced by spin-orbit coupling mechanism.

The heavy atom induced spin-orbit coupling is affected by both the nuclear charge of the heavy atom and the position of the heavy atom in the molecule. Meanwhile, spin-orbit

coupling can happen due to either internal heavy atom effect (chemical bond) or external heavy atom effect (in the matrix or solvent). In addition, increased spin-orbit coupling can also cause decreased phosphorescence and fluorescence lifetime, increased phosphorescence quantum yield, increased oscillator strength for $S_0 \rightarrow T_1$ absorption, and red-shifted emission.

In this dissertation, the spin-orbit coupling is greatly enhanced by platinum and iridium metal ions through chemical bonding of conjugated organic molecule with metal centers, which in turn greatly improves the ISC rate. As a result, high quantum yield of the triplet excited-state is expected. For excited-states with significant contribution from metal-based orbitals, ISC normally occurs at a rate constant of the order of $10^{12}\,s^{-1}$,[18] which greatly exceeds the typical radiative rate constants from singlet excited-states ($\sim 10^8\,s^{-1}$). Phosphorescence is substantially forbidden in purely organic compounds, with a rate constant (typically $< 10^3\,s^{-1}$) that is too slow to allow phosphorescence to compete with non-radiative decay at room temperature. However, in the presence of the Pt(II) or Ir(III) ions that have high spin-orbit coupling constants, k_{ISC} is accelerated typically to values of the order of $10^5 - 10^7\,s^{-1}$, and triplet emission on the microsecond timescale can then be observed.

1.1.5. Energy Transfer and Electron Transfer

In the presence of an energy acceptor A, deactivation of the excited-state D* could occur by a bimolecular energy transfer process, according to the equations below.

$$D + h\nu \rightarrow D* \tag{1.10}$$

$$D* \rightarrow h\nu' + D \tag{1.11}$$

$$h\nu' + A \rightarrow A* \tag{1.12}$$

Energy transfer can occur in case of D* is higher in energy than A*, and the time scale of the energy transfer process should be shorter than the lifetime of D*. Many types of energy transfer process exist, depending on the distance between the donor and the acceptor molecules. Radiative energy transfer can reach up to 100 Å. Otherwise, the dipole-dipole

energy transfer mechanism (Förster mechanism) is proportional to the value of $1/R^6$ (R is the distance between the donor and acceptor), and allows for a relatively long distance of $50 -100$ Å. Both radiative and Förster energy transfer mechanism require the overlap between the emission of the donor and absorption of the acceptor. As the donor and acceptor approach each other close enough ($10 - 15$ Å), exchange mechanism, which involves the overlap between the donor and acceptor orbitals, can take place.

Electron transfer is another interesting deactivation pathway for the excited-states. Photoinduced electron transfer (PET) involves the transfer of an electron from a donor D to an appropriate acceptor A, by either exciting the donor or the acceptor molecule.[19]

$$D*+A \rightarrow D^+ + A^- \tag{1.13}$$

$$D+A* \rightarrow D^+ + A^- \tag{1.14}$$

Without the excitation of donor (or acceptor), an electron transfer process would be highly endothermic. However, once the donor is photexcited, one of its electrons is promoted to a higher energy level, making electron transfer process much more feasible. The PET process produces reactive radical cations, which can undergo a chemical reaction. Marcus developed a theoretical description of electron transfer in 1960's.[20] According to Marcus' theory, no chemical bonds are broken in the electron transfer process. The changes take place in the molecular structure of reactants and the neighboring solvent molecules. The rate constant for electron transfer can be expressed by the following equation:[21]

$$k_{et} = \frac{2\pi}{\hbar} |H_{AB}|^2 \frac{1}{\sqrt{4\pi\lambda\kappa_b T}} exp\left(-\frac{(\lambda + \Delta G^0)^2}{4\lambda\kappa_b T}\right) \tag{1.15}$$

In equation 1.15, k_{et} is the rate constant for electron transfer; $|H_{AB}|$ is the electronic coupling between the beginning and ending states; λ is the reorganization energy, which corresponds to energy required to distort the reactant structure to that of the product without electron transfer; k_b is Boltzmann constant; T is absolute temperature; ΔG^0 is the Gibbs free energy change for the electron transfer reaction.

1.1.6. Excited-state Absorption and Reverse Saturable Absorption

The probability of an absorption process by a molecule is defined as the absorption cross section (σ), and the probabilities of the ground-state absorption and excited-state absorption of a molecule are defined as ground-state absorption cross section (σ_0) and excited-state absorption cross section (σ_{ex}), respectively. If the excited-states (S_1 or T_1) of molecules are long lived, the excited molecules can be populated to a higher energy state (S_n or T_n), which is defined as excited-state absorption (ESA). ESA occurs when the incident light is very strong, and it is a nonlinear optical process because the molecules can take more than one photons. There are two scenarios for ESA, satuable absorption (SA) and reverse saturable absorption (RSA). In SA, the excited-state absorption cross section is smaller than that of the ground-state, thus the transmittance of light will increase when the incident fluence increases. In RSA, the cross section of the excited-state is higher than that of the ground-state, and the transmittance will decrease with the increased population of the excited-state. Chromophores showing RSA have been widely studied regarding their potential applications in laser beam shaping, optical switching, and beam compression.[22]

Several criteria need to be addressed for an ideal reverse saturable absorber. First of all, the ratio between the excited-state absorption cross section (σ_{ex}) and the ground-state absorption cross section (σ_0) should be large. Secondly, the lifetime of the excited-states should be longer than the pulse width of the incident laser pulse. Thirdly, the excited-state quantum yield should be high to generate large population of the molecules at the excited-states and facilitate the absorption from the excited-states. Note that excited-state absorption includes both the singlet excited-states and triplet excited-states. When the laser pulse is shorter than the lifetime of the intersystem crossing, the singlet-excited-state absorption dominates in the ESA. On the other hand, when the laser pulse is longer than the lifetime of intersystem crossing, ESA is dominated by the triplet excited-states absorption.

1.2. Platinum(II) Complexes: Basic Photophysics and Representative Examples

For the complexes discussed in this dissertation, platinum is in +2 oxidation state with d^8 electronic configuration, which prefers to adopt a square-planar geometry in the presence of strong-field ligands thermodynamically. This preference can be illustrated in Figure 1.3.[23] In the square-planar geometry, the energy of the unoccupied orbital ($d_{x^2-y^2}$) is pushed to a higher energy, while substantial stabilization of the three occupied orbitals (d_{z^2}, d_{xz}, d_{yz}) is facilitated. It is the four-coordinate square-planar geometry that makes Pt(II) complexes unique among the transition metal complexes.
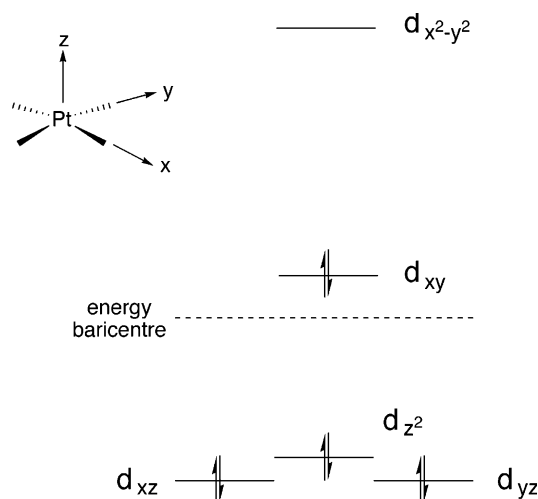
Figure 1.3. Ligand field splitting diagram for Pt(II) complexes. (Reprinted with the permission from Ref. 23)

1.2.1. Ligand Field (d-d) Excited-states and Axial Interactions

Ligand field d-d excited-state is formed upon the population of the strongly antibonding $d_{x^2-y^2}$ orbital. The d-d excited-state causes a significant distortion of the molecular geometry and an eloneged Pt – L bond. As shown in Figure 1.4 (a),[23] the energy minimum of the d-d excited-state is significantly displaced with respect to the ground-state by comparing their potential energy surfaces. This circumstance is unfavorable for the stability of an excited-state, because nonradiative internal conversion or intersystem crossing to the ground-state can occur through the isoenergetic crossing point.
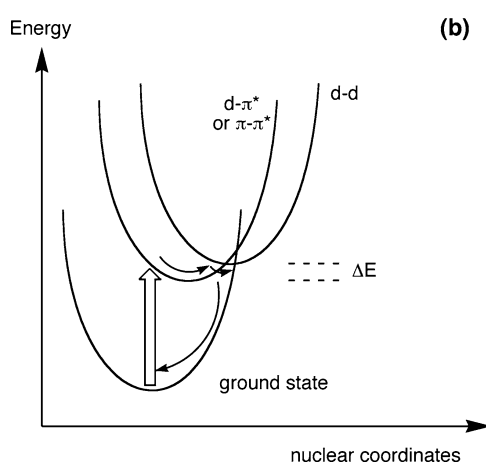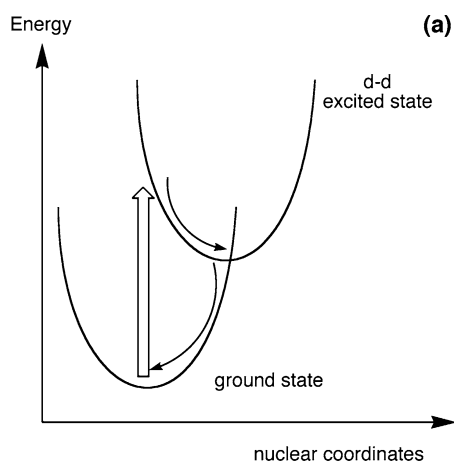
Figure 1.4. (a) Potential energy surface for the d-d excited-state is displaced to the ground-state. (b) Non-radiative decay pathway provided by the d-d excited-state to the lower energy excited-state. Reprinted with permission from Ref. 23.

Besides itself being subject to nonradiative decay pathway, the d-d excited-state can also serve as a nonradiative decay pathway to other excited-state(s), even though these excited-state may lie at lower energy level than the d-d excited-state. For example, the energy level of the ligand-centered (LC) (π-π* or n-π*) and charge-transfer (metal to ligand charge-transfer, MLCT, d- π*) excited-states shown in Figure 1.4 (b) is lower than the d-d states, thus having intrinsically faster k_r values than the d-d state. However, the d-d excited-state can still exert a negetive effect on MLCT or LC state as long as ΔE in Figure 1.4 (b) is comparable to kT. As a result, the d-d excited-state is thermally accessible from the lowest energy excited-state because the room temperature is high enough to produce a kT

13

comparable or even larger than ΔE. This adds a decay pathway for the lowest excited-state, resulting in a rapid decay of the lowest excited-state and thus reducing the emission quantum yield and lifetime.

However, most of the Pt(II) complexes discussed in this dissertation have large ΔE values because of two alternating or combined reasons: (1) the energy of the emissive state is low enough, and/or (2) the energies of d-d states are pushed to an energy that is high enough to be thermally accessible.

Another character of the Pt(II) complexes is that they are subject to inter-molecular interactions due to the their square planar geometry. Different axial interactions can take place, such as intermolecular π-π stacking or dimerization in the ground state, and excimer or exciplex formation in the excited state(s). Ground-state stacking of Pt(II) complexes may produce particular metal–metal interactions: i.e. weakly bonding and antibonding dσ and dσ* molecular orbitals can be formed between two d_{z^2} orbitals from two different molecules, because the d_{z^2} orbital is perpendicular to the molecular plane. The metal-metal separation range for the formation of d_{σ} and $d_{\sigma*}$ orbitals is 3.0 – 3.5 Å.[24] On the other hand, for complexes with planar and conjugated aromatic ligands, π-π interactions between the ligands of adjacent or packing molecules are also possible. The d^8-d^8 and π-π interactions can be illustrated by Figure 1.5 for a dinuclear platinum complex reported by Che.[25]
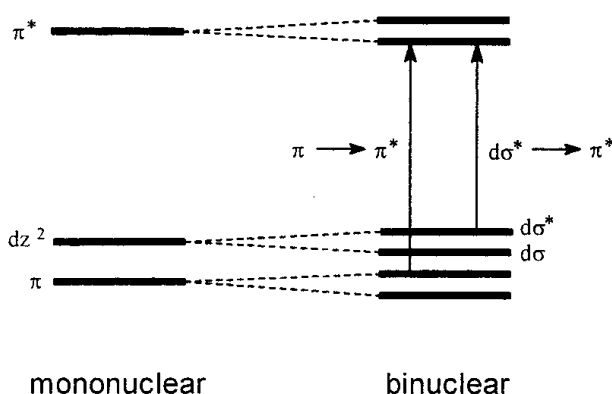
Figure 1.5. Molecular orbital diagram for d^8-d^8 and π-π interactions. Reprinted with permission from Ref. 25.

14

1.2.2. Platinum(II) Diimine Complexes Containing Acetylide Ligands

Extensive investigations have been conducted on platinum(II) diimine complexes containing acetylide ligands, with general structure shown in Chart 1.1. The introduction of strong field acetylide ligands into the coordination sphere of Pt(II) efficiently raises deactivating metal centered d-d states. As a result, the emission properties of these complexes are significantly improved and stable triplet excited-states are expected for these complexes.
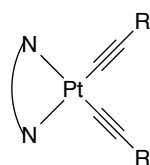
Chart 1.1. General strucuture of Pt(II) diimine complexes with acetylide ligands.

Reported by Che in 1994,[26] Pt(phen)(-C≡C-Ph)$_2$ (complex **1** in Chart 1.2) is the first example of such complexes. At room temperature in CH$_2$Cl$_2$, Pt(phen)(-C≡C-Ph)$_2$ exhibited broad and structureless emission that was attributed to the ^{3}MLCT (d-π*) excited-state. Following that, Eisenberg[27] and Schanze[28] groups independently did extensive studies on structure–property relationships in platinum diimine complexes with acetylide ligands (complexes **2** − **8** illustrated in Chart 1.2). They found that the highest occupied molecular orbital (HOMO) could be efficiently adjusted by varying the substituents on the aryl acetylide ligands, while the lowest unoccupied molecular orbital (LUMO) energy could be adjusted by varying the substituents on the diimine motif. Recently, Castellano's group[29] reported a striking example that showcased the interplay between ^{3}π-π* and ^{3}MLCT. In their study, conjugated aromatic units connected to the coordinating acetylene were varied, such as 1-pyrene, 1-anthracene and 1-perylene (complexes **9** − **11** in Chart 1.2). In complex **9**, long-lived (τ = 48.5 μs) and structured phosphorescence from the ^{3}π-π* state of the pyrenyl−C≡C unit was observed by excitation at the ^{1}MLCT bands of the complex in solution at room temperature. Facilitated by the intersystem crossing promoted by the Pt(II) metal center,

various platinum(II) diimine complexes featuring long-lived intraligand phosphorescence (^{3}IL) were also synthesized and investigated, exemplified by complex **12** reported by Zhao and Castellano.[30] Complex **12** showed room temperature phosphorescence with a lifetime of 124 μs and a quantum yield of 0.22, which is from the $^3\pi$-π* state localized at the naphthalimide ligand. This is the first time that phosphorescence was observed from naphthalimide. Similar examples including complexes **13** and **14** were studied by Zhao later.[31, 32]
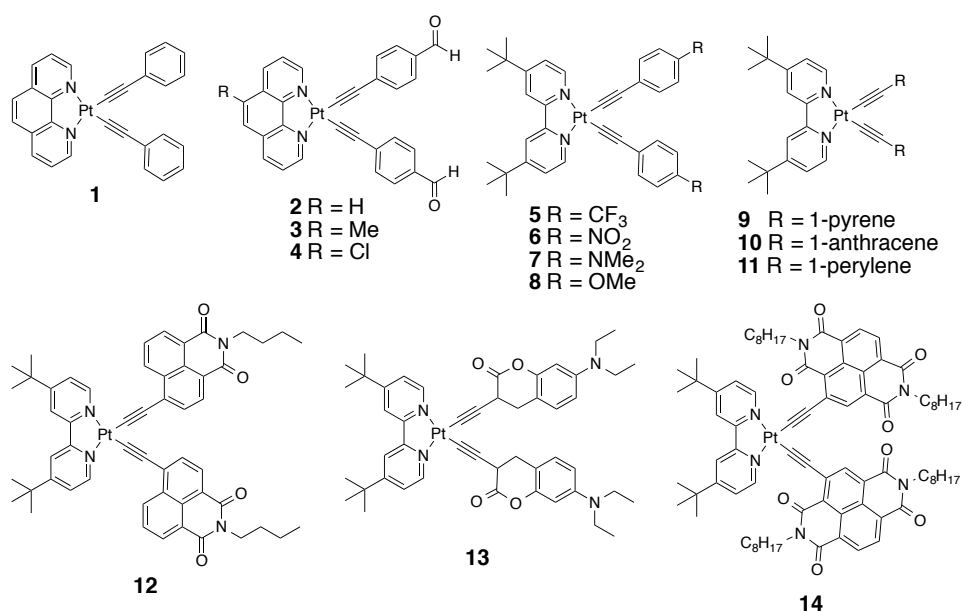
Chart 1.2. Examples of Pt(II) diimine complexes with acetylide ligands.

Since 2010, our group has reported the systematic photophysical studies and reverse saturable absorption of Pt(II) diimine complexes with various substituents on the acetylide ligands. These examples are shown in Chart 1.3 and their key photophysical data are summarized in Table 1.1.

15 R = H
16 R = CHO
17 R = NO$_2$
18 R = benzothiazol-2'-yl
19 R = NPh$_2$
20 R = 2-naphthalene
21 R = 9-anthracene
22 R = 1-pyrene
23 R = 10-phenothiazine
24 R = 4-nitrophenylacetylene
25 R = 4-diphenylaminophenylacetylene

26

27 n = 0
28 n = 1

29 – 33

29-L

30-L

31-L

32-L

33-L

34 n = 0
35 n = 1
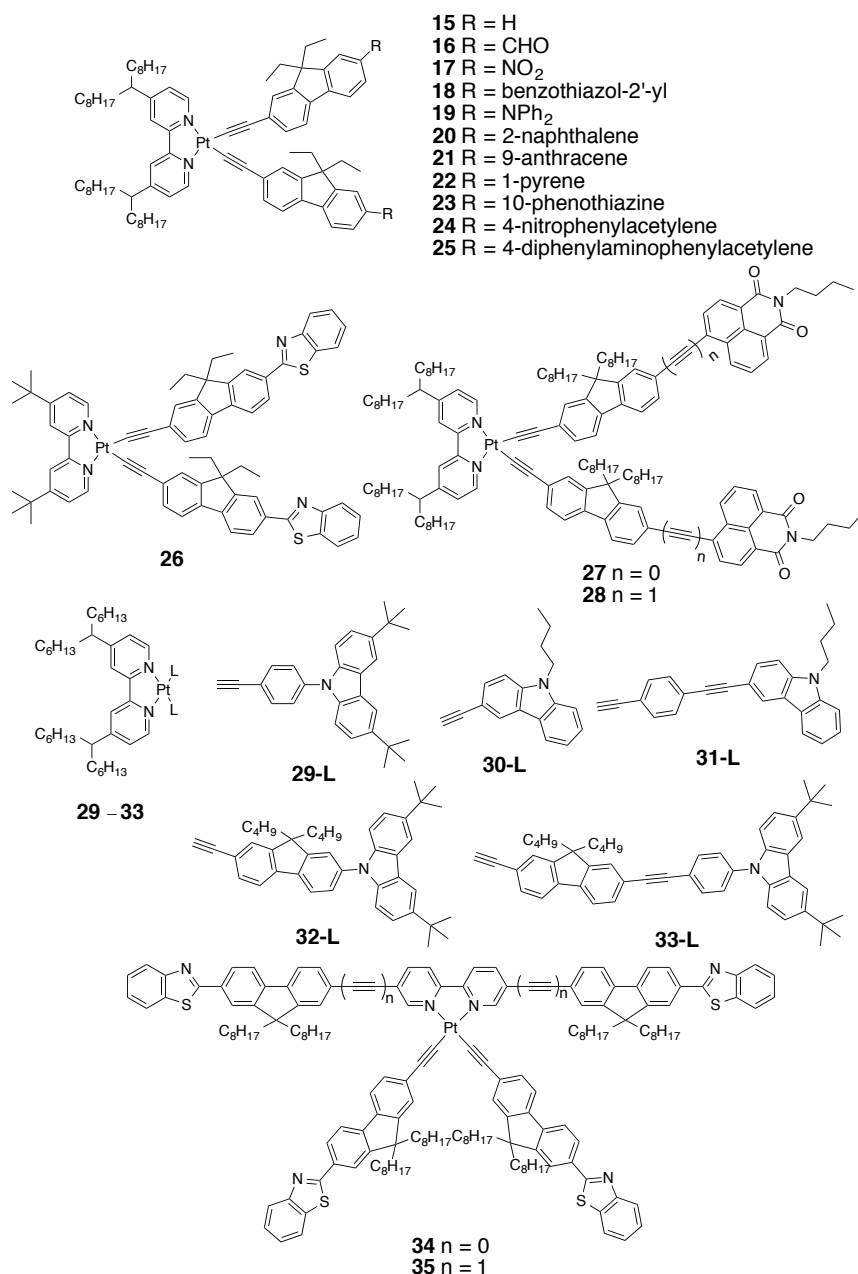
Chart 1.3. Selected examples of Pt(II) diimine complexes containing arylacetylide ligands studied by our group.

For the complexes shown in Chart 1.3, the energy levels of the π-π* state and the charge transfer state(s) (MLCT/LLCT/ILCT) can be substantially adjusted by substituents and solvent polarity as discussed in detail below. In most cases, the lowest-energy singlet electronic transition is dominated by charge transfer state (^{1}MLCT/^{1}LLCT) for these complexes. However, in the case of strong electron withdrawing group on the acetylide ligand (complex **17**),[33] ligand-localized ^{1}π-π* transition also contributes significantly. The

effect of structural variation on the emitting state can be best illustrated in complexes **20** – **23**.[34] Although the triplet emitting state for complexes **20**, **21** and **23** are dominated by $^3\pi$-π^* localized on the fluorenylacetylide motif, charge transfer state (^{3}ML'CT, metal to fluorenylacetylide charge transfer) still present. In complex **22**, the triplet emitting state is predominately from pyrene-localized $^3\pi$-π^* state. The difference in the triplet emitting states is resulted from the degree of π conjugation between the substituent and the fluorenyl motif. It was also discovered that most of these complexes exhibit broadband excited-state absorption from the visible to the NIR region (illustrated by the TA spectrum of complex **26** in Figure 1.6) and long-lived triplet excited-state. The other common factor that affects the emitting state is the solvent polarity. For example, complexes **16**[33], **18**[33], **26**[9], and **33**[35] showed structured emission in polar solvents, which was from the $^3\pi$-π^* excited-state; while in less polar solvents such as toluene and hexane, the emission was switched to ^{3}MLCT state characterized by the structureless feature of the emission spectra and reduced lifetime, in the scales of hundreds of ns to several μs. This character is illustrated by the emission spectra of complex **16** in Figure 1.7.
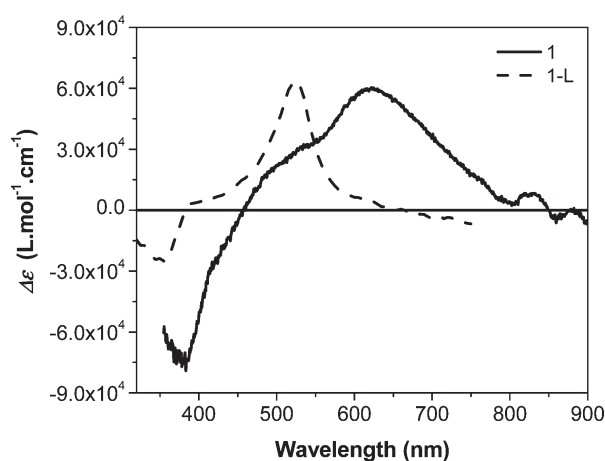
Figure 1.6. Nanosecond transient difference absorption of complex **26** (solid line). Reprinted with permission from Ref. 9.
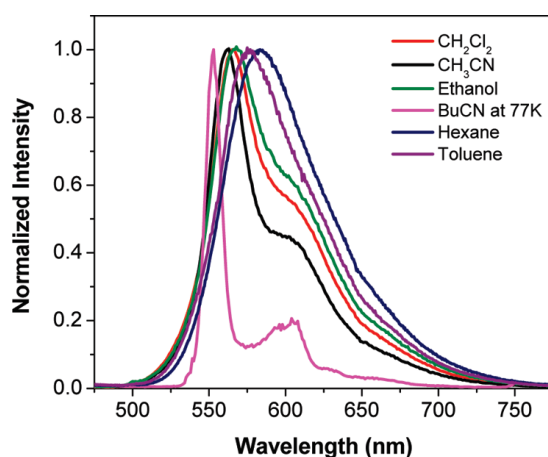
Figure 1.7. Normalized emission spectra of **26** in different solvents. Reprinted with permission from Ref. 9.

Table 1.1. Photophysical data of complexes **15** – **34**.

	λ_{abs}/nm (logε/Lmol^{-1}cm^{-1})	λ_{em}/nm (τ/μs); Φ_{em} R.T.	λ_{em}/nm (τ/μs); 77 K	$\lambda_{T_1-T_n}$/nm (τ_T/μs; log$\varepsilon_{T_1-T_n}$/L mol^{-1} cm^{-1}; Φ_T)[c]
15	310 (4.89), 324 (4.89), 391 (4.12)	577 (0.31); 0.023	525 (3.7)	568 (0.75; 4.61; 0.41)
16	365 (4.87), 432(4.06)	551 (4.8); 0.16	543 (33.0)	601 (1.6; 4.80; 0.22)
17	289 (4.67), 397 (4.81)	579 (-); 0.017	565 (122.1)	530 (4.8; 4.63; 0.16)
18	369 (5.05), 449 (4.07)	564 (9.7); 0.083	562 (87.0)	589 (1.5; 4.92; 0.18)
19	297 (4.85), 371 (4.99), 459 (4.04)	590 (-); -	543 (8.9)	517 (-; -; -)
20	357 (5.07), 446 (4.07)	580 (0.34); 0.085	542 (75.7)	490 (0.35; 4.69; 0.11)
21	337 (4.90), 388 (4.57), 438 (4.05)	573 (0.35); 0.009	538 (15.8)	440 (28.8; 4.91; 0.064)
22	360 (5.05), 442 (4.09)	626 (-); 0.002	618 (0.11)	530 (20.1; 4.64; 0.066)
23	340 (4.96), 431 (4.03)	604 (0.55); -	511 (12.1)	480 (0.08; 4.47; 0.26)
24	314 (4.78), 338 (4.75), 397 (4.85)	576 (0.03); 0.001	570 (109)	500 (3.2; 4.86; 0.15)
25	300 (4.81), 373 (5.18), 450 (4.14)	568 (0.97); 0.07	561 (93)	550 (0.61; -; -)
26	288 (4.55), 374 (5.03), 423 (4.33)	565 (10.7);0.2	552 (289)	620 (10.8; 4.78; 0.14)
27	337 (4.95), 404 (4.70)	589 (-); 0.012	-	535 (21.6; 4.80; 0.11)
28	349 (4.96), 436 (4.91)	500 (-); 0.051	-	565 (29.6; 4.84; 0.091)
29	298 (4.98), 350 (4.29), 400 (4.05)	584 (0.05); 0.019	503 (3.8)	385 (0.23; 4.46; 0.34)
30	290 (5.07), 368 (4.04), 449 (3.85)	629 (-); 0.0026	541 (2.8)	390 (0.03; 3.98; 0.20)
31	334 (5.01), 356 (4.99), 403 (4.19)	564 (0.31); 0.083	527 (50)	385 (0.48; 3.93; 0.78)
32	298 (4.90), 353 (5.03), 400 (4.14)	584 (0.12); 0.038	517 (38)	445 (0.33; 4.93; 0.13)

Table 1.1. Photophysical data of complexes **15 – 34** (continued).

	λ_{abs}/nm (logε/Lmol^{-1}cm^{-1})	λ_{em}/nm (τ/μs); Φ_{em} R.T.	λ_{em}/nm (τ/μs); 77 K	$\lambda_{T_1-T_n}$/nm (τ_T/μs; log$\varepsilon_{T_1-T_n}$/L mol^{-1} cm^{-1}; Φ_T)^c
33	298 (4.90), 354 (5.14), 404 (4.50)	561 (1.8); 0.047	552 (149)	600 (-; 4.60; 0.031)
34	306 (4.84), 351 (5.15), 369 (5.21), 389 (5.28), 431 (4.94), 478 (4.09)	610 (0.45); 0.046	-	537 (52.6; 5.50; 0.022)
35	326 (4.96), 361 (5.25), 390 (5.23), 430 (5.01), 452 (4.95), 500 (4.01)	660 (-); 0.0046	-	525 (47.1; 5.36; 0.012)

15 – 19, **24**, and **25**: UV-vis in CH_2Cl_2; RT emission in CH_2Cl_2 at the concentration of 1×10^{-5} mol/L, with Ru(bpy)$_3$Cl$_3$ in aqueous solution (Φ_{em} = 0.042; λ_{ex} = 436 nm) as the standard for quantum yield calculation; 77 K emission in methyl-tetrahedrafuran glassy matrix; ns TA in CH_3CN/CH_2Cl_2 (9/1) with SiNc as standard (ε_{590} = 53400 L mol^{-1} cm^{-1}, Φ_T = 0.20). **26**: UV-vis in CH_2Cl_2; RT emission in CH_2Cl_2, with Ru(bpy)$_3$Cl$_3$ in aqueous solution (Φ_{em} = 0.042; λ_{ex} = 436 nm) as the standard for quantum yield calculation; 77 K emission in BuCN glassy matrix; ns TA in CH_2Cl_2 with SiNc as standard (ε_{590} = 53400 L mol^{-1} cm^{-1}, Φ_T = 0.20). **27** and **28**: UV-vis in CH_2Cl_2; RT emission in CH_2Cl_2 at the concentration of 1×10^{-5} mol/L, with Ru(bpy)$_3$Cl$_3$ in aqueous solution (Φ_{em} = 0.042; λ_{ex} = 436 nm) as the standard for quantum yield calculation; ns TA in MeCN with SiNc as standard (ε_{590} = 53400 L mol^{-1} cm^{-1}, Φ_T = 0.20). **20 – 23**, **29 – 33**: UV-vis in CH_2Cl_2; RT emission in CH_2Cl_2 at the concentration of 1×10^{-5} mol/L, with Ru(bpy)$_3$Cl$_3$ in aqueous solution (Φ_{em} = 0.042; λ_{ex} = 436 nm) as the standard for quantum yield calculation; 77 K emission in BuCN glassy matrix; ns TA in toluene with SiNc as standard (ε_{590} = 53400 L mol^{-1} cm^{-1}, Φ_T = 0.20). **34** and **35**: UV-vis in CH_2Cl_2; RT emission in CH_2Cl_2 at the concentration of 1×10^{-5} mol/L, with Ru(bpy)$_3$Cl$_3$ in aqueous solution (Φ_{em} = 0.042; λ_{ex} = 436 nm) as the standard for quantum yield calculation; ns TA in toluene with SiNc as standard (ε_{590} = 53400 L mol^{-1} cm^{-1}, Φ_T = 0.20).

Platinum(II) diimine acetylide complexes have wide applications in light-emitting devices, lower-power upconversion, oxygen sensor, nonlinear absorption, etc. As illustrated by the example shown in Figure 1.8, Che and co-workers reported the application of platinum(II) diimine acetylide complexes as organic light-emitting materials, in which different substituted bipyridine or phenathroline were utilized as the diimine ligand and phenylacetylide was employed as the acetylide ligand.[36] Zhao and co-workers demonstrated that, with long-lived triplet excited-state, complex **14** could be used as triplet sensitizer for upconversion by Zhao.[32] In the presence of complex **14**, emission of perylene at 440 nm – 600 nm region was observed with 532 nm laser excitation of the ^{1}MLCT band of complex **14**,

as shown in Figure 1.9. Zhao also explored the oxygen sensing properties of complexes **12** and **13** as luminescent chromophore, as illustrated in Figure 1.10 for complex **13**.[30, 31]
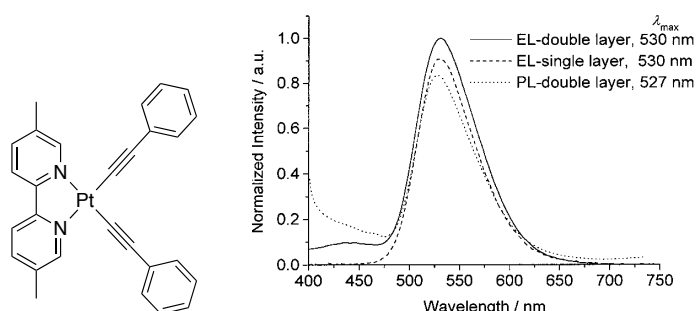
Figure 1.8. 5,5'-Diimine platinum bisphenylacetylide is an example among many similar complexes investigated by Che and coworkers.[23q] The electroluminescence and photoluminescence in spin-coated poly(*N*-vinylcarbozole) (90 wt %) film is shown. Superior electroluminescence was obtained with the maximum luminance of 620 DC m^{-2} at a driving voltage of 30 V. Reprinted with permission from Ref. 36.
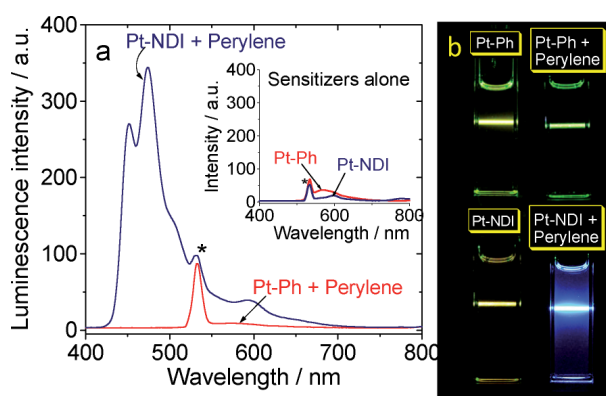
Figure 1.9. Using complexes **14** (PT-NDI) as triplet sensitizer, the emission of the acceptor perylene was observed. Same experiments were also carried out on complex Pt-Ph (which possesses same diimine part with complex **14**, but phenylacetylene as the arylacetylene part) for comparison. Reprinted with permission from Ref. 32.
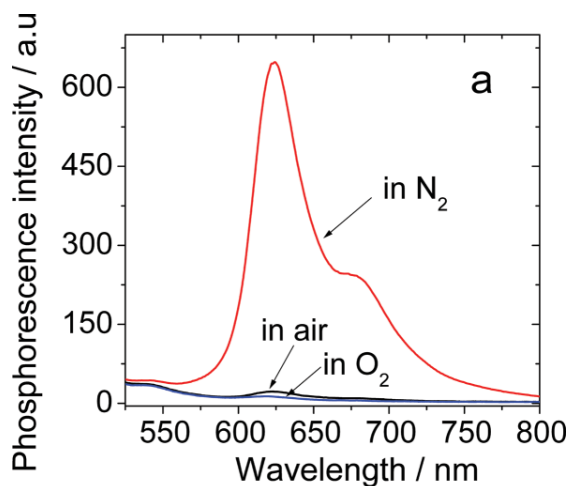
Figure 1.10. Emission of **13** in toluene saturated with air, oxygen, and nitrogen. Reprinted with permission from Ref. 31.

Based on the large ratios of the excited-state absorption cross section with respect to the ground-state absorption cross section in the visible and near-IR region, and on the significant two-photon absorption cross section in the near-IR region of most of the Pt(II) diimine complexes synthesized in our group, our group demonstrated the reverse saturable absorption upon 532 nm ns laser irradiation. Most of the complexes exhibit strong transmittance decreases up increasing the incident fluence. For instance, the transmittance of the dichloromethane solutions of complexes **26**, **34**, and **35** decreased from 80% at low incident energy to 20% or less at high incident energy, which clearly manifests the strong RSA. The degree of RSA is significantly influenced by the degree of π-conjugation on the acetylide ligand, with a better π-conjugation in complexes **20** and **22**, the RSA is much stronger than those in complexes **21** and **23**, as shown in Figure 1.11. Similarly, the RSA of complexes **24** and **25** is much stronger than those in complexes **17** and **19**, respectively, as shown in Figure 1.12. In addition, different substituents at the 7-position of fluorenyl group show a distinct effect on the RSA. As exemplified in Figure 1.13, complex **19** with strong electron donating substituent exhibits a stronger RSA than the ones with electron withdrawing substituents (complexes **16** and **17**).

22
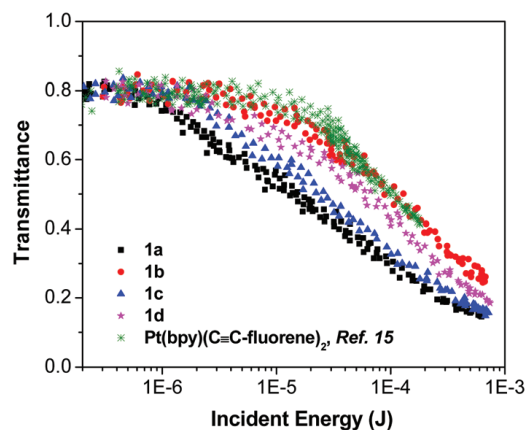
Figure 1.11. Nonlinear transmission curves for **20 – 23** (1a, **20**; 1b, **21**; 1c, **22**; 1d, **23**) in CH$_2$Cl$_2$ for 4.1 ns laser pulse at 532 nm. The linear transmission for all samples was adjusted to 80% in a 2 mm cuvette. Reprinted with permission from Ref. 34.
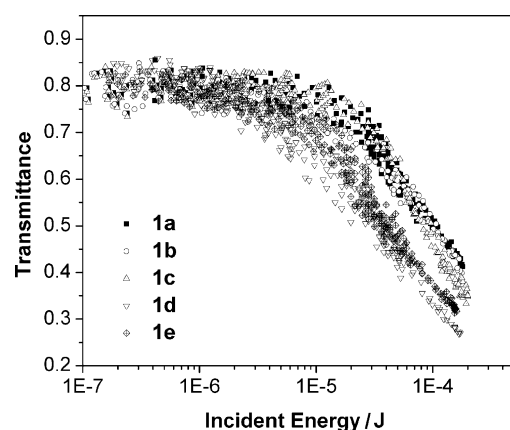
Figure 1.12. Nonlinear transmission curves for **15 – 19** (1a, **15**; 1b, **16**; 1c, **17**; 1d, **18**; 1e, **19**) in CH$_2$Cl$_2$ for 4.1 ns laser pulse at 532 nm. The linear transmission for all samples was adjusted to 80% in a 2 mm cuvette. Reprinted with permission from Ref. 33.
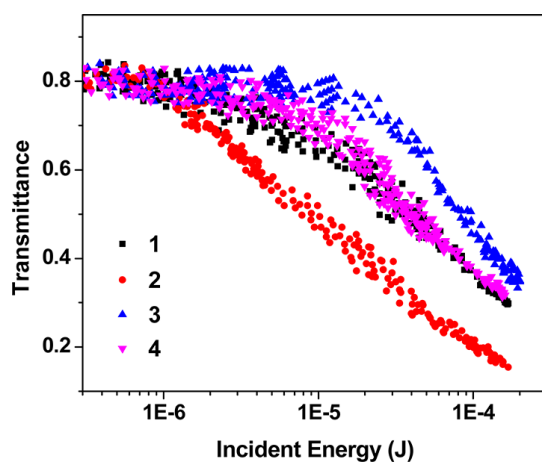
Figure 1.13. Nonlinear transmission curves for **24 – 25** (1, **24**; 2, **25**) in CH$_2$Cl$_2$ for 4.1 ns laser pulse at 532 nm. The linear transmission for all samples was adjusted to 80% in a 2 mm cuvette. Reprinted with permission from Ref. 37.

1.2.3. Synthesis of Pt(II) Diimine Complexes Containing Acetylide Ligands

The synthesis of Pt(II) diimine complexes containing acetylide ligands can be illustrated by the general procedure in Scheme 1.1. The coordination reaction of diimine and K_2PtCl_4 is carried out in refluxing water with catalytic amount of H^+. The resulted diimine platinum(II) chloride is then treated with substituted acetylene in refluxing CH_2Cl_2 in presence of base and catalyst CuI. Both reactions should be protected under inert atmosphere such as nitrogen or argon to prevent possible side reactions.
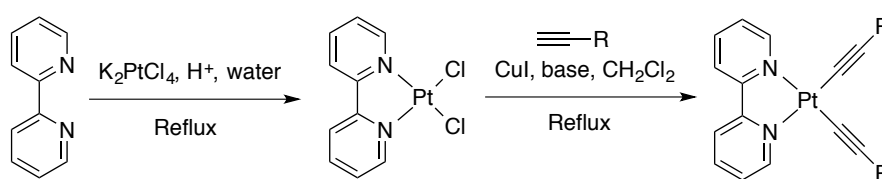
Scheme 1.1. Synthetic routes for Pt(II) diimine complexes containing acetylide ligands

1.2.4. Cyclometallated Pt(II) Complexes with Tridentate N^N^C Ligand

Complexes containing a covalent metal–carbon bond along with one or two traditional coordination bonds are defined as cyclometallated complexes. As a result, cyclometallated complexes belong to organometallic complexes considering the existence of metal–carbon bond in the structure. For example, 2-phenylpyridine (ppy) is a typical cyclometallating ligand and it can bond to a variety of second and third row transition metal ions. The bonding process that results in a 5-membered chelating ring involves a net deprotonation of the aromatic carbon. The deprotonation results in a C^- ligating atom that is a very strong σ donor. Considering the π-accepting ability of the pyridyl part, a synergism of electron delocalization are formed in the 5–membered chelating ring between the metal center, the σ-donor carbon anion and the π-acceptor pyridine, in which electron density is transferred from carbon anion to the metal ion and then back to the pyridyl part of the ligand. The synergism can significantly enhance the metal-ligand interaction and offer the metal ion a very strong ligand-field. Comparing to analogous bidentate N^N complexes that could be

venerable to D_{2d} distortion, the energy of deactivating d-d state in tridentate N^N^C complexes is raised efficiently, thus promoting stable emitting ^{3}MLCT or $^3\pi,\pi^*$ excited-state with high quantum yield.

Examples of platinum(II) complexes with N^N^C ligands are shown in Chart 1.4. Complex **36** is an early example of such complexes,[38] in which one of the two pendent phenyl rings adopts coplanar geometry with the N^N motif and coordinates to platinum(II). Complex **36** is highly emissive at room temperature in CH_2Cl_2, with emission parameters of λ_{max} = 550 nm, τ_{em} = 14 μs, and Φ = 0.21. Complexes **37 – 43** that contain 6-phenyl-2,2'-bipyridine as the N^N^C coordination ligand were studied by Che's and other groups.[39 – 42] Although substituents vary in these complexes, the emission of these complexes all originates from the ^{3}MLCT state.[40] Interestingly, while the structure variation from **37** to **42** barely affect the emission band maximum (562 nm – 568 nm),[40, 41] the attachment of a longer alkoxyl chain seems efficiently facilitated the interaction between the pendent phenyl ring with the N^N^C coordination core, which is reflected by the much red-shifted emission band maximum (590 nm).[42] Complexes with extended π-conjugation such as complexes **44 – 49** were also synthesized and investigated systematically by Che's group.[43] The emission energy of **44 – 49** in solution is substantially tuned by the substituent. The emission is assigned from triplet excited-state with contribution from both ^{3}MLCT and $^3\pi$-π^*. The extended conjugation in complexes **44 – 49** sufficiently increases the electron delocalization, thus reducing the bond displacement at the excited-state. As a result, the non-radiative decay can be substantially suppressed due to extended π-conjugation.
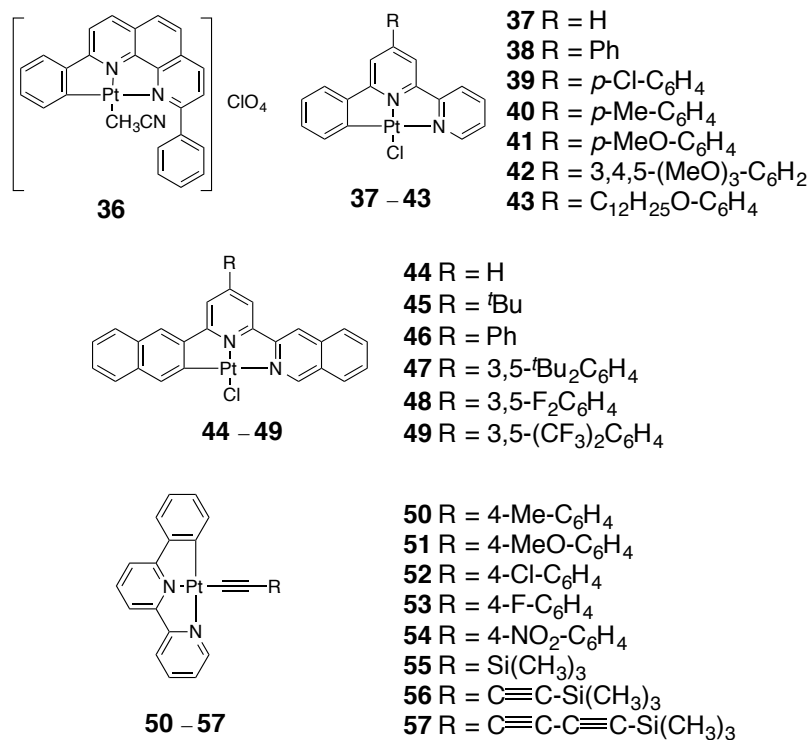
Chart 1.4. Examples of Pt(II) complexes with N^N^C ligands

One of the most important applications of platinum(II) complexes containing N^N^C

ligands is as organic light-emitting materials, exemplified by complex **50** in Chart 1.4.[44]

Intense orange emission was observed for OLED using **50** as electrophosphorescnct material,

with luminance of 3900 cd m^{-2} at 12 V (λ_{max} = 580 nm; CIE coordinates: x = 0.508, y = 0.466)

and EL efficiency of 1.4 cd A^{-1} (η_{ext} = 0.6%) at 20 mA cm^{-2} at 4% doping level. The emission

energies (emission color) of this kind of complexes can be efficiently tuned through the

variation of the substituents on the phenylacetylide ligands, as demonstrated by complexes **51**

– **57** in Chart 1.4.[44] In these complexes, acetylide ligands are employed to destabilize the

non-radiative d-d state as well as to tune the triplet excited-states. From complex **51** to

complex **54**, the emission energy blue-shifted from 630 nm for **51** to 560 nm for **54**.[44] This

trend can be well explained by the fact that the electron withdrawing group will stabilize the

N^N^C localized HOMO of the complex. The extent of conjugation also plays an role on the

emission energy demonstrated by complexes **55** – **57**.[44] The emission energy blue-shifts as

the conjugation length increases from **55** (570 nm) to **57** (557 nm), indicating the stabilized

acetylide/Pt(II) based HOMO energy due to longer conjugation in the acetylide ligand.
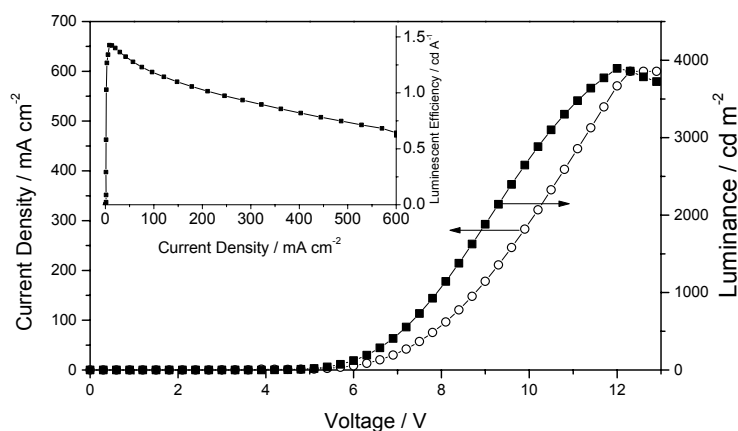
Figure 1.14. Current density, voltage and luminance characteristics (inset: luminesence efficieny vs. current density) for OLED using 50 as emitter at 4% doping level. Reprinted with permission from Ref. 44.

Because of the relatively sturdy structure and stable excited-states, our group has

conducted a systematic study on the platinum complexes with modified N^N^C ligands.

Selected examples are shown in Chart 1.5, and the key photophysical parameters for

complexes **62** − **72** are summarized in Table 1.2. Complexes **58** − **61** are several early

examples investigated by our group.[45] The UV-vis and ns transient absorption study revealed

that the length of conjugation on the acetylide ligand exerted significant effect on both the

singlet and triplet excited-states while the replacement of CH_3 with OCH_3 showed minor

effect. Other than arylacetylide auxiliary ligand, complex **62** employed alkylacetylide

auxiliary ligand.[46] Moderate room temperature emission was observed for complex **62** with

maximum at 591 nm in CH_3CN, which is attributed to ^{3}MLCT. Notably, relatively high

triplet quantum yield (0.51) was observed for complex **62**. By incorporating alkoxyl group -

OC_7H_8 on the phenyl ring, complexes **63** − **67** exhibit much longer emission lifetimes (~ 100

ns for **62**, 460 ns − 670 ns for **63** and **64**) and higher emission quantum yield.[47] This

phenomenon is accounted for by the electron-donating ability of the alkoxyl group, which

admixes intra ligand charge transfer (^{3}ILCT) character to the metal/ligand to ligand charge

27

transfer state (^{3}MLCT/^{3}LLCT). Further study was carried out by incorporating fluoreneyl unit at the central pyridine, as shown in complexes **68 – 71**.[48] The electron-donating ability of fluorenyl unit further increased the triplet excited-state lifetime and quantum yield and the ratios between the excited-state absorption cross section and ground-state absorption cross section. Complex **72** embraces fluorenyl unit directly to the N^N^C coordination core.[10] The ground-state of complex **72** featured ligand-centered π-π* transition in the UV and blue region and a broad and structureless ^{1}MLCT/^{1}LLCT absorption band in the visible region, as shown in Figure 1.15 and Figure 1.16. The emission of the complex at room temperature and at 77 K is dominated by $^3\pi,\pi$* character with minor contribution from ^{3}MLCT state, while the degree of ^{3}MLCT contribution can be adjusted by solvent polarities. In contrast, both the nanosecond (in CH$_3$CN) and femtosecond (in CH$_2$Cl$_2$) transient absorptions are dominated by $^3\pi,\pi$* state.

58 – 61

58 R = CH$_3$, n = 1
59 R = CH$_3$, n = 2
60 R = OCH$_3$, n = 1
61 R = OCH$_3$, n = 2

62 – 65

62 R = C≡C-C$_3$H$_7$, R' = H
63 R = Cl, R' =OC$_8$H$_{17}$
64 R = C≡C-C$_3$H$_7$, R' =OC$_8$H$_{17}$
65 R = C≡C-C$_6$H$_5$, R' =OC$_8$H$_{17}$

66

67

68 – 71

68 R = Cl, R' = H
69 R = Cl, R' =OC$_8$H$_{17}$
70 R = C≡C-C$_3$H$_7$, R' =H
71 R = C≡C-C$_6$H$_5$, R' =H

72
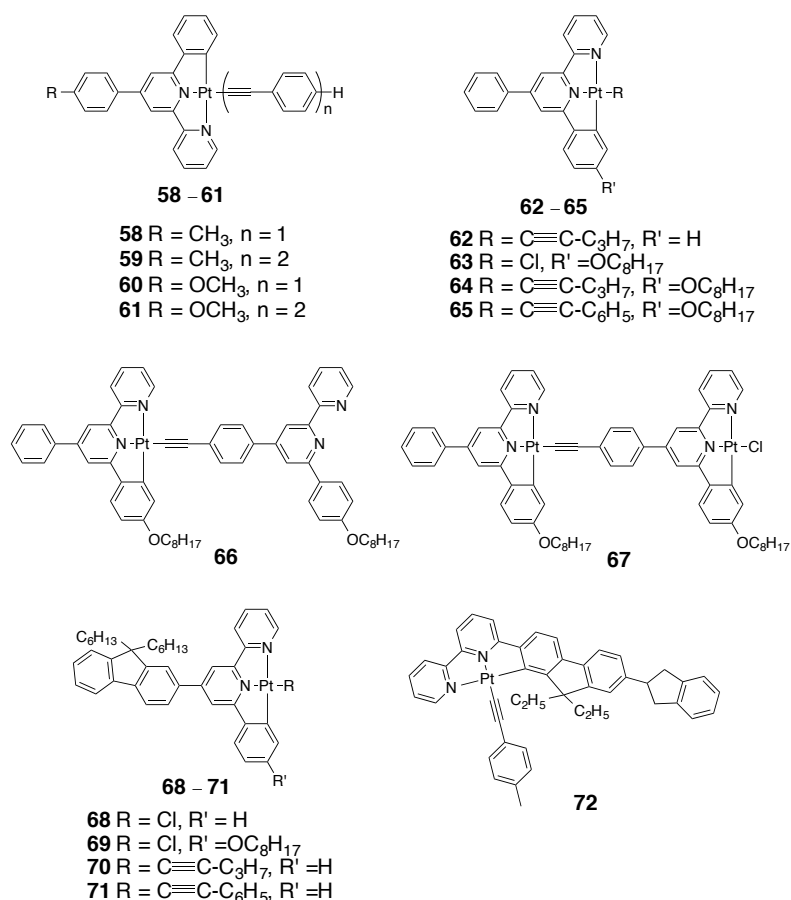
Chart 1.5. Pt(II) complexes with N^N^C ligands studied by our group

Table 1.2. Photophysical data of complexes **58 – 72**.

	λ_{abs}/nm (logε/Lmol^{-1}cm^{-1})	λ_{em}/nm (τ/μs); Φ_{em} R.T.	$\lambda_{T_1-T_n}$/nm (τ_T/μs; log$\varepsilon_{T_1-T_n}$/L mol^{-1} cm^{-1}; $_T$)^c
62	- (-)	589 (0.1); 0.25	587 (0.09; 3.69; 0.51)
63	286 (4.61), 300 (4.63), 367 (4.24), 431 (3.58)	590 (0.74); 0.033	468 (0.3; 3.47; 0.27)
64	293 (4.66), 342 (4.25), 368 (4.26), 439 (3.76), 464 (3.70)	596 (0.67); 0.19	502 (0.54; 3.49; 0.34)
65	292 (4.72), 344 (4.25), 366 (4.28), 439 (3.86), 464 (3.82)	590 (0.98); 0.15	630 (0.67; 3.94; 0.42)
66	294 (4.86), 329 (4.76), 441 (4.06), 464 (4.03)	590 (0.97); 0.21	650 (0.75; 3.46; 0.11)
67	286 (4.77), 299 (4.78), 366 (4.48), 436 (4.05)	592 (0.87); 0.008	590 (4.8; 3.42; 0.06)
68	282 (4.58), 336 (4.47), 354 (4.51), 421 (3.93), 439 (3.94)	568 (0.96); 0.075	656 (0.21; 3.70; 0.08)
69	291 (4.57), 323 (4.49), 354 (4.58), 419 (3.89), 439 (3.83)	591 (0.95);0.047	665 (0.68; 3.68; -)
70	288 (4.58), 355 (4.49), 443 (3.96), 463 (3.90), 529 (3)	593 (0.68); 0.073	635 (0.66; 3.58; 0.11)
71	284 (4.68), 355 (4.49), 441 (4.01), 465 (3.96), 530 (3.08)	593 (0.98); 0.076	645 (0.8; 3.22; 0.24)
72	265 (4.36), 286 (4.34), 352 (4.51), 387.5 (4.57), 458 (3.63)	591 (1.43); 0.067	633 (14.0; 4.65; 0.28)

62: UV-vis data not reported; RT emission in CH$_3$CN at the concentration of 3.4×10^{-5} mol/L, λ_{ex} = 432 nm; quantum yield relative to Ru(bpy)$_3$Cl$_3$ in aqueous solution (Φ_{em} = 0.042; λ_{ex} = 436 nm); ns TA in CH$_3$CN with SiNc as standard (ε_{590} = 53400 L mol^{-1} cm^{-1}, Φ_T = 0.20). **63 – 71**: UV-vis in CH$_2$Cl$_2$; RT emission in CH$_2$Cl$_2$, emission lifetime is intrinsic lifetime, emission quantum yield relative to Ru(bpy)$_3$Cl$_3$ in aqueous solution (Φ_{em} = 0.042; λ_{ex} = 436 nm); ns TA in CH$_3$CN with SiNc as standard (ε_{590} = 53400 L mol^{-1} cm^{-1}, Φ_T = 0.20). **63 – 71**: UV-vis in CH$_2$Cl$_2$; RT emission in CH$_2$Cl$_2$, emission lifetime is intrinsic lifetime, emission quantum yield relative to Ru(bpy)$_3$Cl$_3$ in aqueous solution (Φ_{em} = 0.042; λ_{ex} = 436 nm); ns TA in CH$_2$Cl$_2$ with SiNc as standard (ε_{590} = 53400 L mol^{-1} cm^{-1}, Φ_T = 0.20).
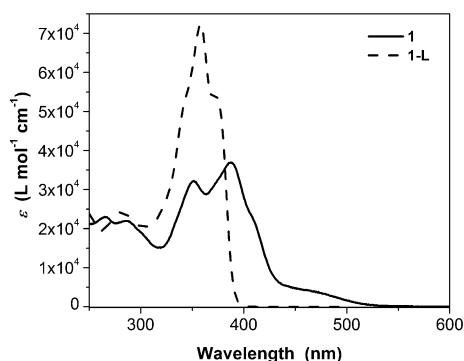
Figure 1.15. UV-vis spectrum of complex **72** (1) in CH$_2$Cl$_2$. Reprinted with permission from Ref. 10.
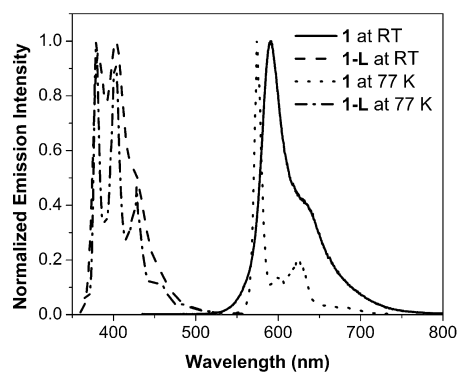
Figure 1.16. Emission of complex **72** (1) at room temperature in CH_2Cl_2, and at 77 K in butylnitrile. Reprinted with permission from Ref. 10.

Complexes **58** − **72** all exhibit strong nonlinear absorption. The reverse satuable absorption are demonstrated by applying 532 nm ns laser pulses through the sample solutions in 2 mm cuvettes. Complexes **58** − **61** exhibit excited-state absorption cross section to ground-state absorption cross section ratio up to 20.[45] This value was improved to 160 for complex **62** at the wavelength of 570 nm.[46] Incorporation of electron-donating substituents such as alkoxyl or fluorenyl units on the N^N^C ligand in complexes **63** − **71** caused the admixture of ^{3}MLCT/^{3}LLCT/^{3}ILCT characters in the triplet excited stats, which induced broad triplet excited-state absorption and strong reverse saturable absorption at 532 nm, as demonstrated in Figure 1.17 for the triplet excited-state absorption and Figure 1.18 for the reverse saturable absorption of complexes **68** − **71**. Similarly, strong and broad triplet excited-state absorption was observed for complex **72**, as illustrated in Figure 1.19. As a result, detailed nonlinear optical characterizations were carried out for complex **72**. Z-scan experiments with ns and ps laser pulses at 532 nm and with ps laser pulses at a variety of visible and near-IR wavelengths were carried out, and the results indicated that this complex exhibited large ratios of excited-state absorption to ground-state absorption from 430 to 680 nm (the ration between excited-state absorption cross section to ground-state absorption cross section up to the scale of 10^4) and strong two-photon absorption from 740 to 910 nm, making

30

complex **72** a promising broadband nonlinear absorbing material. The reverse saturable

absorption of **72** is shown in Figure 1.20.
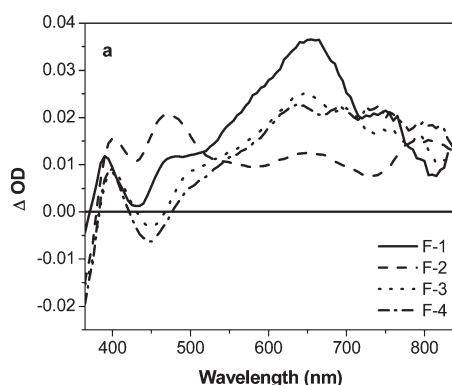
Figure 1.17. Triplet excited-state absorption of complexes **68 − 71** (**68**, F-1; **69**, F-2; **70**, F-3; **71**, F-4) in argon-degassed CH_3CN at the zero-time decay after 355 nm excitation. Reprinted with permission from Ref. 48.
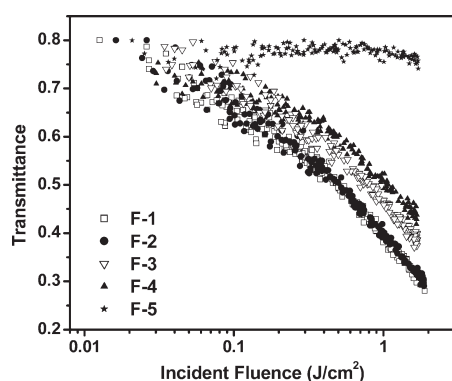
Figure 1.18. Reverse saturable absorption of complexes **68 − 71** in CH_2Cl_2 for 4.1 ns laser at 532 nm in a 2 mm cuvette. The linear transmission was adjusted to 80%. Reprinted with permission from Ref. 48.
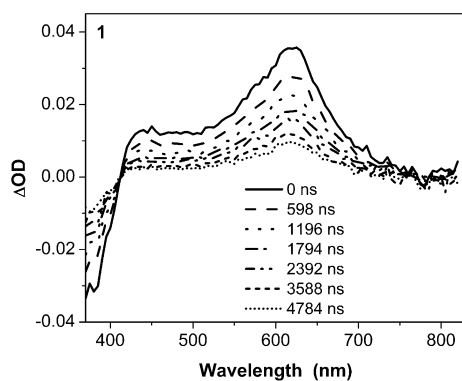
Figure 1.19. Time-resolved triplet excited-state absorption of **72** in argon-degassed CH_3CN after 355 nm excitation. Reprinted with permission from Ref. 10.

31
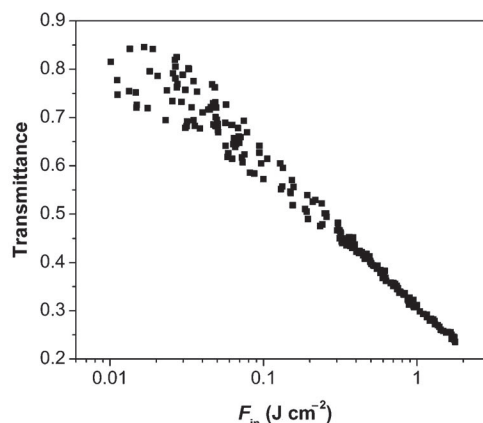
Figure 1.20. Reverse saturable absorption of **72** in CH_2Cl_2 for 4.1 ns laser at 532 nm in a 2 mm cuvette. The linear transmission was adjusted to 80%. Reprinted with permission from Ref. 10.

1.2.5. Synthesis of Cyclometallated Pt(II) Complexes with Tridentate N^N^C Ligand

The ligand synthesis is the prerequisite for the synthesis of Pt(II) complexes with N^N^C ligand. N^N^C ligand can be synthesized following the general procedure shown in Scheme 1.2. The N^N^C ligand included in this dissertation is obtained by consecutive utilization of Stille coupling[49] and Suzuki[50] coupling from 2-bromopyridine. Organotin compound py-Sn is synthesized by treating 2-bromopyridine with BuLi, then with Bu_3SnCl. Stille reaction between the py-Sn with 2,6-dibromopyridine lead to bipyridine compound bpy-Br. Treatment of bpy-Br with BuLi followed by 2-isopropoxy-4,4,5,5-tetramethyl-1,3,2-dioxaborolane affords the protected arylbronic acid bpy-B. The Suzuki coupling reaction between bpy-B and substituted 7-bromofluorene leads to the tridentate N^N^C ligand.
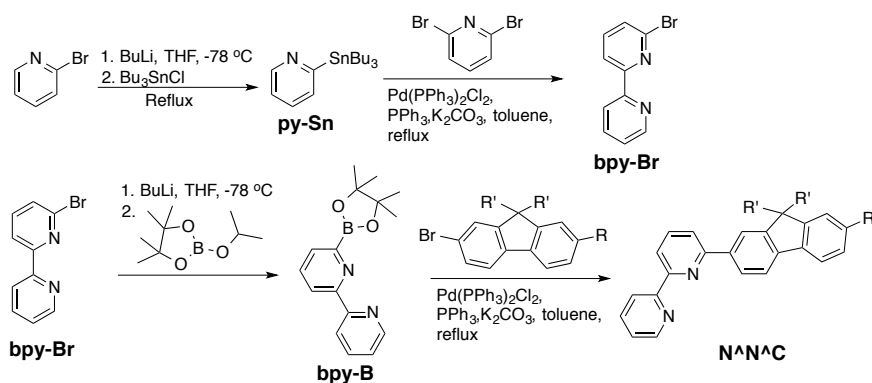
Scheme 1.2. Synthetic routes for N^N^C ligand

The coordination of N^N^C ligand into the coordination sphere of Pt(II) can be readily accomplished by the reaction between K_2PtCl_4 and the ligand in acetic acid under refluxing temperature, as shown in equation 1.16. Protection under inert atmosphere of nitrogen is suggested.

$$K_2PtCl_4 + N^\wedge N^\wedge CH \rightarrow (N^\wedge N^\wedge C)PtCl \tag{1.16}$$

1.3. Bis-cyclomatalated Iridium(III) Complexes

1.3.1. Characteristics of Ir(III) Complexes

Comparing to d^8 platinum(II), iridium(III) have d^6 electronic configuration and the complexes formed adopt octahedral geometry. The octahedral structure around the metal center makes Ir(III) well protected by ligands from the surrounding environment. Deactivation pathways such as axial interaction, ground-state aggregation and solvent molecule binding can be efficiently reduced in iridium complexes. In addition, the spin-orbit coupling constant of iridium metal is the largest among transition metals.[51] As a result, high triplet excited-state quantum yields are expected due to rapid intersystem crossing. The large spin-orbit coupling constant also facilitates the spin-forbidden absorption from the singlet ground state to triplet excited state. Figure 1.21 illustrates the general molecular orbital energy diagram of octahedral iridium complexes.[52] The subscript M or L for each molecular orbital denote the predominant localization of the orbital. For example, in the ground electronic configuration of transition metal complexes in their normal oxidation states, the σ_L and π_L orbitals are completely filled, the π_M orbitals are either partially or completely filled, and the higher orbitals are usually empty.
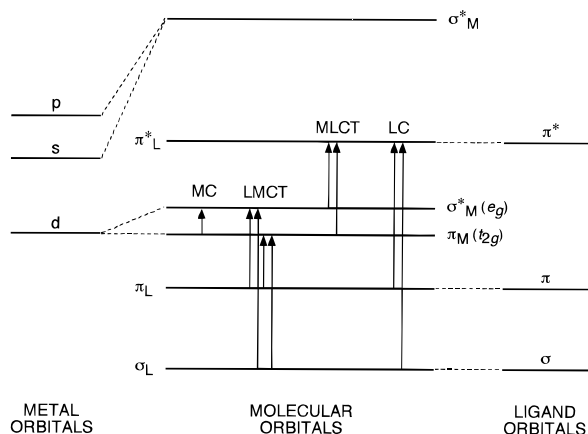
Figure 1.21. Energy-level diagram and electronic transitions for octahedral metal complexes (Reprinted with permission from Ref. 52)

Various electronic transitions exist in iridium(III) complexes, as indicated by the vertical arrows in Figure 1.21. The electronic transition between two d orbitals of the metal center is called metal centered transitions (MC). Ligand to metal charge transfer (LMCT) is the electronic transitions from the ligand's σ_L or π_L orbital to the metal's vacant d orbital center, while metal to ligand charge transfer (MLCT) is the electronic transitions from the metal's filled d orbitals to the ligand's π_L* orbitals. Ligand centered (LC) transitions is the electronic transitions within the ligand from the lower energy σ_L, π_L, or n orbitals to higher σ_L* or π_L* orbitals.

1.3.2. Photophysics and Applications of Selected Examples

Photophysics and applications of iridium(III) complexes have drawn intense attention. Two of the prototype bis-cyclometalated iridium(III) complexes, [Ir(bpy)(ppy)$_2$]$^+$ and Ir(ppy)$_3$, are shown in Chart 1.6.[53, 54] In the two complexes, bpy denotes for 2,2'-bipyridine while ppy denotes for 2-phenylpyridine. The coordination geometry for both complexes is octahedral. [Ir(bpy)(ppy)$_2$]$^+$ is cationic regarding to the inner coordination sphere. The complexes show intense electronic absorption from ligand centered transitions in the ultraviolet region and moderate absorption in the violet to blue region from the ^{1}MLCT transition.[53, 54] Notably, [Ir(bpy)(ppy)$_2$]$^+$ showed spin-forbidden transitions 3MLCT/3LLCT

in its UV-vis absorption spectrum.[55] The emission of the complex is from the ^{3}MLCT state with the lifetime in the scale of several hundred of nanosecond.[53] Ir(ppy)$_3$ is a neutral complex. The electronic absorption of Ir(ppy)$_3$ features intense absorption band (ligand centered $^1\pi$-π^*) in the ultraviolet region and both spin-allowed and spin-forbidden charge transfer band (MLCT) in the region of 330 nm – 450 nm, which effectively mix with each other by the strong spin-orbit coupling of Ir(III).[54] The emission of Ir(ppy)$_3$ is featured by strong phosphorescence both at 77 K and at room temperature from a mixture of ^{3}LC/^{3}MLCT, with the lifetime in the scale of several microseconds and quantum yield nearly unity.[54]

[Ir(bpy)(ppy)$_2$]$^+$ Ir(ppy)$_3$
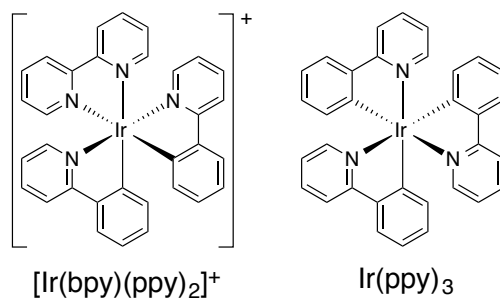
Chart 1.6. Two prototype iridium(III) complexes

Recent studies on bis-cyclometalated Ir(III) complexes widely employ different ligands such as bpy/ppy, 1-phenylpyrazol, benzimidazol, 2-phenyl benzothiozol, benzoquinoline, etc. These ligands are further modified by attaching different substituents with electron donating or withdrawing abilities or extended π-conjugation. Examples of Ir(III) complexes with three bidentate ligands are illustrated in Chart 1.7.

Chart 1.7. Selected examples of bis-cyclometalated Ir(III) complexse

As illustrated by complexes **73 – 87**, Thompson and co-workers conducted systematic studies on the photophysics of bis-cyclometalated Ir(III) complexes and explored their applications as organic light emitting materials.[56] Employing monoanionic, bidentate acetylacetonate ancillary ligand, different cyclometalating ligands were utilized to tune the ground- and excited-state properties. Particularly, the emission energy was tuned to emit from blue to red. Except for the $^1\pi\text{-}\pi^*$ absorption bands, all the complexes showed both ^{1}MLCT and ^{3}MLCT absorption bands. For example, the ^{1}MLCT (410 nm) and ^{3}MLCT bands (460 nm) for complex **73** in 2-methyltetrahedralfuran were both observed, and the intensity for ^{3}MLCT absorption is comparable to the ^{1}MLCT absorption, indicating the strong spin-obit coupling effect of the metal center. The strong spin-orbit coupling of the metal center also facilitated efficient triplet excited-state emission, with the quantum yields of **73 – 87**

varying in the range of 0.1 – 0.6 and the lifetimes in the range of 1 – 14 μs. The triplet excited-states of these complexes were assigned to be $^3\pi$-π^*/^{3}MLCT, the percentage of which depended on the virtue of the bis-cyclometalating ligands. Complexes **73**, **77**, and **80** were employed as the dopant for organic light emitting diodes (OLEDs) as green, red, and yellow emitters respectively. The resultant OLED devices gave relatively high external efficiencies, from 6% to 12.3%. Complex **77** gave saturated red electroluminescence with an efficiency of 2.1 lm/W.

Rather than varying the cyclometalating ligands in complexes **73** – **87**, cationic complexes **88** – **93** contain different diimine ligand with different conjugation extension while maintaining the cyclometalating 1-phenyl-isoquinoline ligand.[57] As shown in Figure 1.22, the electronic absorption of these complexes are composed of $^1\pi$-π^* in the < 400 nm region, ^{1}MLCT/^{1}LLCT in the 400 – 500 nm region, and ^{3}MLCT in the region above 500 nm. Featuring mixed ^{3}MLCT/^{3}LLCT/$^3\pi$-π^* excited-states, the emission wavelength of these complexes can be tuned from 586 nm for **88** and **89** to 732 nm for **93**, resulted from different conjugation extension of the diimine ligands. The emission spectra of complexes **88** – **93** are shown in Figure 1.23.
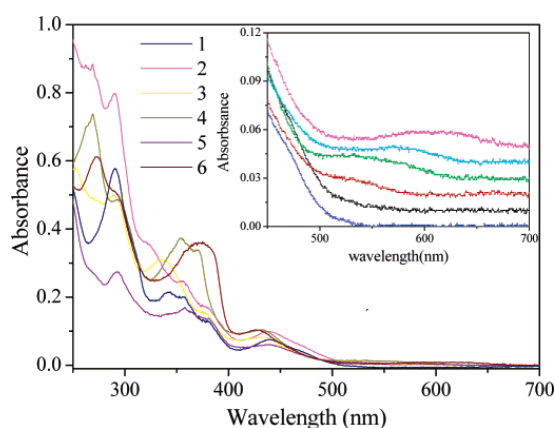
Figure 1.22. Absorption spectra of **88 - 93** (**88**, 1; **89**, 2; **90**, 3; **91**, 4; **92**, 5; **93**, 6) at room temperature in CH_2Cl_2. Reprinted with permission from Ref. 57.
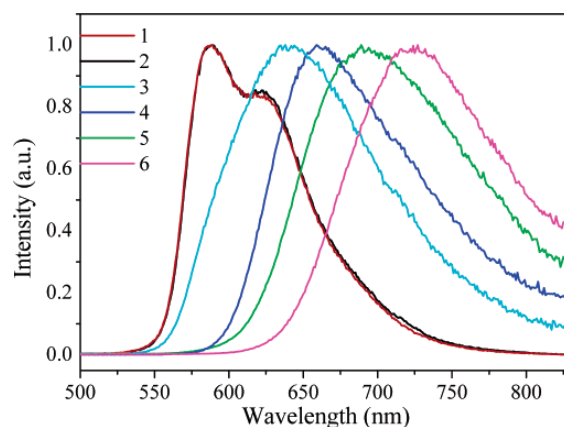
Figure 1.23. Photoluminescence of **88** - **93** (**88**, 1; **89**, 2; **90**, 3; **91**, 4; **92**, 5; **93**, 6) at room temperature in CH$_2$Cl$_2$. Reprinted with permission from Ref. 57.

Complex **94** illustrated the application of Ir(III) complex as nonlinear optical material, as reported by Schanze.[58] The electronic absorption of complex **94** in THF featured a broad band at 500 nm, which was attributed to the mixture of $^1\pi$-π^*/^{1}MLCT transitions. Weak emission with a band maximum at 730 nm was observed for complex **94** in THF with a lifetime of 513 ns and quantum yield of 0.003, which was also observed under two-photon excitation with 1064 nm laser. Notably, complexes **94** exhibited strong transient absorption (Figure 1.24) in the spectral region of visible to near-IR, indicating its application as broadband nonlinear absorbing material. Unsurprisingly, complex **94** showed remarkable nonlinear absorption for 1064 nm ns laser, which occured through two-photon absorption at 1064 nm followed by intersystem crossing to the absorbing triplet excited-states. In addition, reverse saturable absorption was observed at 532 nm. This dual-mechanism nonlinear absorption can be elucidated by Figure 1.25.
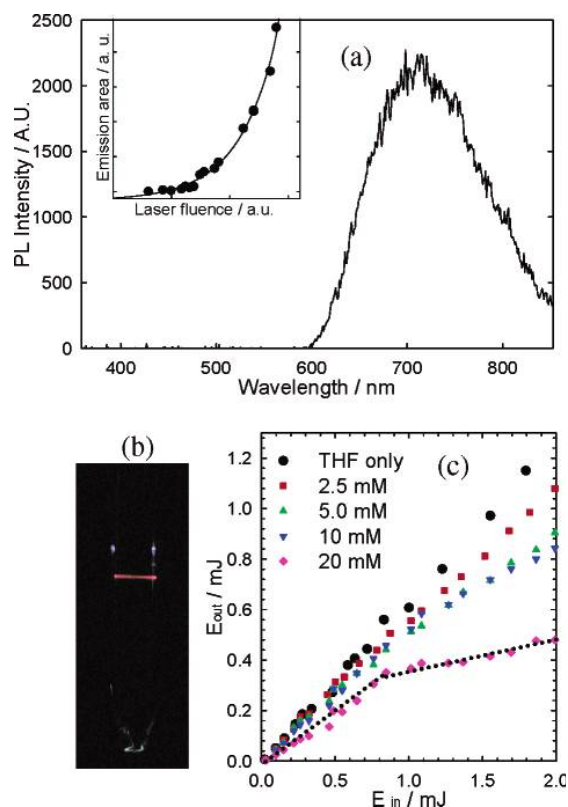
Figure 1.24. (a) Emission spectrum of **94** in 5 mM THF solution, λ_{ex} = 1064 nm. (b) Photograph of the visible emission under 1064 nm excitation. (c) Transmittance of 1064 nm pulsed beam at various concentrations of **94** in THF. Reprinted with permission from Ref. 58.
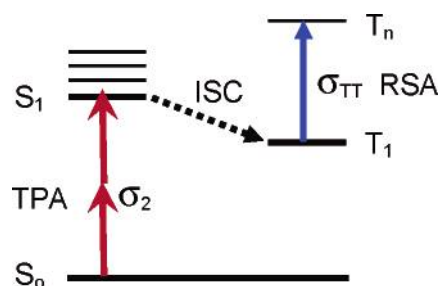
Figure 1.25. Energy diagram for **94**, which exhibits two-photon absorption and reverse saturable absorption. Reprinted with permission from Ref. 58.

Complexes **95 – 98**, reported by our group recently, are cationic Ir(III) complexes featuring benzothiazofluorene (BTZ) substituents on either diimine ligand or cyclometalating 2-phenylpyridine ligand.[59] In these complexes, the structure-property relationship was examined by variation of the position of the BTZ or the extent of π-conjugation. As shown in Figure 1.26, the electronic absorptions of **95 – 98** feature $^1\pi$-π* transitions admixed with ^{1}MLCT/^{1}LLCT in the < 475 nm region and spin-forbidden ^{3}MLCT/^{3}LLCT above 475 nm.

The emitting states varies significantly in the four complexes: ^{3}MLCT/^{3}LLCT for **95**, $^3\pi$-π*

for **96**, and admixed ^{3}MLCT/^{3}LLCT/$^3\pi$-π* for **97** and **98**. Broadband transient absorptions are

observed, and they are much stronger for **95 – 97** than for **98**, as shown in Figure 1.27. This

trend in transient absorption is reproduced in the reverse saturable absorption of **95 – 98** for

532 nm ns laser, in which the strength follows the trend of **95 $\approx$ 96 $\approx$ 97 > 98**. Nevertheless,

the strength of the transient absorption is not the solely factor that governs the strength of

reverse satuable absorption, and the ground-state absorption and triplet-excited state quantum

yield should all be considered.
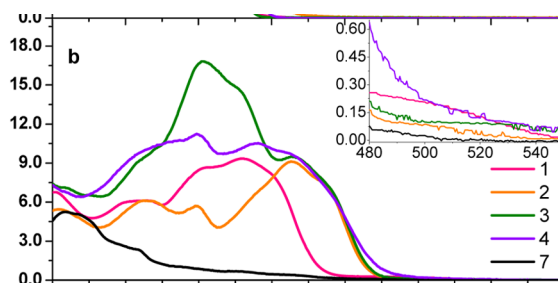
Figure 1.26. Electronic absorption of **95 – 98** in CH$_2$Cl$_2$ (**95**, 1;
96, 2; **97**, 3; **98**, 4). Reprinted with permission from Ref. 59.
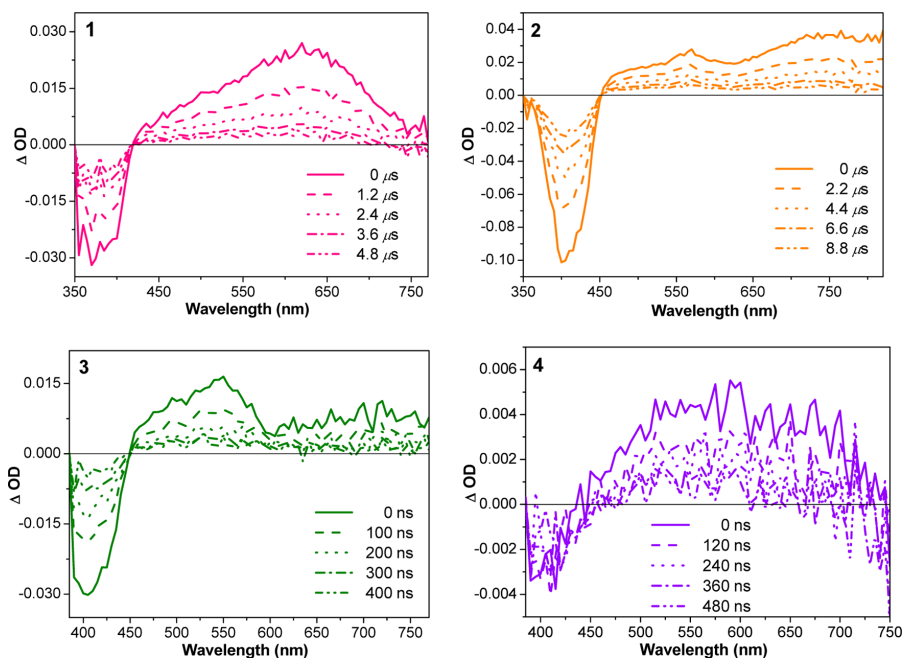
Figure 1.27. Time-resolved transient absorptiop of **95 – 98** in toluene, λ_{ex} = 355
nm, A$_{355}$ = 0.4. (**95**, 1; **96**, 2; **97**, 3; **98**, 4). Reprinted with permission from Ref. 59.
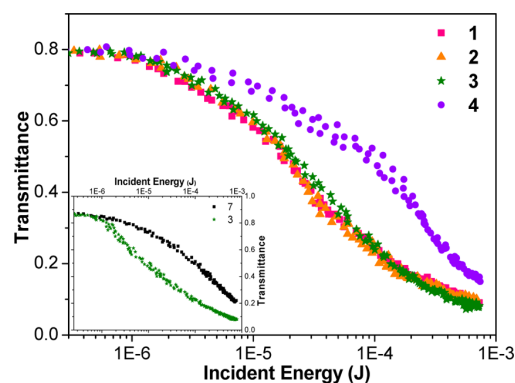
Figure 1.28. Reverse saturable absorption for complexes **95 – 98** in 2 mm thick toluene solution (80% linear transmission) for 4.1 ns laser pulses at 532 nm. Reprinted with permission from Ref. 59.

Table 1.3. Photophysical data of complexes **95 – 98**.

	λ_{abs}/nm (logε/Lmol^{-1}cm^{-1})	λ_{em}/nm (τ/μs); Φ_{em} R.T.	$\lambda_{T_1-T_n}$/nm (τ_T/μs; log$\varepsilon_{T_1-T_n}$/L mol^{-1} cm^{-1}; Φ_T)^c
95	314 (4.79), 355 (4.94), 379 (4.97)	582 (1.20); 0.33	620 (5.30; 4.98; 0.13)
96	313 (4.79), 348 (4.76), 413 (4.96), 430 (4.89)	600 (6.80); 0.097	735 (8.35; 4.76; 0.30)
97	307 (4.95), 353 (5.22), 378 (5.17), 414 (4.98)	608 (1.39); 0.14	550 (0.20; 4.65; 0.16)
98	322 (5.02), 349 (5.05), 390 (5.02), 413 (4.99)	609 (1.32); 0.027	590 (0.30; 5.06; 0.015)

UV-vis in CH$_2$Cl$_2$; RT emission in CH$_2$Cl$_2$ at the concentration of 1×10^{-5} mol/L, emission quantum yield relative to Ru(bpy)$_3$Cl$_3$ in aqueous solution (Φ_{em} = 0.042; λ_{ex} = 436 nm); ns TA in toluene with SiNc as standard (ε_{590} = 53400 L mol^{-1} cm^{-1}, Φ_T = 0.20).

1.3.3. Synthesis of Ir(III) Complexes

The coordination reactivity of the iridium center is relatively inert. However, many methods have been developed to facilitate the coordination of iridium to different kinds of ligands. In this dissertation, the synthesis of the mononuclear iridium complexes was realized in a two-step procedure illustrated in Chart 1.8.[60]
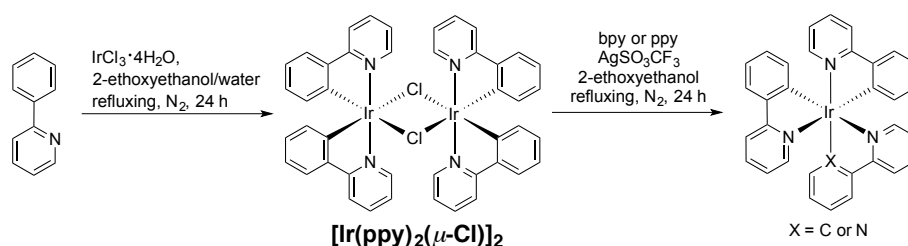
Chart 1.8. General synthesis route for Ir(III) complexes. bpy: 2,2'-bipyridine; ppy: 2-phenylpyridine

41

In this procedure, dinuclear $[Ir(ppy)_2(\mu\text{-}Cl)]_2$ complex was first synthesized by treating iridium trichloride with at least two equivalent of cyclometalating ligand (2-phenylpyridine as an example) under reflux in mixed solvent of 2-ethoxyethanol and water (v/v = 3/1) for 24 hours. The dinuclear complex was then treated with the third ligand (bpy or ppy) in refluxing 2-ethoxyethanol for 24 hour to afford the target mononuclear iridium complex. Both steps should be protected under nitrogen to prevent possible side reactions as well as considering the stability of the dinuclear complex.

1.4. Designing Criteria for Nonlinear Absorbing Materials

The research of our group has been focused on the nonlinear absorption of platinum(II) complexes based on their excited-state absorption (ESA) and/or two-photon absorption (TPA). The ultimate goal is to reduce the transmittance of high intensity lasers by RSA or TPA/ESA mechanism. To date, we have discovered many complexes that show excellent reverse saturable absorption (RSA) and/or TPA, and devices based on these complexes have been explored for laser pulse compression applications. In order to enhance the RSA of complexes, the materials have to have large ratios of ESA cross section (σ_{ex}) relative to those of their ground-state (σ_0). This requires us to reduce the ground-state absorption but increase the ESA at the interested wavelengths. To reach this goal, understanding the structure-property correlation is the key. The nonlinear absorption of metal complexes relies on the σ_{ex}/σ_0 for reverse saturable absorbers and on the TPA cross sections (σ_2) for two-photon absorbing materials. Increase of either value leads to stronger nonlinear absorption. To increase the σ_{ex}/σ_0 value, we need to minimize the ground-state absorption (but not to zero!) and/or maximize the excited-state absorption in the expected RSA region. In addition, having a long-lived excited-state that can absorb light before decay to ground-state is the preliminary requirement. Meanwhile, since the ligand-centered $^1\pi,\pi^*$ states generally have strong ground-state absorption while ^{1}MLCT/^{1}LLCT states absorb weakly,

blue-shift of the ligand-centered $^1\pi,\pi^*$ states to the UV-region and red-shift of the ^{1}MLCT/^{1}LLCT band would not only improve the RSA in the visible to the NIR region but also expand the RSA spectral region. To increase the σ_2 value, molecules should contain more conjugated π-electron system as the ligand and the degree of charge transfer should be large. On the other hand, although increasing the π-conjugation of the ligand could potentially increase the TPA of the molecule and admixture the $^3\pi,\pi^*$ character into the low-energy charge-transfer state to increase the lifetime of the lowest triplet excited-state, the extended π-conjugation of the ligand could red-shift the major absorption band, which would reduce the RSA. Therefore, there is a fine balance when adjusting the conjugation length of the ligand.

Ligand field strength of the metal center is very important in determining the excited-state properties of the transition-metal complexes. Generally, the ligand field strength of transition metals increases from the first-row to the third-row metals. As a result, most first-row transition metal complexes have a short-lived excited-state due to the accessibility of non-radiative deactivating d,d state. In contrast, second- and third-row transition metals complexes can reach stable and long-lived excited-state. Both Pt and Ir metals belong to third-row transition metal, especially the ligand field strength of Ir(III) is even stronger than Pt(II). The non-radiative deactivating d,d state is pushed to a higher energy level for the Ir(III) complexes, which could generate long-lived triplet excited-states. This is another desirable feature for ideal nonlinear absorbing materials. In addition, Ir(III) complexes have been reported to exhibit faster intersystem crossing, which could enhance the quantum yield of the triplet excited-state and facilitate the RSA for ns and longer pulsewidth lasers. Furthermore, it is possible to incorporate more desirable substituents on each of the bidentate ligand to enhance the RSA and TPA in the Ir(III) complexes. From practical viewpoints, the octahedral coordination geometry of Ir(III) could reduce the intermolecular interactions,

which could increase the solubility of the Ir(III) complexes. Moreover, iridium salt is cheaper than platinum salt, which could reduce the cost for practical applications.

1.5. Objective of My Dissertation Research

As discussed above in this chapter, Pt(II) and Ir(III) complexes show interesting photophysical and nonlinear absorption. By utilizing the strong intersystem crossing induced by the large spin-orbit coupling constant of these metal centers, two major research objectives are merged in this dissertation: (1) understanding the structure property relationship of Pt(II) and Ir(III) complexes by studying the photophysics, including electronic absorption, emission and transient absorption, of the structurally-related complexes with different substituents on the ligands; (2) optimizing the RSA and/or TPA of these complexes. To realize these goals, five series of Pt(II) or Ir(III) complexes were developed and studied in detail:

(1) Synthesis, photophysics and nonlinear absorption of bipyridyl platinum(II) bisstilbenylacetylide complexes with different auxiliary substituents

(2) Tunable photophysics and reverse saturable absorption of a series of platinum chloride complexes containing 6-[7-R-9,9-di(2-ethylhexyl)-9H-fluoren-2-yl]-2,2'-bipyridinyl ligand

(3) Synthesis, photophysics, and reverse saturable absorption of platinum complexes bearing extended π-conjugated C^N^N ligand

(4) Synthesis, photophysics, and nonlinear absorption of 7-(benzothiazol-2-yl)-9,9-di(2-ethylhexyl)-9H-fluoren-2-yl tethered [Ir(bpy)(ppy)$_2$]PF$_6$ and Ir(ppy)$_3$

(5) Synthesis, photophysics, and nonlinear absorption of a series of bipyridyl iridium(III) complexes with different cyclometallating arylpyridine ligands

1.6. References

[1] Lu, W.; Mi, B.-X.; Chan, C.-W.; Hui, Z.; Che, C.-M.; Zhu, N.; Lee, S.-T. *J. Am. Chem. Soc*. **2004**, *126*, 4958.

[2] He, Z.; Wong, W.-Y.; Yu, X.; Kwok, H.-S.; Lin*, Z. Inorg. Chem*. **2006**, *45*, 10922.

[3] Lamansky, S.; Djurovich, P.; Murphy, D.; Abdel-Razzaq, F.; Lee, H. E.; Adachi, C.; Burrows, P. E.; Forrest, S. R.; Thompson, M. E. *J. Am. Chem. Soc.* **2001**, *123*, 4304.

[4] Thomas, K. R. J.; Velusamy, M.; Lin, J. T.; Chien, C. H.; Tao, Y. T.; Wen, Y. S.; Hu, Y. H.; Chou, P. T. *Inorg. Chem.* **2005**, *44*, 5677.

[5] Wu, W.; Xu, X.; Yang, H.; Hua, J.; Zhang, X.; Zhang, L.; Long, Y.; Tian, H. *J. Mater. Chem*. **2011**, *21*, 10666.

[6] Keck, M. V.; Lippard, S. J. *J. Am. Chem. Soc.* **1992**, *114*, 3386.

[7] Lo, K. K. W.; Hui, W. K.; Chung, C. K.; Tsang, K. H. K.; Ng, D. C. M.; Zhu, N. Y.; Cheung, K. K. *Coord. Chem. Rev*. **2005**, *249*, 1434.

[8] Zhang, K.Y.; Lo, K. K.W. *Inorg. Chem*. **2009**, *48*, 6011.

[9] Sun, W.; Zhang, B.; Li, Y.; Pritchett, T. M.; Li, Z.; Haley, J. E. *Chem. Mater*. **2010**, *122*, 6384.

[10] Zhang, B.; Li, Y.; Liu, R.; Pritchett, T. M.; Azenkeng, A.; Ugrinov, A.; Haley, J. E.; Li, Z.; Hoffmann, M. R.; Sun, W. *Chem. Eur. J.* **2012**, *18*, 4593.

[11] Atkins, P. W. *Molecular Quantum Mechanics*; Oxford University Press, New York, **1983**.

[12] Rohatgi-Mukherjee, K. K. *Fundamentals of Organic Chemistry*; John Wiley & Sons, New York and Toronto, **1978**.

[13] McGlynn, S. P. *Molecular Spectroscopy of the Triplet State*; Prentice Hall, New Jersey, **1969**.

[14] Zimmermann, J.; Zeug, A.; Roder, B. *Phys. Chem. Chem. Phys.* **2003**, *5*, 2964.

[15] Wayne, R. P. *Principles and Applications of Photochemistry*; Oxford University Press,

New York, **1988**.

[16] Turro, N. J. *Modern Molecular Photochemistry*; University Science Books, **1991**.

[17] Gibert, A.; Baggott, J. *Essentials of molecular photochemistry*; Blackwell Scientific Publication, Inc., **1991**.

[18] Yeh, A.T.; Shank, C. V.; McCusker, J. K. *Science* **2000**, *289*, 935.

[19] Cowan, D. O. *Elements of Organic Photochemistry*; Plenum Press, New York and London, **1976**.

[20] Marcus, R. A. *Disc. Faraday Soc.* **1960**, *29*, 21.

[21] Marcus, R. A.; Sutin, N. *Biochim. Biophys. Acta.* **1985**, *811*, 265.

[22] Harter, D. J.; Sand, M. L.; Band, Y. B. *J. Appl. Phys.* **1984**, *56*, 865.

[23] Williams, J. A. G. *Top. Curr. Chem.* **2007**, *281*, 205.

[24] Miskowski, V. M.; Houlding, V. H. *Inorg. Chem.* **1991**, *30*, 4446.

[25] Lai, S.-W.; Lam, H.-W.; Lu, W.; Cheung, K.-K.; Che, C.-M. *Organometallics* **2002,** *21,* 226.

[26] Chan, C.-W.; Cheng, L.-K.; Che, C.-M. *Coord. Chem. Rev.* **1994**, *132*, 87.

[27] Wadas, T. J.; Lachicotte, R. J.; Eisenberg, R. *Inorg. Chem.* **2003**, *42*, 3772.

[28] Whittle, C. E.; Weinstein, J.A.; George, M. W.; Schanze, K. S. *Inorg. Chem.* **2001**, *40*, 4053.

[29] Castellano, F. N.; Pomestchenko, I. E.; Shikhova, E.; Hua, F.; Muro, M. L.; Rajapakse, N. *Coord. Chem. Rev.* **2006**, *250*, 1819.

[30] Guo, H.; Muro-Small, M. L.; Ji, S.; Zhao, J.; Castellano, F. N. *Inorg. Chem.* **2010**, *49*, 6802.

[31] Sun, H.; Guo, H.; Wu, W.; Liu, X.; Zhao, J. *Dalton Trans.* **2011**, *40*, 7834.

[32] Liu, Y.; Wu, W.; Zhao, J.; Zhang, X.; Guo, H. *Dalton Trans.* **2011**, *40*, 9085.

[33] Liu, R.; Zhou, D.; Azenkeng, A.; Li, Z.; Li, Y.; Glusac, K. D.; Sun, W. *Chem. Eur. J.*

2012, *18*, 11440.

[34] Liu, R.; Dandu, N.; Li, Y.; Kilina, S.; Sun, W. *Dalton Trans.* **2013**, *42*, 4398.

[35] Liu, R.; Chen, H.; Chang, J.; Li, Y.; Zhu, H.; Sun, W. *Dalton Trans.* **2013**, *42*, 160.

[36] Chan, S.-C.; Chan, M. C. W.; Wang, Y.; Che, C.-M.; Cheung, K.-K.; Zhu, N. *Chem. Eur. J.* **2001**, *19*, 4180.

[37] Liu, R.; Azenkeng, A.; Zhou, D.; Li, Y.; Glusac, K. D.; Sun, W. *J. Phys. Chem. A* **2013**, *117*, 1907.

[38] Chan, C-W.; Lai, T-F.; Che, C-M.; Peng, S-M. *J. Am. Chem. Soc.* **1993**, *115*, 11245.

[39] Constable, E. C.; Henney, R. P. G.; Leese, T. A.; Tocher, D. A. *J. Chem. Soc. Chem. Commun.* **1990**, 513.

[40] Cheung, T-C.; Cheung, K-K.; Peng, S-M.; Che, C-M. *J. Chem. Soc. Dalton Trans.* **1996**, 1645.

[41] Lai, S-W.; Chan, MC-W.; Cheung, T-C.; Peng, S-M.; Che, C-M. *Inorg. Chem.* **1999**, *38*, 4046.

[42] Neve, F.; Crispini, A.; Campagna, S. *Inorg. Chem.* **1997**, *36*, 6150.

[43] Kui, S. C. F.; Sham, I. H. T.; Cheung, C. C. C.; Ma, C.-W.; Yan, B.; Zhu, N.; Che, C.-M.; Fu, W.-F. *Chem. Eur. J.* **2007**, *13*, 417.

[44] Lu, W.; Mi, B. X.; Chan, M. C. W.; Hui, Z.; Che, C-M.; Zhu, N.; Lee, S. T. *J. Am. Chem. Soc.* **2004**, *126*, 4958.

[45] Sun, W.; Wu, Z-X.; Yang, Q.-Z.; Wu, L-Z.; Tung, C-H. Appl. Phys. Lett. **2003**, *82*, 850.

[46] Shao, P.; Li, Y.; Sun, W. *J. Phys. Chem. A* **2008**, *112*, 1172.

[47] Shao, P.; Li, Y.; Azenkeng, A.; Hoffmann, M. R.; Sun, W. *Inorg. Chem.* **2009**, *48*, 2407.

[48] Shao, P.; Li, Y.; Yi, J.; Pritchett, T. M.; Sun, W. *Inorg. Chem.* **2010**, *49*, 4507.

[49] Milstein, D.; Stille, j. K. *J. Am. Chem. Soc.* **1978**, *100*, 3636.

[50] Miyaura, N.; Suzuki, A. *Chem. Rev.* **1995**, *95*, 2457.

[51] Cotton, F. A.; Wilkinson, G. *Advanced Inorganic Chemistry: A Comprehensive Text*; Wiley, New York, **1980**.

[52] Vincenzo, B.; Alberto, J.; Margherita, V. *Chem. Rev.* **1996,** 96, 759.

[53] Garces, F. O.; King, K. A.; Watts, R. J. *Inorg. Chem.* **1988**, *27*, 3464.

[54] Tamayo, A. B.; Alleyne, B. D.; Djurovich, P. I.; Lamansky, S.; Tsyba, I.; Ho, N. N.; Bau, R.; Thompson, M. E. *J. Am. Chem. Soc.* **2003**, *125*, 7377.

[55] Wu, S.-H.; Ling, J.-Y.; Lai, S.-H.; Huang, M.-J.; Cheng, C. H.; Chen, I-C. *J. Phys. Chem. A* **2010**, *114*, 10339.

[56] Lamansky, S.; Djurovich, P.; Murphy, D.; Abdel-Razzaq, F.; Lee, H-E.; Adachi, C.; Burrows, P. E.; Forrest, S. R.; Thompson, M. E. *J. Am. Chem. Soc.* **2001**, *123*, 4304.

[57] Zhao, Q.; Liu, S.; Shi, M.; Wang, C.; Yu, M.; Li, L.; Li, F.; Yi, T.; Huang, C. *Inorg. Chem.* **2006**, *45*, 6152.

[58] Kim, K.-Y.; Farley, R. T.; Schanze, K. S. *J. Phys. Chem. B* **2006**, *110*, 17302.

[59] Li, Y.; Dandu, N.; Liu, R.; Hu, L.; Kilina, S.; Sun, W. *ACS Appl. Mater. Interfaces* **2013**, *5*, 6556.

[60] Lamansky, S.; Djurovich, P.; Murphy, D.; Abdel-Razaq, F.; Kwong, R.; Tsyba, I.; Bortz, M.; Mui, B.; Bau, R.; Thompson, M. E. *Inorg. Chem.* **2001**, *40*, 1704.

CHAPTER 2. SYNTHESIS, PHOTOPHYSICS, AND NONLINEAR ABSORPTION OF BIPYRIDYL PLATINUM(II) BISSTILBENYLACETYLIDE COMPLEXES WITH DIFFERNET AUXILIARY SUBSTITUENTS

2.1. Introduction

Photophysical and photochemical properties of platinum complexes have been of intense interest for researchers for decades. The interests arise from the unique structural and spectroscopic properties of the platinum complexes and their promising potential applications in the fields of organic light emitting diodes (OLEDs),[1, 2] low power photon upconversion sensitizers,[3] dye-sensitized solar cells (DSSCs),[4] DNA intercalators,[5] photodynamic therapy (PDT),[6] *etc*. Among the reported complexes, platinum diimine bis(acetylide) complexes are of particular interest. Systematic investigations on the photophysics and potential applications of these complexes have been reported by several groups. In 1994, Che and co-workers reported their study on the $Pt(phen)(C{\equiv}CC_6H_5)_2$ complexes and proposed that the emissive state for these complexes has a metal-to-ligand charge transfer character (MLCT).[7,8] Following that, comprehensive work by Eisenberg's group discovered that the lowest occupied molecular orbital (LUMO) of the Pt(II) diimine complexes could be adjusted by the variation of the substituents on diimine, while the highest occupied molecular orbital (HOMO) is slightly affected by the variation of the arylacetylide ligands.[9] Schanze and co-workers later reported that the intraligand $^3\pi,\pi^*$ state largely localized on the arylacetylide ligand could also play a role in the photophysics of the Pt(II) diimine complex with strong electron-withdrawing group on the phenylacetylide ligands.[10] In recent years, Castellano and co-workers demonstrated the interplay of the ^{3}MLCT and $^3\pi,\pi^*$ states in Pt(II) diimine complexes bearing more conjugated aromatic rings, *i.e.* 1-pyrene, 1-anthracene and 1-perylene on the acetylide ligands.[11, 12] In accordance with these results, our group recently revealed the admixture of the ^{3}MLCT and $^3\pi,\pi^*$ characters in the lowest excited states of a

2,2'-bipyridine Pt(II) complex bearing 2-(benzothiazol-2'-yl)-9,9-diethyl-7-ethynylfluorene ligands.[13]

In addition to the interesting photophysical studies, the potential applications of the Pt(II) diimine complexes in OLEDs,[14] molecular photochemical devices,[15, 16] and as vapoluminescent materials[17] and nonlinear absorbing materials[13] have been explored. A detailed nonlinear absorption study reported by our group on the 2,2'-bipyridine Pt(II) complex bearing 2-(benzothiazol-2'-yl)-9,9-diethyl-7-ethynylfluorene ligands[13] revealed that this complex exhibit extremely large ratios of the excited-state absorption relative to that of the ground state in the visible spectral region and large two-photon absorption (TPA) in the near-IR region. This discovery is quite exciting; however, the two-photon absorption cross sections of this complex is still moderate compared to the best organic two-photon absorbing materials.[18] In order to improve the TPA of the Pt(II) bipyridyl complex in the near-IR region, we are interested in introducing the stilbene component to the acetylide ligand, because the TPA of stilbene and its derivatives have been extensively investigated.[19, 20, 21] The ultimate goal is to explore whether the TPA of the Pt(II) bipyridyl complexes could be improved by incorporation of the stilbene component while retaining the strong excited-state absorption of the Pt(II) bipyridyl complexes.

Schanze's group has reported the photochemistry and photophysics of four platinum complexes bearing stilbenylacetylide ligands.[22] It is found that the triplet excited states of these complexes are localized on one of the 4-ethynylstilbene ligands, and the coordination geometry can affect the extent of delocalization through the metal center. However, the effects of the substituents on the 4-ethynylstilbene ligands on the ground- and excited-state properties of the platinum diimine bisstilbenylacetylide complexes have not been explored; and the nonlinear absorption characteristics of these complexes have not been investigated either.

In this study, we synthesized a series of platinum diimine bisstilbenylacetylide complexes (Chart 1) and systematically investigated their photophysics and excited-state absorption. The nonlinear transmission performances of these complexes are evaluated at 532 nm using ns laser pulses. Although the ultimate goal of this project is to enhance the TPA of the Pt(II) complexes in the near-IR region, the linear optical properties of these complexes and their dependence on the substituents are in close relationship to the nonlinear absorption of the complexes. As such, we first focus on understanding of how the auxiliary substituents on the stilbenylacetylide ligand influence the ground-state and excited-state characteristics of the complexes. To reach this goal, both photophysical experiments and time dependent density functional theory (TD-DFT) calculations were carried out.

2.2. Experimental Section

2.2.1. Synthesis and Characterization

All of the reagents and solvents for synthesis were purchased from Aldrich Chemical Co. or Alfa Aesar and used as is unless otherwise stated. Silica gel for chromatography is purchased from Sorbent Technology (60 Å, 230 - 400 mesh, 500 - 600 m^2/g, pH: 6.5 - 7.5). Complexes **2-1** – **2-6** were characterized by ^{1}H NMR, electrospray ionization mass spectrometry (ESI-MS), and elemental analyses. Ligands **2-3-L** – **2-6-L** were characterized by ^{1}H NMR and elemental analyses. Each intermediate is characterized by ^{1}H NMR. ^{1}H NMR was obtained on Varian Oxford-VNMR spectrometers (300 MHz, 400 MHZ, or 500 MHz). ESI-MS analyses were performed at a Bruker BioTOF III mass spectrometer. Elemental analyses were conducted by NuMega Resonance Laboratories, Inc. in San Diego, California.
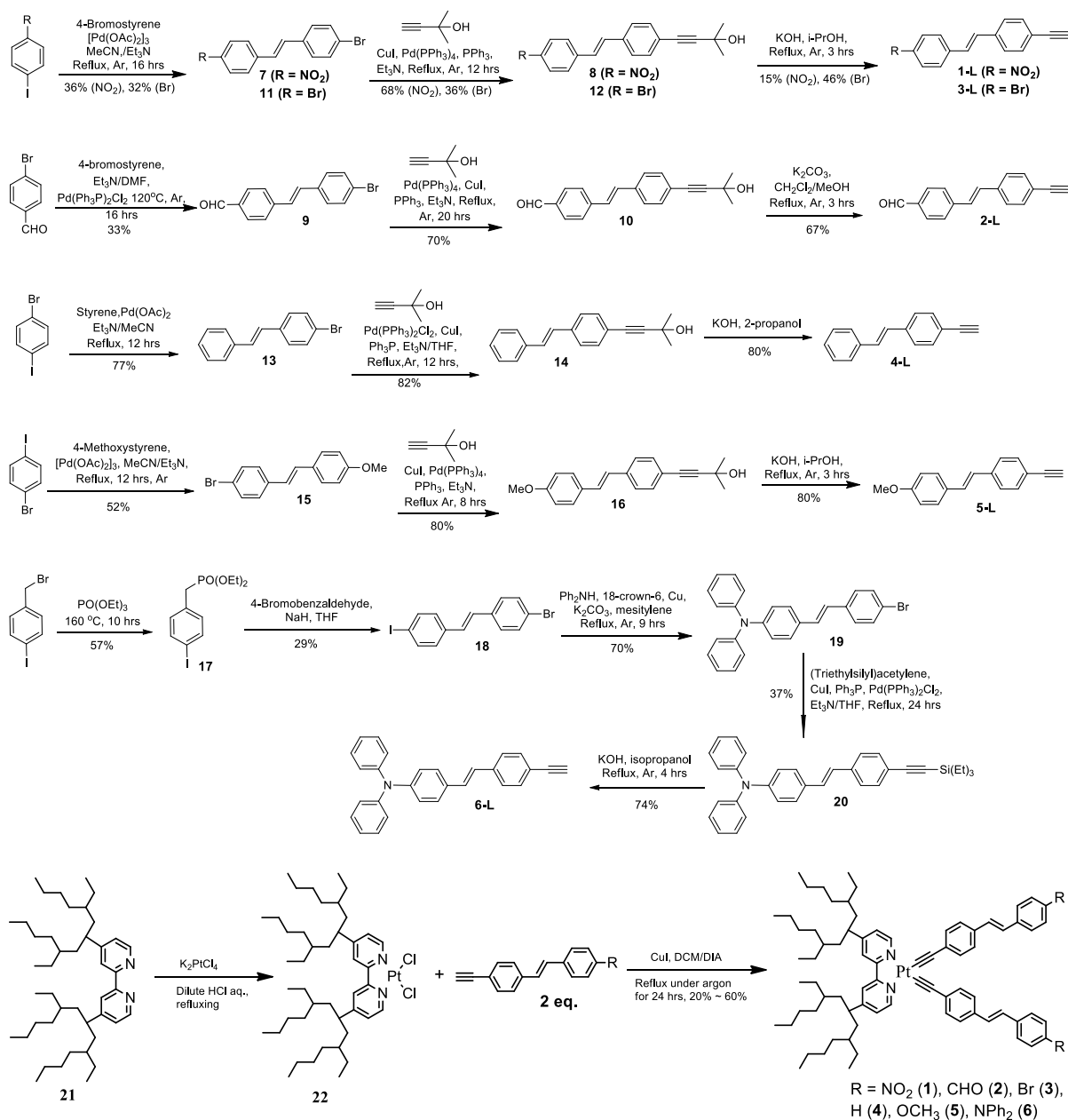
Scheme 2.1. Synthetic routes and structures for complexes **2-1 – 2-6**.

4,4'-di(5,9-diethyl-7-tridecanyl)-2,2'-bipyridine (**21**) was synthesized following the literature procedure.[23] Complex **22** was synthesized by the reaction of K_2PtCl_4 with **21** in refluxing aqueous HCl solution.[9] Compounds **7, 9, 11, 13,** and **15** were synthesized by Heck reaction.[24] Compound **18** was synthesized by Wittig reaction.[25] Compound **19** was synthesized by Ullmann reaction[26] from **18**. Sonogashira coupling reaction[27] of **7**, **9**, **11**, **13**, **15**, and **19** with ethynyltrimethylsilane or 2-methyl-3-buytn-2-ol followed by hydrolysis with

K$_2$CO$_3$ or KOH in *i*-PrOH afforded ligands **1-L** − **6-L**. The synthesis of **1-L** − **6-L** was all previously reported[22, 28 − 31] except **3-L**.

11. The mixture of 4-bromostyrene (1.82 g, 1.4 mL, 10 mmol), 1-bromo-4-iodobenzene (2.83 g, 10 mmol), [Pd(OAc)$_2$]$_3$ (67 mg, 0.1 mmol), MeCN (15 mL), and Et$_3$N (10 mL) was heated to reflux under argon for 12 hrs. After reaction, the solvent was removed by distillation. The residue was dissolved in dichloromethane, and the undissolved part was removed via filtration. The filtrate was washed with brine and dried over Na$_2$SO$_4$. The crude product was purified by silica gel column chromatography with hexane used as eluent. 1.08 g white powder was collected as the product (yield: 32%). ^{1}H NMR (CDCl$_3$, 400 MHz): 6.99 (s, 2H), 7.32 − 7.35 (m, 4H), 7.44 − 7.46 (m, 4H).

12. The mixture of **11** (0.39 g, 1.15 mmol), 2-methyl-3-buytn-2-ol (0.11 mL, 1.15 mmol), CuI (5 mg), Pd(PPh$_3$)$_4$ (5 mg), and PPh$_3$ (5 mg) in Et$_3$N (20 mL) were heated to reflux under argon for 12 hrs. After reaction, the precipitate was removed by filtration and the solvent in filtrate was removed by distillation. The residue was purified by silica gel column chromatography with hexane and dichloromethane (v/v = 1/1) used as the eluent. 0.14 g yellow powder was collected as the product (yield: 36 %). ^{1}H NMR (CDCl$_3$, 400 MHz): 1.61 (s, 6H), 1.98 (s, 1H), 7.02 (d, J = 0.8 Hz, 2H), 7.32 − 7.47 (m, 8H).

3-L. Compound **12** (140 mg, 0.41 mmol), KOH (0.14 g, 2.5 mmol), and *i*-PrOH (20 mL) were refluxed under argon for 3 hrs. After reaction, *i*-PrOH was removed by distillation and the residue was dissolved in dichloromethane (50 mL). The resultant solution was washed with water (3 × 50 mL) and dried over Na$_2$SO$_4$. After removal of the solvent, the residue was purified by silica gel column chromatography with hexane and dichloromethane (v/v = 1/1) used as eluent. 53 mg white powder was collected as the product (yield: 46%). ^{1}H NMR (CDCl$_3$, 400 MHz): 3.11 (s, 1H), 3.75 (s, 1H), 7.03 (s, 2H), 7.34 − 7.36 (m, 2H), 7.42 − 7.47 (m, 6H).

21. Colorless oil, 1.13 g, yield: 89%. ^{1}H NMR (400 MHz, CDCl$_3$): 8.55 (d, J = 4.8 Hz, 2H), 8.23 (s, 2H), 7.08 (dd, J = 5.2, 1.6 Hz, 2H), 2.80 (m, 2H), 1.42 – 1.62 (m, 8H), 0.98 – 1.40 (m, 36H), 0.70 – 0.90 (m, 24H).

22. Yellow solid, 1.03 g, yield: 64%. ^{1}H NMR (400 MHz, CDCl$_3$): 0.72 – 0.87 (m, 24H), 0.92 – 1.37 (m, 36H), 1.55 (m, 8H), 7.32 (dd, J = 6.0, 1.6 Hz, 2H), 7.60 (s, 2H), 9.64 (d, J = 6 Hz, 2H).

General procedure for synthesis of complexes 2-1 – 2-6. The mixture of **22** (0.10 mmol), stilbenylacetylide ligand (0.24 mmol), CuI (5 mg), CH$_2$Cl$_2$ (15 mL), and diisopropylamine (5 mL) was heated to reflux under argon for 24 hrs. After reaction, the solvent and diisopropylamine was removed by rotary evaporation, and the residue was purified by flash silica gel column chromatography using dichloromthane as the eluent. The unreacted ligands were removed first, and then the yellow or red layer was collected as product. The crude product was recrystallized from dichloromethane and hexane to yield yellow or red powders.

2-1. Red powder, 60 mg, yield: 49%. ^{1}H NMR (CDCl$_3$, 400 MHz): 9.57 (s, br., 2H), 8.17 – 8.20 (m, 4H), 7.72 (s, 2H), 7.59 – 7.61 (m, 8H), 7.45 (m, 4H), 7.40 (m, 2H), 7.23 (d, J = 16.4 Hz, 2H), 7.08 (d, J = 16.4 Hz, 2H), 2.92 (m, 2H), 1.56 (m, 8H), 1.05 – 1.38 (m, 36H), 0.75 – 0.89 (m, 24H). ESI-HRMS: m/z Calc. for [C$_{76}$H$_{96}$N$_4$O$_4$Pt+Na]$^+$: 1347.6994; Found: 1347.6966. Anal. Calc. for C$_{76}$H$_{96}$N$_4$O$_4$Pt·2H$_2$O·CH$_2$Cl$_2$: C, 63.97; H, 7.11; N, 3.88; Found: C, 63.96; H, 7.61; N, 4.20.

2-2. Red powder, 72 mg, yield: 55%. ^{1}H NMR(CDCl$_3$, 400 MHz): 9.96 (s, 2H), 9.65 (s, br., 2H), 7.84 (d, J = 8.4 Hz, 4H), 7.71 (s, 2H), 7.62 (d, J = 8.4 Hz, 4H), 7.55 (m, 4H), 7.38 – 7.44 (m, 6H), 7.23 (d, J = 16.4 Hz, 2H), 7.08 (d, J = 16.4 Hz, 2H), 2.91 (m, 2H), 1.57 (m, 8H), 1.04 – 1.40 (m, 36H), 0.75 – 0.89 (m, 24H). ESI-HRMS: m/z Calc. for

$[C_{76}H_{98}N_2Pt+Na]^+$: 1312.7174; Found: 1312.7166. Anal. Calc. for $C_{78}H_{98}N_2O_2Pt \cdot 2H_2O$: C, 70.40; H, 8.03; N, 2.11; Found: C, 70.29; H, 8.22; N, 2.48.

2-3. Red powder, 57 mg, yield: 41%. ^{1}H NMR (CDCl$_3$, 400 MHz): 9.68 (d, J = 4.8 Hz, 2H), 7.69 (s, 2H), 7.52 (d, J = 8.0 Hz, 4H), 7.42 − 7.45 (m, 4H), 7.33 − 7.40 (m, 10H), 7.05 (d, J = 16.4 Hz, 2H), 6.96 (d, J = 16.4 Hz, 2H), 2.90 (m, 2H), 1.56 (m, 8H), 1.04 − 1.39 (m, 36H), 0.75 − 0.89 (m, 24H). ESI-HRMS: m/z Calc. for $[C_{76}H_{96}N_2Br_2Pt+Na]^+$: 1415.5478; Found: 1415.5461. Anal.Calc. for $C_{76}H_{96}Br_2N_2Pt$: C, 65.55; H, 6.95; N, 2.01; Found: C, 65.59; H, 7.17; N, 2.34.

2-4. Yellow powder, 26 mg, yield: 21%. ^{1}H NMR (CDCl$_3$, 400 MHz): 9.71 (d, J = 5.6 Hz, 2H), 7.69 (s, 2H), 7.48 − 7.54 (m, 8H), 7.31 − 7.42 (m, 10H), 7.19 − 7.24 (m, 2H), 7.09 (d, J = 16.4 Hz, 2H), 7.04 (d, J = 16.4 Hz, 2H), 2.91 (m, 2H), 1.53 − 1.58 (m, 8H), 1.05 − 1.38 (m, 36H), 0.75 − 0.90 (m, 24H). ESI-HRMS: m/z Calc. for $[C_{76}H_{98}N_2Pt+Na]^+$: 1256.7276; Found: 1256.7227. Anal. Calc. for $C_{76}H_{98}N_2Pt \cdot 0.5C_6H_{14}$: C, 74.26; H, 8.28; N, 2.19; Found: C, 74.53; H, 8.40; N, 2.37.

2-5. Yellow powder, 78 mg, yield: 60%. ^{1}H NMR (CDCl$_3$, 400 MHz): 9.71 (d, J = 5.6 Hz, 2H), 7.68 (s, 2H), 7.51 (d, J = 8.0 Hz, 4H), 7.40 − 7.43 (m, 4H), 7.36 − 7.38 (m, 6H), 7.01 (d, J = 16.4 Hz, 2H), 6.93 (d, J = 16.4 Hz, 2H), 6.86 − 6.88 (m, 4H), 3.81 (s, 6H), 2.90 (m, 2H), 1.50 − 1.73 (m, 8H), 1.04 − 1.36 (m, 36H), 0.70 − 0.99 (m, 24H). ESI-HRMS: m/z Calc. for $[C_{78}H_{102}N_2O_2Pt+Na]^+$: 1316.7487; Found: 1316.7515. Anal. Calc. for $C_{78}H_{102}N_2O_2Pt$: C, 72.36; H, 7.94; N, 2.16; Found: C, 71.87; H, 8.25; N, 2.29.

2-6. Red powder, 71 mg, yield: 45%. ^{1}H NMR (CDCl$_3$, 400 MHz): 9.69 (s, br., 2H), 7.69 (s, 2H), 7.51 (d, J = 8.4 Hz, 4H), 7.35 − 7.38 (m, 10H), 7.20 − 7.26 (m, 8H), 7.07 − 7.10 (m, 8H), 6.99 − 7.04 (m, 10H), 6.95 (d, J = 16.4 Hz, 2H), 2.91 (m, 2H), 1.57 (m, 8H), 1.05 − 1.41 (m, 36H), 0.75 − 0.90 (m, 24H). Anal. Calc. for $C_{100}H_{116}N_4Pt \cdot 0.5CH_2Cl_2$: C, 74.90; H, 7.32; N, 3.48; Found: C, 75.20; H, 7.72; N, 3.74.

2.2.2. DFT Calculations

The ground- and excited-state properties of complexes **2-1** – **2-6** were studied using DFT and linear response TD-DFT. All calculations – ground state geometry optimization, electronic structure, excited states and optical spectra – were performed using Gaussian09 quantum chemistry software package.[32] Geometries of all molecules were optimized for the ground state (closed-shell singlet S_0). For calculations of emission spectra, the geometry was optimized in the lowest-energy excited singlet (S_1) and triplet (T_1) states. All procedures were done utilizing the hybrid CAM-B3LYP functional.[33] The LANL08 basis set was used for the heavier Pt atom, while the remaining atoms were modeled with the 6-31G* basis set. The chosen method represents one of the currently most accurate DFT functionals and basis sets that have already shown good agreement with experimental data for different organometallic complexes.[34–36] All calculations have been performed in solvent using CPCM reaction field model,[37, 38] as implemented in Gaussian09. Dichloromethane (CH_2Cl_2, $\varepsilon_r = 9.08$) was chosen as a solvent for consistency with the experimental studies. As was found for several organometallic complexes, inclusion of the solvent into calculations is very important to reproduce experimental optical spectra.[39–41]

The excited states have been studied using linear response TD-DFT formalism,[42] in which the adiabatic approximation for the exchange-correlation kernel is used. For the absorption spectra of the complexes, 40 lowest singlet optical transitions were considered to reach the transition energies of ~ 4.9 eV. Each spectral line obtained from the TDDFT calculation was broadened by a Gaussian function with the line width of 0.1 eV to match the experimentally observed homogeneous broadening. The fluorescence energies were determined by calculating vertical transition energies for the optimized lowest singlet excited state (S_1) geometries (both excited state geometry optimization and vertical transitions have been performed with the TD-DFT). The phosphorescence energies were calculated by first

optimizing the lowest triplet state geometry followed by the vertical triplet excitations calculated via TD-DFT.

In order to analyze the nature of the singlet and triplet excited states, natural transition orbital (NTO) analysis was performed based on the calculated transition densities.[43] This method offers the most compact representation of the transition density between the ground and excited states in terms of an expansion into single-particle transitions (hole and electron for each given excited state). Here we refer to the unoccupied NTO as the "electron" transition orbital, and the occupied NTO as the "hole" transition orbital. Note that electron and hole NTOs are not the same as unoccupied and occupied molecular orbitals (MOs) in their ground state. Upon photoexcitation, the excitonic couplings (Coulomb interaction between the photoexcited electron-hole pair) mix the ground state MOs, so that the representation of an excitation via the pair of ground state MOs is not valid. In contrast, electron and hole NTOs obtained from TD-DFT calculations allow for representation of the excited state electronic density. NTOs shown in this paper were produced with the isovalue of 0.02 and visualized with the GaussView 5.1 graphical software.[44]

2.2.3. Photophysical Measurements

The solvents used for photophysical experiments are spectroscopic grade, which are purchased from VWR International and used as is without further purification. An Agilent 8453 spectrophotometer was used to record the UV-vis absorption spectra in different solvents. A SPEX fluorolog-3 fluorometer/phosphorometer was used to record the steady-state emission spectra in different solvents. The emission quantum yields were determined by the relative actinometry method[45] in degassed solutions, in which a degassed 1 N sulfuric acid solution of quinine bisulfate ($\Phi_{em} = 0.546$, $\lambda_{ex} = 347.5$ nm)[46] was used as the reference.

The laser system for the fs transient absorption measurement was described previously.[47] Briefly, the 800 nm laser pulses were produced at a 1 kHz repetition rate (fwhm

= 110 fs) by a mode-locked Ti:sapphire laser (Hurricane, Spectra-Physics). The output from the Hurricane was split into pump (85%) and probe (10%) beams. The pump beam (800 nm) was sent into an optical paramagnetic amplifier (OPA-400, Spectra Physics) to obtain 310, 330, and 350 nm excitation sources (E < 1 μJ/pulse), and to a second harmonic generator (Super Tripler, CSK) to obtain 400 nm beam (E ~ 2 μJ/pulse). The probe beam was focused into a rotating CaF_2 crystal or a sapphire crystal for white light continuum generation between 350 and 750 nm or between 400 and 800 nm. The flow cell (Starna Cell Inc. 45-Q-2, 0.9 ml volume with 2 mm pathlength), pumped by a Fluid Metering RHSY Lab pump (Scientific Support Inc.), was used to prevent photodegradation of the sample. After passing through the cell, the continuum was coupled into an optical fiber and input into a CCD spectrograph (Ocean Optics, S2000). The data acquisition was achieved using in-house LabVIEW (National Instruments) software routines. The group velocity dispersion of the probing pulse was determined using nonresonant optical Kerr effect (OKE) measurements.[48] Sample solutions were prepared at a concentration needed to have absorbance of A~0.6-0.8 at the excitation wavelength.

The nanosecond transient absorption (TA) spectra and decays were measured in degassed solutions on an Edinburgh LP920 laser flash photolysis spectrometer. The third harmonic output (355 nm) of a Nd:YAG laser (Quantel Brilliant, pulsewidth 4.1 ns, repetition rate was set at 1 Hz) wasused as the excitation source. Each sample was purged with argon for 30 min before each measurement. The triplet excited-state absorption coefficient (ε_T) at the TA band maximum was determined by the singlet depletion method.[49] quation 2.1 was used to calculate the ε_T.[49]

$$\varepsilon_T = \varepsilon_S \frac{\Delta OD_T}{\Delta OD_S} \tag{2.1}$$

In equation 2.1, ΔOD_S is minimum of the bleaching band and ΔOD_T is the maximum of the absorption band in the TA spectrum, and ε_S is the ground-state molar extinction

58

coefficient at the wavelength of the bleaching band minimum. After the ε_T value is obtained, the $\boldsymbol{\Phi}_T$ could be obtained by the relative actinometry, in which SiNc in benzene was used as the reference ($\varepsilon_{590} = 70000$ M^{-1} cm^{-1}, $\boldsymbol{\Phi}_T = 0.20$).[50]

2.2.4. Nonlinear Transmission

The reverse saturable absorption of complexes **2-1 − 2-6** was characterized by nonlinear transmission experiment at 532 nm using a Quantel Brilliant laser. The pulse width of the laser is 4.1 ns and the repetition rate is set at 10 Hz. The complexes were dissolved in CH$_2$Cl$_2$. The concentration of the sample solutions was adjusted to obtain a linear transmission of 80% at 532 nm in a 2-mm-thick cuvette. The experimental setup and details are similar to that reported previously.[51] A 40-cm plano-convex lens was used to focus the beam to the center of the 2-mm thick sample cuvette.

2.3. Results and Discussion

2.3.1. Molecular Geometries.

The optimized geometries of complexes **2-1 − 2-6** are reported in Table 2.1. Optimization of the ground singlet state of the complexes **2-1 − 2-6** with DFT resulted in their essentially planar geometry. The stilbenyl components of the stilbenylacetylide ligands are twisted relative to the Pt coordination plane by ~ 1 degree, while substituent groups stay in the stilbenyl plane (except for NPh$_2$-group, which is twisted in the propeller-like shape). Pt-N bonds are on average of 2.087 Å, and are not affected by the stilbenylacetylide substituent group. Pt-C bond lengths are ~1.940 Å, and are very slightly affected by the substituent groups (in the fourth decimal digit).

Table 2.1. Optimized molecular structures of complexes **2-1** – **2-6** via DFT calculation.

2-1	**2-2**
2-3	**2-4**
2-5	**2-6**
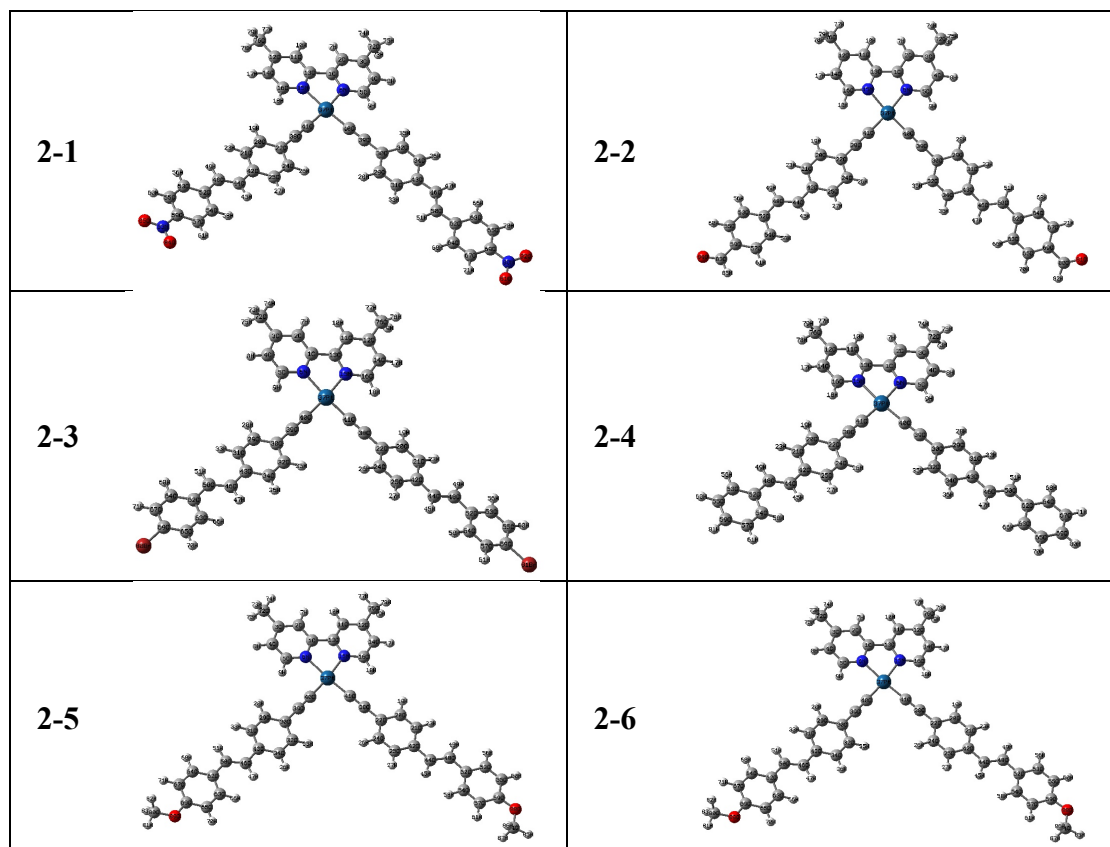
2.3.2. Electronic Absorption

The UV-Vis spectra of complexes **2-1** – **2-6** are shown in Figure 2.1. The absorption of all complexes obeys Beer's law in the concentration range of our study (1×10^{-6} to 1×10^{-4} mol/L), suggesting that no ground-state aggregation occurs in this concentration range. The major absorption bands of complexes **2-1** – **2-6** resemble those of their ligands, which are exemplified in Figures 2.1a for complexes **2-1** – **2-6** and Figure 2.1b for **2-1**, **2-4**, **2-5**, and **2-6**, indicating that these bands arise from the stilbenylacetylide ligand-centered transitions. This assignment is supported by the molar extinction coefficients of these bands, which at least doubles those of their corresponding ligands. The red-shift of these bands suggests delocalization induced by the *d*π orbital of platinum.
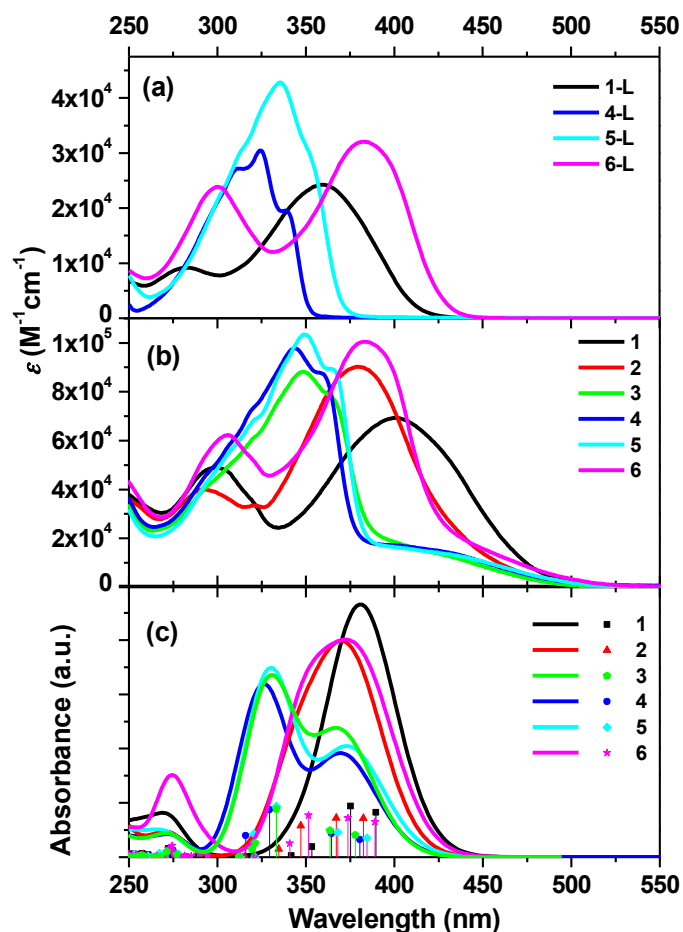
Figure 2.1. (a) UV-vis absorption of ligands **2-1-L**, **2-4-L**, **2-5-L** and **2-6-L** measured in CH_2Cl_2; (b) UV-vis absorption spectra of complexes **2-1** – **2-6** measured in CH_2Cl_2; (c) Calculated absorption spectra for complexes **2-1** – **2-6**, vertical lines resemble excited states and the corresponding oscillator strength.

The absorption of complexes **2-3**, **2-4**, and **2-5** in the region of 300 nm and 375 nm features well resolved vibronic structure, which is indicative of the $^1\pi,\pi^*$ transitions localized on the stilbenylacetylide ligands. However, at the wavelengths above 380 nm, a broad shoulder that is absent in the ligands absorption spectra is observed. Compared to the major absorption bands centered at ca. 340 – 350 nm, this shoulder exhibits significant negative solvatochromic effect (as illustrated in Figure 2.2a), which is consistent with the other Pt(II) diimine complexes reported in the literature[7-10] and implies a charge transfer nature of this absorption band. In contrast, the absorption spectra of **2-1**, **2-2**, and **2-6** are broad and red-shifted relative to the major absorption bands of **2-3**, **2-4**, and **2-5**. The vibronic structures are not clearly observed for **2-1**, **2-2** and **2-6**. Absorption of complexes **2-1** and **2-6** is also found

to exhibit a negative solvatochromic effect, as illustrated in Figure 2.2c for **2-1**. All of these features lead to the attribution of the absorption of **2-1**, **2-2** and **2-6** partially to charge transfer processes, probably mixing ligand-to-ligand charge transfer (LLCT) and metal-to-ligand charge transfer (MLCT) from $d\pi$ (platinum) to π^* (diimine). However, considering the large molar extinction coefficients of **2-1**, **2-2** and **2-6**, the lowest-energy absorption band in these three complexes should have dominant contribution from the acetylide ligand π,π^* transition.
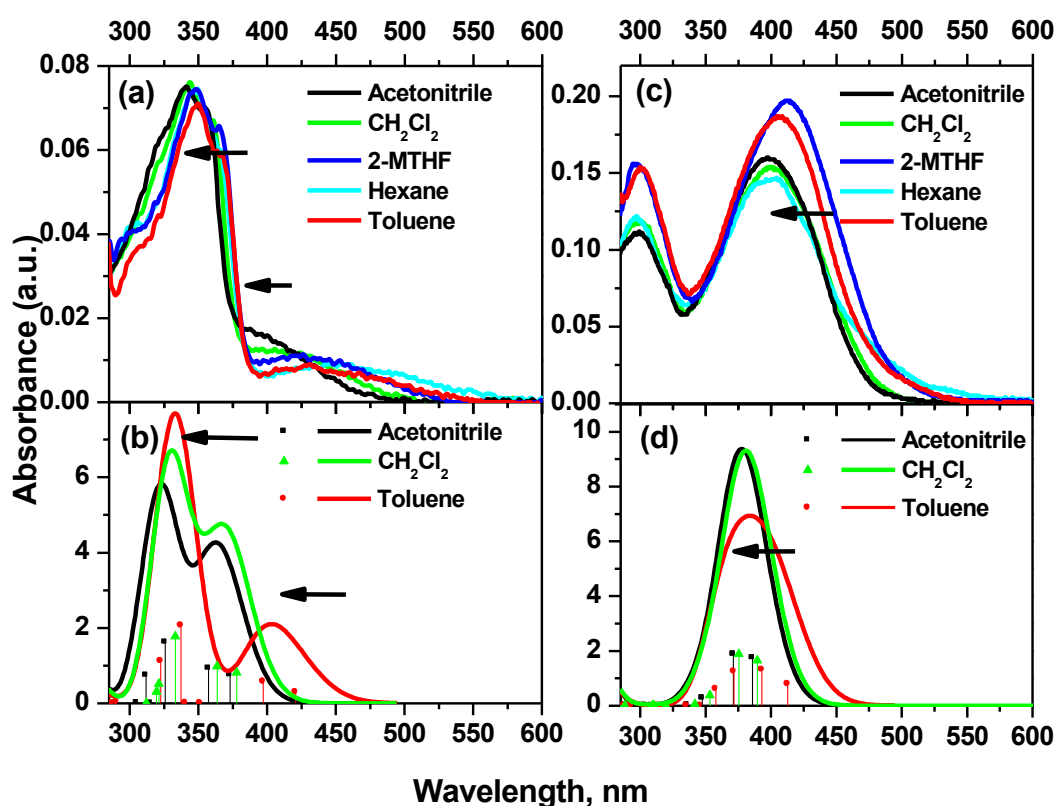
Figure 2.2. Left: experimental (a) and calculated (b) absorption spectra of complex **2-4** in different solvents; Right: experimental (c) and calculated (d) absorption spectra of **2-1** in different solvents. Arrows indicate the blue-shift of the absorption bands with increasing solvent polarity.

In general, the major absorption band(s) of all substituted stilbenylacetylide complexes are red-shifted relative to that of complex **2-4**, and similar pattern is observed in the ligands' absorption. This result agrees with the previous studies on the push-pull conjugated oligomers[52, 53] and suggests that electronic structures of the Pt-complexes

discussed in this work can be effectively tuned by varying the substituents at the 4'-position of the stilbenylacetylide ligands, which consequently influences the photophysical properties.

These trends, as well as the overall spectral assignment are supported by the linear response TD-DFT calculations. Calculated absorption spectra (Figure 2.1c) show a substantial agreement with the experimental data, as can be seen in Figures 2.1 and 2.2. Although theoretically predicted absorption energies (Figure 2.1c) are blue-shifted compared to experimental ones, they clearly reproduce the experimental trends of absorption spectra and are found to be highly dependent on solvent polarity (Figure 2.2b). Experimental and theoretical absorption properties are summarized and compared in Table 2.2. Unlike **2-1**, **2-2** and **2-6**, complexes **2-3**, **2-4** and **2-5**, which are substituted with weak electron-donor/acceptor groups, exhibit a lower-intensity shoulder in the spectral region above 380 nm. As resolved by the DFT studies, the shoulder involves two excitations with the mixed MLCT and LLCT characters, while higher energy peak has dominant ligand π,π^* character.

Table 2.2. Experimental and calculated electronic absorption parameters for complexes **2-1** – **2-6** and ligands **2-1-L**, **2-4-L**, **2-5-L**, and **2-6-L** in CH_2Cl_2.

	λ_{abs}/nm (ε_{max}/M^{-1}cm^{-1})[a]	$^{Theor}\lambda_{abs}$/nm (ex. State; f_{osc})[b]
2-1	401 (69330), 298 (48900)	389 (S1; 1.6529), 375 (S2; 1.8782), 353 (S3; 0.3870)
2-2	380 (90250), 292 (40080)	383 (S1; 1.4325), 367 (S2; 1.4423), 347 (S3; 1.1505)
2-3	420 (14580), 363 (78730), 349 (88280), 333 (74500)	378 (S1; 0.8110), 364 (S2, 0.9787), 333 (S3; 1.7741)
2-4	410 (16480), 360 (87300), 344 (97850), 325 (77380)	381 (S1; 0.6476), 364 (S2; 0.8692), 329 (S3; 1.7507)
2-5	415 (14980), 365 (89250), 349 (103480), 335 (87230)	384 (S1; 0.7001), 368 (S2; 0.9100), 333 (S3; 1.8807)
2-6	385 (100480), 305 (62130)	389 (S1; 1.3019), 374 (S2; 1.4375), 352 (S3; 1.5416)
2-1-L	360 (24260), 283 (9190)	
2-4-L	340 (19470), 325 (30500), 311 (26980)	
2-5-L	354 (28960, sh.), 336 (42850), 314 (30940, sh.)	
2-6-L	384 (32130), 300 (24020)	

[a]λ_{abs} is absorption wavelength, ε_{max} is molar extinction coefficient. [b] $^{Theor}\lambda_{abs}$ is calculated wavelength corresponding to the transition between the ground and excited state of interest (number of excited state is shown in parentheses), f_{osc} is calculated oscillator strength for the corresponding excitations.

The excited state character of the studied complexes can be easily seen from the natural transition orbital, NTO plots, shown in Table 2.3 and in Supporting Information. Thus, the lowest energy transitions of complexes **2-3**, **2-4** and **2-5** involve a transfer of the Pt *d*-electrons from the top of the valence band (see the diagram in Figure 2.3) and the stilbenylacetylide ligand to the bipyridine (bpy) moiety. The MLCT/LLCT characters of these transitions explain their relatively small oscillator strengths (intensities of peaks in absorption spectra). Due to unequal interaction of the ligand field with the participating Pt *d*-orbitals of different symmetry, these excited states are noticeably separated (by ~ 0.5 eV) from higher-energy states, which explain the appearance of the well-separated, low-intensity shoulder in the absorption spectra of these compounds. Second absorption band of compounds **2-3**, **2-4** and **2-5** can mainly be described as the π,π^* intraligand transition within the stilbenylacetylide ligands with an admixture of the MLCT/LLCT character (see NTOs for the 3rd excited state, S3, in Table 2.3). This band is more sensitive to the type of the substituent and red-shifted in case of the stronger electron donor or acceptor attached to the stilbenyl moiety.

Table 2.3. Natural transition orbitals (NTOs)[a] representing transitions that correspond to the first and the second lower energy "bands" for complexes **2-1**, **2-4**, and **2-6**. Excited state number, corresponding oscillator strengths and excitation energies are shown.

Excited state number and properties	Hole	Electron
S1 f_{osc} = 1.6529 3.19 eV (389 nm)		
1		
S3 f_{osc} = 0.3870 3.51 eV (353 nm)		

Table 2.3. Natural transition orbitals (NTOs)[a] representing transitions that correspond to the first and the second lower energy "bands" for complexes **2-1**, **2-4**, and **2-6**. Excited state number, corresponding oscillator strengths and excitation energies are shown (continued).

Excited state number and properties	Hole	Electron
4		
S1 f_{osc} = 0.6476 3.26 eV (381 nm)		
S3| f_{osc} = 1.7507 3.77 eV (329 nm)		
6		
S1 f_{osc} = 1.3019 3.19 eV (389 nm)		
S3 f_{osc} = 1.5416 3.53 eV (352 nm)		

[a] Note that excited state NTOs differ from the ground state MOs, and rather can be considered as the linear combination of the ground state MOs that contribute to a given excited state.

In contrast, the lowest-energy absorption band of complexes **2-1**, **2-2** and **2-6**, is predicted to have strong contribution of the π,π^* intraligand transition with some mixture of the MLCT and LLCT characters (see Table 2.3). Significant ligand π,π^* character of these transitions gives rise to the intensity of the lowest-energy absorption band of these complexes, as can be seen in Fig 2.1c. NTOs in Table 2.3 for complexes **2-1** and **2-6** illustrate the delocalized nature of the lowest-energy excited states that contribute to the absorption band, which results in larger oscillator strengths for these transitions. The higher-lying

excitations can rather be characterized as the LLCT transitions from the stilbenylacetylides to the bpy moiety mixed with MLCT character, which explains their lower intensity.
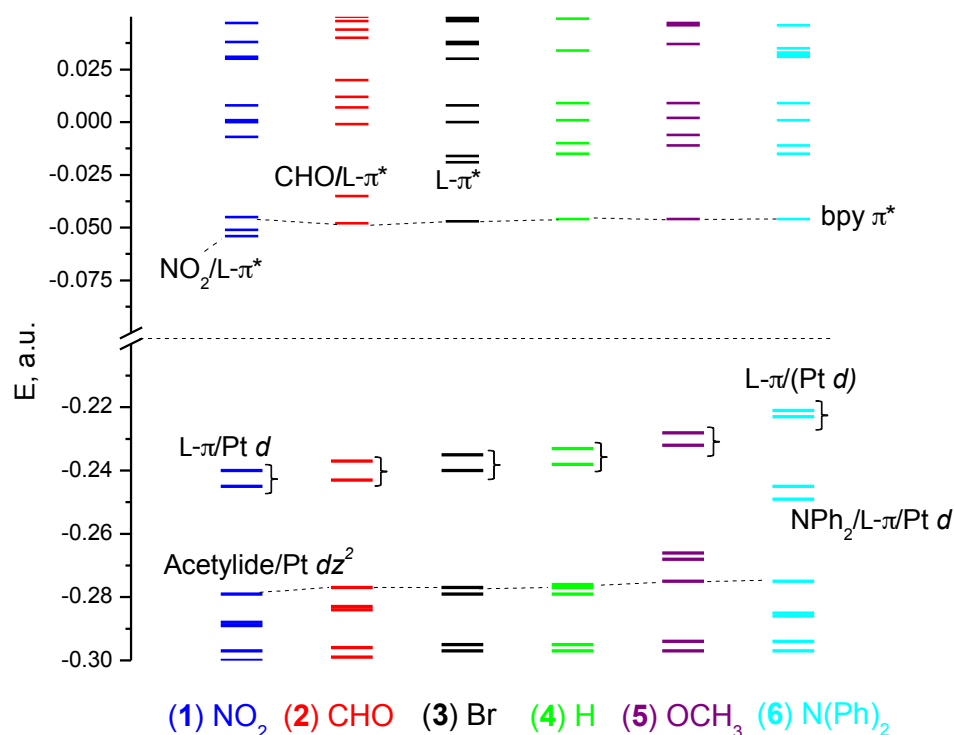
Figure 2.3. Ground state molecular orbital energy diagram for complexes **2-1 – 2-6** calculated with DFT (CAM-B3LYP//LANL08/6-31G*) in dichloromethane.

In general, shape of the absorption spectra of the discussed Pt-complexes with the stilbenylacetylide ligands depends on the interplay between the states with charge transfer character (LLCT and MLCT) and the intraligand π,π^* transitions. Thus the complexes with the weak donor/acceptor substituents (**2-3**, **2-4**, **2-5**) exhibit an MLCT/LLCT shoulder in the lower energy region of spectra. In the cases when the stilbenylacetylides are substituted with a stronger electron-donor/acceptor substituent (**2-1**, **2-2** and **2-6**), the lower energy MLCT/LLCT states strongly mix with the intraligand π,π^* transitions that cause larger transition dipole moments and stronger absorption intensity. The ground state MO diagram shown in Figure 2.3 provides a better understanding of the effect of substituent on energy

levels and absorption spectra of the Pt-complexes discussed herein. The highest occupied orbitals are delocalized over the stilbenylacetylide ligands (L-π) and have noticeable Pt-d contribution, while the lowest unoccupied orbitals are predominantly delocalized over the bipyridine ligand (bpy π^*) except for complex **2-1**. Addition of the electron-donating groups, such as OCH_3 (**2-5**) and NPh_2 (**2-6**), increases the ground state dipole moment and raises the energies of the HOMOs. For complex **2-6,** HOMO and HOMO-1 can be characterized as the pure ligand π (L- π) orbitals with very little Pt-d admixture. Addition of electron-withdrawing substituents, such as NO_2 (**2-1**) and CHO (**2-2**), lowers the energies of the unoccupied levels, which lie very closely to or even below (as in complex **2-1)** the bpy-π^* level. Therefore, addition of stronger electron-donor or stronger electron-acceptor groups leads to a smaller HOMO-LUMO gap (red-shift in absorption spectra) and change in the character of the lowest-energy absorption bands.

Addition of polar solvents compensates the static and the transition dipole moments induced by the strong electron donating/accepting groups, and stabilizes the donor/acceptor electronic levels. This is equivalent to shifting HOMOs to lower energies, while LUMO localized on the stilbenyl moves to the higher energy, resulting in blue shifts (larger gap between levels) of the absorption bands with increase in the solvent polarity, as shown in Figure 2.2. The blue-shift of the absorption bands with solvent polarity is observed both for the complexes with the weak electron-donor/acceptor groups (**2-3**, **2-4** and **2-5**) and with strong electron-donor/acceptor groups (**2-1**, **2-2** and **2-6**), while the overall shape of the absorption spectra is negligibly affected by solvent polarity.

2.3.3. Photoluminescence

All of the complexes exhibit weak emission both at room temperature in dichloromethane solution and at 77 K in butyronitrile glassy matrix. The emission spectra of complexes **2-1** – **2-6** at room temperature are shown in Figure 2.4, and the emission data are

summarized in Table 2.4. The emission band(s) of **2-2** – **2-5** at room temperature are mirror images to those of their respective major absorption band(s) with Stokes shifts smaller than 80 nm; while the emission of **2-1** and **2-6** at room temperature is broad and structureless, with a Stokes shift of 129 nm and 107 nm, respectively. The emission lifetimes of these complexes could not be detected by our spectrometer due to the very short lifetime (< 5 ns). These features suggest that the observed emission for complexes **2-1** – **2-6** at room temperature emanates from the singlet excited state of the stilbenylacetylide ligand. At 77 K, the emission of **2-1** – **2-6** appears at 625 - 667 nm (Figure 2.4c), which is assigned to the phosphorescence of the complexes. However, due to the very weak signal, the phosphorescence lifetimes have not been determined.
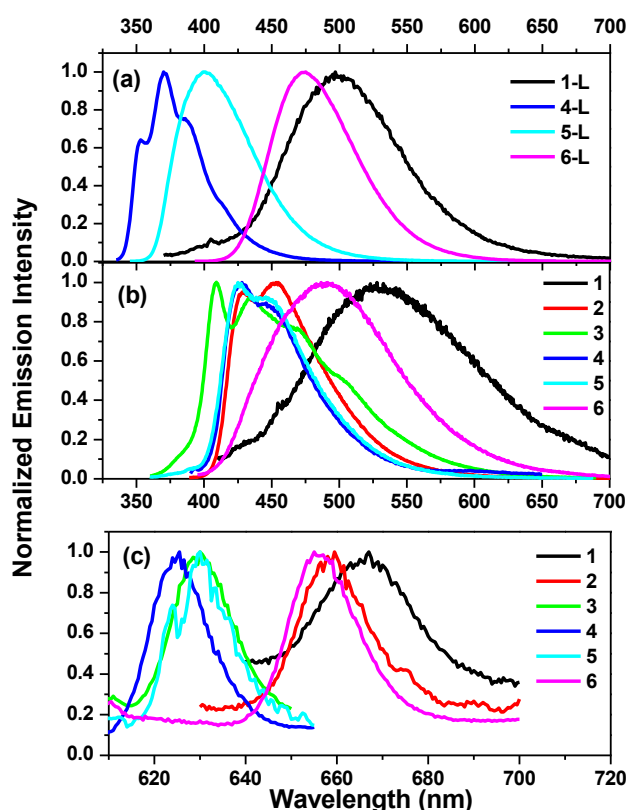
Figure 2.4. Normalized emission spectra of (a) ligands **2-1-L**, **2-4-L**, **2-5-L**, and **2-6-L** and (b) complexes **2-1** – **2-6** in dichloromethane at room temperature; (c) complexes **2-1** – **2-6** in butyronitrile glassy matrix at 77 K (phosphorescence).

In previous studies[17] of compound **2-4**, singlet $^1\pi,\pi^*$ state has been proposed to relax predominantly through the intersystem crossing into triplet $^3\pi,\pi^*$ state, which explains the observed relatively weak fluorescence. The triplet ^{3}MLCT emission has also been observed in a similar series of complexes, but shown to undergo a quick nonradiative decay through the relaxation of the stilbene ligand(s) into *cis*-conformation.[17] The energy levels of the $^3\pi,\pi^*$ states relative to the ^{3}MLCT states have been shown to strongly depend on the type of substituent on the 4,4'-position of the bpy ligand, because of a strong influence of the substituent on the ^{3}MLCT energies.[54–56] Similar to previous studies, we found a strong effect on relative positioning between the $^3\pi,\pi^*$ and ^{3}MLCT states that is caused by the strength of the electron-donor/accepter substituent on the stilbene.

Table 2.4. Photoluminescence and excited-state absorption parameters for complexes **2-1** – **2-6** and ligands **2-1-L**, **2-4-L**, **2-5-L** and **2-6-L**.

	λ_{em}/nm $(\Phi_{em})^a$ R. T.	λ_{em}/nm[b] 77 K	$\lambda_{T_1-T_n}$/nm (τ_T/ns; $\varepsilon_{T_1-T_n}$/M^{-1} cm^{-1}; Φ_T)^c	$\lambda_{S_1-S_n}$/nm (τ_S/ps)^d	$^{theor}\lambda_{fluo}$ /nm	$^{theor}\lambda_{phos}$ /nm
1	530 (0.012)	667	480 (385; 67825; -), 750 (401; 98760; 0.17)	495 (59), 580 (58)	497	663
2	454 (0.008)	659	510 (225; 184760; 0.079)	532 (77), 626 (74)	472	-
3	409 (0.017)	630	435 (48; -; -)	465 (14)	449	638
4	425 (-)	625	460 (64; -; -)	460 (69)	452	638
5	428 (0.009)	630	460 (73; -; -)	468 (205)	460	-
6	492 (0.003)	656	520 (198; 235510; 0.075)	526 (18)	463	668
1-L	499 (0.007)	-	435 (-), 602 (-)	467 (91), 562 (121)	-	-
4-L	370 (0.10)	-	505 (-)	606 (43)	-	-
5-L	401 (0.03)	-	510 (-)	550 (22)	-	-
6-L	474 (0.58)	-	470 (-)	444 (95), 602 (59)	-	-

^{a}In CH_2Cl_2. ^{b}In BuCN glassy matrix. ^{c}Triplet excited-state absorption band maximum ($\lambda_{T_1-T_n}$), molar extinction coefficient ($\varepsilon_{T_1-T_n}$), quantum yield (Φ_T) and lifetime (τ_T) measured in CH_3CN/CH_2Cl_2 solution (v/v = 10:1). ^{d}Singlet excited-state absorption band maximum ($\lambda_{S_1-S_n}$) and lifetime (τ_S) measured in CH_3CN/CH_2Cl_2 solution.

To elucidate the nature of emission of complexes **2-1** – **2-6**, their spectra are compared to the emission of the corresponding ligands, **2-1-L**, **2-4-L**, **2-5-L** and **2-6-L** (Figure 2.4a). The emission of **2-4-L** can be assigned to $^1\pi,\pi^*$ transition by comparing to the *trans*-stilbene emission reported in the literature.[57] The $^1\pi,\pi^*$ character of the singlet emission in this ligand is also well presented in the NTOs, as shown in Table 2.5. Compound **5-L** emits at a similar level as **4-L,** while the **1-L** and **6-L** spectra are significantly red-shifted due to a presence of strong electron accepting/donating groups. NTOs for the relaxed singlet excited state geometries, corresponding to the fluorescence, show that strong electron donating substituent NPh$_2$ delocalizes the hole NTO (HOTO) over both the stilbene and the substituent group, while showing more localized character of the electron NTO (LUTO) on the stilbene with insignificant electron density on the substituent group (see the bottom panel in Table 2.5). The strong electron withdrawing NO$_2$ group has an opposite effect, with the more delocalized character of the electron NTO than the hole. Such a difference in delocalization between the electron and hole NTOs explains the red shift in fluorescence of ligands **2-1-L** and **2-6-L**, compared to other ligands.

Table 2.5. NTO plots for the optimized singlet (S$_1$) and triplet (T$_1$) transitions (corresponding to the fluorescence and phosphorescence, respectively) for complexes **2-1**, **2-4**, **2-6** and their corresponding ligands, **2-1-L**, **2-1-L**, and **2-6-L**.

	S$_1$		T$_1$	
	HOTO	LUTO	HOTO	LUTO
2-1				
2-4				
2-6				
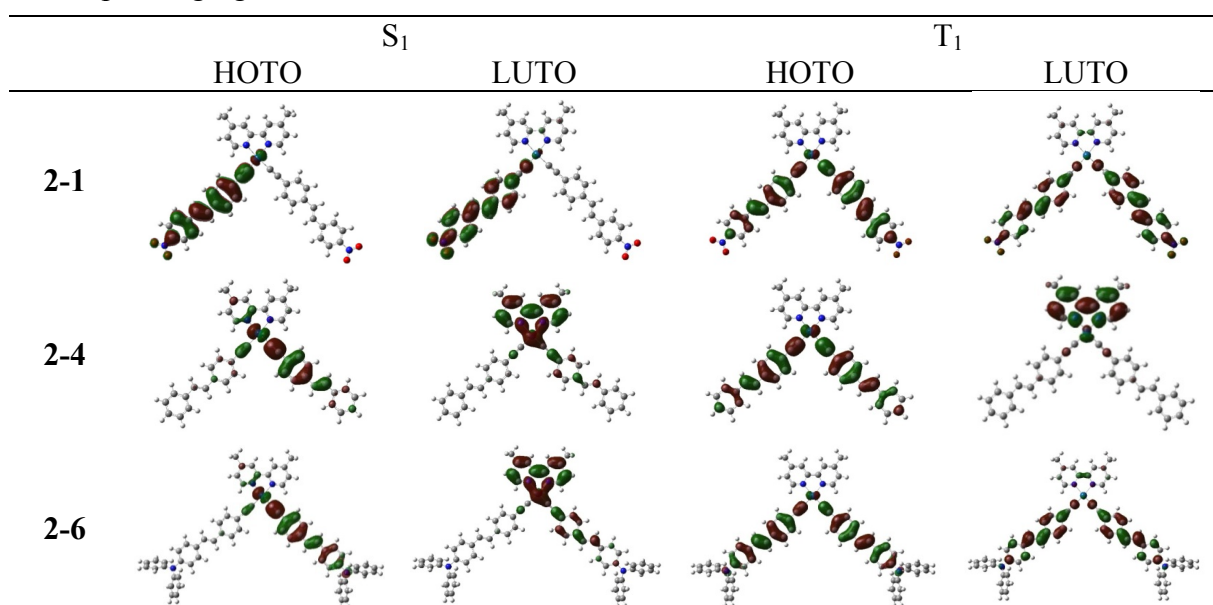
Table 2.5. NTO plots for the optimized singlet (S_1) and triplet (T_1) transitions (corresponding to the fluorescence and phosphorescence, respectively) for complexes **2-1**, **2-4**, **2-6** and their corresponding ligands, **2-1-L**, **2-1-L**, and **2-6-L** (continued).

	S_1		T_1	
	HOTO	LUTO	HOTO	LUTO
2-1-L				
2-4-L				
2-6-L				

The emission spectra of complexes **2-1** and **2-6** very closely represent emission of their ligands, slightly shifted to the red, which is indicative of the predominant intraligand character of the photoluminescence in this range (see Figure 2.4). However, the width of the spectra significantly increases as a result of some interactions with Pt d-orbitals, as well as strong electron-vibrational couplings. The other complexes emit at substantially lower energy compared to their corresponding ligands, which suggests a strong delocalization induced by platinum $d\pi$ orbitals, and significant contribution from ^{1}MLCT/^{1}LLCT as being discussed in the following paragraph.

Overall, TD-DFT calculations of the singlet and triplet emission repeat the trends observed experimentally, as summarized in Table 2.4. NTOs for the relaxed singlet and triplet excited state geometries (corresponding to fluorescence and phosphorescence, respectively) are illustrated in Table 2.4 and compared with the NTOs contributing to the singlet emission of the corresponding stilbenylacetylide ligands. The singlet emission of complex **2-1** stems from the intraligand ${}^1\pi,\pi^*$ transition in one of the single stilbenylacetylide ligands, which become slightly twisted relative to the Pt coordination plane and, thus, hinders the ^{1}MLCT character of fluorescence in this compound. Interestingly, the character of the NTOs contributing to singlet emission of this compound have a very different nature,

71

compared to NTOs contributing the lowest energy absorption (compare NTOs in Table 2.4 with S_1 in Table 2.3 for **2-1**). Such a significant difference in NTOs is a sign of a strong exciton-vibration coupling, which is evident by a broadening of the fluorescence peak of complex **2-1** compared to those of **2-1-L** shown in Figure 2.4. In all other complexes NTOs contributing to fluorescence are strongly mixed with the ^{1}MLCT from Pt to bpy moiety, as well as LLCT between the stilbene and bpy. Strong charge transfer character of the NTOs involved in the singlet emission explains the experimentally observed red-shift in the emission maxima of these complexes versus the fluorescence energies of their ligands.

Triplet state emission for compounds **2-1** and **2-6** involves a symmetric $^3\pi,\pi^*$ transition in both stilbenylacetylide ligands (Table 2.5, right panel); while phosphorescence of complexes with the weaker donor/acceptor substituents predominantly carries the ^{3}LLCT/^{3}MLCT character. The red-shift of the photoluminescence spectra observed for complexes with the stronger electron accepting/donating groups (**2-1** and **2-6**) can be explained by the interplay between the $^3\pi,\pi^*$ electronic levels of the stilbenylacetylide ligands and the ^{3}MLCT/^{3}LLCT states, similar to the picture discussed in the absorption section. Strong electron donating/accepting groups lower the energies of the stilbene $^3\pi,\pi^*$ transitions relative to those of the ^{3}MLCT/^{3}LLCT states, so that the lowest excited states bear more of the $^3\pi,\pi^*$ character. This process is highly sensitive to the solvent polarity, as polar solvent can partially stabilize the dipole moment induced by the substituent group and raise the intraligand transition energies. In other words, in a less polar solvent, $^3\pi,\pi^*$ transitions have more admixture of ^{3}MLCT/^{3}LLCT character.

Combining all the evidences discussed above, the emission parentage of the complexes are assigned as follows: the emission of complexes **2-1** and **2-6** is dominated by the ligand centered π,π^* transition localized on the stilbenylacetylide ligands, but complex **2-6** has some admixture of the ^{1}MLCT/^{1}LLCT characters in its fluorescence. The emission of

complexes **2-2**, **2-3**, **2-4**, and **2-5** can be characterized by the mixture of major MLCT/LLCT and little intraligand π,π^* transitions. The short-lived and weak fluorescence of the complexes at room temperature can be accounted for by existence of the twisted geometry of the ligands, which may serve as a nonradiative decay pathway of the excited state.[22] Overall, variation of substituent at the 4'-position of the stilbenylacetylide ligands has a significant influence on the emission energy and electronic state of the complexes.

2.3.4. Transient Absorption

The nanosecond and femtosecond transient absorption measurements (TA) for complexes **2-1** − **2-6** and ligands **2-1-L**, **2-4-L**, **2-5-L** and **2-6-L** were carried out. From the TA experiment, we can obtain the spectral features and lifetimes of the singlet and triplet excited states. The spectral region where the excited-state absorption is stronger than the ground-state absorption can be identified from the positive absorption band(s) of the TA spectrum; while the excited-state lifetime can be deduced from the decay of the TA and the triplet excited-state quantum yield is determined by the relative actinometry.

The nanosecond TA spectra of complexes **2-1** − **2-6** and ligands **2-1-L**, **2-4-L**, **2-5-L** and **2-6-L** in CH_3CN/CH_2Cl_2 (v/v = 10/1) solution at zero delay after excitation are shown in Figure 2.5. All of the complexes exhibit strong TA signals that are well time resolved (illustrated by the time-resolved spectra of **2-1** − **2-6** in Figure 2.6). The TA of the complexes are significantly enhanced compared to those of their corresponding ligands, indicating enhanced intersystem crossing (ISC) induced by the heavy-atom effect of Pt. Complexes **2-1** and **2-2** that bear strong electron-withdrawing substituents show especially broad and strong transient absorptions; while the shape of the TA spectra of the other complexes resemble those of their corresponding ligands. For all complexes, a bleaching band was observed at $\lambda <$ 450 nm, which is consistent with the position of the major absorption band in their UV-Vis absorption spectra. The triplet lifetime deduced from the decay of the TA and the molar

extinction coefficient of the triplet excited-state absorption determined from the singlet depletion method[49] for **2-1**, **2-2** are **2-6** and listed in Table 2.4. Similar to those trends observed from the UV-Vis absorption and emission spectra, the bleaching band and TA absorption band are red-shifted for complexes **2-1**, **2-2** and **2-6** in comparison to those of **2-3**, **2-4** and **2-5**. The triplet excited-state lifetimes of **2-1**, **2-2** and **2-6** are also significantly longer than those of **2-3**, **2-4** and **2-5**, which indicate different natures of the excited state that gives rise to the transient absorption. For complex **2-4**, the feature of the TA spectrum and the lifetime are quite similar to those reported by Schanze and co-workers for a similar Pt(II) bipyridyl bis(ethynylstilbene) complex, in which the transient is believed to be a stilbene-localized $^3\pi,\pi^*$ state with the double bond in the *trans* geometry.[22] The short lifetime should be attributed to the rapid nonradiative decay induced by the C=C bond rotation in the stilbene moiety. The similar TA pattern for **2-3** and **2-5** to those of their respective ligands and to **2-4** implies that the excited state that gives rise to the TA is the stilbene-localized $^3\pi,\pi^*$ state as well.
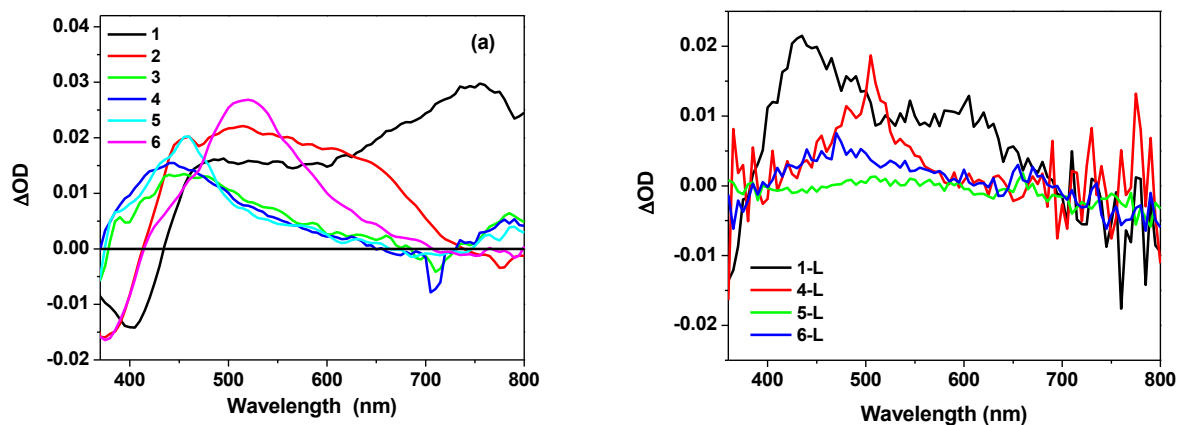
Figure 2.5. Nanosecond transient difference absorption spectra of complexes **2-1 – 2-6** (left) and **2-1-L**, **2-4-L**, **2-5-L**, and **2-6-L** (right) at zero time decay in CH_3CN /CH_2Cl_2 (v/v = 10/1) immediately after 4.1 ns laser excitation.

For complexes **2-1** and **2-2**, the TA spectra are much broader and a strong new absorption band appears at 750 nm for **2-1**. With reference to the TA study reported by Castellano and co-workers for Pt terpyridyl acetylide complexes bearing π-conjugated

arylacetylides,[58] the near-IR TA band of **2-1** could possibly originate from the acetylide cation generated from the LLCT/ILCT (intraligand charge transfer from the stilbene to the nitro group) processes. Therefore, the excited state that gives rise to the observed TA for **2-1** is tentatively assigned to the stilbene localized $^3\pi,\pi^*$ state, mixed with LLCT/ILCT characters. We believe the TA for **2-2** has similar origin.
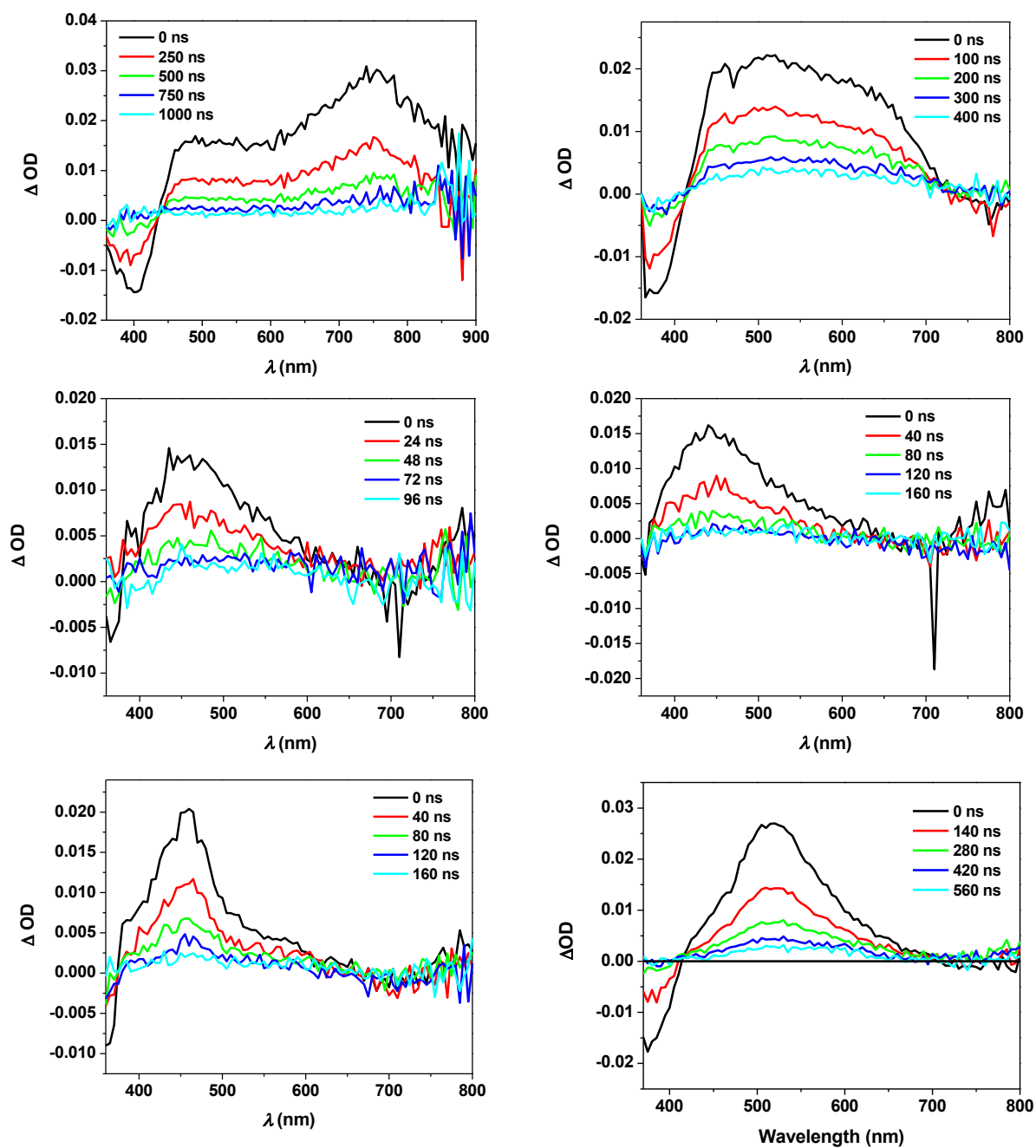
Figure 2.6. Time-resolved ns transient absorption spectra of complex **2-1** – **2-6** in CH$_3$CN/CH$_2$Cl$_2$ (v/v = 10/1). λ_{ex} = 355 nm. $A_{355\ nm}$ = 0.4 in a 1-cm cuvette.

75

The femtosecond time-resolved TA spectra of **2-1 – 2-6** in a mixed CH_3CN/CH_2Cl_2 solution are shown in Figure 2.7. The TA spectra of **2-2 – 2-5** resemble those of their ns TA spectra, thus are assigned to the same transients as those contributing to the ns TA, which could be from the singlet excited state or the triplet excited state in case the intersystem crossing is very fast.
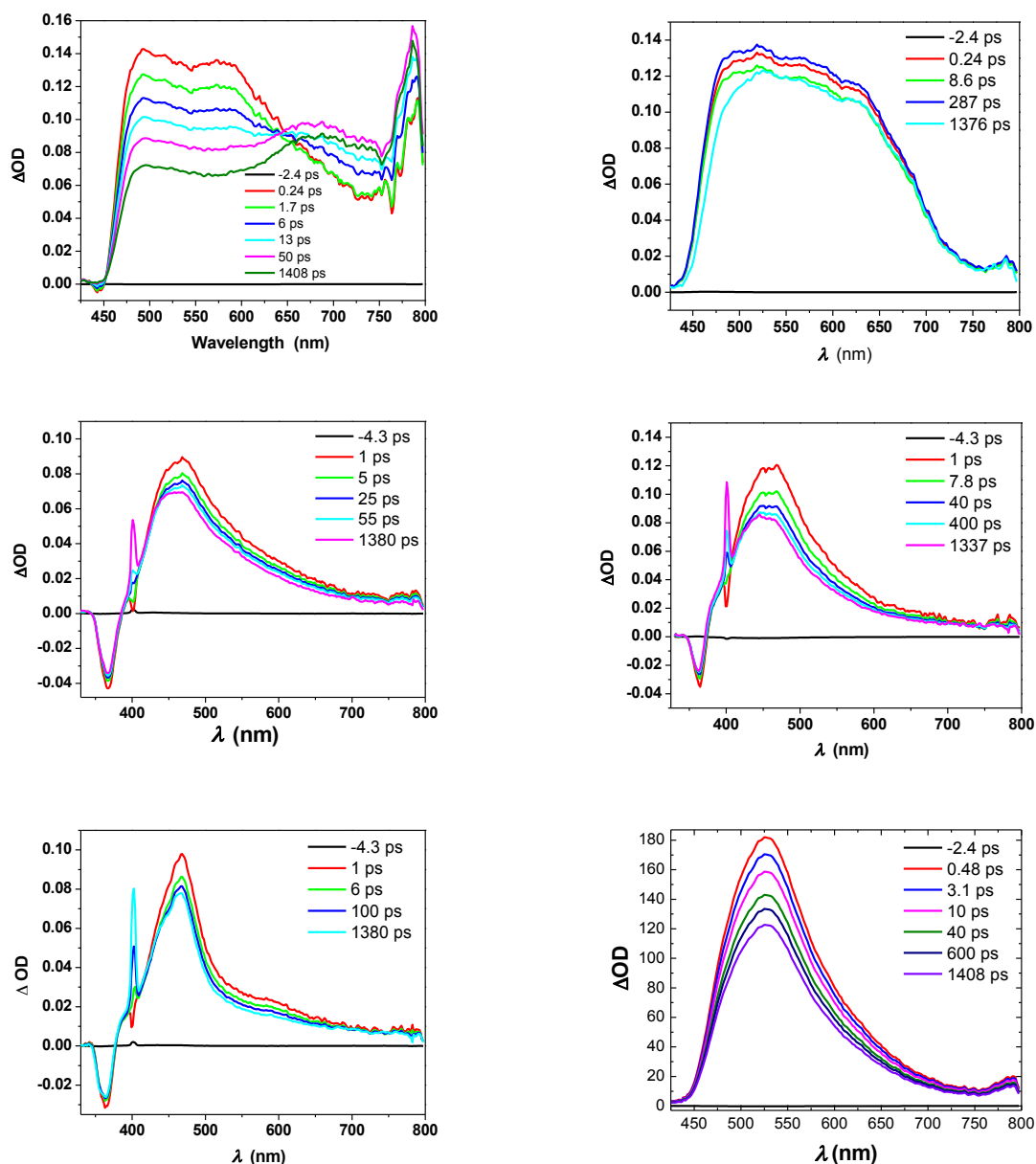
Figure 2.7. Femtosecond time-resolved transient difference absorption spectrum of complex **2-1 – 2-6** in CH_3CN/CH_2Cl_2 (v/v = 10/1). λ_{ex} = 400 nm.

However, the femtosecond TA spectrum of complex **2-1** exhibits a different time-resolved pattern. As shown in Figure 2.7, at 0.24 ps delay after laser excitation, two broad

bands at 493 nm and 577 nm and a narrow band at 785 nm appear, which are similar to those observed in its nitrostilbenylethyne ligand (Figure 2.8). The intensities of the 493 and 577 nm bands are gradually reduced while the 785 nm band increases and a new broad band at 683 nm emerges. An isosbestic point is observed at 647 nm. At 50-ps delay, the intensities of the bands at 683 nm and 785 nm reach the maxima, and the full spectrum resembles that of the ns TA. These characteristics suggest the intersystem crossing from the singlet to the triplet excited state completed within 50 ps. At longer delay time, the TA spectrum slowly decays, reflecting the longer lifetime of the triplet excited state. The singlet TA band maxima and the lifetime of the singlet excited state deduced from the decay of the fs TA for **2-1** – **2-6** are listed in Table 2.4.
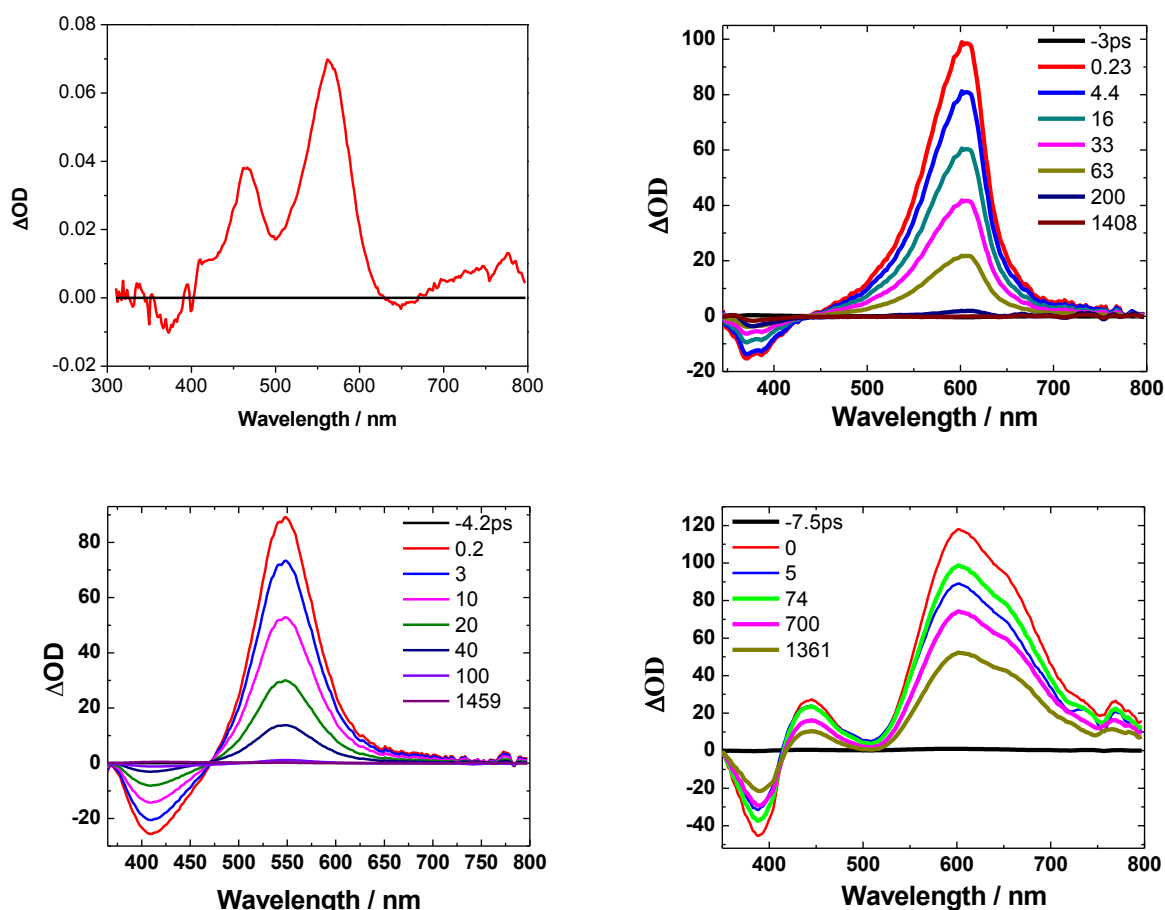
Figure 2.8. Femtosecond transient absorption spectrum of ligand **2-1-L**, **2-4-L**, **2-5-L** and **2-6-L** in CH_3CN/CH_2Cl_2 (v/v = 9/1) at zero delay after 400 nm laser excitation.

77

2.3.5. Reverse Saturable Absorption

As discussed above, both the ns and fs TA spectra of **2-1** – **2-6** exhibit positive absorption at 532 nm, indicating a stronger excited-state absorption than that of the ground state. In addition, the triplet excited-state lifetime is longer than the ns laser pulse width (4.1 ns). Therefore, it is expected that reverse saturable absorption (RSA), defined as a decreased transmission upon increase of incident fluence, would occur for ns laser pulse at 532 nm. To demonstrate this, nonlinear transmission experiment using complexes **2-1** – **2-6** at 532 nm for ns laser pulses was carried out in dichloromethane solution at a linear transmittance of 80% in a 2-mm cuvette. The results are shown in Figure 8. The transmission of the complexes drastically decreases with increased incident fluence, clearly demonstrating a strong RSA. The degree of RSA of the complexes increases in the order of **2-1** < **2-3** < **2-5** < **2-4** < **2-2** < **2-6**. The degree of RSA for **6** is even stronger than the 2,2'-bipyridine Pt(II) complex bearing 2-(benzothiazol-2'-yl)-9,9-diethyl-7-ethynylfluorene complex reported by our group earlier.[13] The stronger RSA of **2-2** and **2-6** can be accounted for by their much stronger excited-state absorption (both singlet and triplet) at 532 nm relative to other complexes, which is clearly evident from the ns and fs TA spectra.
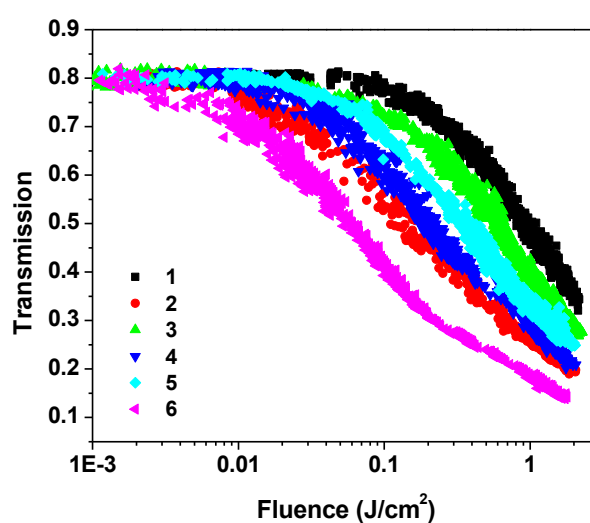
Figure 2.9. Nonlinear transmission curves of **2-1** – **2-6** in CH$_2$Cl$_2$ solution for 4.1 ns laser pulses at 532 nm. The pathlength of the cuvette is 2 mm, and the linear transmission of the solution is adjusted to 80% at 532 nm in the 2-mm cuvette.

2.4. Conclusion

A series of platinum bipyridyl platinum(II) bisstilbenylacetylide complexes with different auxiliary substituents on the stilbenylacetylide ligands were synthesized, and the photophysics of these complexes were systematically characterized by spectroscopic measurements and TD-DFT theoretical calculations. The absorption and emission characteristics of these complexes can be substantially adjusted by the auxiliary ligands. While the substitution of H on the 4'-position of stilbene by Br and OMe groups does not alter the photophysical properties of the complexes eminently, the absorption and the emission characteristics are significantly tuned by the CHO, NO_2 and NPh_2 substituents. The lowest-energy absorption band of **2-3**, **2-4**, and **2-5** are dominated by the MLCT/LLCT transitions with admixture of the π,π^* character, while the lowest absorption bands for complexes **2-1, 2-2** and **2-6** are dominated by the ligand-centered π,π^* transition with the admixture of MLCT/LLCT characters (in a strong dependence on solvent polarity). Emission processes very similar trends. The ns and fs transient difference absorption of the complexes feature strong absorption in the visible spectral region, which can be attributed to stilbene-localized π,π^* state with the double bond in the trans geometry. The TA spectra of complexes **2-1** and **2-2** that bear strong electron-withdrawing substituents are very broad and extend to the near-IR region, suggesting contribution from the acetylide ligand cation that results from the LLCT/ILCT transitions. All complexes exhibit strong reverse saturable absorption for ns laser pulse at 532 nm, with complex **2-6** showing the strongest RSA due to the very strong excited-state absorption relative to that of the ground state at 532 nm. This makes complex **2-6** a very promising candidate for devices that require strong RSA.

2.5. References

[1] Lu, W.; Mi, B.-X.; Chan, C.-W.; Hui, Z.; Che, C.-M.; Zhu, N.; Lee, S.-T. *J. Am. Chem. Soc.* **2004**, *126*, 4958.

[2] He, Z.; Wong, W.-Y.; Yu, X.; Kwok, H.-S.; Lin, Z. *Inorg. Chem.* **2006**, *45*, 10922.

[3] Du, P.; Eisenberg, R. *Chem. Sci.* **2010**, *1*, 502.

[4] Wu, W.; Xu, X.; Yang, H.; Hua, J.; Zhang, X.; Zhang, L.; Long, Y.; Tian, H. *J. Mater. Chem.* **2011**, *21*, 10666.

[5] Keck, M. V.; Lippard, S. J. *J .Am. Chem. Soc.* **1992**, *114*, 3386.

[6] Lottnera, C.; Knuechelb, R.; Bernhardtc, G.; Brunner, H. *Cancer Lett.* **2004**, *203*, 171.

[7] Chan, C.-W.; Cheng, L.-K.; Che, C.-M. *Coord. Chem. Rev.* **1994**, *132*, 87.

[8] Miskowski, V. M.; Houlding, V. H.; Che, C.-M.; Wang, Y. *Inorg. Chem.* **1993**, *32*, 2518.

[9] Hissler, M.; Connick, W. B.; Geiger, D. K.; McGarrah, J. E.; Lipa, D.; Lachicotte, R. J.; Eisenberg, R. *Inorg. Chem.* **2000**, *39,* 447.

[10] Whittle, C. E.; Weinstein, J. A.; George, M. W.; Schanze, K. *Inorg. Chem.* **2001**, *40,* 4053.

[11] Castellano, F. N.; Pomestchenko, I. E.; Shikhova, E.; Hua, F.; Muro, M. L.; Rajapakse, N. *Coord. Chem. Rev.* **2006**, *250*, 1819.

[12] Pomestchenko, I. E.; Luman, C. R.; Hissler, M.; Ziessel, R.; Castellano, F. N. *Inorg. Chem.* **2003**, *42*, 1394.

[13] Sun, W.; Zhang, B.; Li, Y.; Pritchett, T. M.; Li, Z.; Haley, J. E. *Chem. Mater.* **2010**, *122*, 6384.

[14] Chan, S.-C.; Chan, M. C. W.; Wang, Y.; Che, C.-M.; Cheung, K.-K.; Zhu, N. *Chem. Eur. J.* **2001**, *7*, 4180.

[15] Hissler, M.; McGarrah, J. E.; Connick, W. B.; Geiger, D. K.; Cummings, S. D.; Eisenberg, R. *Coord. Chem Rev.* **2000**, *208*, 115.

[16] McGarrah, J. E.; Kim, Y.-J.; Hissler, M.; Eisenberg, R. *Inorg. Chem.* **2001**, *40*, 4510.

[17] Lu, W.; Chan, M. C. W.; Zhu, N.; Che, C.-M.; He, Z.; Wong, K. Y. *Chem. Eur. J.* **2003**, *9*, 6155.

[18] He, G. S.; Tan, L.-S.; Zheng, Q.; Prasad, P. N. *Chem. Rev.* **2008**, *108*, 1245.

[19] Svetlichnyi, V. A.; Meshalkin, Y. P.; *Opt. Commun.* **2007**, *280,* 379.

[20] Huang, Z.; Wang, X.; Li, B.; Lv, C.; Xu, J.; Jiang, W.; Tao, X.; Qian, S.; Chui, Y.; Yang, P. *Opt. Mater.* **2007**, *29,* 1084.

[21] Zhou, X.; Ren, A.-M.; Feng, J.-K.; Liu, X.-J. *Chem. Phy. Lett.* **2002**, *362,* 541.

[22] Haskins-Glusac, K.; Ghiviriga, I.; Abboud, K. A.; Schanze, K. *J. Phys. Chem. B* **2004**, *108,* 4969.

[23] Domínguez-Gutiérrez, D.; De Paoli, G.; Guerrero-Martínez, A.; Ginocchietti, G.; Ebeling, D.; Eiser, E.; De Cola, L.; Elsevier, C. J. *J. Mater. Chem.* **2008**, *18,* 2762.

[24] Heck, R. F.; Nolley, J. P. *J. Org. Chem.* **1972**, *37,* 2320.

[25] Reinhard, W. H. *Angew. Chem. Int. Ed.* **2001**, *40,* 1411.

[26] Hassan, J.; Sévignon, M.; Gozzi, C.; Schulz, E.; Lemaire, M. *Chem. Rev.* **2002**, *102,* 1359.

[27] Sonogashira, K.; Tohda, Y.; Hagihara, N. *Tetrahedron Lett.* **1975**, *16,* 4467.

[28] Hockless, D. C. R.; Whittall, I. R.; Humphrey, M. G. *Acta. Cryst. C* **1996**, *52,* 3222.

[29] Rodrí, J. G.; Lafuente, G. A.; Arranz, J. *J. Polym. Sci., Part A: Polym. Chem.* **2005**, *43,* 6438.

[30] Zhao, H.; Yuan, W. Z.; Tang, L.; Sun, J. Z.; Xu, H.; Qin, A.; Mao, Y.; Jin, J. K.; Tang, B. Z. *Macromolecules*, **2008**, *41,* 8566.

[31] Rigamonti, L.; Babgi, B.; Cifuentes, M. P.; Roberts, R. L.; Petrie, S.; Stranger, R.; Righetto, S.; Teshome, A.; Asselberghs, I.; Clays, K.; Humphrey, M. G. *Inorg. Chem.* **2009**, *48,* 3562.

[32] Gaussian 09, Revision A.1, Frisch, M. J.; Trucks, G. W.; Schlegel, H. B.; Scuseria, G. E.; Robb, M. A.; Cheeseman, J. R.; Scalmani, G.; Barone, V.; Mennucci, B.; Petersson, G. A.; Nakatsuji, H.; Caricato, M.; Li, X.; Hratchian, H. P.; Izmaylov, A. F.; Bloino, J.; Zheng, G.; Sonnenberg, J. L.; Hada, M.; Ehara, M.; Toyota, K.; Fukuda, R.; Hasegawa, J.; Ishida, M.; Nakajima, T.; Honda, Y.; Kitao, O.; Nakai, H.; Vreven, T.; Montgomery, Jr., J. A.; Peralta, J.

E.; Ogliaro, F.; Bearpark, M.; Heyd, J. J.; Brothers, E.; Kudin, K. N.; Staroverov, V. N.; Kobayashi, R.; Normand, J.; Raghavachari, K.; Rendell, A.; Burant, J. C.; Iyengar, S. S.; Tomasi, J.; Cossi, M.; Rega, N.; Millam, N. J.; Klene, M.; Knox, J. E.; Cross, J. B.; Bakken, V.; Adamo, C.; Jaramillo, J.; Gomperts, R.; Stratmann, R. E.; Yazyev, O.; Austin, A. J.; Cammi, R.; Pomelli, C.; Ochterski, J. W.; Martin, R. L.; Morokuma, K.; Zakrzewski, V. G.; Voth, G. A.; Salvador, P.; Dannenberg, J. J.; Dapprich, S.; Daniels, A. D.; Farkas, Ö.; Foresman, J. B.; Ortiz, J. V.; Cioslowski, J.; Fox, D. J. Gaussian, Inc., Wallingford CT, **2009**.

[33] Yanai, T.; Tew, D.; Handy, N. *Chem. Phys. Lett.* **2004**, *393*, 51.

[34] Roy, L. E.; Scalmani, G.; Kobayashi, R.; Batista, E. R. *Dalton Trans.* **2009**, *38*, 6719.

[35] Peach, M. J. G.; Benfield, P.; Helgaker, T.; Tozer, D. J. *J. Chem. Phys.* **2008**, *128,* 044118.

[36] Jr. Vlček, A.; Záliš, S. *Coord. Chem. Rev.* **2007**, *251*, 258.

[37] Barone, V.; Cossi, M.; Tomasi, J. *J. Comput. Chem.* **1998**, *19*, 404.

[38] Cossi, M.; Rega, N.; Scalmani, G.; Barone, V. *J. Comput. Chem.* **2003**, *24*, 669.

[39] Batista, E. R.; Martin, R. L. *J. Phys. Chem. A* **2005**, *109*, 3128.

[40] Fantacci, S.; De Angelis, F.; Selloni, A. *J. Am. Chem. Soc.* **2003**, *125*, 4381.

[41] Filippo, D. A.; Simona, F.; Annabella, S. *Chem. Phys. Lett.* **2004**, *389*, 204.

[42] Furche, F.; Ahlrichs, R. *J. Chem. Phys.* **2002**, *117,* 7433.

[43] Martin, R. L. *J. Chem. Phys.* **2003**, *118*, 4775.

[44] GaussView Version 4.1, Dennington-II, R.; Keith, T.; Millam, J.; Semichem Inc., Shawnee Mission, KS, **2007**.

[45] Demas, J. N.; Crosby, G. A. *J. Phys. Chem.* **1971**, *75*, 991.

[46] Eaton, D. F. *Pure Appl. Chem.* **1988**, *60*, 1107.

[47] Li, G.; Glusac, K. D. *J. Phys. Chem. A* **2008**, *112*, 4573.

[48] Yamaguchi, S.; Hamaguchi, H. O. *Appl. Spectr.* **1995**, *49,* 1513.

[49] Carmichael, I.; Hug, G. L. *J. Phys. Chem. Ref. Data.* **1986**, *15*, 1.

[50] Firey, P. A.; Ford, W. E.; Sounik, J. R.; Kenney, M. E.; Rodgers, M. A. J. *J. Am. Chem. Soc.* **1988**, *110,* 7626.

[51] Guo, F.; Sun, W.; Liu, Y.; Schanze, K. S. *Inorg. Chem.* **2005**, *44*, 4055.

[52] Badaeva, E. A.; Timofeeva, T. V.; Masunov, A.; Tretiak, S. *J. Phys. Chem. A* **2005**, *109*, 7276.

[53] Meyers, F.; Bredas, J. L. *Synth. Metals* **1992**, *49*, 181.

[54] Hissler, M.; Connick, W. B.; Geiger, D. K.; McGarrah, J. E.; Lipa, D.; Lachicotte, R. J.; Eisenberg, R. *Inorg. Chem.* **2000**, *39*, 447.

[55] Wadas, T. J.; Lachicotte, R. J.; Eisenberg, R. *Inorg. Chem.* **2003**, *42*, 3772.

[56] Whittle, C. E.; Weinstein, J. A.; George, M. W.; Schanze, K. S. *Inorg. Chem.* **2001**, *40*, 4053.

[57] Waldeck, D. H. *Chem. Rev.* **1991**, *91*, 415.

[58] Wang, X.; Goeb, S.; Ji, Z.; Castellano, F. N. *J. Phys. Chem. B* **2010**, *114*, 14440.

CHAPTER 3. PLATINUM CHLORIDE COMPLEXES CONTAINING 6-[9,9-DI(2-ETHYLHEXYL)-7-R-9*H*-FLUOREN-2-YL]-2,2'-BPYRIDINE LIGAND (R = NO$_2$, CHO, BENZOLTHIAZOL-2-YL, *n*-Bu, CARBOZOL-9-YL, NPh$_2$)

3.1. Introduction

Platinum(II) complexes have been fascinating for decades due to their rich photophysics and potential applications in various photonic devices and in cancer treatment.[1] For instance, Lippard's group has extensively investigated the application of platinum complexes as anticancer reagents;[2] Che and co-workers employed platinum(II) diimine arylacetylide complexes and cyclometalated 6-aryl-2,2'-bipyridine arylacetylide platinum complexes in organic light emitting devices (OLEDs);[3, 4] Eisenberg,[5] Schanze,[6] and Yam[7] groups independently studied the application of platinum complexes in dye sensitized solar cells (DSSCs); our group and several other groups reported the utilization of platinum complexes as chemical sensors.[8 – 14] In recent years, our group and Schanze group have also extensively explored the application of various Pt(II) complexes as nonlinear transmission materials.[15 – 31]

Compared to bidentate ligands, terdentate ligands are more resistant to distortion towards D_{2d} conformations when coordinated with d^8 transition metals, and thus disfavor non-radiative processes.[32] Terpyridine ligands stand out for their preference to adopt planar geometries. Unfortunately, the binding angle of terpyridine is not ideal when forming square planar configuration,[33] which reduces the ligand field and thus facilitates the accessibility of deactivating metal-centered *d-d* state. In contrast, terdentate cyclometalating ligands with C^N^N framework, by incorporating an hydrocarbon aryl unit at the 6-position of 2,2'-bipyridine, have shown several merits over terpyridine ligands. Firstly, cyclometalation makes it possible to construct neutral inner coordination sphere. Secondly, the strong σ

donating ability of the ligating C⁻ atom and good π accepting capability of the bipyridine motif offer the metal center a strong ligand field, which increases the *d-d* excited state and consequently reduces the deactivation of the lowest-energy charge transfer excited state via the *d-d* excited state. Thirdly, the C^N^N type ligand would form less-distorted square-planar geometry with the d^8 transition metals, which reduces the radiationless decay as well. Fourthly, the stronger π-donating ability of the 6-aryl ring could also introduce some intraligand charge transfer character into the lowest excited states, resulting in long-lived triplet excited state.

In one of our previous studies, we found that incorporation of fluorenyl substituent to the 4-position of the center pyridine ring of the terpyridine ligand could efficiently increase the emission efficiency, prolong the triplet excited-state lifetime, and increase the ratio of the excited-state absorption cross section relative to the ground-state absorption cross section in Pt(II) complexes.[17] As a result, stronger reverse saturable absorption was obtained. Inspired by this investigation and by the merit of C^N^N ligand vs. terpyridine ligand, we recently designed a complex with the C^N^N framework that incorporates fluorene at the 6-position of the bipyridine.[34] The complex features large ratios of excited-state absorption cross section to ground-state absorption cross section in the visible spectral region, and strong two-photon absorption in the near-IR region. Both of them account for the strong nonlinear transmission of the complex. These results are quite exciting, however, the structure-property correlations in Pt(II) complexes with this type of C^N^N ligand have not been explored yet. In addition, in order to further improve the reverse saturable absorption of this type of Pt(II) complexes, it is critical to reduce the ground-state absorption of the complexes in the visible spectral region. This could be realized by replacing the 4-tolylacetylide co-ligand by chloride co-ligand, which would reduce the contribution of the ligand-to-ligand charge transfer (LLCT) to the lowest excited state and cause hyposochromic shift of the charge transfer absorption

band. Taking these factors into account, we designed and synthesized six new Pt(II) complexes (structures of the new complexes **3-1 – 3-6** are illustrated in Scheme 3.1) with different electron-donating or withdrawing substituents at the 7-position of the fluorene component. In order to increase the solubility of the Pt(II) complexes, branched alkyl chains (2-ethylhexyl) were introduced at the 9-positon of the fluorene. Here we report the synthesis, photophysics and reverse saturable absorption of these complexes. Insights into the nature of optical transitions have also been obtained from the time-dependent density functional theory (TD-DFT) calculations.

3.2. Experimental Section

3.2.1. Synthesis and Characterization

The synthetic routes for **3-1 – 3-6** are illustrated in Scheme 3.1. All of the reagents and solvents were purchased from Aldrich Chemical Co. or Alfa Aesar and used as is unless otherwise stated. Silica gel for column chromatography was purchased from Sorbent Technology (60 Å, 230 - 400 mesh, 500 - 600 m^2/g, pH: 6.5 - 7.5). The synthesis of precursors **Br-F8-I**,[35] **Br-F8-CHO**,[36] **CHO-F8-B**,[37] **Br-F8**,[38] **NO₂-F8-Br**,[39] **NO₂-F8-B**,[39] **BTZ-F8-Br**,[40] **CBZ-F8-B**,[41] **NPh₂-F8-B**,[18] **C₄H₉-F8**-B,[42] and **BPY-Br**[43] followed the literature procedures. **BTZ-F8-B** was obtained by reacting **BTZ-F8-Br** in THF solution at -78 °C with 1 equivalent of BuLi followed by addition of 1 equivalent of 2-isopropoxy-4,4,5,5-tetramethyl-1,3,2-dioxaborolane. All intermediates were characterized by ^{1}H NMR. The synthetic details and ^{1}H NMR data of these intermediates are provided in Supporting Information. The general procedures for the synthesis of ligands **3-1-L – 3-6-L** and for complexes **3-1 – 3-6** are provided below. Ligands **3-1-L – 3-6-L** and complexes **3-1 – 3-6** were all characterized by ^{1}H NMR, electrospray ionization high-resolution mass spectrometry (ESI-HRMS), and elemental analyses. ^{1}H NMR spectra were obtained on Varian Oxford-VNMR spectrometers (300 MHz, 400 MHZ, or 500 MHz). ESI-HRMS analyses were

performed on a Bruker BioTOF III mass spectrometer. Elemental analyses were conducted by NuMega Resonance Laboratories, Inc. in San Diego, California.
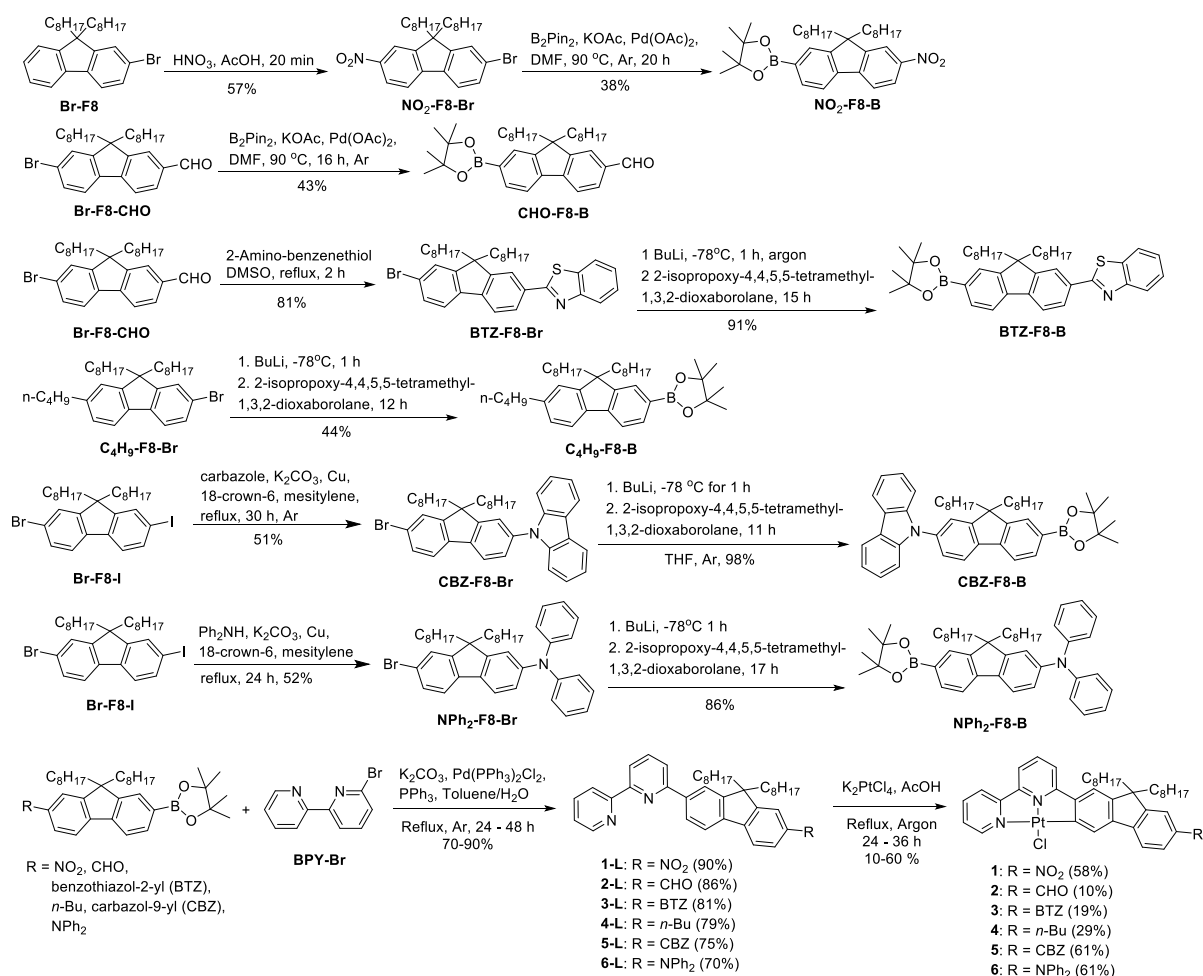
Scheme 3.1. Synthetic routes and structures for complexes **3-1 – 3-6** (C_8H_{17} = 2-ethylhexyl)

BTZ-F8-Br. The mixture of Br-F8-CHO (1.36 g, 2.7 mmol), 2-aminobenzenethiol (0.34 g, 2.7 mmol), and DMSO (6 mL) was heated to reflux for 2 hours. After the reaction mixture was cooled down to room temperature, 100 mL Et_2O was added and the mixture was washed with brine for four times. The organic layer was collected and dried with $MgSO_4$. After removal of solvent, the residue orange oil was purified by column chromatography (silica gel) eluted with mixed CH_2Cl_2/hexane (1:3 v/v). 1.34 g colorless oil was collected as the final product (yield: 81%). ^{1}H NMR ($CDCl_3$, 400 MHz): 8.04 – 8.12 (m, 3H), 7.88 – 7.91

(m, 1H), 7.74 – 7.76 (m, 1H), 7.59 (d, J = 8.0 Hz, 1H), 7.52 – 7.55 (m, 1H), 7.46 – 7.48 (m, 2H), 7.34 – 7.38 (m, 1H), 1.95 – 2.12 (m, 4H), 0.48 – 0.96 (m, 30H).

BTZ-F8-B. Compound BTZ-F8-Br (1.34 g, 2.2 mmol) was dissolved in THF (30 mL) and the solution was cooled down to -78 $^{\circ}$C under argon. BuLi (1.8 mL 2.5 M hexane solution, 4.5 mmol) was then added dropwise. The solution was stirred under argon at -78 $^{\circ}$C for 1 hour. 2-Isopropoxy-4,4,5,5-tetramethyl-1,3,2-dioxaborolane (0.67 mL (d = 0.912 g/mL), 3.3 mmol) was added dropwise and the mixture was allowed to warm up to room temperature and kept stirring for 15 hours. After reaction, the organic layer was washed with saturated NH_4Cl aqueous solution and brine, and dried with $MgSO_4$. Then the solvent was removed and the residue was purified by column chromatography (silica gel) eluted with hexane/ethyl acetate (10:1 v/v). 1.3 g light yellow oil was collected as the final product (yield: 91%). ^{1}H NMR (CDCl$_3$, 500 MHz): 8.09 – 8.15 (m, 3H), 7.88 – 7.93 (m, 2H), 7.83 – 7.85 (m, 2H), 7.76 (d, J = 7.5 Hz, 1H), 7.51 (t, J = 7.5 Hz, 1H), 7.39 (t, J = 7.5 Hz, 1H), 2.10 – 2.11 (m, 4H), 1.39 (s, 12H), 0.51 – 0.97 (m, 30H).

C$_4$H$_9$-F8-B. Compound n-Bu-F8-Br (1.24 g, 2.4 mmol) was dissolved in THF (10 mL) and the solution was cooled down to -78 $^{\circ}$C under argon. BuLi (1.0 mL 2.5 M hexane solution, 2.5 mmol) was then added dropwise. The solution was stirred under argon at -78 $^{\circ}$C for 1 hour. 2-Isopropoxy-4,4,5,5-tetramethyl-1,3,2-dioxaborolane (0.6 mL (d = 0.912 g/mL), 3.0 mmol) was added dropwise and the mixture was allowed to warm up to room temperature and kept stirring for 12 hours. After reaction, the organic layer was washed with saturated NH_4Cl aqueous solution and brine, and then dried with $MgSO_4$. Then the solvent was removed and the residue was purified by column chromatography (silica gel) eluted with hexane/CH_2Cl_2 (3:1 v/v). 0.6 g colorless was collected as the final product (yield: 44%). ^{1}H NMR (CDCl$_3$, 400 MHz): 7.78 (d, J = 6.8 Hz, 1H), 7.74 (d, J = 7.6 Hz, 1H), 7.61 (d, J = 7.6 Hz, 1H), 7.57 (d, J = 7.6 Hz, 1H), 7.15 (m, 1H), 7.09 (dd, J = 7.8, 1.4 Hz, 1H), 2.64 (t, J =

7.6 Hz, 2H), 1.88 – 2.02 (m, 4H), 1.54 – 1.63 (m, 2H), 1.34 (s, 12H), 1.29 – 1.38 (m, 2H), 0.41 – 0.94 (m, 33H).

CBZ-F8-Br. The mixture of I-F8-Br (1.70 g, 2.86 mmol), carbazole (0.50 g, 3.00 mmol), K_2CO_3 (0.83 g, 6.00 mmol), Cu-bronze (0.96 g, 1.50 mmol), and 18–crown–6 (0.16 g, 0.62 mmol), and mesitylene (30 mL) was heated to reflux under argon for 30 hours. After the reaction, 50 mL dichloromethane was added to the mixture and the solid was removed by filtration. The organic solution was washed with brine twice and dried with $MgSO_4$. After removal of the solvent, the residue was purified by column chromatography (silica gel) eluted with mixed CH_2Cl_2/hexane (1:3 v/v). 1.0 g colorless oil was collected as the final product (yield: 51%). ^{1}H NMR ($CDCl_3$, 400 MHz): 8.19 (d, J = 7.6 Hz, 2H), 7.89 (d, J = 8.0 Hz, 1H), 7.65 (dd, J = 8.0, 1.0 Hz, 1H), 7.50 – 7.60 (m, 4H), 7.30 – 7.45 (m, 6H), 1.93 – 2.10 (m, 4 H), 0.54 – 1.01 (m, 30 H).

CBZ-F8-B. To the stirred THF solution of Br-F8-CBZ (1.0 g, 1.5 mmol) under argon at -78 ^{o}C, BuLi (5.0 mL 2.5 M hexane solution, 12.5 mmol) was added dropwise. After kept stirring at -78 ^{o}C for 1 hour, 2-isopropoxy-4,4,5,5-tetramethyl-1,3,2-dioxaborolane (1.0 mL, 5.0mmol) was added. The system was allowed to warm up to room temperature and kept stirring for 11 hours. Saturated NH_4Cl aqueous solution (20 mL) was then added. The organic layer was collected and washed with brine and dried with $MgSO_4$. After the solvent was removed, the residue was purified using column chromatography (silica gel) eluted with mixed hexane/CH_2Cl_2 (4:1 v/v). 1.0 g colorless oil was collected as the final product (yield: 98%). ^{1}H NMR ($CDCl_3$, 400 MHz): 8.15 (d, J = 7.6 Hz, 2H), 7.92 (d, J = 8.0 Hz, 1H), 7.87 (d, J = 7.2 Hz, 1H), 7.84 (d, J = 7.6 Hz, 1H), 7.76 (d, J = 7.6 Hz, 1H), 7.52 – 7.54 (m, 1H), 7.46 – 7.50 (m, 1H), 7.26 – 7.40 (m, 6H), 1.90 – 2.12 (m, 4H), 1.37 (s, 12H), 0.50 – 0.96 (m, 30H).

CHO-F8-B. To the degassed DMF (20 mL) solution of Br-F8-CHO (1.0 g, 2.0 mmol) and bis(pinacolato)diboron (1.2 g, 4.7 mmol), KOAc (1.8 g, 18.0 mmol) and Pd(OAc)$_2$ (37 mg) were added and the mixture was degassed again. Then the mixture was heated to 90 ^{o}C for 16 hours. After the reaction, 100 mL ethyl acetate was added and solid was removed by filtration. The solution was washed with brine twice (30 mL × 2) and dried with MgSO$_4$. After removal of solvent, the residue was purified by column chromatography (silica gel) eluted with mixed CH$_2$Cl$_2$/hexane (2:1 v/v). 0.47 g colorless oil was collected as the final product (yield: 43%). ^{1}H NMR (CDCl$_3$, 400 MHz): 10.04 (s, 1H), 7.84 – 7.92 (m, 4H), 7.81 (d, J = 7.6 Hz, 1H), 7.75 (d, J = 7.6 Hz, 1H), 1.98 – 2.09 (m, 4H), 1.35 (s, 12H), 0.38 – 0.96 (m, 30H).

NO$_2$-F8-Br. Fuming nitric acid (10 mL) was added to the stirred AcOH (30 mL) solution of Br-F8 (2.36 g, 5.0 mmol) at 60 ^{o}C. The mixture was stirred at 60 ~ 70 ^{o}C for 20 minutes. After that, AcOH was removed by distillation. Purification was carried out by column chromatography (silica gel) eluted with hexane/CH$_2$Cl$_2$ (5:1 v/v). 1.46 g yellow oil was collected as the product (yield: 57%). ^{1}H NMR (CDCl$_3$, 400 MHz): 8.21 – 8.26 (m, 2H), 7.75 – 7.77 (m, 1H), 7.62 – 7.64 (m, 1H), 7.56 – 7.59 (m, 1H), 7.51 – 7.54 (m, 1H), 1.96 – 2.07 (m, 4H), 0.38 – 0.96 (m, 30H).

NO$_2$-F8-B. To the degassed DMF (20 mL) solution of Br-F8-NO$_2$ (1.45 g, 2.8 mmol) and bis(pinacolato)diboron (1.07 g, 4.2 mmol), KOAc (2.48 g, 25 mmol) and Pd(OAc)$_2$ (55 mg) were added and the mixture was degassed again and heated to 90 ^{o}C for 20 hours. After the reaction, 100 mL diethyl ether was added. The organic phase was collected, washed with brine twice, and dried over MgSO$_4$. The solvent was removed and the residue was purified by column chromatography (silica gel) eluted with mixedCH$_2$Cl$_2$/hexane (1:3 v/v). 0.60 g colorless oil was collected as the final product (yield: 38%). ^{1}H NMR (CDCl$_3$, 400 MHz):

8.24 – 8.25 (m, 2H), 7.75 – 7.90 (m, 4H), 1.99 – 2.09 (m, 4H), 1.36 (s, 12H), 0.36 – 0.85 (m, 30H).

NPh₂-F8-Br. The mixture of I-F8-Br (1.09 g, 1.8 mmol), Ph₂NH (0.34 g, 2.0 mmol), K₂CO₃ (0.9 g, 6.5 mmol), Cu-bronze (0.43 g), 18–crown–6 (0.26 g, 1.0 mmol), and mesitylene (30 mL) was heated to reflux under argon for 24 hours. After the reaction, 50 mL CH₂Cl₂was added to the mixture and the solid was removed by filtration. The organic solution was washed with brine twice, and dried with MgSO₄. The solvent was removed and the residue was purified by column chromatography (silica gel) eluted with mixed CH₂Cl₂/hexane (1:3 v/v). 0.6 g yellow oil was collected as the final product (yield: 52%). ^{1}H NMR (CDCl₃, 400 MHz): 7.52 – 7.55 (m, 1H), 7.40 – 7.48 (m, 2H), 7.21 – 7.29 (m, 4H), 6.98 – 7.12 (m, 9H), 1.76 – 1.94 (m, 4H), 0.47 – 1.07 (m, 30H).

NPh₂-F8-B. To the stirred THF solution of NPh₂-F8-Br (0.6 g, 0.94 mmol) under argon at -78 °C, BuLi (5.0 mL 2.5 M hexane solution, 12.5 mmol) was added dropwise. After stirring at -78 °C for 1 hour, 2-isopropoxy-4,4,5,5-tetramethyl-1,3,2-dioxaborolane (0.61 mL, 3.00 mmol) was added. The mixture was allowed to warm up to room temperature and kept stirring for 17 hours. After the reaction, the organic layer was washed with saturated NH₄Cl aqueous solution (20 mL) and brine, and then dried with MgSO₄. Then the solvent was removed and the residue was purified by column chromatography (silica gel) eluted with hexane/CH₂Cl₂ (4:1 v/v). 0.55 g yellow oil was collected as pure product (yield: 86%). ^{1}H NMR (CDCl₃, 400 MHz): 7.74 – 7.78 (m, 2H), 7.57 – 7.60 (m, 2H), 7.19 – 7.24 (m, 4H), 6.96 – 7.10 (m, 8H), 1.95 – 1.99 (m, 2H), 1.79 (m, 2H), 1.34 (s, 12H), 0.46 – 0.89 (m, 30H).

General Procedure for the Synthesis of Ligands 3-1-L – 3-6-L. The mixture of **R-F8-B** (1 mmol), 6-bromo-2,2'-bipyridine (235 mg, 1 mmol), K₂CO₃ (410 mg, 3 mmol), Pd(PPh₃)₂Cl₂ (30 mg), and PPh₃ (60 mg) in toluene (20 mL) and water (10 mL) was heated to reflux under argon for 40 hours. After reaction, the organic layer was collected, washed with

brine (30 mL × 3), and dried over MgSO$_4$. Then the solvent was removed to obtain the crude

product. The crude product was purified using column chromatography.

3-1-L. Purified by silica gel column chromatography eluted with dichloromethane. 0.53 g pale yellow solid was obtained (yield: 90%). ^{1}H NMR (CDCl$_3$, 400 MHz): 8.70 – 8.71 (m, 1H), 8.63 – 8.65 (m, 1H), 8.40 – 8.42 (m, 1H), 8.27 – 8.29 (m, 2H), 8.19 – 8.22 (m, 2H), 7.80 – 7.94 (m, 5H), 7.32 – 7.35 (m, 1H), 2.08 – 2.18 (m, 4H), 0.48 – 0.83 (m, 30H). ESI-HRMS: *m/z* calc. for [C$_{39}$H$_{47}$N$_3$O$_2$+H]$^+$: 590.3741; Found: 590.3734. Anal. Calc. for C$_{39}$H$_{47}$N$_3$O$_2$: C, 79.42; H, 8.03; N, 7.12; Found: C, 79.13; H, 8.06; N, 7.15.

3-2-L. Purified by silica gel column chromatography eluted with dichloromethane. 0.49 g yellow oil was obtained (yield: 86%). ^{1}H NMR (CDCl$_3$, 400 MHz): 10.07 (s, 1H), 8.69 – 8.70 (m, 1H), 8.64 – 8.66 (m, 1H), 8.40 (d, *J* = 8.0 Hz, 1H), 8.16 – 8.21 (m, 2H), 7.94 – 7.97 (m, 1H), 7.80 – 7.92 (m, 6H), 7.31 – 7.34 (m, 1H), 2.06 – 2.19 (m, 4H), 0.46 – 0.86 (m, 30H). ESI-HRMS: *m/z* calc. for [C$_{40}$H$_{48}$N$_2$O+H]$^+$: 573.3839; Found: 573.3823. Anal. Calc. for C$_{40}$H$_{48}$N$_2$O: C, 83.87; H, 8.45; N, 4.89; Found: C, 83.49; H, 8.80; N, 4.82.

3-3-L. Purified by silica gel column chromatography eluted with hexane/ethyl acetate (10:1 v/v). 0.55 g yellow oil was obtained (yield: 81%). ^{1}H NMR (CDCl$_3$, 400 MHz): 8.64 – 8.70 (m, 2H), 8.36 – 8.39 (m, 1H), 8.07 – 8.19 (m, 5H), 7.80 – 7.91 (m, 6H), 7.46 – 7.50 (m, 1H), 7.30 – 7.38 (m, 2H), 2.15 – 2.17 (m, 4H), 0.48 – 0.95 (m, 30H). ESI-HRMS: *m/z* calc. for [C$_{46}$H$_{51}$N$_3$S+H]$^+$: 678.3876; Found: 678.3884. Anal. Calc. for C$_{46}$H$_{51}$N$_3$S·0.33DMF·0.33CH$_2$Cl$_2$: C, 77.81; H, 7.45; N, 6.39; Found: C, 77.51; H, 7.50; N, 6.46.

3-4-L. Purified by silica gel column chromatography eluted first with hexane/dichloromethane (2:1 v/v), then with hexane/ethyl acetate (5:1 v/v). 0.47 g yellow oil was obtained (yield: 79%). ^{1}H NMR (CDCl$_3$, 400 MHz): 8.65 – 8.69 (m, 2H), 8.35 (dd, *J* = 7.6, 0.8 Hz, 1H), 8.08 – 8.13 (m, 2H), 7.73 – 7.88 (m, 4H), 7.62 (d, *J* = 7.6 Hz, 1H), 7.28 –

7.32 (m, 1H), 7.20 (s, 1H), 7.13 (dd, J = 7.8, 1.4 Hz, 1H), 2.67 (t, J = 7.6 Hz, 2H), 1.96 –

2.12 (m, 4H), 1.59 – 1.64 (m, 2H), 1.31 – 1.39 (m, 2H), 0.47 – 0.96 (m, 33H). ESI-HRMS:

m/z calc. for $[C_{43}H_{56}N_2+H]^+$: 601.4516; Found: 601.4514. Anal. Calc. for $C_{43}H_{56}N_2 \cdot 0.67$

toluene: C, 86.44; H, 9.33; N, 4.23; Found: C, 86.80; H, 9.70; N, 4.60.

3-5-L. Purified by silica gel column chromatography eluted with dichloromethane.

0.78 g yellow oil was collected as the product (yield: 75%). ^{1}H NMR (CDCl$_3$, 400 MHz):

8.68 – 8.72 (m, 2H), 8.40 (d, J = 7.6 Hz, 1H), 8.16 – 8.24 (m, 4H), 7.97 (d, J = 7.6 Hz, 1H),

7.83 – 7.94 (m, 4H), 7.51 – 7.61 (m, 2H), 7.28 – 7.43 (m, 7H), 1.98 – 2.25 (m, 4H), 0.52 –

0.98 (m, 30H). ESI-HRMS: m/z calc. for $[C_{51}H_{55}N_3+H]^+$: 710.4469; Found: 710.4475. Anal.

Calc. for $C_{51}H_{55}N_3 \cdot 0.17CH_2Cl_2$: C, 84.86; H, 7.70; N, 5.80; Found: C, 85.08; H, 7.98; N,

5.74.

3-6-L. Purified by silica gel column chromatography eluted with dichloromethane.

0.50 g yellow oil was obtained (yield: 70%). ^{1}H NMR (CDCl$_3$, 400 MHz): 8.64 – 8.69 (m,

2H), 8.34 (d, J = 7.6 Hz, 1H), 8.12 (dd, J = 8.2, 1.4 Hz, 1H), 8.06 (m, 1H), 7.83 – 7.89 (m,

2H), 7.78 (d, J = 7.6 Hz, 1H), 7.71 (m, 1H), 7.60 – 7.63 (m, 1H), 7.29 – 7.33 (m, 1H), 7.19 –

7.24 (m, 4H), 7.05 – 7.13 (m, 6H), 6.67 – 7.01 (m, 2H), 1.84 – 2.08 (m, 4H), 0.51 – 1.02 (m,

30H). ESI-HRMS: m/z calc. for $[C_{51}H_{57}N_3+H]^+$: 712.4625; Found: 712.4623. Anal. Calc. for

$C_{51}H_{57}N_3$: C, 86.03; H, 8.07; N, 5.90; Found: C, 86.29; H, 8.20; N, 5.71.

General Procedure for the Synthesis of Complexes 3-1 – 3-6. The mixture of

ligand (0.5 mmol), K$_2$PtCl$_4$ (0.5 mmol), and acetic acid (10 mL) was heated to reflux under

argon for 24 hours. After reaction, the solvent was removed. The red residual was dissolved

in dichloromethane, washed with brine (10 mL × 3), and dried over MgSO$_4$. Purification was

carried out by running flash silica gel column chromatography eluted with dichloromethane,

and then recrystallization from dichloromethane and hexane.

3-1. 237 mg orange powder was obtained (yield: 58%). ^{1}H NMR (CDCl$_3$, 400 MHz): 9.15 – 9.19 (m, 1H), 8.21 – 8.29 (m, 3H), 8.03 – 8.08 (m, 1H), 7.85 – 7.95 (m, 3H), 7.58 – 7.67 (m, 3H), 7.38 (m, 1H), 1.98 – 2.08 (m, 4H), 0.44 – 0.93 (m, 30H). ESI-HRMS: m/z calc. for [C$_{39}$H$_{46}$N$_3$O$_2$ClPt+H]$^+$: 820.3001; Found: 820.3003. Anal. Calc. for C$_{39}$H$_{46}$N$_3$O$_2$ClPt: C, 57.17; H, 5.66; N, 5.13; Found: C, 56.98; H, 5.68; N, 5.11.

3-2. 40 mg red powder was obtained (yield: 10%). ^{1}H NMR (CDCl$_3$, 400 MHz): 10.05 (s, 1H), 8.88 – 8.93 (m, 1H), 8.12 – 8.23 (m, 1H), 7.84 – 7.92 (m, 5H), 7.73 – 7.79 (m, 1H), 7.56 (d, J = 8.0 Hz, 1H), 7.43 – 7.50 (m, 2H), 7.33 (d, J = 2.8 Hz, 1H), 1.96 – 2.09 (m, 4H), 0.42 – 0.93 (m, 30H). ESI-HRMS: m/z calc. for [C$_{40}$H$_{47}$N$_2$ClOPt+H]$^+$: 803.3100; Found: 803.3072. Anal. Calc. for C$_{40}$H$_{47}$ClN$_2$OPt: C, 59.88; H, 5.90; N, 3.49; Found: C, 59.88; H, 6.28; N, 3.37.

3-3. 86 mg yellow powder was obtained (yield: 19%). ^{1}H NMR (CDCl$_3$, 400 MHz): 9.14 – 9.17 (m, 1H), 8.18 (s, 1H), 8.01 – 8.11 (m, 4H), 7.88 – 7.94 (m, 3H), 7.80 – 7.85 (m, 1H), 7.60 – 7.64 (m, 1H), 7.53 – 7.57 (t, J = 7.8 Hz, 2H), 7.45 – 7.49 (m, 1H), 7.33 – 7.37 (m, 2H), 1.98 – 2.13 (m, 4H), 0.45 – 0.93 (m, 30H). ESI-HRMS: m/z calc. for [C$_{46}$H$_{50}$N$_3$ClSPt+H]$^+$: 908.3137; Found: 908.3132. Anal. Calc. for C$_{46}$H$_{50}$ClN$_3$PtS: C, 60.88; H, 5. 55; N, 4.63; S, 3.53; Found: C, 60.73; H, 5.90; N, 4.47; S, 3.92.

3-4. 120 mg orange powder was obtained (yield: 29%). ^{1}H NMR (CDCl$_3$, 500 MHz): 8.80 (dd, J = 22, 5.3 Hz, 1H), 8.03 – 8.10 (m, 1H), 7.83 – 7.92 (m, 2H), 7.66 – 7.73 (m, 2H), 7.50 – 7.53 (m, 1H), 7.36 – 7.45 (m, 2H), 7.25 – 7.30 (m, 1H), 7.17 (s, 1H), 7.13 – 7.15 (m, 1H), 2.68 (t, J = 7.5 Hz, 2H), 1.93 – 2.03 (m, 4H), 1.60 – 1.67 (m, 2H), 1.32 – 1.42 (m, 2H), 0.48 – 1.00 (m, 33H). ESI-HRMS: m/z calc. for [C$_{43}$H$_{55}$ClN$_2$Pt+H]$^+$: 831.3778; Found: 831.3796. Anal. Calc. for C$_{43}$H$_{55}$ClN$_2$Pt·0.25toluene: C, 62.98; H, 6.73; N, 3.28; Found: C, 62.68; H, 6.93; N, 3.37.

3-5. 287 mg yellow powder was obtained (yield: 61%). ^{1}H NMR (CDCl$_3$, 400 MHz): 9.16 – 9.19 (m, 1H), 8.24 (m, 1H), 8.16 (d, J = 7.6 Hz, 2H), 8.02 – 8.07 (m, 2H), 7.95 (d, J = 8.0 Hz, 1H), 7.83 – 7.87 (m, 1H), 7.49 – 7.66 (m, 5H), 7.34 – 7.44 (m, 5H), 7.26 – 7.31 (m, 2H), 1.94 – 2.10 (m, 4H), 0.54 – 0.97 (m, 30H). ESI-HRMS: m/z calc. for [C$_{51}$H$_{54}$ClN$_3$Pt+H]$^+$: 940.3733; Found, 940.3729. Anal. Calc. for C$_{51}$H$_{54}$ClN$_3$Pt: C, 65.20; H, 5.79; N, 4.47; Found: C, 64.94; H, 6.08; N, 4.44.

3-6. 287 mg red powder was obtained (yield: 61%). ^{1}H NMR (CDCl$_3$, 400 MHz): 9.19 – 9.22 (m, 1H), 8.02 – 8.06 (m, 2H), 7.89 – 7.91 (d, J = 8.0 Hz, 1H), 7.77 – 7.82 (td, J = 8.0, 2.0 Hz, 1H), 7.68 – 7.71 (m, 1H), 7.62 – 7.66 (m, 1H), 7.48 – 7.52 (t, J = 8.4 Hz, 2H), 7.19 – 7.26 (m, 5H), 6.96 – 7.10 (m, 8H), 1.78 – 1.93 (m ,4H), 0.49 – 1.02 (m, 30H). ESI-HRMS: m/z calc. for [C$_{51}$H$_{56}$ClN$_3$Pt+H]$^+$: 942.3889; Found: 942.3878. Anal. Calc. for C$_{51}$H$_{56}$ClN$_3$Pt: C, 65.06; H, 5.99; N, 4.46; Found: C, 64.71; H, 6.25; N, 4.43.

3.2.2. Crystallographic Analysis

Single crystals of complex **3-1** were obtained by slow diffusion of hexane into the dilute dichloromethane solution of **3-1**. Single crystal X-ray diffraction data of **3-1** were collected on a Bruker Apex Duo diffractometer with an Apex 2 CCD area detector at T = 100 K. Mo radiation was used. All structures were processed with Apex 2 v2010.9-1 software package (SAINT v. 7.68A, XSHELL v. 6.3.1).[44 - 46] Direct method was used to solve the structure after multi-scan absorption corrections. Details of data collection and refinement are given in Table 3.1.

Table 3.1. Single crystal X-ray parameters and refinement data for **3-1**.

T (K)	100(2)
λ (Å)	0.71073
Formula	C$_{39}$H$_{46}$ClN$_3$O$_2$Pt·CH$_2$Cl$_2$
MW	904.25
Crystal size(mm)	0.33×0.12×0.09
Crystal system	monoclinic
Space group,	P2(1)/n

Table 3.1. Single Crystal X-ray Parameters and Refinement Data for **3-1** (continued).

a (Å)	12.7116(9)
b (Å)	17.5310(11)
c (Å)	17.1311(11)
α (degree)	90
β (degree)	90.489(1)
γ (degree)	90
V (Å^3)	3817.5(4)
Z	4
ρ_{calc} (g/cm^3)	1.573
μ (cm^{-1})	3.924
Radiation type	Mo
$F(000)$	1816
Reflections collected	65292
Unique reflections	11451
no of reflns (I $\geq 2\sigma$)	8722
Resolution (Å)	0.7
Goodness-of-fit on F^2	1.022
R_1/wR_2 (I $\geq 2\sigma(I)$)[a]	0.0317/0.0732
R_1/wR_2 (all data)[a]	0.0529/0.0827

[a]$R_1 = \Sigma||F_0| - |F_c|| / \Sigma|F_0|$, $wR_2 = [\Sigma(w(F_o^2 - F_c^2)^2) / \Sigma w(F_o^2)^2]^{1/2}$ for $F_o^2 > 2\sigma(F_o^2)$, $w = 1/[\sigma^2(F_o^2) + (AP)^2 + BP]$ where $P = (F_o^2 + 2F_c^2)/3$; A (B) = 0.0370 (5.4894).

3.2.3. Photophysical Measurements

The solvents used for photophysical experiments were spectroscopic grade, and were purchased from VWR International and used as is without further purification. An Agilent 8453 spectrophotometer was used to record the UV-vis absorption spectra in different solvents. A SPEX fluorolog-3 fluorometer/phosphorometer was used to measure the steady-state emission spectra in different solvents. The emission quantum yields were determined by the relative actinometry method[47] in degassed solutions, in which a degassed aqueous solution of [Ru(bpy)$_3$]Cl$_2$ (Φ_{em} = 0.042, λ_{ex} = 436 nm)[48] was used as the reference for complexes **3-1** – **3-6**, and a degassed 1 N sulfuric acid solution of quinine bisulfate (Φ_{em} = 0.546, λ_{ex} = 347.5 nm)[49] was used as the reference for ligands **1-L** – **6-L**.

The nanosecond transient difference absorption (TA) spectra and decays were measured in degassed solutions on an Edinburgh LP920 laser flash photolysis spectrometer. The third harmonic output (355 nm) of a Nd:YAG laser (Quantel Brilliant, pulsewidth: 4.1

ns, repetition rate was set at 1 Hz) was used as the excitation source. Each sample was purged with argon for 30 min prior to measurement. The triplet excited-state absorption coefficient (ε_T) at the TA band maximum was determined by the singlet depletion method.[50] After obtaining the ε_T value, the Φ_T could be determined by the relative actinometry using SiNc in benzene as the reference ($\varepsilon_{590} = 70000$ M^{-1} cm^{-1}, $\Phi_T = 0.20$).[51]

3.2.4. Nonlinear Transmission Experiment

The reverse saturable absorption of complexes **3-1 – 3-6** was characterized by nonlinear transmission experiment at 532 nm using a Quantel Brilliant laser as the light source. The pulse width of the laser was 4.1 ns and the repetition rate was set at 10 Hz. The complexes were dissolved in CH$_2$Cl$_2$. The concentration of the sample solutions was adjusted to obtain a linear transmission of 90% at 532 nm in a 2-mm-thick cuvette. The experimental setup and details are similar to that reported previously.[16] A 40-cm plano-convex lens was used to focus the beam to the center of the 2-mm thick sample cuvette.

3.2.5. Computational Details

The ground-state properties of complexes **3-1 – 3-6** were studied using density functional theory (DFT), while the excited states were simulated using linear response time dependent DFT (TDDFT). All calculations – the geometry optimization, the ground-state and excited-state electronic structures, and optical spectra – were performed using Gaussian 09 quantum chemistry software package.[52] All procedures were done utilizing the long-rang corrected functionalCAM-B3LYP.[53] The LANL08 basis set[54] was used for the heavier Pt atom, while the remaining atoms were modeled with the 6-31G* basis set. The chosen method represents one of the currently most accurate DFT functionals and basis sets that have already shown good agreement with experimental data for different organometallic complexes.[55 - 57] All calculations have been performed in solvent using Conductor Polarized

97

Continuum Model (CPCM),[58, 59] as implemented in Gaussian 09. Dichloromethane (CH_2Cl_2, ε_r = 9.08) was chosen as the solvent for consistency with the experimental studies. Implementation of solvent also helps to avoid any unnatural charge transfer states within the energy gap of these complexes.[60 - 62]

The excited states energies and oscillator strengths have been studied using linear response TDDFT formalism,[63] in which the adiabatic approximation for the exchange-correlation kernel was used. These calculations were done using the same basis sets and functional as used in the ground state DFT calculations. For absorption spectra, 40 lowest singlet optical transitions were considered to reach the transition energies of ~ 5 eV (250 nm). Each spectral line obtained from the TDDFT calculation was broadened by a Gaussian function with the line width of 0.1 eV to match the experimentally observed homogeneous broadening. The phosphorescence energies were calculated by first optimizing the lowest triplet state geometry followed by the vertical triplet excitations calculated via TDDFT.

In order to analyze the nature of the singlet and triplet excited states, natural transition orbital (NTO) analysis was performed based on the calculated transition densities.[64] This method offers the most compact representation of the transition density between the ground and excited states in terms of an expansion into single-particle transitions (hole and electron for each given excited state). Here we refer to the unoccupied NTO as the "electron" transition orbital, and the occupied NTO as the "hole" transition orbital. NTOs shown in this paper were produced with the isovalue of 0.02 and visualized with the GaussView 5.1 graphical software.[65]

3.3. Results and Discussion

3.3.1. Crystal Structure of 3-1

Single crystals of complex **3-1** were obtained by slow diffusion of hexane into the dichloromethane solution of **3-1**. The crystal structure and packing pattern are illustrated in

Figure 3.1, and selected bond length, bond angles, and torsion angles are compiled in Table

3.2. As shown in Figure 3.1, two diastereomers (Figure 3.1a: *R* configuration at C25, 52%;

Figure 3.1b: *S* configuration at C25, 48%) were observed in the crystal, which could arise

from the racemic starting material 2-ethylhexyl bromide. In contrast, only the *S* configuration

of C33 was observed. Nevertheless, the configuration of C25 or C33 plays a negligible role

on the photophysics and nonlinear absorption of the Pt(II) complexes and thus is not the

focus of this study. As a result, we only pick the diastereomer with *R* configuration at C25

(Figure 3.1a) for structural and packing discussion. The packing pattern is illustrated by two

single cells in *b* axis in Figure 3.1c. Regardless of the two alkyl chains at the 9-position of the

fluorene motif, the complex basically has a planar structure, in which bipyridine, Pt-Cl,

fluorene, and nitro sit roughly in the same plane. The geometry optimization of the molecule

performed by DFT calculations also results in the planar configurations as shown in Figure

3.2.
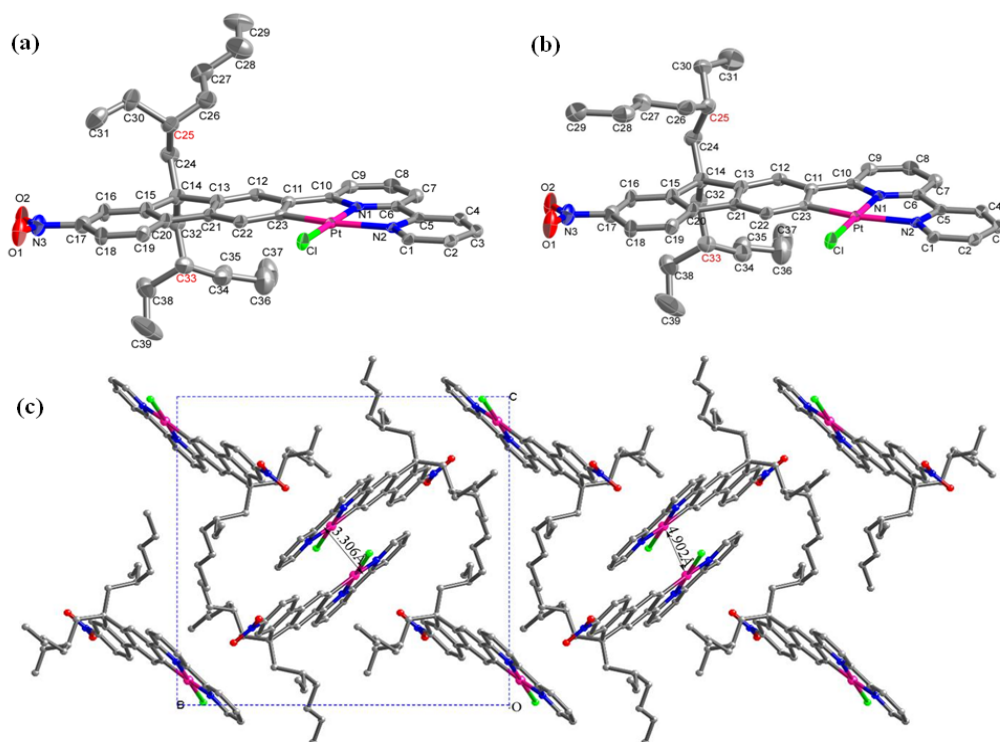
Figure 3.1. (a) The structure of the diastereomer in which C25's configuration is *R*, and the percentage of this diastereomer is 52%; (b) the structure of the diastereomer in which C25's configuration is *S*, and the percentage of this diastereomer is 48%; (c) 3D packing of complex 1 viewed along a axis.

Table 3.2. Selected bond length, bond angle, and torsion angles of complex **3-1**.

Atom 1	Atom 2	Atom 3	Atom 4	Bond Length/ Å or Bond Angle / degree
Pt	Cl			2.296(1)
Pt	N1			1.944(3)
Pt	N2			2.101(3)
Pt	C23			1.986(3)
N1	C10			1.364(4)
N1	C6			1.349(4)
N2	C5			1.359(5)
N2	C1			1.342(4)
C5	C6			1.484(5)
C10	C11			1.467(5)
Cl	Pt	N1		178.49(9)
Cl	Pt	N2		98.42(8)
Cl	Pt	C23		98.97(11)
N1	Pt	N2		80.14(11)
N1	Pt	C23		82.48(13)
N2	Pt	C23		162.56(13)
Pt	N1	C10		117.8(2)
Pt	N1	C6		118.7(2)
C10	N1	C6		123.5(3)
Pt	N2	C5		112.2(2)
Pt	N2	C1		128.3(2)
C5	N2	C1		119.5(3)
Pt	C23	C11		112.3(3)
Pt	C23	C22		129.5(3)
C23	C11	C10		115.0(3)
Cl	Pt	N1	C10	-164(3)
N2	Pt	N1	C10	179.1(3)
C23	Pt	N1	C10	0.5(2)
N1	C6	C5	N2	0.6(4)
C23	C11	C10	N1	-0.6(4)
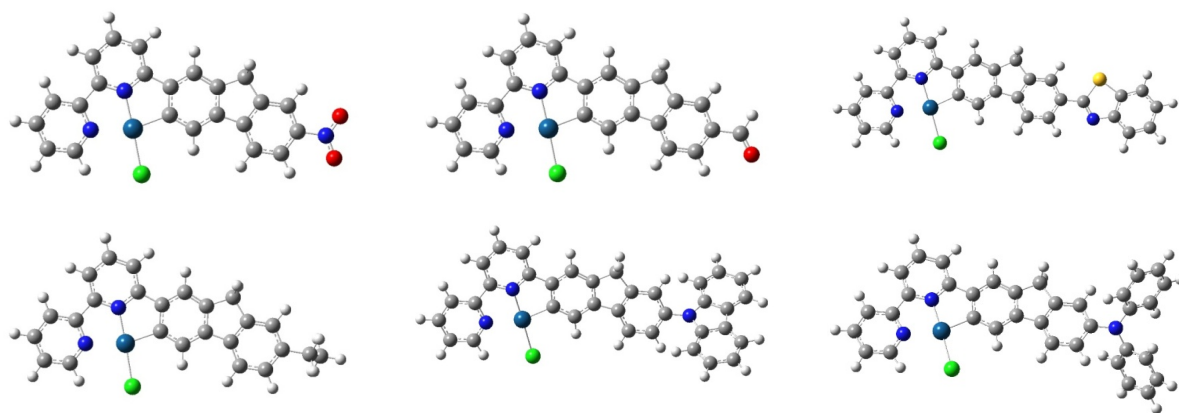
Figure 3.2. Optimized geometries of via DFT calculations (top: **3-1** − **3-3** from left to right; bottom: **3-1** − **3-6** from left to right)

The bond lengths of Pt-N1 (1.944(3) Å), Pt-N2 (2.101(3) Å), and Pt-C23 (1.986(3) Å) resemble our previously published data for a similar core structure in Ref. 34, with the corresponding values for complex **1** in Ref. 34 being 1.980(7) Å, 2.112(8) Å, and 1.997(8) Å, respectively.[34] The shorter bond length of Pt-N1 in this work is probably due to the weaker trans effect of chloride ligand compared to 4-tolylacetylide co-ligand in Ref. 34. The bond angles around the platinum center, Cl-Pt-C23 (98.97(11)), Cl-Pt-N2 (98.42(8)), N1-Pt-C23 (82.48(13)), and N1-Pt-N2 (80.14(11)), reveal deviation of the structure from an ideal square planar configuration around the metal center. The torsion angle between the fluorene and bipyridine components is approximately 0.6 degrees (revealed by the torsion angle of C23-C11-C10-N1), while the NO_2 plane deviates from the fluorene plane by an angle of 6.5 degrees (see the torsion angle of O1-N3-C17-C18).

Four molecules of **3-1** form a single centrosymmetric cell in the crystal matrix. In every single cell, two molecules adopt a head-to-tail packing with their π-conjugated planes opposite to each other; while the other two are in the perpendicular direction of the two packing molecules. The average distance between the two packing π-conjugated planes, defined by the distance of the two planes averaging the 26 atoms within the ring system of each molecule, is 3.306 Å, indicating the presence of π-π interactions between the two molecules in the crystal matrix. The nearest Pt$\cdots$Pt separation is 4.902 Å, which is longer than the Pt$\cdots$Pt association range of 3.09 - 3.71 Å.[66] Therefore, no intermolecular Pt$\cdots$Pt interactions present even if in the crystal form.

3.3.2. Electronic Absorption

The electronic absorption spectra of ligands **3-1-L** – **3-6-L** and complexes **3-1** – **3-6** at different concentrations are recorded in dichloromethane solutions. The absorptions of these compounds obey Beer's Law in the concentration range of 1×10^{-6} – 1×10^{-4} mol/L, indicating the absence of ground state aggregation in the concentration range studied in

dichloromethane. As shown in Figure 3.3a, **3-1-L** – **3-6-L** display intense absorption bands from 300 to 400 nm, which predominantly arise from the $^1\pi,\pi^*$ transitions. However, contribution from intraligand charge transfer cannot be completely ruled out. The predominant $^1\pi,\pi^*$ character of these absorption bands is supported by the minor solvatochromic effect in these ligands, as demonstrated in Figures 3.4. Comparing to **3-4-L**, the major absorption bands of all other ligands are red-shifted, which is likely the sign of electron delocalization induced by the substituent. Stronger electron withdrawing substituent (NO_2 in **3-1-L**) and stronger electron donating substituent (NPh_2 in **3-6-L**) cause the most red-shift of the absorption band. Extended π-conjugation from the BTZ substituent in **3-3-L** also induces a significant red-shift and enhanced extinction coefficient.
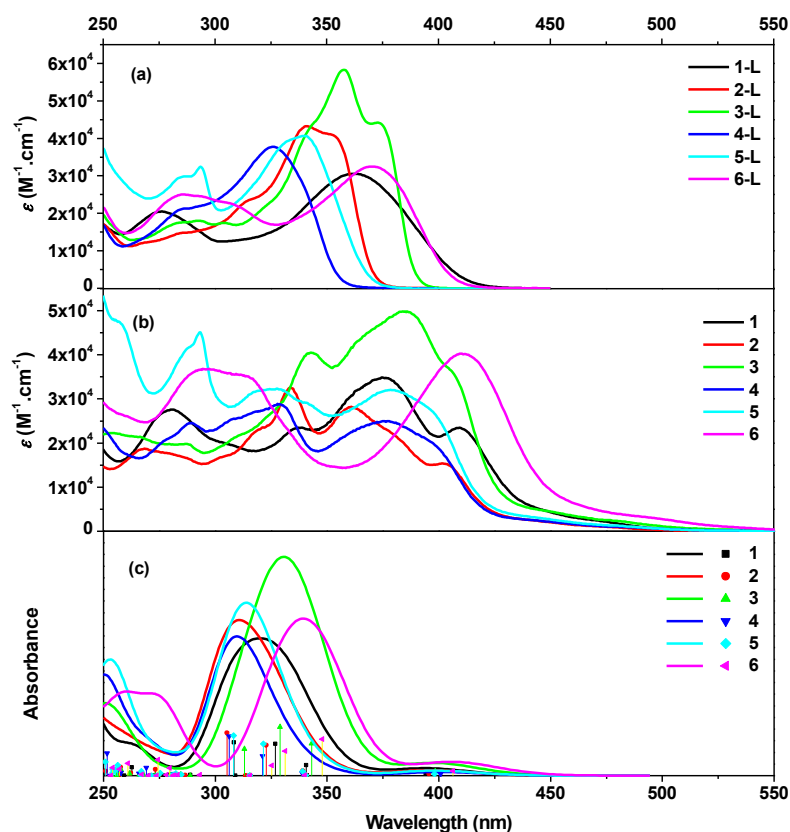
Figure 3.3. (a) UV-vis absorption spectra of ligands **3-1-L** – **3-6-L** measured in CH_2Cl_2; (b) UV-vis absorption spectra of complexes **3-1** – **3-6** measured in CH_2Cl_2; (c) Calculated absorption spectra for complexes **3-1** – **3-6**, vertical lines resemble excited states and the corresponding oscillator strength.
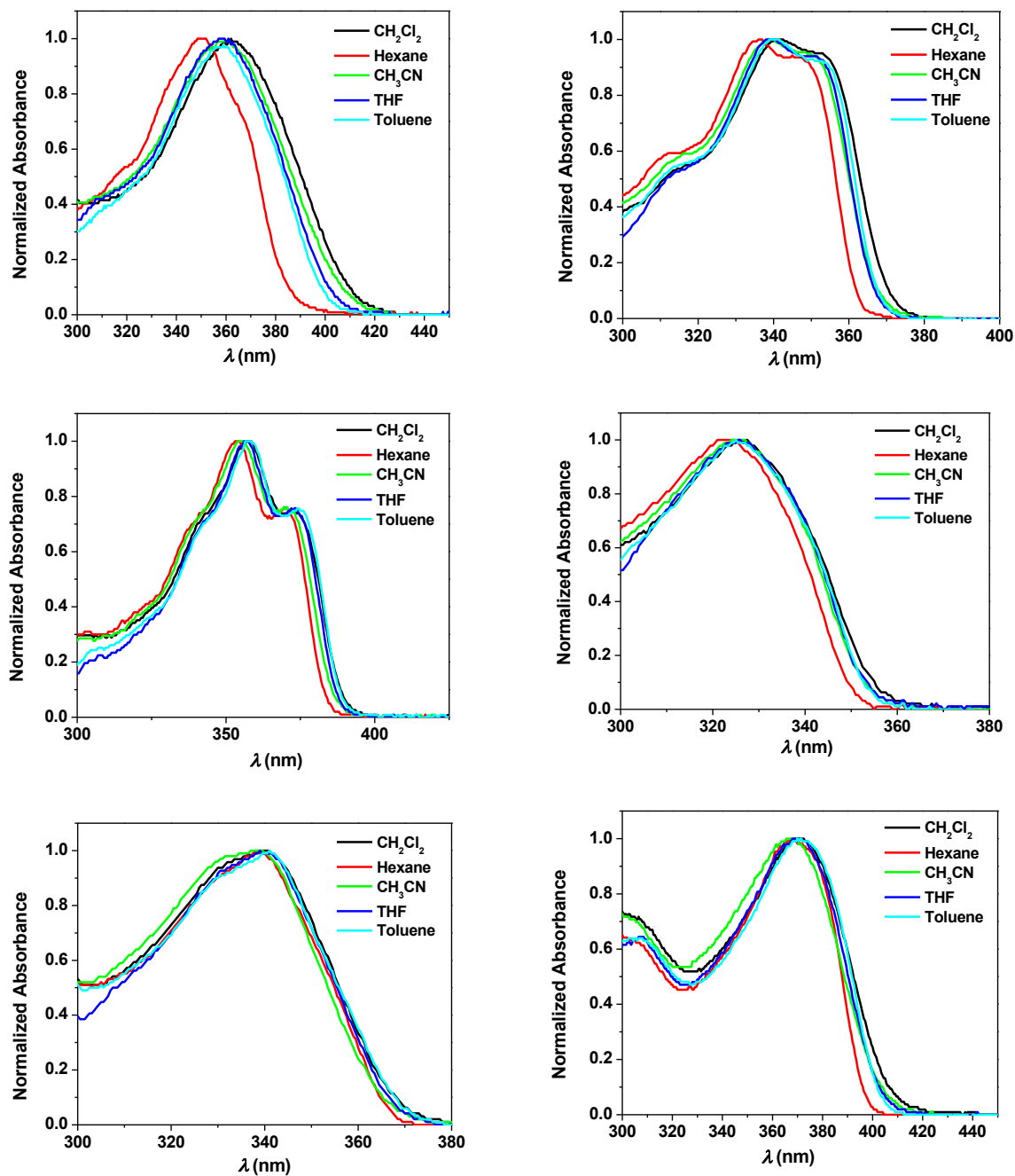
Figure 3.4. Normalized absorption spectra of **3-1-L** – **3-6-L** in different solvents.

For complexes **3-1** – **3-6**, the UV-vis absorption spectra consist of intense absorption bands below 420 nm and broad tail above 420 nm (see spectra in Figure 2.3b). The intense absorption bands below 420 nm in complexes **3-1** – **3-3** (which contain electron-withdrawing substituents at the 7-position of fluorene) exhibit more featured spectra with a few well-distinct peaks than those in complexes **3-4** – **3-6** with electron-donating substituent. Similar to the trend observed in their corresponding ligands, the UV-vis absorption spectra for

complexes with stronger electron-withdrawing or donating substituents (complexes **3-1** and

3-6) and with BTZ substituent (complex **3-3**) are red-shifted compared to the other three

complexes. This trend is well reproduced by our TDDFT calculations illustrated in Figure

2.3c and listed in Table 3.3, although the energies of all complexes are blue-shifted with

respect to experimental data due to a high portion of the Hartree-Fock exchange in the CAM-

B3LYP functional.

Table 3.3. Experimental and calculated electronic absorption parameters for complexes **3-1** – **3-6** and experimental absorption data for ligands **3-1-L** – **3-6-L** in CH_2Cl_2.

	λ_{abs}/nm (ε_{max}/$M^{-1}.cm^{-1}$)[a]	$^{Theor}\lambda_{abs}$/nm (S_n; f_{osc})[b]
1	409 (23430), 375 (34850), 339 (23530)	394 (S_1; 0.0563), 341 (S_2; 0.0094), 340 (S_3; 0.228), 327 (S_4; 0.679), 308 (S_6; 0.710)
2	402 (15400), 361 (28200), 334 (32530)	395 (S_1; 0.0416), 340 (S_2; 0.0091), 339 (S_3; 0.103), 323 (S_4; 0.649), 305 (S_7; 0.914)
3	404 (37320), 385 (49820), 343 (40510)	398 (S_1; 0.096), 343 (S_2, 0.692), 341 (S_3; 0.009), 329 (S_4; 1.047), 313 (S_6; 0.572)
4	376 (24930), 329 (28780)	400 (S_1; 0.0280), 340 (S_2; 0.0096), 339 (S_3; 0.0575), 321 (S_4; 0.420), 306 (S_6; 0.8470)
5	379 (31980), 328 (32330)	398 (S_1; 0.0382), 340 (S_2; 0.0097), 339 (S_3; 0.0966), 321 (S_4; 0.682), 308 (S_6; 0.863)
6	411 (40130), 310 (35550)	406 (S_1; 0.104), 348 (S_2; 0.782), 340 (S_3; 0.0103), 331 (S_4; 0.525)
1-L	362 (30540), 276 (20490)	
2-L	341 (43250)	
3-L	373 (44200), 358 (58250)	
4-L	326 (37730)	
5-L	340 (40650)	
6-L	370 (32500), 285 (25000)	

[a] λ_{abs} is absorption wavelength, ε_{max} is molar extinction coefficient. [b] $^{Theor}\lambda_{abs}$ is calculated wavelength corresponding to the transition between the ground and excited state of interest (number of excited state is shown in parentheses), f_{osc} is calculated oscillator strength for the corresponding excitations.

The natural transition orbitals (NTOs) listed in Table 3.4 clearly indicate that the

transitions contributing to the absorption bands around 400-410 nm and 360-380 nm for **3-1** –

3-3 are featured by mixed ^{1}MLCT ($d\pi$(Pt)→π^*(bpy)), ^{1}LLCT (π(Cl)→π^*(bpy)), $^1\pi,\pi^*$, and

^{1}ILCT (intraligand charge transfer) characters, while the band at ca. 340 nm primarily arises

from the mixed $^1\pi,\pi^*$/^{1}ML'CT ($d\pi$(Pt)→π^*(fluorene)) transitions. In contrast, the major

absorption bands for **3-4** and **3-5** (with weak or moderate electron-donating substituents at the

7-position of fluorene) originate from the ^{1}MLCT/$^1\pi,\pi*$/^{1}ILCT transitions, while complex **3-6** with strong electron-donating substituent is featured predominantly with $^1\pi,\pi*$/^{1}MLCT transitions in its major absorption band at ca. 410 nm, with a minor contribution from ^{1}LLCT/^{1}ILCT in its high-energy shoulder around 380 nm (see NTOs in Table 3.4). Such a pronounced $^1\pi,\pi*$ character of optical transitions at ~ 410 nm is a result of the NPh$_2$ substituent in complex **3-3** − **3-6** that strongly delocalizes both the hole and electron orbitals via spreading the charge density towards the NPh$_2$ group. Increase in π-conjugation provides the most pronounced red-shift in the main absorption band of **3-6**, compared to those in complexes **3-4** and **3-5**, in which the electron is primarily localized on the bpy component, while the hole is spread over fluorene motif. Note that although for all complexes except **3-6**, the substituents are not directly involved in the NTOs contributing to the lower-energy edge of the main absorption band (380 - 420 nm), they play an important role in overall delocalization of the charge density over fluorene. Thus, the large red-shift of complex **3-3** is also associated with the increase in π-conjugation due to the substituent, which tends to partially spread both the hole and electron charge density over fluorene towards the BTZ substituent. The same trend is also noticeable (but less pronounced) in complex **3-1** with the strong electron withdrawing substituent pulling the charge density to the fluorene, which explains its red-shift with respect to complex **3-2**.

Table 3.4. Natural transition orbitals (NTOs)[a] representing transitions corresponding to the main absorption bands for **3-1** − **3-6**.

	Excited state and properties	Hole	Electron
1	**S$_3$** $f_{osc} = 0.2279$ 340 nm		
	S$_4$ $f_{osc} = 0.6786$ 327 nm		
	S$_6$ $f_{osc} = 0.7102$ 308 nm		

Table 3.4. Natural transition orbitals (NTOs)[a] representing transitions corresponding to the main absorption bands for **3-1** – **3-6** (continued).
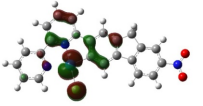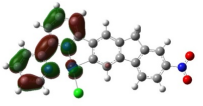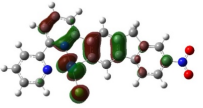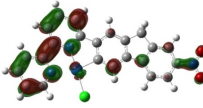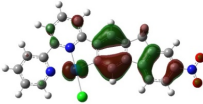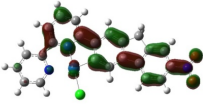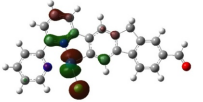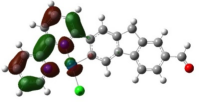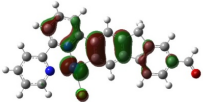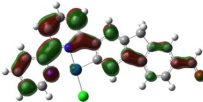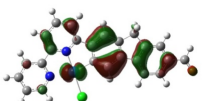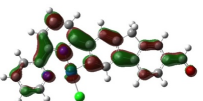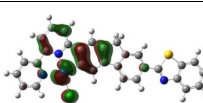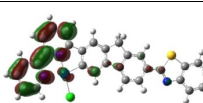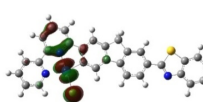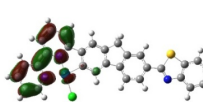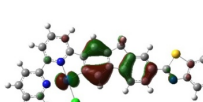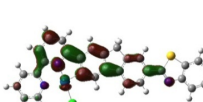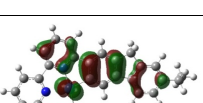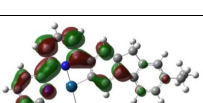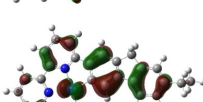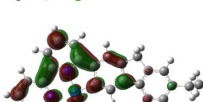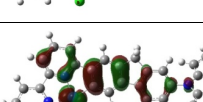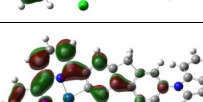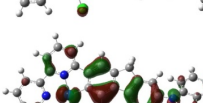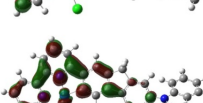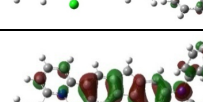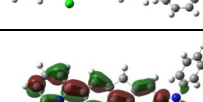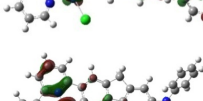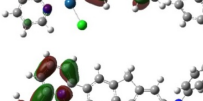
	Excited state and properties	Hole	Electron
	S_3 $f_{osc} = 0.1034$ 339 nm		
2	S_4 $f_{osc} = 0.6492$ 323 nm		
	S_7 $f_{osc} = 0.9140$ 305 nm		
	S_2 $f_{osc} = 0.6915$ 343 nm		
3	S_4 $f_{osc} = 1.0472$ 329 nm		
	S_6 $f_{osc} = 0.5719$ 313 nm		
	S_4 $f_{osc} = 0.4201$ 321 nm		
4	S_6 $f_{osc} = 0.8470$ 306 nm		
	S_4 $f_{osc} = 0.6820$ 321 nm		
5	S_6 $f_{osc} = 0.8630$ 308 nm		
	S_2 $f_{osc} = 0.7823$ 348 nm		
6	S_4 $f_{osc} = 0.5252$ 331 nm		

[a]Note that excited state NTOs differ from the ground state MOs, and rather can be considered as the linear combination of the ground state MOs that contribute to a given excited state.

In addition to the major absorption bands, a well pronounced tail appears at the low-energy end of the major absorption bands and extends to 550 nm in the absorption spectra of

complexes **3-1** – **3-6**, as seen in Figures 3.3b and 3.3c. These tails become more distinguishable from the major absorption bands in MTHF, toluene and hexane as shown in Figures 3.5. The calculated NTOs contributing to the lowest-energy, low-intensity transition (Table 3.5) reveal that this tail features ^{1}MLCT/$^1\pi,\pi*$/^{1}ILCT characters for all complexes. However, in accordance with the trend observed from the major absorption bands, this tail bathochromically shifts to longer wavelengths in complexes **3-1**, **3-3** and **3-6** compared to those in **3-2**, **3-4** and **3-5**, with the most pronounced red-shift and the highest intensity in complex **3-6**, due to the strongest delocalization of NTOs over the fluorene promoted by the strongest electron donating NPh$_2$ group (Table 3.5).
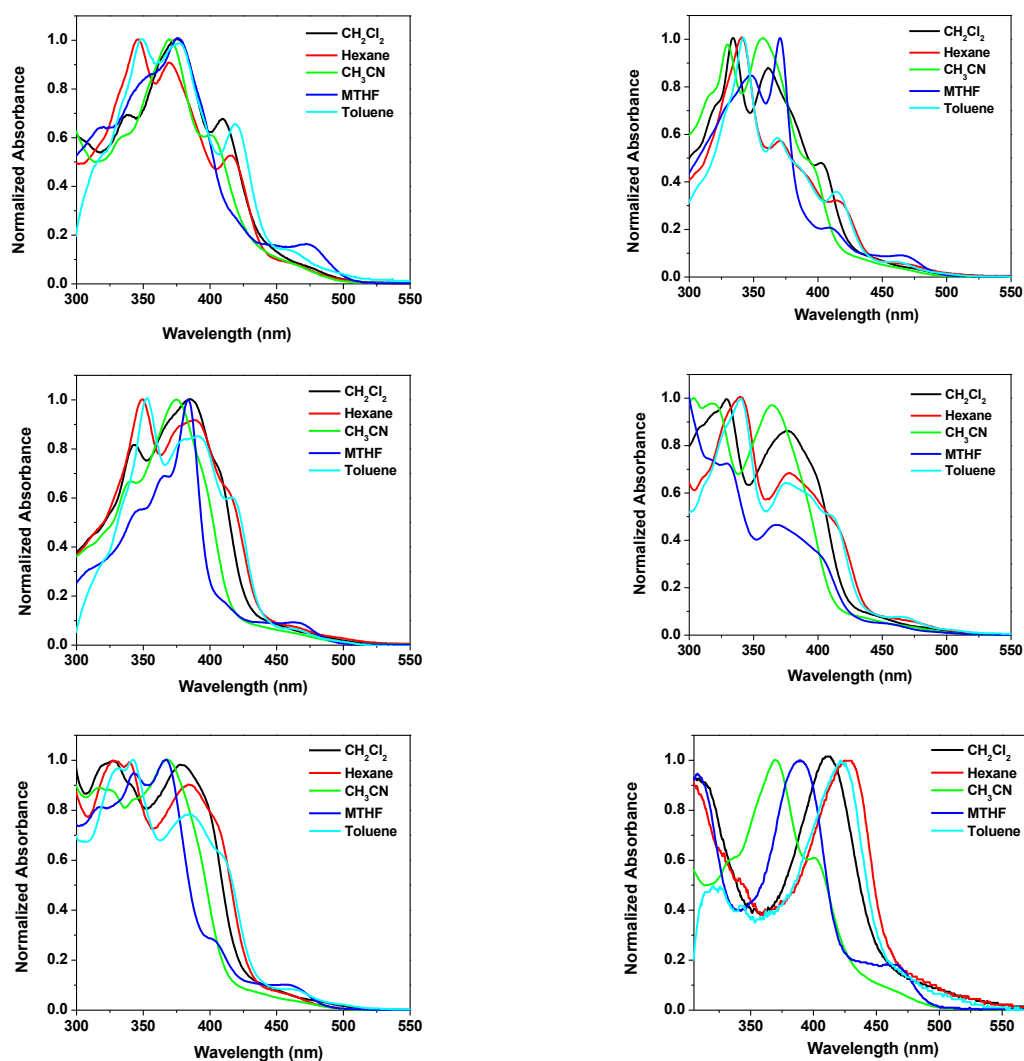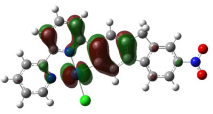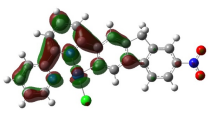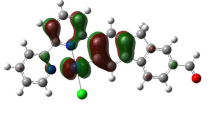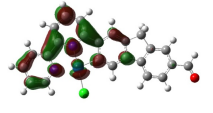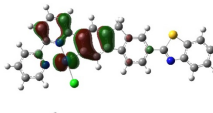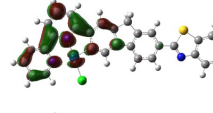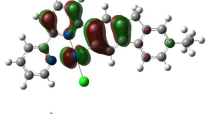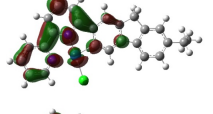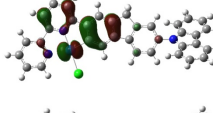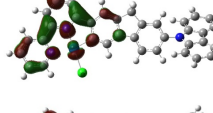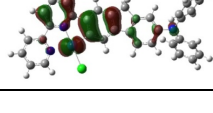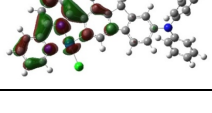
Figure 3.5. Normalized absorption spectra of **3-1** – **3-6** in different solvents.

Table 3.5. Natural transition orbitals contributing to the lowest-energy absorption 'tail' for complexes **3-1 – 3-6**.

	Excited state number and properties	Hole	Electron
3-1	**S$_1$** f_{osc} = 0.0563 394 nm		
3-2	**S$_1$** f_{osc} = 0.0416 395 nm		
3-3	**S$_1$** f_{osc} = 0.096 398 nm		
3-4	**S$_1$** f_{osc} = 0.0280 400 nm		
3-5	**S$_1$** f_{osc} = 0.0382 398 nm		
3-6	**S$_1$** f_{osc} = 0.1044 406 nm		

3.3.3. Photoluminescence

Photoluminescence of ligands **3-1-L – 3-6-L** and Pt(II) complexes **3-1 – 3-6** were studied at room temperature in different solvents and at 77 K in butyronitrile glassy matrix. The spectra are presented in Figures 3.6, 3.7, and 3.8. The emission parameters are summarized in Table 3.6 and 3.7. As shown in Figure 3.6a and in Tables 3.6 and 3.7, ligands **3-L – 6-L** exhibit intense fluorescence in all solvents in the region of 350 nm – 550 nm with the emission quantum yield in the range of 0.50 – 0.91. The emission of **1-L** and **2-L** at room temperature is much weaker in comparison to those of **3-L – 6-L**. Ligand **1-L** exhibits dual emission in CH$_2$Cl$_2$ solution when excited at 325 nm, with a slightly structured $^1\pi,\pi^*$ fluorescence at ca. 414 nm and a structureless ^{1}ILCT fluorescence at ca. 480 nm. When excited at 400 nm, only the ^{1}ILCT fluorescence is observed. The charge transfer nature of the 480 nm band is supported by the positive solvatochromic effect of this emission band and by the fact that this emission band is only observed in polar solvents like CH$_2$Cl$_2$ and CH$_3$CN

(Figure 3.7). For **2-L**, only the $^1\pi,\pi^*$ fluorescence was observed in all of the solvents when excited below 330 nm. However, ^{1}ILCT was detected in CH$_3$CN solution when excited at 374 nm. The absence of charge transfer emission in solvents other than CH$_3$CN implies a weaker admixture of the ^{1}ILCT character in the lowest singlet excited state in **2-L** compared to **1-L**. This is reasonable because of the weaker electron-withdrawing ability of the formyl substituent with respect to the nitro substituent. In contrast, **3-L** only displays $^1\pi,\pi^*$ fluorescence with clear vibronic structure independent of the solvent polarity and the excitation wavelength. This feature can be attributed to the extended π-conjugation induced by the BTZ substituent and the weaker electron-withdrawing ability of the BTZ substituent.

The emission characteristics of **4-L** – **6-L** (all with electron-donating substituents) at room temperature are quite similar. As exemplified in Figure 3.7 for **6-L**, the fluorescence spectrum becomes significantly red-shifted and featureless going from nonpolar solvents (hexane and toluene) to polar solvents (THF, CH$_2$Cl$_2$, CH$_3$CN), indicating a transition from $^1\pi,\pi^*$ fluorescence in nonpolar solvents to ^{1}ILCT fluorescence in polar solvents. The positive solvatochromic effect is more pronounced in **6-L** than in **5-L** and **4-L**, and the ^{1}ILCT emission energy apparently decreases from **4-L** to **5-L** to **6-L**. This trend is consistent with the strength of the electron-donating ability of the substituent in these compounds. With the increased electron-donating ability (*i.e.* NPh$_2$ > CBZ > *n*-Bu), the degree of intraligand (intramolecular) charge transfer is enhanced, which consequently induces the red-shift of the charge transfer emission.

The emission of **3-1-L** – **3-6-L** at 77 K in butyronitrile glassy matrix was investigated in order to understand the phosphorescence from these compounds. As illustrated in Figure 3.6c, structured phosphorescence between 500 and 700 nm was observed only in **1-L** and **2-L**. The emission detected below 500 nm for **2-L** – **6-L** is low-temperature fluorescence,

which becomes narrower, structured and slightly blue-shifted due to the rigidochromic effect.[67 - 70]
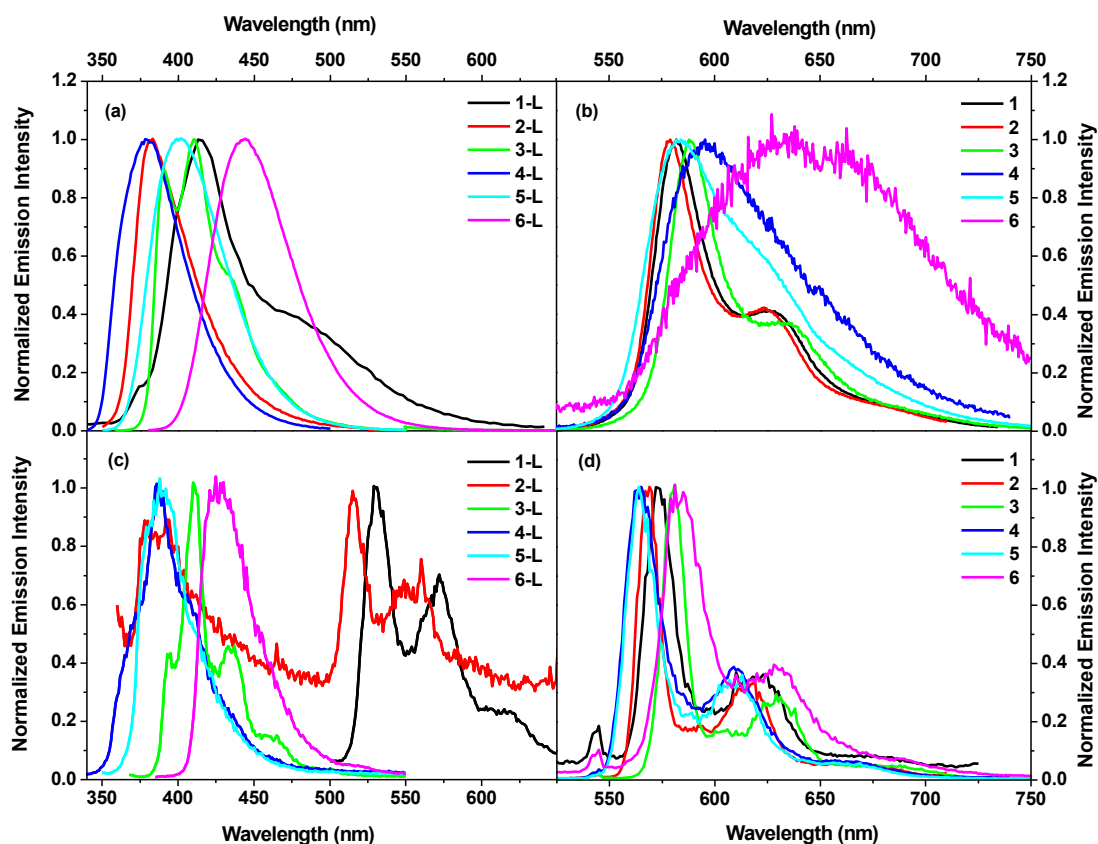
Figure 3.6. (a) Normalized emission spectra of ligands **3-1-L** – **3-6-L** (λ_{ex} was 325 nm for **3-1-L**, 320 nm for **3-2-L**, 348 nm for **3-3-L**, 326 nm for **3-4-L**, 340 nm for **3-5-L**, and 370 nm for **3-6-L**) in CH$_2$Cl$_2$ at the concentration of 1×10^{-5} mol/L for **3-2-L** – **3-6-L** and 5×10^{-4} mol/L for **3-1-L**; (b) Normalized emission spectra of complexes **3-1** – **3-6** (λ_{ex} was 372 nm for **3-1**, 360 nm for **3-2**, 383 nm for **3-3**, 375 nm for **3-4**, 380 nm for **3-5**, and 410 nm for **3-6**) in CH$_2$Cl$_2$ at the concentration of 1×10^{-5} mol/L; (c) Normalized emission spectra of **3-1-L** – **3-6-L** at 77 K in glassy BuCN matrix (λ_{ex} was 405 nm for **3-1-L**, 350 nm for **3-2-L**, 358 nm for **3-3-L**, 326 nm for **3-4-L**, 340 nm for **3-5-L**, and 375 nm for **3-6-L**); (d) Normalized emission spectra of complexes **3-1** – **3-6** at 77 K in glassy BuCN matrix at the concentration of 1×10^{-5} mol/L (λ_{ex} was 372 nm for **3-1**, 360 nm for **3-2**, 383 nm for **3-3**, 375 nm for **3-4**, 380 nm for **3-5**, and 410 nm for **3-6**).
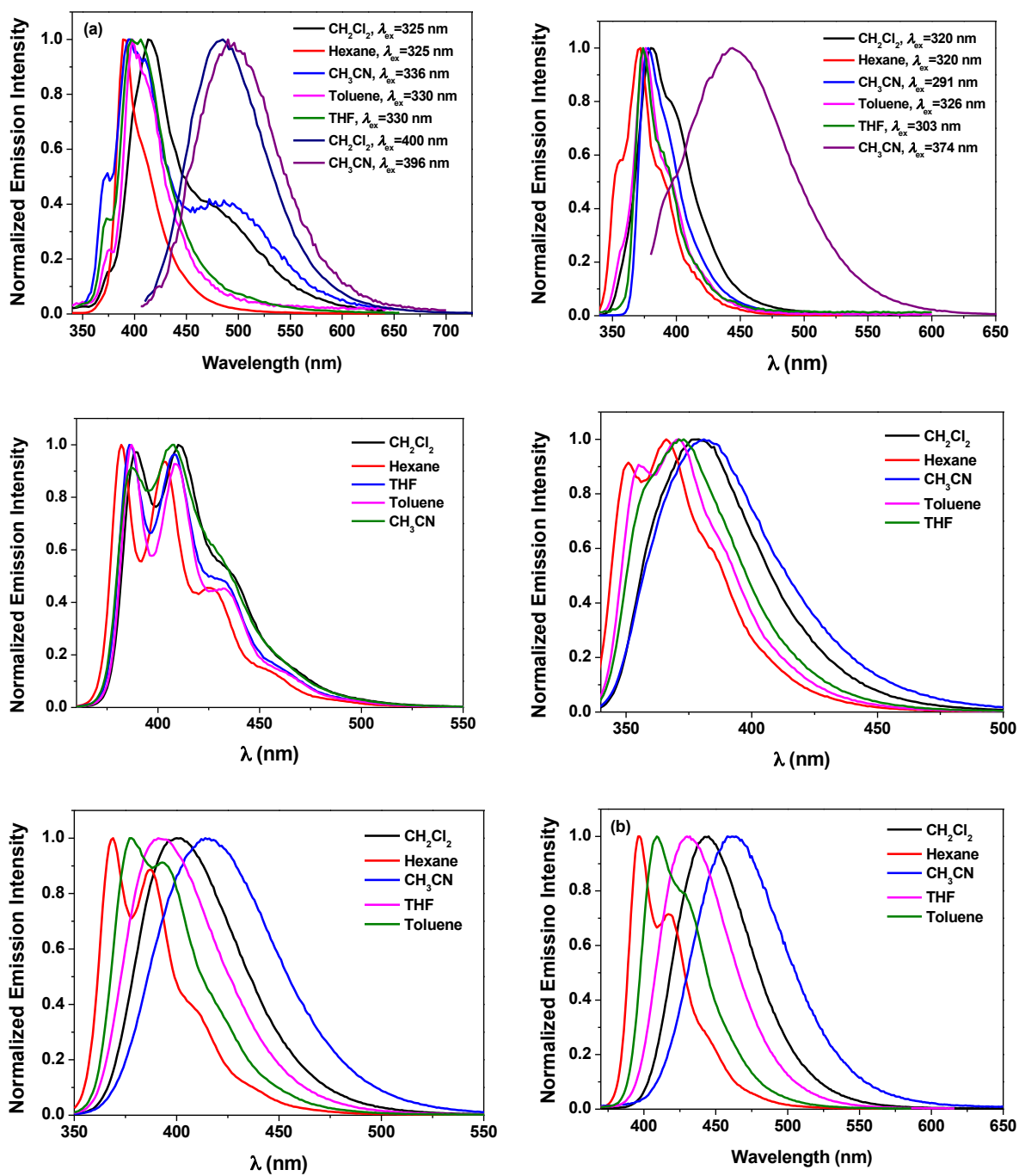
Figure 3.7. Normalized emission spectra of **3-1-L** – **3-6-L** in different solvents.
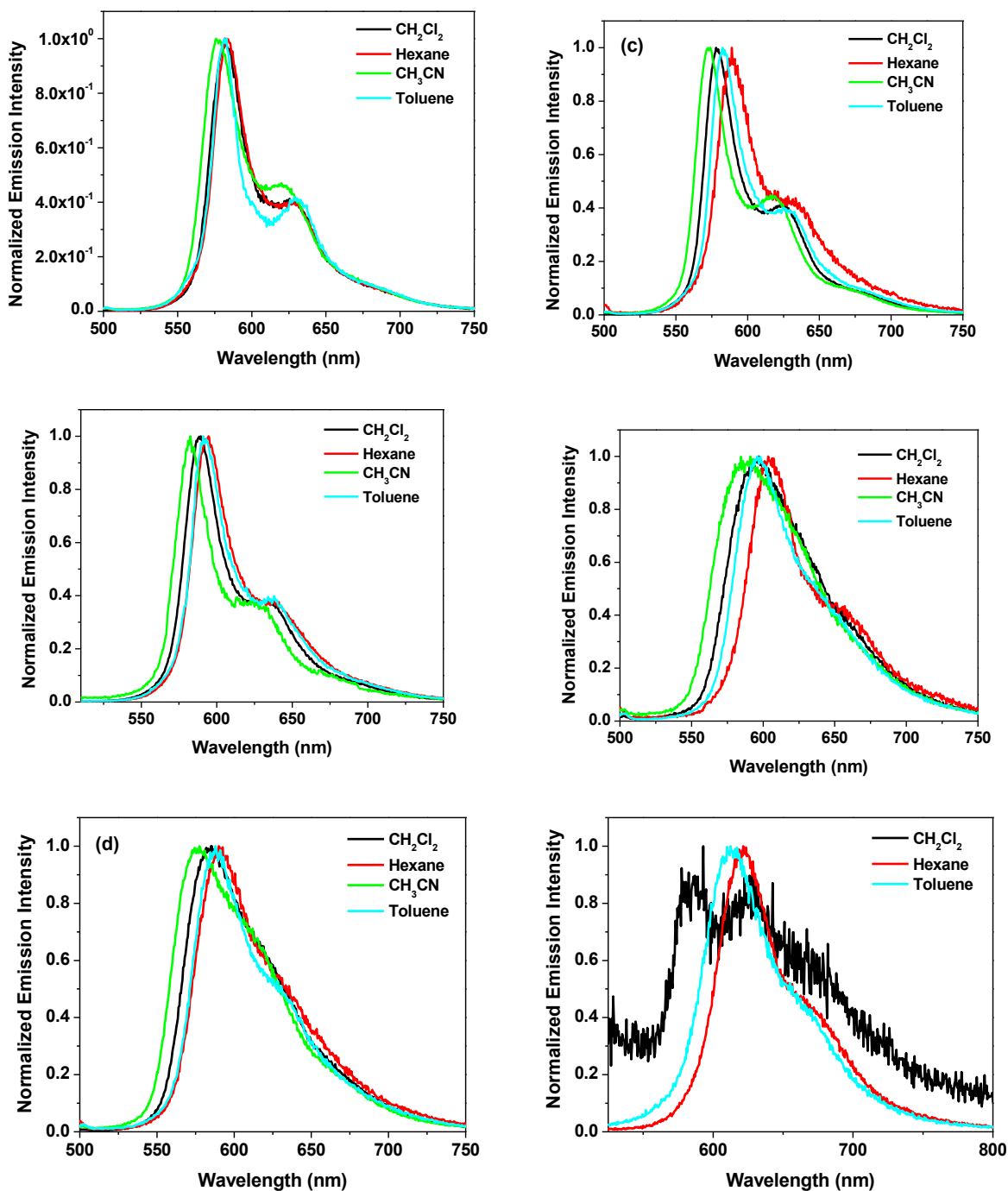
Figure 3.8. Normalized emission spectra of **3-1** – **3-6** (λ_{ex} = 436 nm) in different solvents.

Complexes **3-1**, **3-2**, and **3-3** exhibit well-structured emission at room temperature (Figure 3.6b) with the band maximum at 582 nm, 579 nm, and 588 nm, respectively, which show somewhat negative solvatochromic effect as shown in Figure 3.8. The vibronic progressions are 1208, 1220, and 1234 cm^{-1} for **3-1**, **3-2**, and **3-3**, respectively, and the emission lifetimes of **3-1** – **3-3** are in the range of 5.3 μs – 6.1 μs. These features suggest

that the emission of complexes **3-1**, **3-2**, and **3-3** emanate predominantly from the ligand-localized $^3\pi,\pi*$ state. This assignment is confirmed by the calculated NTOs contributing to the lowest-energy triplet transition, as shown in Table 3.8. However, the calculated NTOs suggest that the emission of **3-1** and **3-2** has some contributions from the ^{3}MLCT states. In contrast, the emission spectra of **3-4**, **3-5**, and **3-6** are broad and less structured (or structureless for **3-3 – 3-6**) in CH_2Cl_2 solution at room temperature (as shown in Figure 3.6b), with apparently shorter lifetimes (*i.e.* 1.33 μs for **3-4** and 2.10 μs for **3-5**, and the lifetime for **3-6** was unable to be measured due to very weak signal) and lower quantum yields (see Table 3.6). The emission of **3-4** and **3-5** shows a negative solvatochromic effect in different solvents, as shown in Figure 3.8. The emission of complex **3-6** was substantially quenched in polar solvents such as CH_2Cl_2 and CH_3CN. Taking all these facts into account, we conclude that the emission of **3-4**, **3-5**, and **3-6** has significant contribution from a triplet charge transfer state. Our TD-DFT calculations confirm that the triplet transitions of complexes **3-4** and **3-5** admix ^{3}MLCT/$^3\pi,\pi*$ characters, while the triplet transition of **3-6** primarily has ^{3}ILCT character, which are quite distinct from the $^3\pi,\pi*$ dominated character of the triplet transitions in complexes **3-1 – 3-3**, as illustrated in Table 3.8.

The emission of **3-1 – 3-6** at room temperature is concentration-dependent. As exemplified in Figure 3.9 for complex **3-1**, the emission intensity increases in the concentration range of 1×10^{-6} - 2×10^{-5} mol/L, but decreases when the concentration is higher than 2×10^{-5} mol/L. Meanwhile, the emission lifetime keeps decreasing with increased concentration. Both facts suggest the occurrence of self-quenching in these complexes. The self-quenching rate constants deduced for **3-1 – 3-6** are provided in Table 3.6, which are on the order of 10^9 L.mol^{-1}.s^{-1} and are in line with those reported in literatures for other Pt(II) terdentate or diimine complexes.[16, 17, 71 - 76] On the other hand, in view of the strong

absorption at the respective excitation wavelength of each complex, the reduced emission

intensity at high concentrations should also have contribution from primary inner-filter effect.
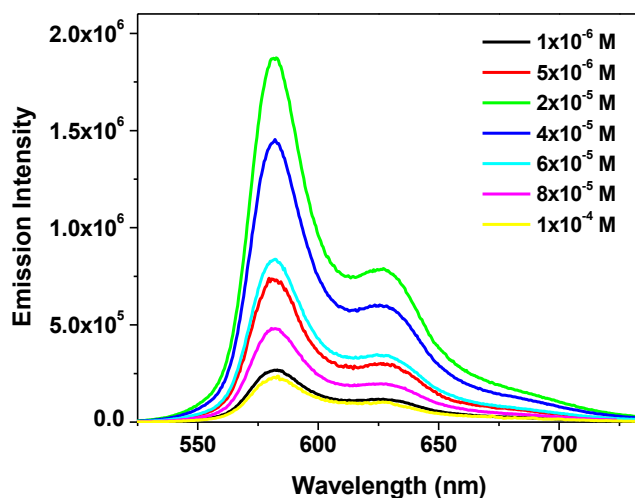
Figure 3.9. Concentration-dependent emission spectra of **3-1** in CH$_2$Cl$_2$. λ_{ex}= 372 nm.

Table 3.6. Emission and excited-state absorption parameters for complexes **3-1 – 3-6** and ligands **3-1-L – 3-6-L.**

	λ_{em}/nm (τ_0/μs; k_{sq}/L.mol^{-1}.s^{-1}); Φ_{em}[a] R. T.	λ_{em}/nm (τ_{em}/μs)[b] 77 K	$\lambda_{T_1-T_n}$/nm (τ_T/μs; $\varepsilon_{T_1-T_n}$/M^{-1} cm^{-1}; Φ_T)[c]	$^{theor}\lambda_{phos}$/nm
1	582 (6.0; 2.04×10^9), 626 (6.2; 1.83×10^9); 0.077	573 (15.7), 621 (16.0)	655 (6.1; 18530; 0.56)	621
2	579 (5.3; 1.46×10^9), 623 (5.5; 1.62×10^9); 0.11	569 (19.3), 617 (19.3)	580 (5.5; 27910; 0.40)	621
3	588 (6.1; 1.44×10^9), 634 (6.1; 9.33×10^8); 0.092	581 (24.0), 630 (28.0)	625 (8.2; 56980; 0.33)	634
4	595 (1.3; 3.49×10^9); 0.031	565 (22.1), 610 (20.0)	555 (2.1; 14870; 0.50)	600
5	584 (2.1; 2.00×10^9); 0.06	564 (21.5), 609 (21.2)	560 (3.8; 13170; 0.32)	601
6	638 (-); 0.003	583 (24.9), 629 (20.9)	530 (1.4; 35680; 0.38), 755 (1.1; 20990; 0.38)	618
1-L	414 (-), 483 (-); -	530, 572	655 (18.6; -; -)	
2-L	383 (-); 0.066	378, 515, 549	535 (4.9; -; -)	
3-L	410 (-); 0.80	410	580 (5.4; -; -)	
4-L	378 (-); 0.69	385	520 (10.1; -; -)	
5-L	401 (-); 0.91	388	445 (10.0; -; -)	
6-L	444 (-); 0.84	425	460 (-; -; -)	
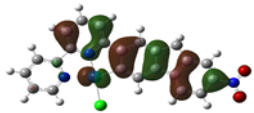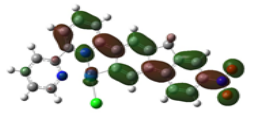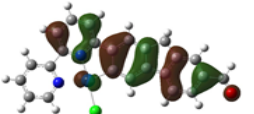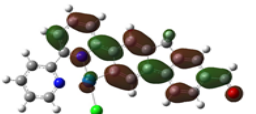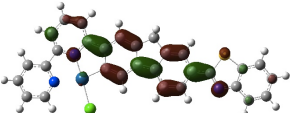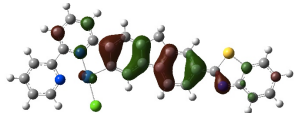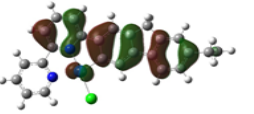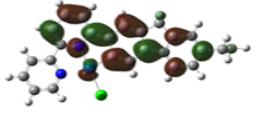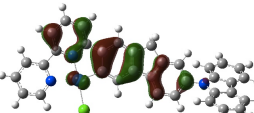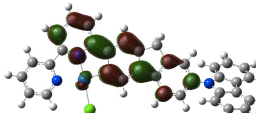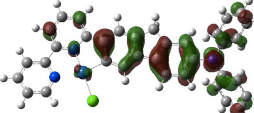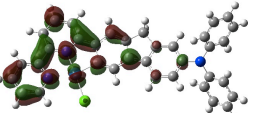
[a]Emission wavelength (λ_{em}), intrinsic lifetime (τ_0), self-quenching rate constant (k_{sq}), and emission quantum yield measured in CH$_2$Cl$_2$. [b]In BuCN glassy matrix. [c]Triplet excited-state absorption band maximum ($\lambda_{T_1-T_n}$), molar extinction coefficient ($\varepsilon_{T_1-T_n}$), quantum yield (Φ_T) and lifetime (τ_T) measured in CH$_3$CN for **3-1 – 3-5**; **3-6** was measured in toluene.

Table 3.7. Fluorescence quantum yields of **3-1-L – 3-6-L** in different solvents[a]; and Emission quantum yields of **3-1 – 3-6** in different solvents[b]

	CH$_2$Cl$_2$	Hexane	CH$_3$CN	THF	Toluene
3-1-L	-[c]	-[c]	-[c]	-[c]	-[c]
3-2-L	0.066	0.060	0.058	0.062	0.068
3-3-L	0.795	0.727	0.783	0.785	0.800
3-4-L	0.693	0.624	0.498	0.606	0.713
3-5-L	0.907	0.819	0.806	0.875	0.888
3-6-L	0.836	0.684	0.363	0.835	0.826
3-1	0.077	0.036	0.054		0.062
3-2	0.11	0.015	0.087		0.059
3-3	0.092	0.037	0.02		0.064
3-4	0.031	0.01	0.024		0.034
3-5	0.060	0.028	0.048		0.035
3-6	-	0.021	-		0.028

[a]1 N sulfuric acid solution of quinine bisulfate (Φ_{em} = 0.546, λ_{ex} = 347.5 nm) was used as the reference. [b]Degassed aqueous solution of [Ru(bpy)$_3$]Cl$_2$ (Φ_{em} = 0.042, λ_{ex} = 436 nm) was used as the reference. [c]Too weak to be measured.

Table 3.8. Natural transition orbitals representing the lowest-energy triplet transitions for complexes **3-1 – 3-6**.

	Triplet Energy	Hole	Electron
1	2.00 eV (621 nm)		
2	2.00 eV (621 nm)		
3	1.96 eV (634 nm)		
4	2.07 eV (600 nm)		
5	2.06 eV (601 nm)		
6	2.01 eV (618 nm)		

The emission of **3-1 – 3-6** at 77 K was investigated in butyronitrile glassy matrix and

the results are provided in Figure 3.6d and in Table 3.6. The emission spectra at 77 K for all

complexes are blue-shifted, more structured and become narrower with respect to their corresponding emission spectra at room temperature, reflecting the rigidochromic effect.[67 - 70] The thermally-induced Stokes shifts are 270 cm^{-1} for **3-1**, 304 cm^{-1} for **3-2**, 205 cm^{-1} for **3-3**, 892 cm^{-1} for **3-4**, 607 cm^{-1} for **3-5**, and 1479 cm^{-1} for **3-6**. The much smaller thermally-induced Stokes shifts for **3-1** – **3-3** are consistent with the $^3\pi,\pi^*$ dominated nature of the emission, and the large Stokes shift for **3-6** is in accordance with the charge transfer character in the emitting triplet excited state. The moderate Stokes shifts in **3-4** and **3-5** also reflect the mixed ^{3}MLCT/$^3\pi,\pi^*$ characters in their emitting states.

3.3.4. Transient Absorption

The nanosecond transient absorption (TA) measurements were conducted for ligands **3-1-L** – **3-6-L** and complexes **3-1** – **3-6**. The following information can be obtained through the TA experiments: (1) the spectral feature of the triplet excited-state absorption; (2) the spectral region where the excited state absorbs strongly than the ground state (can be identified from the positive absorption band(s) of the TA spectrum); (3) the excited-state lifetime (can be deduced from the decay of the TA); and (4) the triplet excited-state quantum yield (can be determined by the relative actinometry). The nanosecond TA spectra of ligands **3-1-L** – **3-6-L** at zero delay after excitation are illustrated in Figure 3.9.

All compounds exhibit moderate to strong transient absorption in the visible to the NIR spectral region. Two trends are emerged by examining the shape of the TA spectra of these compounds. First, the TA band maxima of the compounds with electron-withdrawing substituents (**3-1-L** – **3-3-L**) are obviously red-shifted compared to those of **3-4-L** – **3-6-L** that contain electron-donating substituents. Secondly, the TA spectra of **3-1-L**, **3-5-L** and **3-6-L** consist of two major absorption bands with a relatively narrower band between 400 and 500 nm, and a broader band above 500 nm (Figures 3.10). Considering these different features, we tentatively attribute the observed TA to the $^3\pi,\pi^*$ states for these compounds.

116

However, for **1-L**, **5-L** and **6-L**, ^{3}ILCT could also contribute significantly to the observed TA in view of the facile intraligand charge transfer that could admix the ^{3}ILCT character into the $^3\pi,\pi^*$ states.
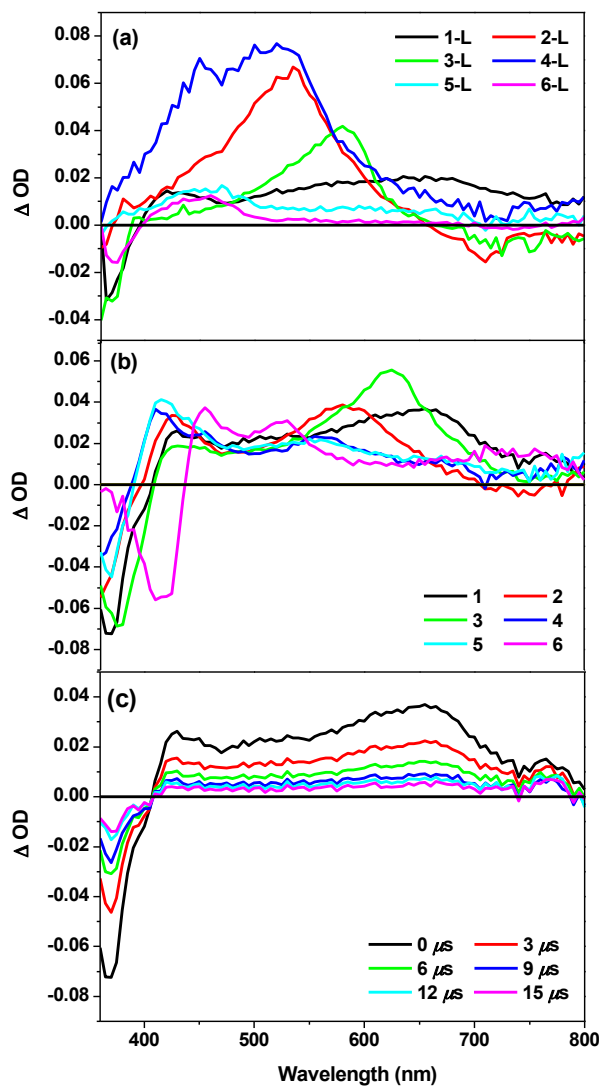
Figure 3.10. Nanosecond transient difference absorption spectra of (a) ligands **3-1-L** – **3-6-L** and (b) complexes **3-1** – **3-6** at zero delay after excitation; (c) time-resolved TA spectra of **3-1-L** – **3-5-L** and **3-1** – **3-5** were measured in CH$_3$CN, **3-6-L** and **3-6** were measured in toluene. λ_{ex} = 355 nm, A_{355} = 0.4 in a 1-cm cuvette.

Figure 3.9b shows the TA spectra of complexes **3-1** – **3-6** at zero delay after excitation. The time-resolved TA spectrum of **3-1** is illustrated in Figure 3.9c, while the others are provided in Figures 3.10.
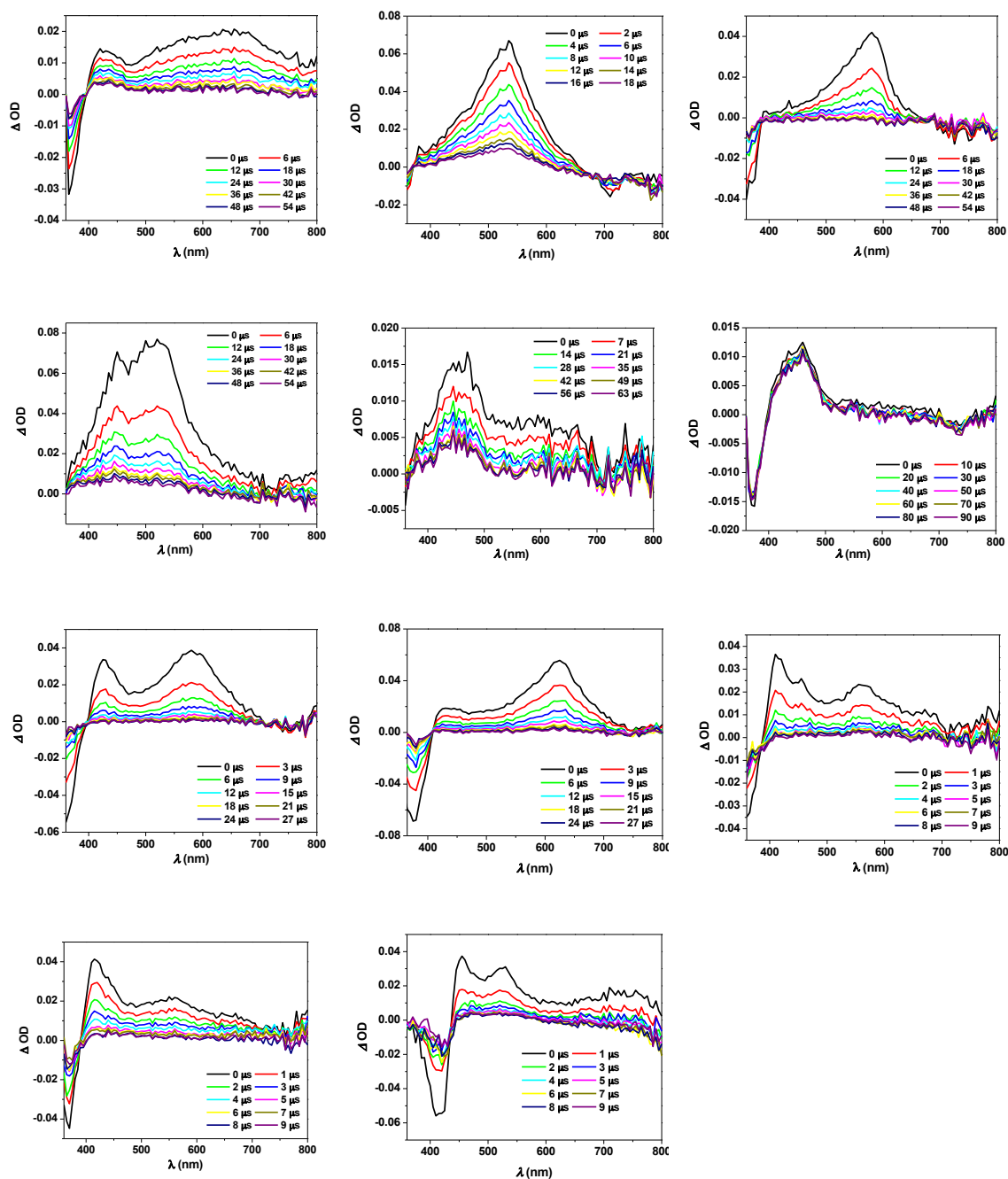
Figure 3.11. Nanosecond time-resolved transient difference absorption spectra of **3-1-L** – **3-6-L**, and **3-2** – **3-6** (**3-6**, in toluene, others in CH$_3$CN) are shown. λ_{ex} = 355 nm.

The TA spectra for all complexes feature two major absorption bands, a narrower one between 400 and 500 nm and a broader one above 500 nm. The low-energy TA bands are stronger than the 400-500 nm absorption bands in **3-1** – **3-3**, but the relative intensity of these two bands is opposite in **3-4** – **3-6**. Compared to the TA spectra of their respective ligands, the low-energy absorption bands of the TA spectra for these complexes are red-shifted, indicating electron delocalization induced by the interaction of Pt(II) center with the ligand.

For all complexes, bleaching occurs at $\lambda < 430$ nm, which is consistent with the position of the major absorption band in their respective UV-vis absorption spectra. The triplet lifetimes deduced from the decay of the TA (Table 3.6) for these complexes are similar to those obtained from the decay of emission, implying that the excited state giving rise to the observed TA could be the same excited state that emits. Based on these features, we tentatively ascribe the TA of **3-1** – **3-5** being predominantly from their $^3\pi,\pi^*$ states, with possible contributions from the ^{3}MLCT states for **3-1**, **3-2**, **3-4** and **3-5**. For complex **3-6**, the TA in CH$_3$CN was too weak to be detected. However, moderately strong TA spectrum was observed in toluene. The absence of TA in polar solvent like CH$_3$CN and the shorter lifetime ($\tau_T = 1.4$ μs in toluene) suggest the charge transfer nature of the triplet excited state that gives rise to the observed TA. Considering the nature of the emitting state of **3-6** discussed earlier, we believe the TA of **3-6** predominantly arises from the ^{3}ILCT state.

3.3.5. Reverse Saturable Absorption

The TA spectra of **3-1** – **3-6** indicate that all complexes exhibit positive absorption at 532 nm, suggesting stronger excited-state absorption than that of the ground state. In addition, the triplet excited-state lifetimes for these complexes are much longer than the ns laser pulse width (4.1 ns). These provide the necessary conditions for reverse saturable absorption (RSA, defined as a decreased transmission upon increase of incident energy) to occur for ns laser pulse at 532 nm. To demonstrate this, nonlinear transmission experiment using complexes **3-1** – **3-6** at 532 nm for ns laser pulses was carried out in CH$_2$Cl$_2$ solution at a linear transmittance of 90% in a 2-mm cuvette. For comparison purpose, the RSA of complex **1** in Ref. 34, which has the similar structure to that of complex **3-3** in this work but with a tolylacetylide co-ligand instead of Cl co-ligand, was also measured under the same experimental condition. The results are displayed in Figure 3.11. The transmission of the complexes drastically decreases with increased incident energy, a clear indication of strong

RSA. The degree of RSA of these complexes increases in the order of **3-4** $\approx$ **3-5** < **3-1** $\approx$ **3-3** < **3-2** < **3-6**, and the RSA of **3-3** is slightly better than complex **1** in Ref. 34. It appears that the RSA is generally stronger in complexes with electron-withdrawing substituents (**3-1** – **3-3**) than in complexes with electron-donating substituents except for **3-6**, which contains the strongest electron-donating substituent. The strongest RSA from **3-6** should be related to its stronger excited-state absorption at 532 nm, which is evident by its TA spectrum, in which one of the absorption bands occurs at ca. 530 nm.
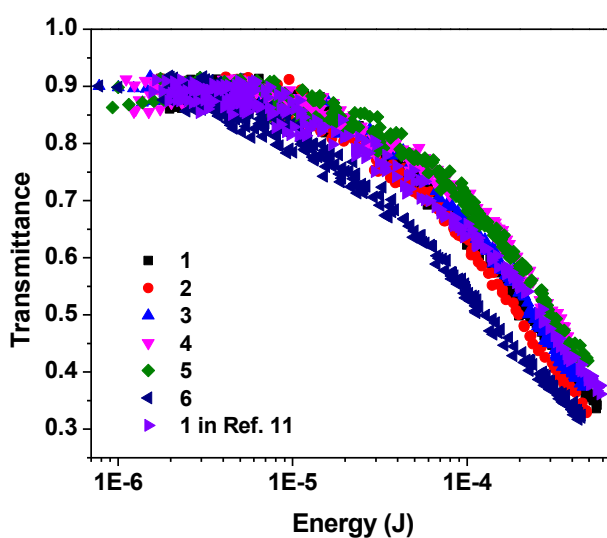
Figure 3.12. Nonlinear transmission curves for **3-1** – **3-6** and complex **1** in Ref. 34 in CH_2Cl_2 in a 2 mm cuvette for 4.1 ns laser pulses at 532 nm. The radius of the beam waist at the focal point was approximately 96 μm. The linear transmission for all samples was adjusted to 90% in a 2 mm cuvette.

To better rationalize the observed RSA trend of these complexes at 532 nm for ns laser irradiation, the ratios of the excited-state absorption cross section (σ_{ex}) relative to the ground-state absorption cross section (σ_0) (which is a key parameter for RSA) at 532 nm for **3-1** – **3-6** have to be evaluated. The σ_{ex} values at 532 nm can be estimated from the ΔODs of the ns TA at zero delay at 532 nm and at the TA band maximum ($\lambda_{T_1-T_n}$), the ground-state absorbance (A) at 532 nm and at the TA band maximum of the same solution for the TA measurement, and the molar extinction coefficient ($\varepsilon_{T_1-T_n}$) at the TA band maximum, as well

as the conversion equation $\sigma = 3.82 \times 10^{-21} \varepsilon$. The detailed procedure for the estimation of these values follows that described by our group previously.[27] The σ_0 values at 532 nm can be deduced from the ground-state absorption molar extinction coefficients using $\sigma = 3.82 \times 10^{-21} \varepsilon$. The resultant σ_{ex} and σ_0 values as well as the ratios of σ_{ex}/σ_0 are compiled in Table 3.9. It is obvious that the σ_{ex}/σ_0 values follow the trend of **4 < 5 < 1 < 3 < 2 < 6**, which correlates very well with the trend of the RSA plots of these complexes. The correspondence between the σ_{ex}/σ_0 values and RSA performances indicates that the RSA mainly arises from the triplet excited states of the complexes. This notion is quite reasonable because the fs TA study on complex **1** in Ref. 34 found that intersystem crossing from the singlet to triplet excited states occurs in ~88 ps ($\tau_{isc} = \tau_s/\Phi_T$); and during the ns excitation, the triplet excited state is the dominant contributor based on the calculated fractional populations of the affected excited states.[34] Considering the similar core structure of complexes **3-1 – 3-6** to that of complex **1** in Ref. 34, it is reasonable to assume that the dominant contributing excited state to the RSA within the ns pulse width should be the triplet excited states for **3-1 – 3-6** as well. Complex **3-6** possesses the strongest triplet excited-state absorption at 532 nm and thus the strongest RSA. The σ_{ex}/σ_0 value for complex **3-3** is also much larger than that for its counterpart with the tolylacetylide ligand (*i.e.* complex **1** in Ref. 34), which has $\sigma_T/\sigma_0 = 69.6$.[34] The much larger ratio for complex **3-3** should be mainly due to the significantly reduced ground-state absorption cross section of **3-3** at 532 nm ($\sigma_0 = 4.3 \times 10^{-19}$ cm^2) with respect to complex **1** in Ref. 34 ($\sigma_0 = 1.48 \times 10^{-18}$ cm^2). This confirms our initial design concept that replacing the tolylacetylide co-ligand with Cl co-ligand could reduce the ground-state absorption in the visible spectral region and thus increase the σ_{ex}/σ_0 ratio and enhance the RSA in the visible spectral region. It is also worth noting that the σ_{ex}/σ_0 ratios for **3-1 – 3-6** are much larger than those of most of the reverse saturable absorbers reported in the literature;[16,17, 22, 23, 20, 34, 72, 73, 77 – 83] and the σ_{ex}/σ_0 value for **3-6** is among the largest value reported to date.

Table 3.9. Ground-state (σ_0) and excited-state (σ_{ex}) absorption cross sections for complexes **3-1 − 3-6** at 532 nm.

	3-1	**3-2**	**3-3**	**3-4**	**3-5**	**3-6**
σ_0/ 10^{-18} cm^2 ^{a}	0.27	0.27	0.43	0.38	0.38	0.88
σ_{ex} /10^{-18} cm^2 ^{b}	46	67	80	44	46	230
σ_{ex}/σ_0	170	248	186	116	121	261

^{a} In CH$_2$Cl$_2$; ^{b}**3-1**–**3-5** in CH$_3$CN and **3-6** in toluene.

3.4. Conclusion

Six new Pt(II) complexes (**3-1 − 3-6**) containing 6-[7-*R*-9,9-di(2-ethylhexyl)-9*H*-fluoren-2-yl]-2,2'-bipyridine (R = NO$_2$, CHO, benzothiazol-2-yl, *n*-Bu, carbazol-9-yl, NPh$_2$) ligands were synthesized, and their photophysics were systematically investigated by spectroscopic techniques and TDDFT theoretical calculations. The absorption and emission characteristics of **3-1 − 3-6** can be substantially adjusted by the 7-substituent. It is found that electron-withdrawing substituents (NO$_2$, CHO, BTZ) and electron-donating substituents (*n*-Bu, CBZ, NPh$_2$) exert distinct effects on the photophysics of the complexes. The lowest-energy absorption bands of **3-1 − 3-6** all feature ^{1}MLCT/^{1}ILCT/$^1\pi,\pi^*$ characters, while the contributions of ^{1}MLCT, ^{1}LLCT, $^1\pi,\pi^*$ and ^{1}ILCT configurations to the major absorption band(s) vary depending on the nature of the substituent. The different substituents influence the nature of the lowest triplet excited states of **3-1 − 3-6** more distinctively, reflected by the fact that the emitting excited state of complexes **3-1 − 3-3** is dominated by the $^3\pi,\pi^*$ characters with a little contribution from ^{3}MLCT in **3-1** and **3-2**, while the emission of **3-4** and **3-5** admixes ^{3}MLCT/$^3\pi,\pi^*$ characters, and **3-6** primarily exhibits very weak ^{3}ILCT emission. It appears that the $^3\pi,\pi^*$ character diminishes while charge transfer character increases when the strength of electron-donating substituent increases. All complexes exhibit broad and strong triplet excited-state absorption from the near-UV to the near-IR spectral region, which originates from the same triplet excited state that emits. The TA band maxima are red-shifted for complexes **3-1 − 3-3** (which possess the electron-withdrawing substituents) compared to those of **3-4 − 3-6** (which contain electron-donating substituents). Due to the

much stronger triplet excited-state absorption than the ground-state absorption of **3-1** – **3-6** in the visible spectral region, all complexes exhibit strong reverse saturable absorption for ns laser pulse at 532 nm, with complex **3-6** showing the strongest RSA due to its strongest excited-state absorption at 532 nm and thus the largest ratio of σ_{ex}/σ_0. The σ_{ex}/σ_0 ratios for the other five complexes are also much larger than most of the reverse saturable absorbers reported in the literature at 532 nm. This makes complexes **3-1** – **3-6**, especially **3-6,** very promising candidates for devices that require strong RSA.

3.5. References

[1] Williams, J. A. G. *Top. Curr. Chem.* **2007**, *281*, 205.

[2] Dhar, S.; Lippard, S. J. *Bioinorganic Medicinal Chemistry*; Wiley-VCH Verlag GmbH & Co. KGaA, Weinheim, Germany, **2010**.

[3] (a) Chan, S. C.; Chan, M. C. W.; Wang, Y.; Che, C. M.; Cheung, K. K.; Zhu, N. *Chem. Eur. J.* **2001**, *7*, 4180.

[4] (b) Lu, W.; Mi, B. X.; Chan, M. C. W.; Hui, Z.; Che, C. M.; Zhu, N.; Lee, S. T. *J. Am. Chem. Soc.* **2004**, *126*, 4958.

[5] Chakraborty, S.; Wadas, T. J.; Hester, H.; Flaschenreim, C.; Schmehl, R.; Eisenberg, R. *Inorg. Chem.* **2005**, *44*, 6865.

[6] Taranekar, P.; Qiao, Q.; Jiang, H.; Ghiviriga, I.; Schanze, K. S.; Reynolds, J. R. *J. Am. Chem. Soc.* **2007**, *129*, 8958.

[7] Kwok, E. C.-H.; Chan, M.-Y.; Wong, K. M.-C.; Lam, W. H.; Yam, V. W.-W. *Chem. Eur. J.* **2010**, *16*, 12244.

[8] Zhang, H.; Zhang, B.; Li, Y.; Sun, W. *Inorg. Chem.* **2009**, *48*, 3617.

[9] Grove, L. J.; Rennekamp, J. M.; Jude, H.; Connick, W. B. *J. Am. Chem. Soc.* **2004**, *126*, 1594.

[10] Mathew, I.; Sun, W. *Dalton Trans.* **2010**, *39*, 5885.

[11] Ji, Z.; Li, Y.; Sun, W. *J. Organometallic Chem.* **2009**, *694*, 4140.

[12] Lu, W.; Chan, M. C. W.; Zhu, N.; Che, C.-M.; He, Z.; Wong, K. Y. *Chem. Eur. J.* **2003**, *9*, 6155.

[13] Wong, K. M.; Tang, W.-S.; Lu, X.-X.; Zhu, N.; Yam, V. W.-W. *Inorg. Chem.* **2005**, *44*, 1492.

[14] Yang, Q.-Z.; Wu, L.-Z.; Zhang, H.; Chen, B.; Wu, Z.-X.; Zhang, L.-P.; Tung, Z.-H. *Inorg. Chem.* **2004**, *43*, 5195.

[15] Sun, W.; Zhang, B.; Li, Y.; Pritchett, T. M.; Li, Z.; Haley, J. E. *Chem. Mater.* **2010**, *122*, 6384.

[16] Guo, F.; Sun, W.; Liu, Y.; Schanze, K. *Inorg. Chem.* **2005**, *44*, 4055.

[17] Shao, P.; Li, Y.; Yi, J.; Pritchett, T. M.; Sun, W. *Inorg. Chem*. **2010**, *49*, 4507.

[18] Ji, Z.; Li, Y.; Pritchett, T. M.; Makarov, N. S.; Haley, J. E.; Li, Z.; Drobizhev, M.; Rebane, A.; Sun, W. *Chem*. *Eur. J.* **2011**, *17*, 2479.

[19] Rogers, J. E.; Slagle, J. E.; Krein, D. M.; Burke, A. R.; Hall, B. C.; Fratini, A.; McLean, D. G.; Fleitz, P. A.; Cooper, T. M.; Drobizhev, M.; Makarov, N. S.; Rebane, A.; Kim, K.-Y.; Farley, R.; Schanze, K. S. *Inorg. Chem.* **2007**, *46*, 6483.

[20] Pritchett, T. M.; Sun, W.; Guo, F.; Zhang, B.; Ferry, M. J.; Rogers-Haley, J. E.; Shensky; W. III; Mott, A. G. *Opt. Lett.* **2008**, *33*, 1053.

[21] Shao, P.; Li, Y.; Sun, W. *J. Phys. Chem. A*. **2008**, *112*, 1172.

[22] Sun, W.; Zhu, H.; Barron, P. M. *Chem. Mater*. **2006**, *18*, 2602.

[23] Liu, R.; Li, Y.; Li, Y.; Zhu, H.; Sun, W. *J. Phys. Chem. A* **2010**, *114*, 12639.

[24] Liu, R.; Azenkeng, A.; Li, Y.; Sun, W. *Dalton Trans.* **2010**, *41*, 12353.

[25] Liu, R.; Zhou, D.; Azenkeng, A.; Li, Z.; Li, Y.; Glusac, K. D.; Sun, W. *Chem. Eur. J.* **2012**, *18*, 11440.

[26] Zhang, B.; Li, Y.; Liu, R.; Pritchett, T. M.; Haley, J. E.; Sun, W. *ACS Appl. Mater. Interfaces* **2013**, *5*, 565.

[27] Li, Y.; Liu, R.; Badaeva, E.; Kilina, S.; Sun, W. *J. Phys. Chem. C* **2013**, *117*, 5908.

[28] Liu, R.; Dandu, N.; Li, Y.; Kilina, S.; Sun, W. *Dalton Trans*. **2013**, *42*, 4398.

[29] Li, Z.; Badaeva, E.; Zhou, D.; Bjorgaard, J.; Glusac, K.; Killina, S.; Sun, W. *J. Phys. Chem. A*. **2012**, *116*, 4878.

[30] Liu, R.; Azenkeng, A.; Zhou, D.; Li, Y.; Glusac, K. D.; Sun, W. *J. Phys. Chem. A* **2013**, *117*, 1907.

[31] Dubinina, G. G.; Price, R. S.; Abboud, K. A.; Wicks G.; Wnuk, P.; Stepanenko, Y.; Drobizhev, M.; Rebane, A.; Schanze, K. S. *J. Am. Chem. Soc.* **2012**, *134*, 19346.

[32] Andrews, L. J. *J. Phys. Chem.* **1979**, *83*, 3203.

[33] McMillin, D. R.; Moore, J. J. *Coord. Chem. Rev.* **2002**, *229*, 113.

[34] Zhang, B.; Li, Y.; Liu, R.; Pritchett, T. M.; Azenkeng, A.; Ugrinov, A.; Haley, J. E.; Li, Z.; Hoffmann, M. R.; Sun, W. *Chem. Eur. J.* **2012**, *18*, 4593.

[35] Maji, M. S.; Pfeifer, T.; Studer, A. *Chem. Eur. J.* **2010**, *16*, 5872.

[36] Montes, V. A.; Perez-Bolivar, C.; Agarwal, N.; Shinar, J.; Anzenbacher, P. Jr. *J. Am. Chem. Soc.* **2006**, *128*, 12436.

[37] Van der Pol, C.; Bryce, M. R.; Wielopolski, M.; Atienza-Castellanos, C.; Guldi, D. M.; Filippone, S.; Martin, N. *J. Org. Chem.* **2007**, *72*, 6662.

[38] Peterson, J. J.; Werre, M.; Simon, Y. C.; Coughlin, E. B.; Carter, K. R. *Macromolecules*. **2009**, *42*, 8594.

[39] Dudek, S. P.; Pouderoijen, M.; Abbel, R.; Schenning, A. P. H. J.; Meijer, E. W. *J. Am. Chem. Soc.* **2005**, *127*, 11763.

[40] Kannan, R.; He, G. S.; Yuan, L.; Xu, F.; Prasad, P. N.; Dombroskie, A. G.; Reinhardt, B. A.; Baur, J. W.; Vaia, R. A.; Tan, L-S. *Chem. Mater.* **2001**, *13*, 1896.

[41] Fisher, A. L.; Linton, K. E.; Kamtekar, K. T.; Pearson, C.; Bryce, M. R.; Petty, M. C. *Chem. Mater.* **2011**, *23*, 1640.

[42] Sonntag, M.; Strohriegl, P. *Liq. Crys.* **2007**, *34*, 49.

[43] Shin, D.; Switzer, C. *Chem. Commun.* **2007**, *42*, 4401.

[44] Bruker Analytical X-ray Systems, Madison, WI, 2010.

[45] Sheldrick, G. M. *Acta Cryst.* **2008**, *A64*, 112.

[46] Blessing, R. H. *Acta Cryst.* **1995**, *A51*, 33.

[47] Demas, J. N.; Crosby, G. A. *J. Phys. Chem.* **1971**, *75*, 991.

[48] Van Houten, J.; Watts, R. *J. Am. Chem. Soc.* **1976**, *98*, 4853.

[49] Eaton, D. F. *Pure Appl. Chem.* **1988**, *60*, 1107.

[50] Carmichael, I.; Hug, G. L. *J. Phys. Chem. Ref. Data.* **1986**, *15*, 1.

[51] Firey, P. A.; Ford, W. E.; Sounik, J. R.; Kenney, M. E.; Rodgers, M. A. J. *J. Am. Chem. Soc.* **1988**, *110,* 7626.

[52] Frisch, M. J.; Trucks, G. W.; Schlegel, H. B.; Scuseria, G. E.; Robb, M. A.; Cheeseman, J. R.; Scalmani, G.; Barone, V.; Mennucci, B.; Petersson, G. A.; Nakatsuji, H.; Caricato, M.; Li, X.; Hratchian, H. P.; Izmaylov, A. F.; Bloino, J.; Zheng, G.; Sonnenberg, J. L.; Hada, M.; Ehara, M.; Toyota, K.; Fukuda, R.; Hasegawa, J.; Ishida, M.; Nakajima, T.; Honda, Y.; Kitao, O.; Nakai, H.; Vreven, T.; Montgomery, Jr., J. A.; Peralta, J. E.; Ogliaro, F.; Bearpark, M.; Heyd, J. J.; Brothers, E.; Kudin, K. N.; Staroverov, V. N.; Kobayashi, R.; Normand, J.; Raghavachari, K.; Rendell, A.; Burant, J. C.; Iyengar, S. S.; Tomasi, J.; Cossi, M.; Rega, N.; Millam, N. J.; Klene, M.; Knox, J. E.; Cross, J. B.; Bakken, V.; Adamo, C.; Jaramillo, J.; Gomperts, R.; Stratmann, R. E.; Yazyev, O.; Austin, A. J.; Cammi, R.; Pomelli, C.; Ochterski, J. W.; Martin, R. L.; Morokuma, K.; Zakrzewski, V. G.; Voth, G. A.; Salvador, P.; Dannenberg, J. J.; Dapprich, S.; Daniels, A. D.; Farkas, Ö.; Foresman, J. B.; Ortiz, J. V.; Cioslowski, J.; Fox, D. J. Gaussian 09, Revision A.1, Gaussian, Inc., Wallingford CT, 2009.

[53] Yanai, T.; Tew, D.; Handy, N. *Chem. Phys. Lett.* **2004**, *393*, 51.

[54] Roy, L. E.; Hay, P. J.; Martin, R. L. *J. Comp. Theor. Chem.* **2008**, *4*, 1029.

[55] Roy, L. E.; Scalmani, G.; Kobayashi, R.; Batista, E. R. *Dalton Trans.* **2009**, 6719.

[56] Peach, M. J. G.; Benfield, P.; Helgaker, T.; Tozer, D. J. *J. Chem. Phys.* **2008**, *128,* 044118.

[57] Vlček, A. Jr.; Záliš, S. *Coord. Chem. Rev.* **2007**, *251*, 258.

[58] Barone, V.; Cossi, M.; Tomasi, J. *J. Comput. Chem.* **1998**, *19*, 404.

[59] Cossi, M.; Rega, N.; Scalmani, G.; Barone, V. *J. Comput. Chem.* **2003**, *24*, 669.

[60] Batista, E. R.; Martin, R. L. *J. Phys. Chem. A.* **2005**, *109*, 3128.

[61] Fantacci, S.; De Angelis, F.; Selloni, A. *J. Am. Chem. Soc.* **2003**, *125*, 4381.

[62] Filippo, D. A.; Simona, F.; Annabella, S. *Chem. Phys. Lett.* **2004**, *389*, 204.

[63] Furche, F.; Ahlrichs, R. *J. Chem. Phys.* **2002**, *117*, 7433.

[64] Martin, R. L. *J. Chem. Phys.* **2003**, *118*, 4775.

[65] GaussView Version 4.1, Dennington-II, R.; Keith, T.; Millam, J., Semichem Inc., Shawnee Mission, KS, 2007.

[66] Stork, J. R.; Olmstead, M. M.; Balch, A. L. *Inorg. Chem.* **2004**, *43*, 7508.

[67] Juris, A.; Balzani, V.; Barigelletti, F.; Campagna, S.; Belser, P.; Von Zelewsky, A. *Coord. Chem. Rev.* **1988**, *84*, 85.

[68] Cummings, S. D.; Eisenberg, R. *J. Am. Chem. Soc.* **1996**, *118*, 1949.

[69] Polo, A. S.; Itokazu, M. K.; Frin, K. M.; Patrocinio, A. O. de T.; Iha, N. Y. M. *Coord. Chem. Rev.* **2006**, *250*, 1669.

[70] Lai, S.-W.; Chan, M. C. W.; Cheung, K.-K.; Che, C.-M. *Inorg. Chem.* **1999**, *38*, 4262.

[71] Hissler, M.; Connick, W. B.; Geiger, D. K.; McGarrah, J. E.; Lipa, D.; Lachicotte, R. J.; Eisenberg, R. *Inorg. Chem.* **2000**, *39*, 447.

[72] Shao, P.; Li, Y.; Sun, W. *Organometallics* **2008**, *27*, 2743.

[73] Ji. Z.; Li. Y.; Sun, W. *Inorg. Chem.* **2008**, *47*, 7599.

[74] Shao, P.; Li, Y.; Azenkeng, A.; Hoffmann, M.; Sun, W. *Inorg. Chem.*. **2009**, *48*, 2407.

[75] Lai, S.-W.; Chan, M. C.-W.; Cheung, T.-C.; Peng, S.-M.; Che, C.-M. *Inorg. Chem*. **1999**, *38*, 4046.

[76] Yam, V. W.-W.; Tang, R. P.-L.; Wong, K. M.-C.; Cheung, K.-K. *Organometallics* **2001**, *20*, 4476.

[77] Sun, W.; Li, Y.; Pritchett, T. M.; Ji, Z.; Haley, J. E. *Nonlinear Opt., Quantum Opt.* **2010**, *40*, 163.

[78] Li, Y.; Pritchett, T. M.; Shao, P.; Haley, J. E.; Zhu, H.; Sun, W. *J. Organomet. Chem.* **2009**, *694*, 3688.

[79] Li, Y.; Pritchett, T. M.; Huang, J.; Ke, M.; Shao, P.; Sun, W. *J. Phys. Chem. A* **2008**, *112*, 7200.

[80] Si, J.; Yang, M.; Wang, Y.; Zhang, L.; Li, C.; Wang, D.; Dong, S.; Sun, W. *Appl. Phys. Lett.* **1994**, *64*, 3083.

[81] McKay, T. J.; Staromlynska, J.; Davy, J. R.; Bolger, J. A. *J. Opt. Soc. Am. B* **2001**, *18*, 358.

[82] Song, Y.; Fang, G.; Wang, Y.; Liu, S.; Li, C.; Song, L.; Zhu, Y.; Hu, Q. *Appl. Phys. Lett.* **1999**, *74*, 332.

[83] Pittman, M.; Plaza, P.; Martin, M. M.; Meyer, Y. H. *Opt. Commun.* **1998**, *158*, 201.

[84] Perry, J. W.; Mansour, K.; Lee, I. Y. S.; Wu, X. L.; Bedworth, P. V.; Chen, C. T.; Ng, D.; Marder, S. R.; Miles, P.; Wada, T.; Tian, M.; Sasabe, H. *Science* **1996**, *273*, 1533.

[85] Guha, S.; Kang, K.; Porter, P.; Roach, J. E.; Remy, D. E.; Aranda, F. J.; Rao, D. V. G. L. N. *Opt. Lett.* **1992**, *17*, 264.

[86] Westlund, R.; Glimsdal, E.; Lindgren, M.; Vestberg, R.; Hawker, C.; Lopez, C.; Malmström, E. *J. Mater. Chem.* **2008**, *18*, 166.

[87] Glimsdal, E.; Carlsson, M.; Eliasson, B.; Minaev, B.; Lindgren, M. *J. Phys. Chem. A* **2007**, *111*, 244.

CHAPTER 4. SYNTHESIS, PHOTOPHYSICS, AND REVVERSE SATURABLE ABSORPTION OF PLATINUM COMPLEXES BEARING EXTENDED π-CONJUGATED C^N^N LIGAND

The majority of this chapter is from my paper published on Dalton Transactions.[1] Reproduced by permission of The Royal Society of Chemistry. The article can be found online at: http://pubs.rsc.org/en/content/articlelanding/2013/dt/c3dt51430g#!divAbstract. However, there are some revisions, and contents including figures and brief discussions are added.

4.1. Introduction

Square-planar platinum(II) complexes have gained intense interest in the past two decades due to their potential applications as antitumor reagents,[2-4] in organic light emitting diodes (OLED),[5-7] photon upconversion,[8-10] and as nonlinear absorbing materials,[11-15] etc. Most of these applications are intrigued by their rich photophysical properties that are closely associated with their long-lived triplet excited states due to the heavy-atom enhanced spin-orbit coupling. It has been reported that the photophysical properties of the Pt(II) complexes can be readily tuned by structural modifications of the ligands. Therefore, understanding the structure-property correlations is critical for designing platinum complexes with a predetermined application. It is found that variation of substituent on the ligand from electron-withdrawing to electron-donating groups,[16] tuning degree of π-conjugation in the ligand,[17] alternation of different linkage between components in ligand,[18] and changing configuration of the Pt(II) complexes (*cis* or *trans*)[19] could all influence the photophysics of the platinum complexes.

Our group has extensively studied the photophysics and nonlinear absorption of platinum complexes bearing polypyridine ligands (terpyridine or diimine) or cyclometalating C^N^N ligands.[11-15] Most of the complexes exhibited excellent reverse saturable absorption

(RSA, *i.e.* an increase of absorptivity of molecules with the increased incident energy, and consequently a decrease of transmission with increased incident energy) for 532-nm ns laser pulses, which is typically related to the large ratios of the excited-state absorption cross section to that of the ground state of the molecule. Studies by our group on platinum bipyridine bisacetylide complexes[14, 15] revealed that the triplet excited states and RSA can be efficiently tuned by the auxiliary substituent on the acetylide ligands. Recently, we studied the effects of substituent at the cyclometalating C^N^N ligand on the photophysics and RSA of a series of Pt(II) complexes and discovered that the electron-donating or withdrawing substituents can significantly influence the excited-state characteristics and RSA.[20] Our studies on Pt(II) bipyridine acetylide complexes discovered that extending the π-conjugation on the bipyridine or/and the acetylide ligands can significantly increase the triplet excited-state lifetime and dramatically improve the RSA at 532 nm for ns laser pulses.[21, 22] Intrigued by these work, we wonder if the extended π-conjugation on the cyclometalating C^N^N ligand could also prolong the triplet excited-state lifetime and enhance the RSA of the Pt(II) complexes; and whether the terminal substituent at the extended π-conjugated C^N^N ligand would influence the photophysics and RSA of the complexes.

To answer these questions, five Pt(II) complexes containing a 6-[9,9-di(2-ethylhexyl)-7-*R*-fluoren-2-yl]-2,2'-bipyridine ligand or a 6-[9,9-di(2-ethylhexyl)-7-(4-(benzothiazol-2-yl)phenyl)-fluoren-2-yl]-2,2'-bipyridine ligand (complexes **4-1** – **4-5** in Scheme 4.1) were synthesized and their photophysics and RSA were systematically investigated. For comparison of the effect of extended π-conjugation, complex **4-6** that was reported previously[20] was also included in this paper. In complexes **4-1** – **4-4**, different substituents were introduced at the 4-position of the ethynylphenyl unit. In complexes **4-2**, **4-5**, and **4-6**, the linkage between the C^N^N core and the benzothiazol-2-yl (BTZ) component was varied from single bond (**4-6**) to phenyl (**4-5**) to ethynylphenyl (**4-2**). Comparison of the

photophysics and RSA of **4-1** – **4-4** would allow the terminal substituent effect to be evaluated; while investigation of **4-2**, **4-5** and **4-6** would help us to better understand the linkage effect and thus the extended π-conjugation effect.

1	R = NO$_2$
2	Benzothiazol-2-yl
3	H
4	OCH$_3$

| **5** | n = 1 |
| **6** | n = 0 |
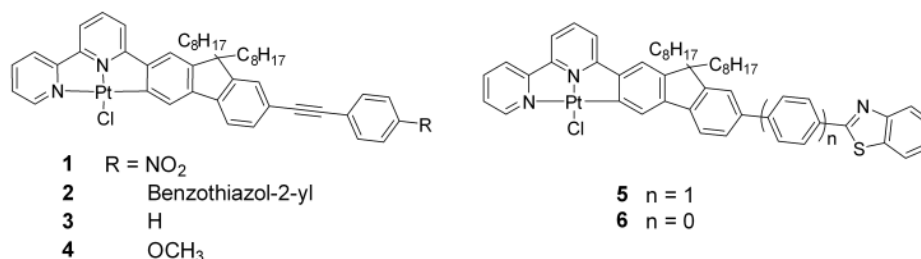
Chart 4.1. Structures for complexes **4-1** – **4-6** (C$_8$H$_{17}$ = 2-ethylhexyl).

4.2. Experiment Section

4.2.1. Synthesis and Characterization

The synthetic routes for ligands **4-1-L** – **4-5-L** and complexes **4-1** – **4-5** are illustrated in Scheme 2. The synthesis of ligand **4-6-L** and complex **4-6** has been reported previously.[20] 1-Ethynyl-4-nitrobenzene (**7a**), phenylacetylene (**7c**), and 1-ethynyl-4-methoxybenzene (**7d**) were purchased from Aldrich Co. All of the other reagents and solvents were purchased from Aldrich Chemical Co. or Alfa Aesar and used as is unless otherwise stated. Silica gel for column chromatography was purchased from Sorbent Technology (60 Å, 230 - 400 mesh, 500 - 600 m^2/g, pH: 6.5 - 7.5). The synthesis of precursors **8**[23] and **11**[24] followed the literature procedures. The synthetic procedures and characterization data for the key precursors **10a** – **10d**, **12**, ligands **4-1-L** – **4-5-L** and complexes **4-1** – **4-5** are provided below. Sonogashira coupling reactions between **7a** – **7d** and **9** respectively yielded **10a** – **10d**. Suzuki coupling reaction between **6** and **11** formed compound **12**. **10a** – **10d** and **12** then reacted with **8** respectively under Suzuki coupling reaction conditions to afford **4-1-L** – **4-5-L**. The ligands **4-1-L** – **4-5-L** reacted respectively with K$_2$PtCl$_4$ in refluxing acetic acid under argon for 24 hours to afford complexes **4-1** – **4-5**. All intermediates, ligands and the Pt(II) complexes were characterized by ^{1}H NMR. Ligands **4-1-L** – **4-5-L** and complexes **4-1** – **4-5** were also characterized by electrospray ionization high-resolution mass spectrometry

(ESI-HRMS), and elemental analyses. ^{1}H NMR spectra were obtained on Varian Oxford-VNMR spectrometers (300 MHz, 400 MHZ, or 500 MHz). ESI-HRMS analyses were performed on a Bruker BioTOF III mass spectrometer. Elemental analyses were conducted by NuMega Resonance Laboratories, Inc. in San Diego, California.
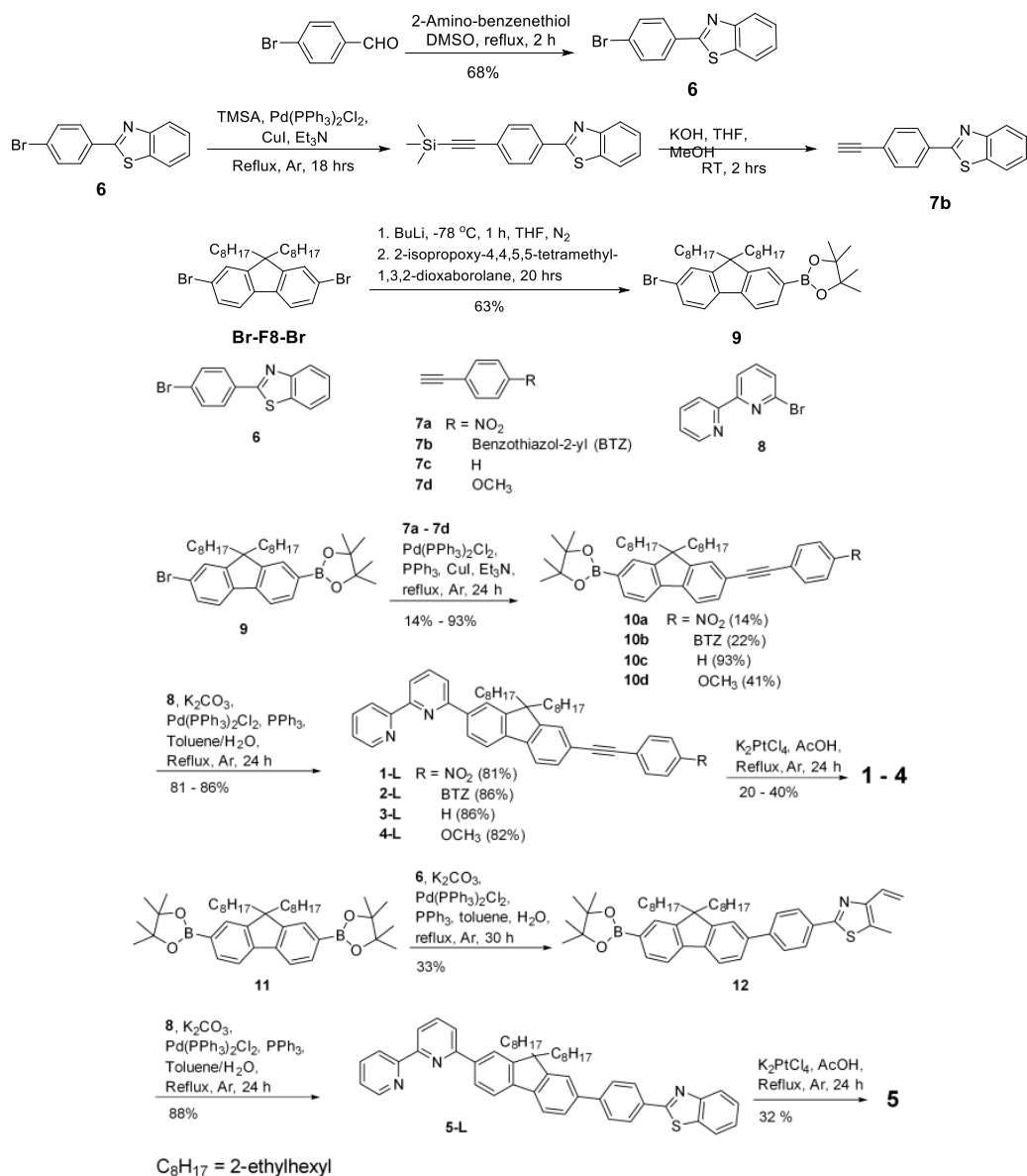
Scheme 4.1. Synthetic routes for ligands **4-1-L** – **4-5-L** and complexes **4-1** – **4-5**.

6. The mixture of 4-bromobenzalhyde (3.7 g, 20 mmol), 2-amino-benzenethiol (2.5 g, 20 mmol), and DMSO (20 mL) was heated to reflux for 2 hrs. After the reaction, the off-white precipitate formed upon cooling was collected and dissolved into dichloromethane. The solution was discolored by stirring with activated carbon pellets under reflux. The

carbon pellets were removed by filtration after the solution cooled down to room temperature. The solvent of the filtrate was then removed by distillation. 3.96 g white powder was collected as the product (yield: 68%). ^{1}H NMR (CDCl$_3$, 400 MHz): 8.03 – 8.06 (m, 1H), 7.92 – 7.96 (m, 2H), 7.87 – 7.90 (m, 1H), 7.59 – 7.62 (m, 2H), 7.46 – 7.50 (m, 1H), 7.36 – 7.40 (m, 1H).

7b. (2 successive steps) In the first step, compound **6** (0.38 g, 1.3 mmol) was dissolved in 30 mL triethylamine and the solution was degassed. Pd(PPh$_3$)$_2$Cl$_2$ (58 mg), PPh$_3$ (98 mg) and CuI (48 mg) was then added. The system was purged with argon again and TMSA (0.5 mL, 3.6 mmol) was injected. The mixture was then heated to reflux for 18 hrs. After reaction, the black precipitate was removed by filtration. The solvent from the filtrate was removed by distillation. The residue was purified by running a silica gel column eluted with a mixed solvent of dichloromethane and hexane (v/v = 1/1). 0.35 g white powder was collected as the product and confirmed as trimethyl-(4-BTZ-phenylethynyl)-silane (yield: 88%). ^{1}H NMR (CDCl$_3$, 400 MHz): 8.04 – 8.06 (m, 1H), 8.00 – 8.02 (m, 2H), 7.88 – 7.90 (m, 1H), 7.54 – 7.56 (m, 2H), 7.46 – 7.50 (m, 1H), 7.35 – 7.39 (m, 1H), 0.25 (s, 9H). In the second step, the mixture of trimethyl-(4-BTZ-phenylethynyl)-silane (0.35 g, 1.1 mmol), KOH (0.56 g, 10 mmol), THF (6 mL), CH$_3$OH (6 mL), and water (1 mL) was stirred at room temperature for 2 hours. After reaction, the solvent was removed by distillation and the residue was dissolved in dichloromethane. The dichloromethane solution was washed with brine twice and dried over MgSO$_4$. After removal of the solvent, 0.26 g yellow powder was collected as the product (yield: 97%). ^{1}H NMR (CDCl$_3$, 400 MHz): 8.03 – 8.07 (m, 3H), 7.88 – 7.90 (m, 1H), 7.58 – 7.60 (m, 2H), 7.46 – 7.50 (m, 1H), 7.36 – 7.40 (m, 1H), 3.20 (s, 1H).

9. Compound Br-F8-Br (5.14 g, 9.4 mmol) was dissolved in 20 mL THF and the solution was degassed and cooled down to -78 ^{o}C. BuLi (4.1 mL, 10.3 mmol) was then

added dropwise. The solution was stirred under argon for 1 hour. 2-Isopropoxy-4,4,5,5-tetramethyl-1,3,2-dioxaborolane (1.92 mL, 0.912 g/mL, 9.4 mmol) was then added dropwise and the reaction mixture was allowed to warm up to room temperature for 20 hours. After the reaction, the organic layer was washed with saturated NH_4Cl aqueous solution and dried over $MgSO_4$. The solvent was removed and the residue was purified by running a silica gel column eluted with a mixed solvent of hexane/CH_2Cl_2 (v/v = 3/1). 3.55 g colorless oil was collected as the product (yield: 63%). ^{1}H NMR (CDCl$_3$, 400 MHz): 7.75 – 7.80 (m, 2H), 7.61 – 7.63 (m, 1H), 7.53 – 7.55 (m, 1H), 7.47 – 7.48 (m, 1H), 7.40 – 7.43 (m, 1H), 1.87 – 2.01 (m, 4H), 1.33 (s, 12H), 0.63 – 0.95 (m, 22H), 0.42 – 0.53 (m, 8H).

General synthetic procedure for 10a – 10d. The mixture of **7a – 7d** (1.0 mmol), **9** (0.94mmol), CuI (40 mg), Pd(PPh$_3$)$_2$Cl$_2$ (40 mg), PPh$_3$ (80 mg), and Et$_3$N (20 mL) was heated to reflux under argon for 24 hours. After reaction, the solid was removed by filtration and Et$_3$N was removed by distillation. Purification was carried out by column chromatography (silica gel) eluted with mixed solvent of hexane and dichloromethane (v/v = 2/1 for **10a** and **10b**; v/v = 5/1 for **10c** and **10d**).

10a. 90 mg yellow oil was collected as the product (yield: 14%). ^{1}H NMR (CDCl$_3$, 500 MHz): 8.19 – 8.22 (m, 2H), 7.77 – 7.84 (m, 2H), 7.64 – 7.71 (m, 4H), 7.49 – 7.55 (m, 2H), 1.93 – 2.06 (m, 4H), 1.34 (m, 12H), 0.45 – 0.95 (m, 30H).

10b. 0.16g light yellow oil was collected as the product (yield: 22%). ^{1}H NMR (CDCl$_3$, 500 MHz): 8.09 – 8.12 (m, 3H), 7.93 – 7.94 (d, J = 8.0 Hz, 1H), 7.81 – 7.88 (m, 2H), 7.68 – 7.73 (m, 5H), 7.51 – 7.60 (m, 3H), 7.36 – 7.43 (m, 3H), 1.97 – 2.10 (m, 4H), 1.39 (s, 12H), 0.50 – 0.99 (m, 30H).

10c. 0.54 g light yellow oil was collected as the product (yield: 93%). ^{1}H NMR (CDCl$_3$, 400 MHz): 7.80 – 7.87 (m, 2H), 7.68 – 7.70 (d, J = 11.2 Hz, 2H), 7.50 – 7.59 (m, 3H), 7.29 – 7.38 (m, 10H), 1.95 – 2.08 (m, 4H), 1.37 (s, 11H), 0.49 – 0.94 (m, 30H).

10d. 0.25 g light yellow oil was collected as the product (yield: 41%). ^{1}H NMR (CDCl$_3$, 400 MHz): 7.77 – 7.83 (m, 2H), 7.65-7.67 (m, 2H), 7.45 – 7.51 (m, 4H), 6.86 – 6.88 (m, 2H), 3.82 (s, 3H), 1.93 – 2.05 (m, 4H), 1.35 (s, 12H), 0.46 – 0.92 (m, 30H).

Synthesis of 12. The mixture of **6** (0.3 g, 1 mmol), **11** (0.65 g, 1 mmol), K$_2$CO$_3$ (0.52 g), Pd(PPh$_3$)$_2$Cl$_2$ (48 mg), PPh$_3$ (78 mg), toluene (15 mL), and water (10 mL) was heated to reflux under argon for 30 hours. After reaction, the solid was removed by filtration and the organic phase was washed with brine and dried over MgSO$_4$. After removal of the solvent, the residue was purified by running a silica gel column eluted with a mixed solvent of dichloromethane and hexane (v/v = 1/3). 0.24 g colorless oil was collected as the product (yield: 33%). ^{1}H NMR (CDCl$_3$, 500 MHz): 8.21 (d, J = 8.0 Hz, 1H), 8.12 (d, J = 8.0 Hz, 1H), 7.94 (d, J = 8.0 Hz, 1H), 7.89 (d, J = 9.0 Hz, 1H), 7.81 – 7.84 (m, 2H), 7.78 (d, J = 8.0 Hz, 2H), 7.74 (d, J = 7.5 Hz, 1H), 7.67 (m, 1H), 7.63 – 7.65 (m, 1H), 7.52 (t, J = 7.5 Hz, 1H), 7.41 (t, J = 7.8 Hz, 1H), 2.05 – 2.14 (m, 4H), 1.39 (s, 12H), 0.52 – 0.91 (m, 30H).

General synthetic procedure for 4-1-L – 4-5-L. The mixture of **8** (0.20 mmol), **10a – 10d** or **12** (0.18 mmol), K$_2$CO$_3$ (0.60 g), Pd(PPh$_3$)$_2$Cl$_2$ (40 mg), PPh$_3$ (60 mg), toluene (10 mL), and water (5 mL) was heated to reflux under argon for 24 hours. After reaction, the solid was removed by filtration and the organic phase was collected and washed with brine and dried over MgSO$_4$. After removal of the solvent, the residue was purified by running a silica gel column eluted with dichloromethane.

4-1-L. 0.10 g yellow oil was collected as the product (yield: 81%). ^{1}H NMR (CDCl$_3$, 400 MHz): 8.68 – 8.69 (m, 1H), 8.64 (d, J = 7.6 Hz, 1H), 8.37 (d, J = 7.6 Hz, 1H), 8.20 – 8.22 (m, 2H), 8.12 – 8.17 (m, 2H), 7.78 – 7.90 (m, 4H), 7.74 (d, J = 7.6 Hz, 1H), 7.65 – 7.69 (m, 2H), 7.57 – 7.60 (m, 1H), 7.54 – 7.56 (m, 1H), 7.30 – 7.33 (m, 1H), 2.00 – 2.16 (m, 4H), 0.51 – 0.95 (m, 30H). Elemental analysis calculated for

$C_{47}H_{51}N_3O_2$•$0.125CH_2Cl_2$•$0.25C_6H_{14}$: C, 80.88; H, 7.64; N, 5.82. Found: C, 81.27; H, 8.07; N, 5.80. ESI-HRMS: m/z calc. for $[C_{47}H_{51}N_3O_2+H]^+$: 690.4054; Found: 690.4035.

4-2-L. 0.12 g yellow solid was collected as the product (yield: 86%). ^{1}H NMR (CDCl$_3$, 400 MHz): 8.68 − 8.70 (m, 1H), 8.64 − 8.66 (m, 1H), 8.35 − 8.38 (m, 1H), 8.11 − 8.17 (m, 1H), 8.06 − 8.10 (m, 3H), 7.77 − 7.91 (m, 5H), 7.72 − 7.74 (d, J = 8.0 Hz, 1H), 7.64 − 7.69 (m, 2H), 7.58 − 7.60 (m, 1H), 7.54 − 7.57 (m, 1H), 7.47 − 7.51 (m, 1H), 7.36 − 7.40 (m, 1H), 7.28 − 7.33 (m, 2H), 2.01 − 2.16 (m, 4H), 0.52 − 0.97 (m, 30H). Elemental analysis calculated for $C_{54}H_{55}N_3S$•$0.25CH_2Cl_2$: C, 81.52; H, 7.00; N, 5.26. Found: C, 81.12; H, 7.35; N, 5.37. ESI-HRMS: m/z calc. for $[C_{54}H_{55}N_3S+H]^+$: 778.4189; Found: 778.4162.

4-3-L. 0.10 g yellow oil was collected as the product (yield: 86%). ^{1}H NMR (CDCl$_3$, 400 MHz): 8.65 − 8.71 (m, 2H), 8.37 − 8.39 (m, 1H), 8.12 − 8.18 (m, 2H), 7.71 − 7.91 (m, 5H), 7.52 − 7.57 (m, 4H), 7.31 − 7.38 (m, 4H), 2.01 − 2.17 (m, 4H), 0.50 − 0.95 (m, 30H). Elemental analysis calculated for $C_{47}H_{52}N_2$•$0.1CH_2Cl_2$: C, 86.58; H, 8.05; N, 4.29. Found: C, 86.89; H, 8.37; N, 4.30. ESI-HRMS: m/z calc. for $[C_{47}H_{52}N_2+H]^+$: 645.4203; Found: 645.4172.

4-4-L. 0.10 g yellow oil was collected as the product (yield: 82%). ^{1}H NMR (CDCl$_3$, 400 MHz): 8.65 − 8.71 (m, 2H), 8.36 − 8.38 (m, 1H), 8.11 − 8.18 (m, 2H), 7.83 − 7.91 (m, 2H), 7.79 − 7.81 (m, 2H), 7.70 − 7.71 (m, 1H), 7.48 − 7.56 (m, 4H), 7.31 − 7.34 (m, 1H), 6.88 − 6.90 (m, 2H), 3.83 (s, 3H), 2.00 − 2.16 (m, 4H), 0.52 − 0.97 (m, 30H). Elemental analysis calculated for $C_{48}H_{54}N_2O$•$0.25CH_2Cl_2$•$0.25C_6H_{14}$: C, 83.25; H, 8.15; N, 3.90. Found: C, 83.21; H, 8.43; N, 4.02. ESI-HRMS: m/z calc. for $[C_{48}H_{54}N_2O+H]^+$: 675.4309; Found: 675.4283.

4-5-L. 0.12 g yellow solid was collected as the product (yield: 88%). ^{1}H NMR (CDCl$_3$, 400 MHz): 8.66 − 8.70 (m, 2H), 8.36 − 8.38 (m, 1H), 8.13 − 8.20 (m, 4H), 8.09 (d, J = 8.4 Hz, 1H), 7.75 − 7.91 (m, 8H), 7.68 (m, 1H), 7.62 − 7.65 (dt, J = 8.0, 1.6 Hz, 1H), 7.47 −

7.51 (m, 1H), 7.36 – 7.40 (m, 1H), 7.30 – 7.33 (m, 1H), 2.07 – 2.21 (m, 4H), 0.51 – 0.92 (m, 30H). Elemental analysis calculated for $C_{52}H_{55}N_3S$: C, 82.82; H, 7.35; N, 5.57. Found: C, 82.42; H, 7.44; N, 5.52.   ESI-HRMS: m/z calc. for $[C_{52}H_{55}N_3S+H]^+$: 754.4189; Found: 754.4167.

General synthetic procedure for 4-1 – 4-5. The mixture of **4-1-L** – **4-5-L** (0.17 mmol), K_2PtCl_4 (72 mg, 0.17 mmol), and acetic acid (10 mL) was refluxed under argon for 24 hours. After reaction, the solvent was removed by distillation. The red solid was purified by column chromatography on silica gel eluted with dichloromethane. Further purification was carried out by recrystallization from dichloromethane and hexane.

4-1. 62 mg red powder was collected as the product (yield: 40%). ^{1}H NMR (CDCl$_3$, 400 MHz): 8.93 – 9.00 (m, 1H), 8.19 – 8.22 (m, 2H), 8.11 – 8.12 (m, 1H), 7.90 – 7.95 (m, 2H), 7.81 – 7.84 (m, 1H), 7.72 – 7.79 (m, 1H), 7.64 – 7.69 (m, 2H), 7.46 – 7.54 (m, 5H), 7.30 – 7.31 (m, 1H), 1.94 – 2.03 (m, 4H), 0.48 – 0.94 (m, 30H). Elemental analysis calculated for $C_{47}H_{50}ClN_3O_2Pt$: C, 61.40; H, 5.48; N, 4.57. Found: C, 61.34; H, 5.72; N, 4.51. ESI-HRMS: m/z calc. for $[C_{47}H_{50}N_3O_2PtCl+H]^+$: 920.3317; Found: 920.3355.

4-2. 52 mg yellow powder was collected as the product (yield: 30%). ^{1}H NMR (CDCl$_3$, 400 MHz): 9.17 – 9.19 (m, 1H), 8.14 (s, 1H), 8.04 – 8.09 (m, 4H), 7.89 – 7.92 (m, 2H), 7.81 – 7.83 (m, 2H), 7.64 – 7.66 (m, 3H), 7.47 – 7.56 (m, 5H), 7.36 – 7.40 (m, 1H), 7.33 (m, 1H), 1.98 – 1.99 (m, 4H), 0.48 – 0.92 (m, 30H). Elemental analysis calculated for $C_{54}H_{54}ClN_3PtS•0.5CH_2Cl_2$: C, 62.34; H, 5.28; N, 4.00. Found: C, 62.48; H, 5.54; N, 4.00. ESI-HRMS: m/z calc. for $[C_{54}H_{54}N_3SPtCl+H]^+$: 1008.3453; Found: 1008.3501.

4-3. 30 mg yellow powder was obtained as the product (yield: 20%). ^{1}H NMR (CDCl$_3$, 500 MHz): 9.04 – 9.08 (m, 1H), 8.14 (s, 1H), 7.93 – 8.01 (m, 2H), 7.77 – 7.84 (m, 2H), 7.52 – 7.58 (m, 7H), 7.33 – 7.39 (m, 4H), 1.97 – 2.05 (m, 4H), 0.52 – 0.96 (m, 30H).

Elemental analysis calculated for $C_{47}H_{51}ClN_2Pt$: C, 64.56; H, 5.88; N, 3.20. Found: C, 64.10; H, 6.21; N, 3.13. ESI-HRMS: *m/z* calc. for $[C_{47}H_{51}N_2PtCl+H]^+$: 875.3466; Found: 875.3432.

4-4. 46 mg yellow powder was obtained as the product (yield: 30%). ^{1}H NMR (CDCl$_3$, 400 MHz): 9.08 – 9.11 (m, 3H), 8.10 (s, 1H), 7.96 – 7.99 (m, 1H), 7.90 (d, J = 8.0 Hz, 1H), 7.75 – 7.80 (m, 2H), 7.45 – 7.59 (m, 7H), 7.29 (d, *J* = 1.6 Hz, 1H), 6.85 – 6.87 (m, 2H), 3.81 (s, 3H), 1.96 – 1.97 (m, 4H), 0.47 – 0.94 (m, 30H). Elemental analysis calculated for $C_{48}H_{53}ClN_2OPt$: C, 63.74; H, 5.91; N, 3.10. Found: C, 63.55; H, 5.91; N, 3.05. ESI-HRMS: *m/z* calc. for $[C_{48}H_{53}N_2OPtCl+H]^+$: 905.3572; Found: 905.3592.

4-5. 53 mg yellow powder was obtained as the product (yield: 32%). ^{1}H NMR (CDCl$_3$, 400 MHz): 9.24 – 9.26 (m, 1H), 8.19 – 8.21 (m, 3H), 8.08 – 8.11 (m, 2H), 7.92 – 7.94 (m, 3H), 7.83 – 7.86 (m, 1H), 7.78 – 7.80 (m, 2H), 7.65 – 7.67 (m, 2H), 7.49 – 7.60 (m, 6), 7.38 – 7.42 (m, 2H), 2.00 – 2.10 (m, 4H), 0.49 – 0.94 (m, 30H). Elemental analysis calculated for $C_{52}H_{54}ClN_3PtS \cdot 0.33CH_2Cl_2$: C, 62.12; H, 5.45; N, 4.15. Found: C, 61.86; H, 5.49; N, 4.14. ESI-HRMS: *m/z* calc. for $[C_{52}H_{54}N_3SPtCl+H]^+$: 984.3452; Found: 984.3462.

4.2.2. Photophysical Measurements

The spectroscopic grade solvents used for the photophysical experiments were purchased from VWR International and used as is without further purification. A Shimadzu UV-2501 spectrophotometer was used to record the UV-vis absorption spectra in different solvents. A SPEX fluorolog-3 fluorometer/phosphorometer was used to measure the steady-state emission spectra. The emission spectra of **4-1** – **4-6** were recorded after their solutions were purged with argon for 30 minutes. The emission quantum yields of **4-1-L** – **4-6-L** and **4-1** – **4-6** were determined by the relative actinometry method[25] (**4-1** – **4-6** were measured in degassed solutions). A degassed aqueous solution of $[Ru(bpy)_3]Cl_2$ (Φ_{em} = 0.042, λ_{ex} = 436 nm)[26] was used as the reference for complexes **4-1** – **4-6**, and a 1 N sulfuric acid solution of

quinine bisulfate (Φ_{em} = 0.546, λ_{ex} = 347.5 nm)[27] was used as the reference for ligands **4-1-L** – **4-6-L**.

The nanosecond transient difference absorption (TA) spectra and decays of **4-1-L** – **4-6-L** and **4-1** – **4-6** were measured in degassed CH$_3$CN solutions on an Edinburgh LP920 laser flash photolysis spectrometer. The third harmonic output (355 nm) of a Nd:YAG laser (Quantel Brilliant, pulse width: 4.1 ns, repetition rate was set at 1 Hz) was used as the excitation source. Each sample was purged with argon for 30 min prior to measurement. The triplet excited-state absorption coefficient (ε_T) at the TA band maximum was determined by the singlet depletion method.[28] The triplet quantum yields (Φ_T) of **4-1** – **4-6** were determined by the relative actinometry using SiNc in benzene as the reference (ε_{590} = 70,000 M^{-1} cm^{-1}, Φ_T = 0.20).[29]

4.2.3. Nonlinear Transmission Experiment

The reverse saturable absorption of complexes **4-1** – **4-6** was characterized by nonlinear transmission experiment at 532 nm using a Quantel Brilliant laser as the light source. The pulse width of the laser was 4.1 ns and the repetition rate was set at 10 Hz. The complexes were dissolved in CH$_2$Cl$_2$. The concentration of the sample solution was adjusted to obtain a linear transmission of 90% at 532 nm in a 2-mm-thick cuvette. The experimental setup is similar to that reported previously,[30] with a 40-cm plano-convex lens being used to focus the beam to the center of the 2-mm-thick sample cuvette.

4.3. Results and Discussion

4.3.1. Electronic Absorption

The electronic absorption of **4-1-L** – **4-6-L** and **4-1** – **4-6** were measured in dichloromethane in the concentration range of 1×10^{-6} – 1×10^{-4} mol/L, and the spectra are shown in Figure 4.1a for the ligands and Figure 4.1b for the complexes. The absorption band

maxima and molar extinction coefficients for the ligands and the complexes are summarized in Table 4.1. No ground-state aggregation was evident in the concentration range studied, as supported by the obedient of the absorption to the Beer's law. The major absorption bands of **4-1-L** – **4-6-L** appear at the 300 nm – 450 nm region with the molar extinction coefficients being on the order of 10^4 L•mol^{-1}•cm^{-1}. Considering the large molar extinction coefficients and the minor solvent effect as shown in Figures 4.2, these bands are ascribed to the $^1\pi,\pi^*$ transitions. The UV-vis absorption spectra of the Pt(II) complexes **4-1** – **4-6** are featured by strong absorption bands below ca. 430 nm (450 nm for **4-1**) and a broad tail from 440 nm (450 nm for **1**) to 500 nm. Comparing to the UV-vis absorption spectra of their respective ligands and with reference to the other Pt(II) C^N^N chloride complexes with similar structures,[31] the major absorption bands are attributed to predominantly the ligand centered $^1\pi,\pi^*$ transitions; while the broad tail is believed to be dominated by the ^{1}MLCT transition, probably mixed with some intraligand charge transfer (from the ethynylfluorene component to the bipyridine component) characters. The $^1\pi,\pi^*$ transitions in the complexes are significantly red-shifted compared to those in their respective ligands, indicating the electron delocalization induced by the interactions with the metal ion.
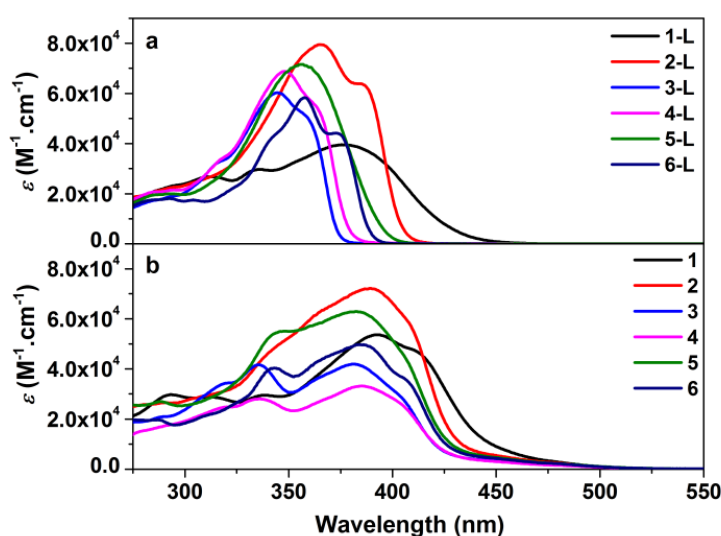
Figure 4.1. (a) UV-vis absorption spectra of ligands **4-1-L** – **4-6-L** measured in CH$_2$Cl$_2$; (b) UV-vis absorption spectra of complexes **4-1** – **4-6** measured in CH$_2$Cl$_2$.

Comparing the UV-vis absorption spectra of **4-1-L** – **4-4-L**, it is very clear that substitution at the 4-position of the ethynylphenyl (regardless electron-donating or electron-withdrawing substituent) causes pronounced red-shifts of the absorption bands and increased molar extinction coefficients, as evidenced by **4-1-L**, **4-2-L** and **4-4-L** compared to **4-3-L**, which suggests electron delocalization induced by the substituents. Notably, the absorption spectrum of **4-1-L** is much broader and red-shifted, but with significantly low molar extinction coefficients with respect to the other ligands. This implies that there could be strong mixing of the intramolecular charge transfer character with the $^1\pi,\pi^*$ transition in **4-1-L**, which decreases the $^1\pi,\pi^*$ transition oscillating strength but increases the intramolecular charge transfer transition oscillating strength. In contrast, the absorption of **4-2-L** – **4-4-L** should be dominated by the $^1\pi,\pi^*$ transitions. Comparison of the UV-vis absorption spectra of **4-2-L**, **4-5-L** and **4-6-L** reveals that with the extended π-conjugation between the BTZ unit and the C^N^N core, the UV-vis absorption spectra of **4-2-L** and **4-5-L** are pronouncedly red-shifted and their molar extinction coefficients are dramatically increased.

Table 4.1. Electronic absorption, emission (room temperature and 77 K), and excited-state absorption parameters for complexes **4-1** – **4-6** and ligands **4-1-L** – **4-6-L**.

	λ_{abs}/nm (ε/L.mol^{-1}.cm^{-1})[a]	λ_{em}/nm (τ_0/μs; k_{sq}/L.mol^{-1}.s^{-1}); Φ_{em}[b] R. T.	λ_{em}/nm(τ_{em}/μs)[c] 77 K	$\lambda_{T_1-T_n}$/nm (τ_T/μs; $\varepsilon_{T_1-T_n}$/L.mol^{-1} cm^{-1}; Φ_T)[d]
4-1	450 (9120), 410 (47670), 393 (53650), 338 (29500)	593 (7.5; 1.53×10^9), 638 (7.0; 1.60×10^9); 0.13	583 (26.1), 632 (23.9)	560 (5.1; 26530; 0.37)
4-2	450 (5490), 410 (55380), 389 (72130), 366 (63380)	592 (6.2; 1.63×10^9), 636 (6.2; 1.26×10^9); 0.053	585 (26.1), 633 (28.1)	675 (8.1; 90010; 0.19)
4-3	450 (3270), 405 (28100), 381 (41910), 336 (41630)	589 (4.7; 1.66×10^9), 630 (4.5; 1.21×10^9); 0.084	577 (22.4), 626 (20.9)	610 (5.7; 37510; 0.43)
4-4	450 (3030), 400 (28300), 385 (33170), 335 (27980)	591 (4.6; 1.69×10^9), 635 (4.5; 1.31×10^9); 0.051	578 (22.9), 627 (23.3)	640 (7.1; 37190; 0.25)

Table 4.1. Electronic absorption, emission (room temperature and 77 K), and excited-state absorption parameters for complexes **4-1 – 4-6** and ligands **4-1-L – 4-6-L** (continued).

	λ_{abs}/nm (ε/L.mol^{-1}.cm^{-1})[a]	λ_{em}/nm (τ_0/μs; k_{sq}/L.mol^{-1}.s^{-1}); Φ_{em}[b] R. T.	λ_{em}/nm(τ_{em}/μs)[c] 77 K	$\lambda_{T_1-T_n}$/nm (τ_T/μs; $\varepsilon_{T_1-T_n}$/L.mol^{-1} cm^{-1}; Φ_T)[d]
4-5	450 (4650), 405 (46110), 382 (62880), 348 (55090)	590 (3.4; 1.79×10^9), 640 (3.4; 1.26×10^9); 0.069	576 (24.7), 623 (23.0)	650 (7.3; 60730; 0.12)
4-6	450 (4310), 404 (37320), 385 (49820), 343 (40510)	588 (6.1; 1.44×10^9), 634 (6.1; 9.33×10^8); 0.092	581 (24.0), 630 (28.0)	625 (8.2; 56980; 0.33)
4-1-L	400 (29080), 377 (39530)	571 (-); 0.032	485	510 (26.7; -; -)
4-2-L	384 (63900), 366 (79400)	428 (-); 0.92	430, 461	625 (12.3; -;-)
4-3-L	357 (52000), 344 (60230)	393 (-); 0.96	378, 392, 413	555 (14.0; -; -)
4-4-L	363 (55150), 348 (68850)	400 (-); 0.99	383, 399, 416	530 (29.6; -; -)
4-5-L	371 (56100), 356 (71580)	427 (-); 0.92	402, 421, 462	610 (15.3; -; -)
4-6-L	373 (44200), 358 (58250)	410 (-); 0.80	395, 410, 437	580 (24.0; -; -)

[a]Absorption band maximum (λ_{abs}) and molar extinction coefficient (ε_{max}) in CH_2Cl_2. [b]Emission wavelength (λ_{em}), intrinsic lifetime (τ_0), self-quenching rate constant (k_{sq}), and emission quantum yield measured in CH_2Cl_2 with Ru(bpy)$_3$Cl$_2$ as the standard for the complexes and quinine for the ligands. [c]In BuCN glassy matrix. [d]Triplet excited-state absorption band maximum ($\lambda_{T_1-T_n}$), molar extinction coefficient ($\varepsilon_{T_1-T_n}$), quantum yield (Φ_T) and lifetime (τ_T) measured in CH_3CN.

Although the effects of terminal substituent and linkage variation on the $^1\pi,\pi^*$ transitions are significant for the ligands, these effects become much weaker in complexes **4-1 – 4-6**. The ligand centered $^1\pi,\pi^*$ transitions of complexes **4-3 – 4-6** are essentially at the same energy except for that they are obviously red-shifted in **4-1** and **4-2**. However, the molar extinction coefficient still increases with the terminal substitution and extended π-linkage except **4-4**. In contrast, the effect of the π-linkage on the charge-transfer tails of **4-2**, **4-5** and **4-6** is more pronounced. The tail in **4-2** and **4-5** are clearly more red-shifted and stronger than that in **4-6**. Furthermore, as shown in Figure 4.2, the absorptions of **4-1 – 4-6**

showed negligible solvatochromic effect, indicating the ligand centered $^1\pi,\pi^*$ transitions nature of the absorptions.
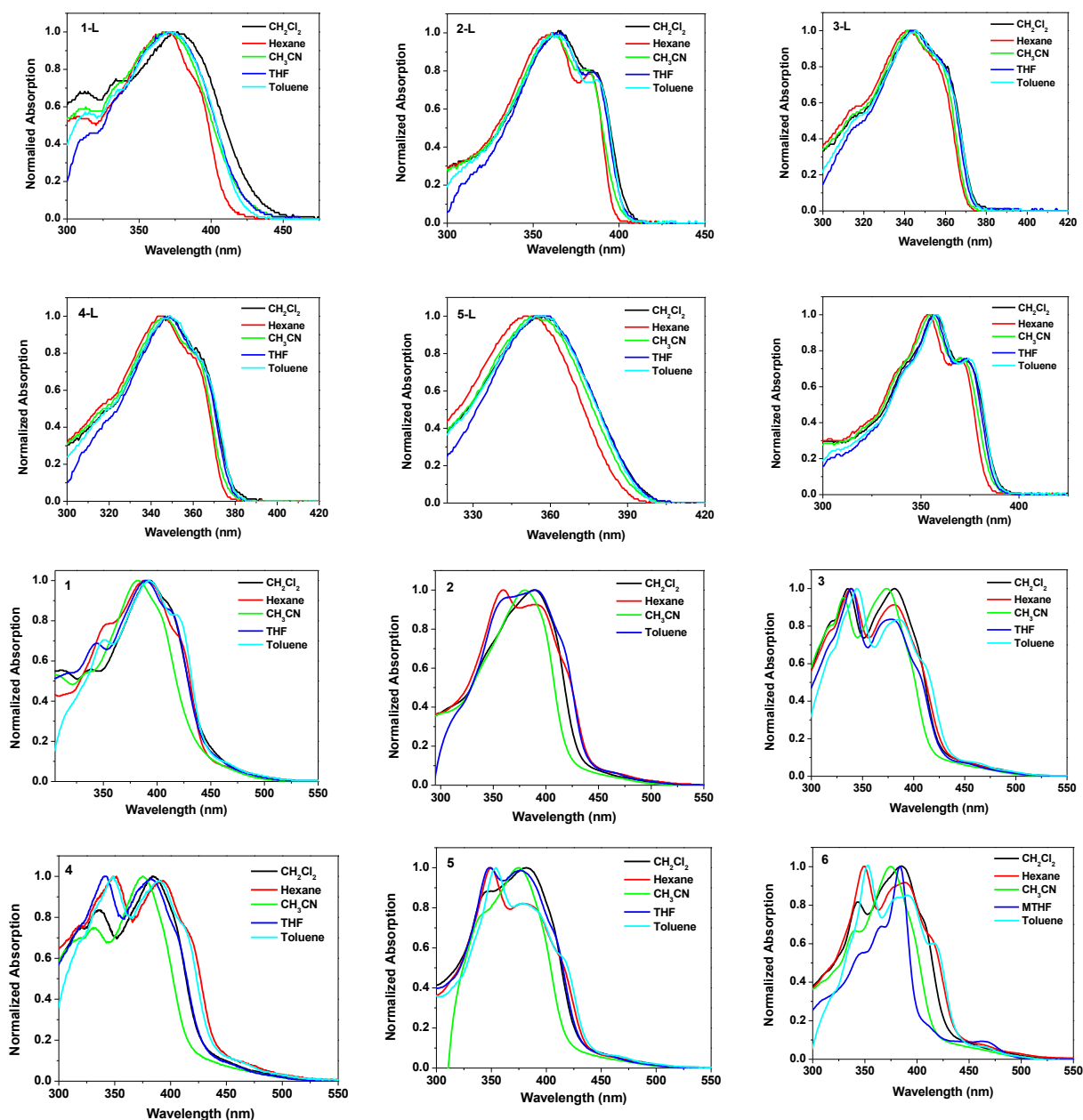
Figure 4.2. Normalized absorption spectra of **4-1-L** – **4-6-L** and **4-1** – **4-6** in different solvents.

4.3.2. Photoluminescence

The emission spectra of **4-1-L** – **4-6-L** and **4-1** – **4-6** in dichloromethane at room temperature and in butyronitrile glassy matrix at 77 K were measured and shown in Figure

4.3. The emission band maxima, lifetimes and quantum yields for the ligands and complexes are summarized in Table 4.1.
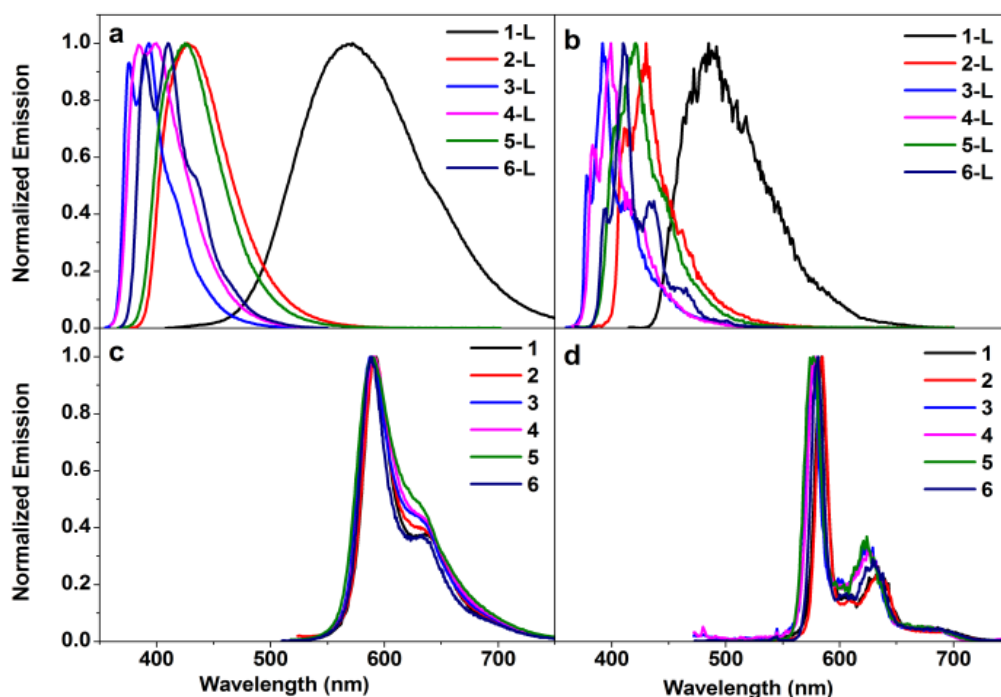
Figure 4.3. (a) Normalized emission spectra of ligands **4-1-L** – **4-6-L** (λ_{ex} = 398 nm for **4-1-L**, 365 nm for **4-2-L**, 345 nm for **4-3-L**, 350 nm for **4-4-L**, 356 nm for **4-5-L**, and 358 nm for **4-6-L**; c = 4×10^{-5} mol/L for **4-1-L** and **4-3-L**, 5×10^{-6} mol/L for **4-2-L**, **4-5-L**, and **4-6-L**, and 1×10^{-6} mol/L for **4-4-L**); (b) Normalized emission spectra of **4-1-L** – **4-6-L** at 77 K in glassy BuCN matrix at the concentration of 1×10^{-5} mol/L (λ_{ex} =398 nm for **4-1-L**, 365 nm for **4-2-L**, 345 nm for **4-3-L**, 350 nm for **4-4-L**, 356 nm for **4-5-L**, and 358 nm for **4-6-L**); (c) Normalized emission spectra of complexes **4-1** – **4-6** (λ_{ex} = 393 nm for **4-1**, 383 nm for **4-2**, 381 nm for **4-3**, 385 nm for **4-4**, 383 nm for **4-5**, and 383 nm for **4-6**) at the concentration of 2×10^{-5} mol/L; (d) Normalized emission spectra of complexes **4-1** – **4-6** at 77 K in glassy BuCN matrix, c = 2×10^{-5} mol/L (λ_{ex} = 393 nm for **4-1**, 383 nm for **4-2**, 381 nm for **4-3**, 385 nm for **4-4**, 383 nm for **4-5**, and 383 nm for **4-6**).

As shown in Figure 4.3a, the emission of the ligands **4-3-L** and **4-6-L** in CH$_2$Cl$_2$ is featured by distinct vibronic structures, while the emission from **4-4-L** is slightly structured. In contrast, the emission from **4-1-L**, **4-2-L** and **4-5-L** is broad and structureless. The lifetimes of the emission from the ligands are too short to be measured on our spectrometer. This suggests that the emission of the ligands predominantly originates from the $^{1}\pi,\pi^{*}$ state for **4-3-L** and **4-6-L**, but predominantly emanates from the ^{1}ILCT (intraligand or intramolecular charge transfer state) for **4-1-L**, **4-2-L** and **4-5-L** in CH$_2$Cl$_2$. For **4-4-L**, the

emission exhibits mixed characters of $^1\pi,\pi^*/^1$ILCT. This assignment is supported by the different solvatochromic effects for these ligands. As demonstrated in Figure 4.4 for **4-1-L** – **4-6-L**, **4-3-L** and **4-6-L** exhibit minor solvatochromic effects, with the similar shape of spectra in both polar and nonpolar solvents and a slight red-shift when the polarity of solvent increases. These features are characteristics of $^1\pi,\pi^*$ fluorescence. However, for the other four ligands, the fluorescence spectra become structureless and drastically red-shifted in polar solvents (such as CH_2Cl_2 and CH_3CN), reflecting the transition from $^1\pi,\pi^*$ character in less polar solvents to ^{1}ILCT character in more polar solvents. Comparing the emission spectra of **4-1-L** – **4-6-L**, it is clear that the fluorescence energy trend follows the similar trend as the UV-vis absorptions, namely, both substitution and extended π-conjugation of the linkage between the BTZ substituent and the C^N^N core effectively lower the fluorescence energy. In addition, both the substitution and extended π-conjugation lead to significant charge transfer characters in their respective fluorescence spectra in polar solvents. It is worth noting that strong electron withdrawing group like NO_2 in **4-1-L** plays the most significant role in switching the emission into charge transfer fluorescence, testified by the solvatochromic study shown in Figure 4.4, in which the emission was only observed in dichloromethane and THF but diminished in nonpolar solvent such as hexane and toluene and in the more polar solvent CH_3CN.

Table 4.2. Fluorescence quantum yields of ligands **4-1-L** – **4-6-L** different solvents

	CH_2Cl_2	Hexane	CH_3CN	THF	Toluene
4-1-L	0.032	0.0077	0.008	0.032	0.017
4-2-L	0.924	0.945	0.848	0.968	0.992
4-3-L	0.957	0.879	0.916	0.920	0.945
4-4-L	0.991	0.912	0.922	0.919	0.978
4-5-L	0.921	0.907	0.857	0.921	0.946
4-6-L	0.795	0.727	0.783	0.785	0.800

The emission spectra of **4-1-L** – **4-6-L** in butyronitrile glassy matrix at 77 K are shown in Figure 4.3b. The spectra become narrower and more structured (except **4-1-L**) in

comparison to those at room temperature but essentially remain the similar energy. Therefore, they are attributed to the low-temperature fluorescence.
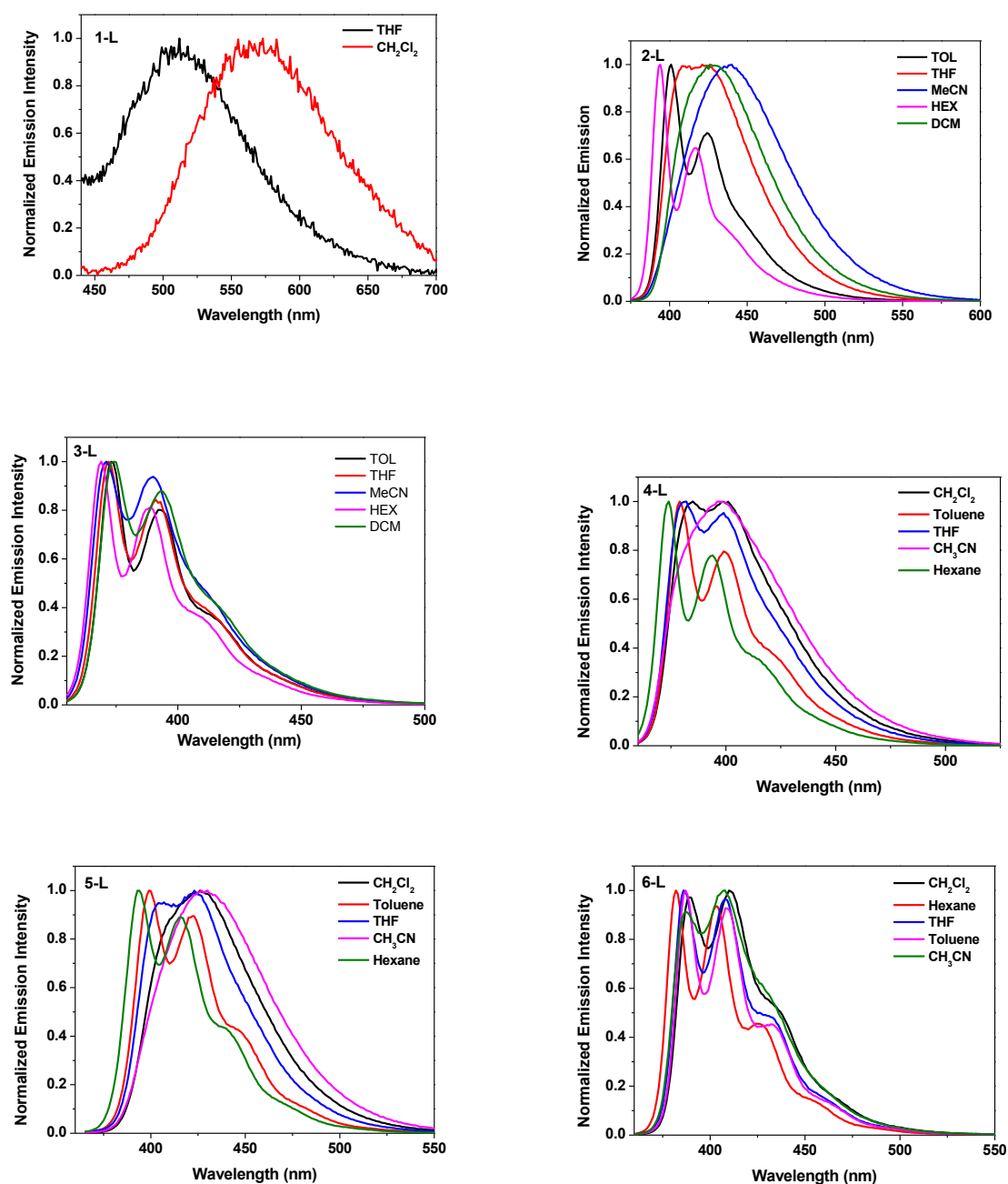
Figure 4.4. Normalized fluorescence spectra of **4-1-L** – **4-6-L** in different solvents. λ_{ex} = 347.5 nm.

The emission spectra of the Pt(II) complexes **4-1** – **4-6** in CH_2Cl_2 at room temperature are displayed in Figure 4.3c. Despite the different substituents and π-linkage, the emission spectra of these complexes all resemble each other, with a remarkable Stokes shift, distinct vibronic structure, long lifetime (3.4–7.5 μs), and minor solvatochromic effect as shown in

147

Figure 4.5. Taking these features into account, we can assign the observed emission of **4-1** – **4-6** to the phosphorescence predominantly from the C^N^N core localized $^3\pi,\pi^*$ state. However, contribution from the ^{3}MLCT state is possible in view of the several microseconds lifetime, which is relatively shorter than a pure $^3\pi,\pi^*$ phosphorescence, and the minor but clear negative solvatochromic effect. This assignment is also supported by the small thermally induced Stokes shifts for these complexes, *i.e.* 289 cm^{-1} for **4-1**, 202 cm^{-1} for **4-2**, 353 cm^{-1} for **4-3**, 381 cm^{-1} for **4-4**, 412 cm^{-1} for **4-5**, and 205 cm^{-1} for **4-6**. This phenomenon is also consistent with that observed from the Pt(II) complexes with a 2-(9,9-dihexadecyl-7-(4-R-phenylethynyl)-fluoren-2-yl)-1,10-phenanthroline ligand.[31]

Table 4.3. Emission characteristics of complexes **4-1** – **4-6** in different solvents at room temperature

λ_{em} /nm (τ_{em}/ns); Φ_{em}				
	CH$_2$Cl$_2$	**Hexane**	**CH$_3$CN**	**THF**	**Toluene**
4-1	594 (5640), 640 (5490); 0.133	598 (1190), 640 (1160); 0.038	588 (3770), 630 (3470); 0.066	591 (295), 639 (280); 0.0060	594 (3240), 634 (3250); 0.052
4-2	593 (3620), 636 (3530); 0.053	599 (1250), 645 (1290); 0.029	586 (6020), 630 (6320); 0.048	-	594 (2230), 635 (1800); 0.067
4-3	588 (4020); 0.084	591 (905); 0.042	583 (3620), 624 (3790); 0.043	588 (290), 632 (290); 0.0063	591 (2040); 0.056
4-4	591 (4120), 635 (4160); 0.051	600 (1100), 650 (1130); 0.020	585 (5010), 625 (5060); 0.048	590 (280), 620 (280); 0.0057	593 (1870), 636 (1810); 0.040
4-5	590 (3120), 640 (3120); 0.069	596 (1180), 645 (1210); 0.032	583 (3640), 625 (3960); 0.059	591 (195), 638 (200); 0.0059	592 (1490), 632 (1160); 0.061
4-6	589 (5430), 632 (5760), 660 (5780); 0.092	594 (1810), 636 (1780), 680 (1950); 0.037*	583 (1790), 600 (1750), 630 (1710); 0.02	-	591 (2310), 638 (2530), 680 (2160); 0.064

*with 5% CH$_2$Cl$_2$
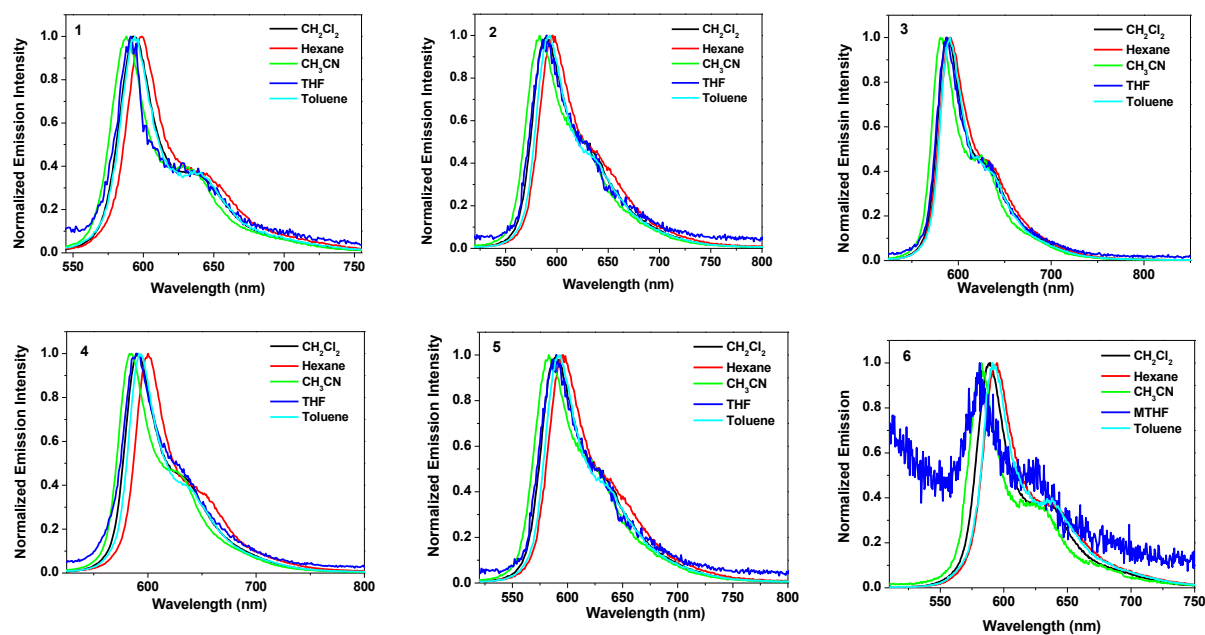
Figure 4.5. Normalized emission spectra of **4-1** – **4-6** in different solvents. λ_{ex} = 436 nm.

Concentration-dependent emission study of **4-1** – **4-6** in CH$_2$Cl$_2$ was conducted. As exemplified in Figure 4.6 for complex **4-3**, the emission intensity increases with increased concentration up to 2×10^{-5} mol/L. Above this concentration, the emission intensity decreases when the concentration gets higher. Considering the remarkable ground-state absorption of this complex at the excitation wavelength (381 nm), primary inner-filter effect is clearly a cause. Contribution from the ground-state aggregation can be excluded because our concentration-dependent UV-vis absorption study described earlier confirms that no ground-state aggregation occurs in the concentration range used in our study. However, lifetime measurements reveal that the lifetime of the solution keeps decreasing with increased concentration, which clearly indicates the presence of self-quenching. The self-quenching rate constant deduced for **4-3** at 589 nm emission wavelength is 1.53×10^9 L.mol^{-1}.s^{-1}, which is in line with those reported for Pt(II) terpyridine, Pt(C^N^N) or Pt(II) diimine complexes.[17,32, 33] Similar phenomena were observed from the other five complexes, and the results are shown in Figure 4.6 and in Table 4.1.

149
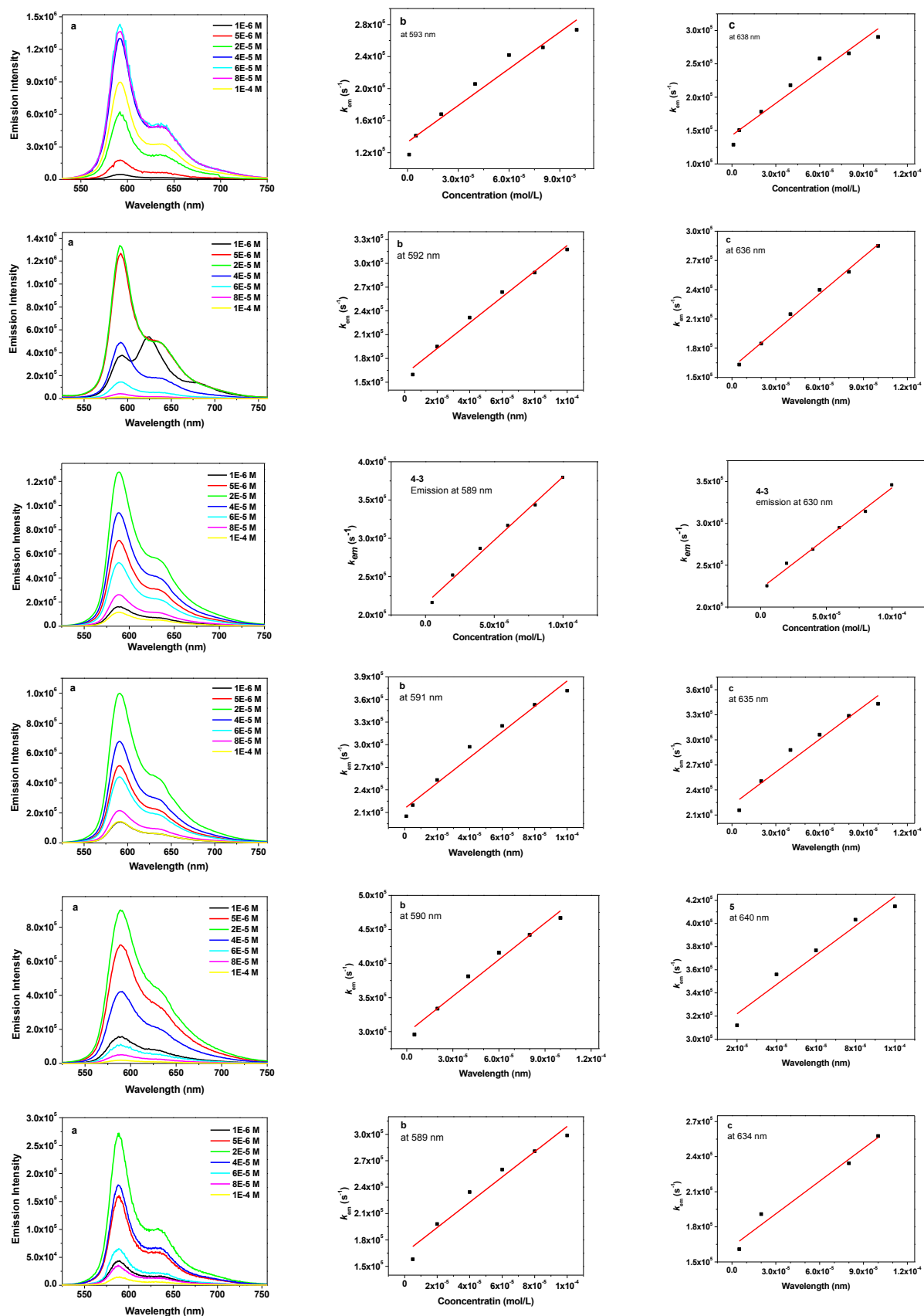
Figure 4.6. (a) Emission spectra of **4-1 – 4-6** at different concentrations in CH₂Cl₂. (b) & (c) Stern-Volmer plots for the emission of **4-1 – 4-6** at the wavelengths indicated in CH₂Cl₂.

The emission spectra of **4-1** – **4-6** at 77 K BuCN glassy matrix are presented in Figure 4.3d. These spectra are somewhat blue-shifted and become more structured and narrower with respect to those at room temperature, which are ascribed to the rigidochromic effect.[34] The vibronic progressions for **4-1** – **4-6** are in the range of 1212–1357 cm^{-1}, and the thermally induced Stokes shifts for these complexes are approximately 200–410 cm^{-1}. All these features indicate the $^3\pi,\pi^*$ nature of the emission at 77 K for these complexes.

4.3.3. Transient Absorption

The nanosecond transient difference absorption (TA) measurements were conducted for ligands **4-1-L** – **4-6-L** and complexes **4-1** – **4-6** in acetonitrile to understand the triplet excited-state characteristics. By performing the transient absorption experiments, the spectral feature of the triplet excited-state absorption can be obtained, and the spectral region where the excited state absorbs stronger than the ground state can be identified from the positive absorption band(s) of the TA spectrum. In addition, the excited-state lifetime and the triplet excited-state quantum yield can be deduced from the decay of the TA and determined by the relative actinometry, respectively.

The nanosecond transient absorption spectra of **4-1-L** – **4-6-L** at zero delay after excitation are displayed in Figure 4.7a. In addition to the bleaching bands in the UV region that correspond to the ground-state absorption bands, all the ligands show moderate to strong transient absorption in the visible spectral region. Compared to **4-3-L**, the TA bands of **4-1-L**, **4-2-L** and **4-4-L** are much broader. For the three ligands with different π-conjugated linkages, *i.e.* **4-2-L**, **4-5-L**, and **4-6-L**, the major TA band is noticeably red-shifted from **4-6-L**, to **4-5-L**, and to **4-2-L** although the TA bands of **4-2-L** and **4-5-L** are weaker. The TAs of all of the ligands show well time-resolved decay as illustrated for **4-1-L** in Figure 4.7b and Figures 4.8 for **4-2-L** – **4-6-L**. The lifetimes deduced from the decay of TA are all tens of μs, implying that the excited state giving rise to the observed TA spectra should be the $^3\pi,\pi^*$.
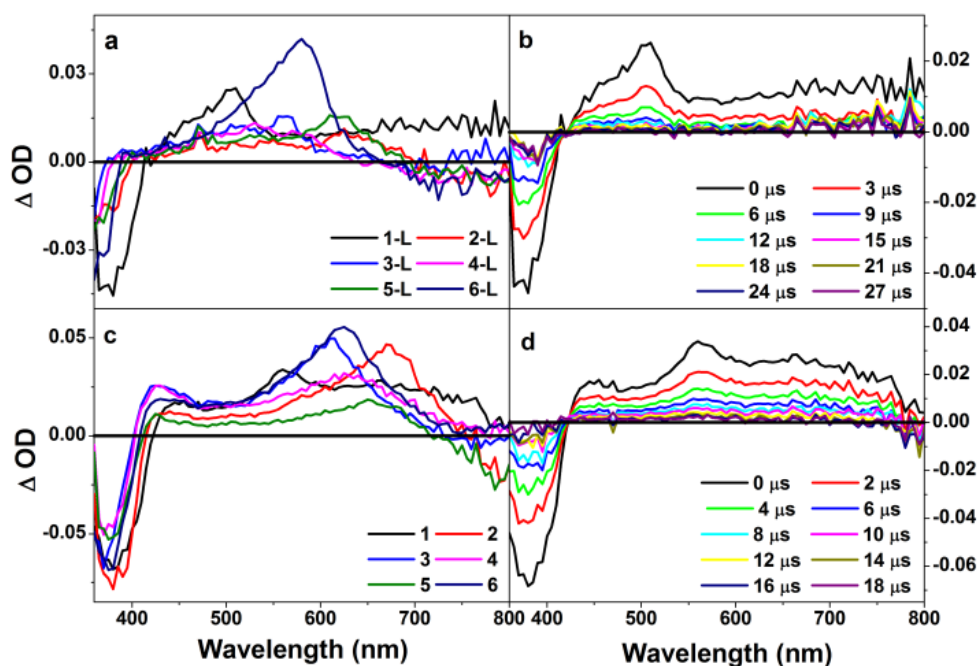
Figure 4.7. Nanosecond transient difference absorption spectra of (a) ligands **4-1-L** – **4-6-L** at zero delay after excitation; (b) time-resolved TA spectra of **4-1-L**; (c) complexes **4-1** – **4-6** at zero delay after excitation; (d) time-resolved TA spectra of **4-1**. All of the spectra were measured in CH_3CN, λ_{ex} = 355 nm, A_{355} = 0.4 in a 1-cm cuvette.

The TA spectra of **4-1** – **4-6** at zero delay after excitation are illustrated in Figure 4.7c. The triplet excited-state lifetimes, extinction coefficients, and quantum yields are deduced or calculated and the results are summarized in Table 4.1. The TAs of all of the complexes show well time-resolved decay as illustrated for **4-1** in Figure 4.7d and Figures 4.8 for **4-2** – **4-6**. The TA spectra of all complexes possess three characteristic bands: the bleaching band in the blue spectral region corresponding to their respective $^1\pi,\pi^*$ absorption band, the moderate and narrow TA band in the wavelength range of 400–500 nm, and the broad and strong TA band in the wavelength range of 500–700 nm. The energy of the 500–700 nm TA band varies with the terminal substituent and the extent of π-conjugation between the C^N^N core and the BTZ unit: both electron-withdrawing and electron- donating substituents (NO_2 in **4-1**, BTZ in **4-2**, and OCH_3 in **4-4**) cause a red-shift of the major TA band, extending the π-conjugation in the linkage also effectively red-shifts the major TA bands in **4-2** and **4-5** compared to that in **4-6**. From the decay of the TA, the triplet lifetimes were deduced to be 5

– 8 μs, suggesting that the TA spectra likely arise from the ligand based $^3\pi,\pi^*$ state as well, which is supported by the red-shift of the major TA bands in **4-1** – **4-6** compared to the TA bands in their corresponding ligands. The red-shifting reflects the interactions between the ligand π orbital and the metal d orbital.
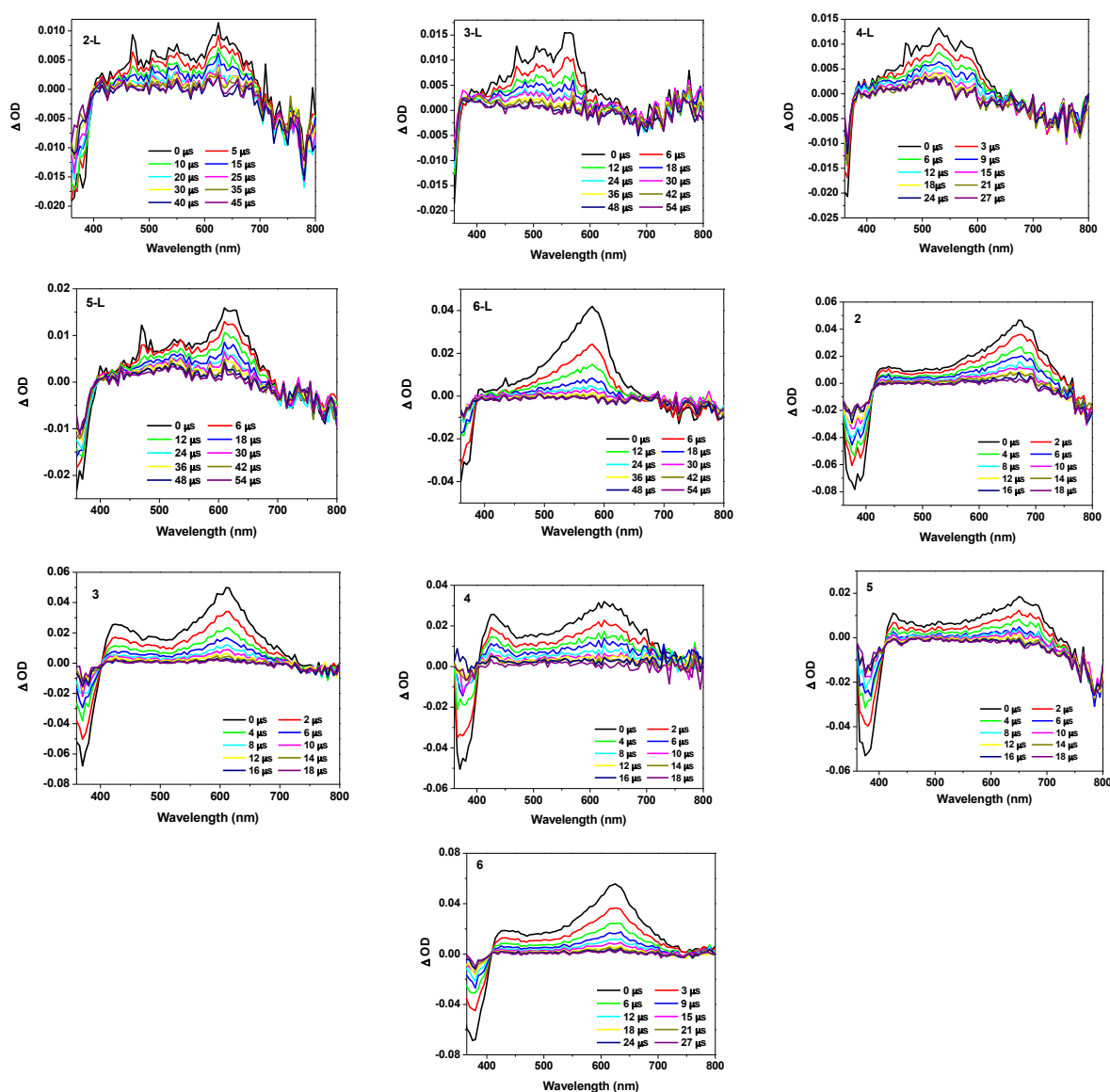
Figure 4.8. Nanosecond time-resolved transient absorption spectra of **4-2-L** – **4-6-L** and **4-2** – **4-6** in CH$_3$CN. λ_{ex} = 355 nm. A$_{355}$ = 0.4 in a 1-cm cuvette.

4.3.4. Reverse Saturable Absorption (RSA)

As manifested by the positive absorption bands in the visible spectral region of the TA spectra, complexes **4-1** – **4-6** all exhibit stronger excited-state absorption than that of the ground state at 532 nm. Meanwhile, the triplet-state lifetimes are significantly longer than

the ns laser pulse width (4.1 ns). Therefore, it is expected that these complexes would exhibit reverse saturable absorption (decrease of transmission with increased incident energy) for ns laser pulses at 532 nm. To verify this assumption, nonlinear transmission experiment was carried out for complexes **4-1 – 4-6** in CH_2Cl_2 solutions at a linear transmittance of 90% in a 2-mm cuvette using the 532-nm ns laser pulses. Figure 6 displays the nonlinear transmission results. The transmissions of all of the complexes decrease remarkably with increased incident energy, which clearly demonstrates a strong RSA from these complexes. The strength of the RSA follows this trend: **4-6**＜**4-4**＜**4-5**＜**4-2**≤**4-3**＜**4-1**. It appears that electron-withdrawing substituents (NO_2 and BTZ) enhance the RSA of **4-1** and **4-2**, while electron-donating substituent (OCH_3 in **4-4**) decreases the RSA at 532 nm. Extending the π-conjugation of the linkage also results in improved RSA, as evident by the trend of **4-6**＜**4-5** ＜**4-2**.
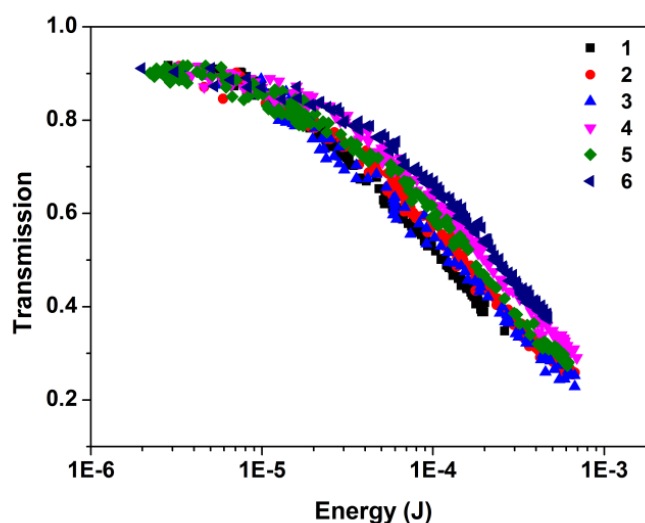
Figure 4.9. Nonlinear transmission curves for **4-1 – 4-6** at 532 nm for 4.1 ns laser pulses. The radius of the beam waist at the focal point was approximately 96 μm. The linear transmission for all sample solutions was adjusted to 90% in a 2 mm cuvette.

To rationalize the trend of RSA performance for these complexes, the ratios of the excited-state absorption cross section with respect to that of the ground state (σ_{ex}/σ_0) at 532 nm, which is the key parameter determining the RSA, have to been evaluated. According to

the ground-state absorption at 532 nm and at the wavelength of the TA band maximum, the

optical density changes (ΔOD) at 532 nm and at the TA band maximum, the molar extinction

coefficient at the TA band maximum ($\varepsilon_{T1\text{-}Tn}$), and the method described by our group

previously,[35] the excited-state absorption cross sections (σ_{ex}) for **4-1** – **4-6** at 532 nm were

estimated and the results are shown in Table 4.4. The calculated ratios of σ_{ex}/σ_0 follow this

trend: **4-6**<**4-4**<**4-5**<**4-2**<**4-3**<**4-1**, which matches the observed RSA trend very well.

Table 4.4. Ground-state (σ_0) and excited-state (σ_{ex}) absorption cross-sections of complexes **4-1** – **4-6** at 532 nm in CH_3CN.

	4-1	**4-2**	**4-3**	**4-4**	**4-5**	**4-6**
$\sigma_0/\ 10^{-18}$ cm	0.35	0.59	0.38	0.57	0.57	0.67
$\sigma_{ex}/\ 10^{-18}$ cm	65	84	59	74	80	80
σ_{ex}/σ_0	186	142	155	130	140	125

4.4. Conclusions

We have synthesized and characterized five new 6-[9,9-di(2-ethylhexyl)-7-*R*-9*H*-

fluoren-2-yl]-2,2'-bipyridine ligands (**4-1-L** – **4-6-L**) and their Pt(II) complexes (**4-1** – **4-6**)

(*R* = 4-R'-phenylethynyl with R'= NO_2, BTZ, H and OCH_3 or *R* = 4'-BTZ-phen-1-yl or BTZ).

The effects of terminal substituents and the different π-conjugated linkages between the BTZ

component and the C^N^N core on the photophysics of these ligands and complexes and on

the RSA of the complexes were systematically investigated. It is found that both the terminal

substitution and extended π-conjugation of the linkage cause pronounced red-shift of the UV-

vis absorption bands and the fluorescence bands in the ligands; and induces significant

intraligand charge transfer character in their fluorescence in polar solvents like CH_2Cl_2 and

CH_3CN. **4-1-L** – **4-6-L** all exhibit moderate triplet transient absorption in the visible spectral

region. Terminal substitution causes a broadening of the TA bands in **4-1-L**, **4-2-L** and **4-4-**

L; while extended π-conjugation in the linkage induces a red-shift of the TA bands in **4-2-L**

and **4-5-L** compared to that in **4-6-L**. After complexation with the Pt(II) ion, the major

absorption bands in the formed complexes **4-1** – **4-6** all bathochromically shift compared to

those of their respective ligands, accompanied by a low-energy charge transfer tail. Terminal substitution and extending π-conjugation exert similar effects to those observed in the ligands. In contrast, the emission spectra and energies are essentially independent of the variation of the substituent and degree of π-conjugation for **4-1** – **4-6**, suggesting a C^N^N core localized $^3\pi,\pi^*$ phosphorescence in nature. Similar to the trend observed in the UV-vis absorption spectra, the TA bands in **4-1** – **4-6** also red-shift with terminal substitution and extended π-conjugation. These bands also notably shift to lower energy compared to those in their corresponding ligands. The ground-state absorption and transient absorption studies demonstrate that the absorption properties of both the ground state and the excited state can be efficiently tuned by structural modifications. As a result, complexes **4-1** – **4-6** exhibit strong RSA for ns laser pulses at 532 nm. The degree of RSA (**4-6**＜**4-4**＜**4-5**＜**4-2**≤**4-3**＜**4-1**) is also affected by the substituents and the π-conjugation on the ligand. The RSA performance is efficiently improved by electron-withdrawing substituents (NO_2 and BTZ) and by extending the π-conjugation; while electron-donating substituent (OCH_3 in **4-4**) decreases the RSA at 532 nm. The broadband excited-state absorption, long triplet lifetime and strong RSA of **4-1** – **4-6** at 532 nm suggest these complexes could be promising nonlinear absorbing materials for photonic device applications.

4.5. References

[1] Li, Z.; Sun, W. *Dalton Trans.* **2013**, *42*, 14021.

[2] Rosenberg, B.; VanCamp, L.; Trosko, J. E.; Mansour, V. H. *Nature* **1969**, *222*, 385.

[3] Chiavarino, B.; Crestoni, M. E.; Fornarini, S.; Scuderi, D.; Salpin, J.-Y. *J. Am. Chem. Soc.* **2013**, *135*, 1445.

[4] Chen, S.; Xu, D.; Jiang, H.; Xi, Z.; Zhu, P.; Liu, Y. *Angew. Chem. Int. Ed.* **2012**, *51*, 12258.

⁵ Xiao, L.; Chen, Z.; Qu, B.; Luo, J.; Kong, S.; Gong, Q.; Kido, J. *Adv. Mater.* **2011**, *23*, 926.

⁶ Sommer, J. R.; Shelton, A. H.; Parthasarathy, A.; Ghiviriga, I.; Reynolds, J. R.; Schanze, K. S. *Chem. Mater.* **2011**, *23*, 5296.

⁷ Wu, Y.; Wu, S.-X.; Li, H.-B.; Geng, Y.; Su, Z.-M. *Dalton Trans.* **2011**, *40*, 4480.

⁸ Du, P. Eisenberg, R. *Chem. Sci.* **2010**, *1*, 502.

⁹ Liu, Y.; Wu, W.; Zhao, J.; Zhang, X.; Guo, H. *Dalton Trans.* **2011**, *40*, 9085.

¹⁰ Singh-Rachford, T. N.; Haefele, A.; Ziessel, R.; Castellano, F. N. *J. Am. Chem. Soc.* **2008**, *130*, 16164.

¹¹ Vestberg, R.; Westlund, R.; Eriksson, A.; Lopes, C.; Carlsson, M.; Eliasson, B.; Glimsdal, E.; Lindgren, M.; Malmströ1m, E. *Macromolecules* **2006**, *39*, 2238.

¹² Sun, W.; Zhang, B.; Li, Y.; Pritchett, T. M.; Li, Z.; Haley, J. E. *Chem. Mater.* **2010**, *122*, 6384.

¹³ Zhang, B.; Li, Y.; Liu, R.; Pritchett, T. M.; Azenkeng, A.; Ugrinov, A.; Haley, J. E.; Li, Z.; Hoffmann, M. R.; Sun, W. *Chem. Eur. J.* **2012**, *18*, 4593.

¹⁴ Li, Z.; Badaeva, E.; Zhou, D.; Bjorgaard, J.; Glusac, K. D.; Killina, S.; Sun, W. *J. Phys. Chem. A* **2012**, *116*, 4878.

¹⁵ Liu, R.; Zhou, D.; Azenkeng, A.; Li, Z.; Li, Y.; Glusac, K. D.; Sun, W. *Chem. Eur. J.* **2012**, *18*, 11440.

¹⁶ Hissler, M.; Connick, W. B.; Geiger, D. K.; McGarrah, J. E.; Lipa, D.; Lachicotte, R. J.; Eisenberg, R. *Inorg. Chem.* **2000**, *39*, 447.

¹⁷ Liu, X.-G.; Sun, W. *Inorg. Chim. Acta.* **2012**, *388*, 140.

¹⁸ Ji, Z.; . Li, S; Li, Y.; Sun, W. *Inorg. Chem.* **2010**, *49*, 1337.

¹⁹ Haskins-Glusac, K.; Ghiviriga, I.; Abboud, K. A.; Schanze, K. S. *J. Phys. Chem. B* **2004**, *108*, 4969.

[20] Li, Z.; Badaeva, E.; Ugrinov, A.; Kilina, S.; Sun, W. *Inorg. Chem.* **2013**, *52*, 7578.

[21] Liu, R.; Azenkeng, A.; Zhou, D.; Li, Y.; Glusac, K. D.; Sun, W. *J. Phys. Chem. A* **2013**, *117*, 1907.

[22] Li, Y.; Liu, R.; Badaeva, E.; Kilina, S.; Sun, W. *J. Phy. Chem. C* **2013**, *117*, 5908.

[23] Shin, D.; Switzer, C. *Chem. Commun.* **2007**, *42*, 4401.

[24] Geng, Y.; Culligan, S. W.; Trajkovska, A.; Wallace, J. U.; Chen, S. H. *Chem. Mater.* **2003**, *15*, 542.

[25] Demas, J. N.; Crosby, G. A. *J. Phys. Chem.* **1971**, *75*, 991.

[26] Van Houten, J.; Watts, R. *J. Am. Chem. Soc.* **1976**, *98*, 4853.

[27] Eaton, D. F. *Pure Appl. Chem.* **1988**, *60*, 1107.

[28] Carmichael, I.; Hug, G. L. *J. Phys. Chem. Ref. Data.* **1986**, *15*, 1.

[29] Firey, P. A.; Ford, W. E.; Sounik, J. R.; Kenney, M. E.; Rodgers, M. A. J. *J. Am. Chem. Soc.* **1988**, *110,* 7626.

[30] Guo, F.; Sun, W.; Liu, Y.; Schanze, K. *Inorg. Chem.* **2005**, *44*, 4055.

[31] Liu, X.-G.; Sun, W. *Eur. J. Inorg. Chem.* **2013** (accepted).

[32] Shao, P.; Li, Y.; Pritchett, T. M.; Sun, W. *Inorg. Chem.* **2010**, *49*, 4507.

[33] Ji, Z.; Azenkeng, A.; Hoffmann, M.; Sun, W. *Dalton Trans.* **2009**, 7725.

[34] Lai, S.; Chan, M C. W.; Cheung, K.; Che, C. *Inorg. Chem.* **1999**, *38*, 4262.

[35] Li, Y.; Liu, R.; Badaeva, E.; Kilina, S.; Sun, W. *J. Phy. Chem. C* **2013**, *117*, 5908.

CHAPTER 5. SYNTHESIS, PHOTOPHYSICS, AND NONLINEAR ABSORPTION OF 7-(BENZOTHIAZOL-2-YL)-9,9-DI(2-ETHYLHEXYL)- 9H-FLUOREN-2-YL TETHERED [Ir(BPY)(PPY)₂]PF₆ AND Ir(PPY)₃ (BPY = 2,2'-BIPYRIDINE, PPY = 2-PHENYLPYRIDINE)

5.1. Introduction

Another important family of transition-metal complexes is iridium(III) complexes. Comparing to the square-planar geometry of platinum(II) complexes, iridium complexes(III) adopt octahedral geometry. Meanwhile, iridium has the largest spin-orbit coupling constant among all transition metals.[1] Thus, strong intersystem crossing to the triplet excited state and high phosphorescence efficiency are expected for iridium(III) complexes. Extensive research has been engaged in utilizing the photoluminescence properties of iridium(III) complexes as dopant for organic light-emitting diodes (OLEDs)[2,3] and light-emitting electrochemical cells (LEECs).[4,5] Other applications of Ir(III) complexes including therapeutic and bioimaging,[6] oxygen sensing,[7] and photocatalic water splitting[8] are also explored.

It has been widely established that the electronic structure can be efficiently controlled by deliberate structural modifications.[8,9] By using different types of diimine or arylpyridine ligands,[10] or varying substituent on the ligands,[11] the nature of the lowest singlet and triplet excited states can be significantly adjusted. For instance, density functional theoty (DFT) calculations and experimental studies carried out by Hay and co-workers[12] revealed that metal d orbital contributions in the low lying metal to ligand charge transfer states varied from 45% to 60% in replacing one ppy ligand (2-phenylpyridine) in Ir(ppy)₃ with acetoylacetonate or benzyolacetonate. In another reported work by Watts and Houten, the energy levels and lifetime of the lowest triplet excited states of iridium 1,10-phenathroline complexes were found to be readily tuned through different substituents such as electron

withdrawing groups (-NO$_2$ and -Cl) or electron donating groups (-Br and -CH$_3$) on the 4, 5, 6, or 7 position of the 1,10-phenathroline ligand.[13]

Further structure-property correlation studies were conducted in more "bulky" molecules with molecule weight up to 3000. In recent reports by Zhao,[14, 15] the photophysics of tris-cyclometalated iridium complexes with varied positions or repeating-unit of the alkylated fluorenyl oligomer on the 2-phenylpyridine ligand was studied. Spectroscopic studies and DFT calculations revealed that both the radiative and nonradiative decay rates, as well as the phosphorescence quantum yield, decrease with increased chain length of the oligofluorene, due to localization of the triplet excitons. Meanwhile, the contribution of the MLCT state to the emissive excited state is significantly affected by the attachment position of the oligofluorene. Particularly, the extended π-conjugation of the substituent at the *para*-position of the cyclometalating carbon of the phenyl ring produced a ligand centered triplet excited state with long lifetime and considerable quantum yield.

Unlike of the extensive study on the light-emitting applications, the research on nonlinear absorption of iridium(III) complexes is quite limited. Schanze[16] first reported the dual mechanism nonlinear absorption of an iridium(III) complex. In the heteroleptic complex with two 2-phenylpyridine ligands and one 4,4′-(2,2′-bipyridine-5,5′-diylbis(ethyne-2,1-diyl))bis(*N,N*-dihexylaniline) ligand, strong excited-state absorption in the near infrared region was observed. Meanwhile, the absorbing excited state can be populated by 5 ns, 1064 nm laser via two-photon absorption. Therefore, both one-photon process and two-photon absorption can induce the nonlinear transmission by the complex. Our group also reported he photophysics and reverse saturable absorptions of fout heteroleptic Ir(III) complexes with extended π-conjugation on the bypyridine and the phenylpyridyl ligands.[17] It was found that extending the π-conjugation of the bypiridine ligand can significantly increase the triplet lifetime by admixing bipyridine-localized $^3\pi,\pi$ character into the lowest triplet excited state;

whilst the extended π-conjugation on the phenylpyridyl ligand decreased the triplet lifetime due to predominantly ^{3}MLCT/^{3}LLCT characters. All complexes exhibited very strong RSA at 532 nm for nanosecond laser. However, there is no report on the nonlinear absorption of the neutral Ir(III) complexes to the best of our knowledge.

In this chapter, five Ir(III) complexes **5-1** – **5-5** were designed, synthesized and studied. The structure of these complexes are shown in Chart 5.1, which features 7-(benzothiazol-2-yl)-9,9-di(2-ethylhexyl)-9H-fluoren-2-yl pedant to the coordination core at the *para-* position of the cyclometalating carbon of the phenyl ring. The ultimate goal of this research is to illustrate the structure-property relationship in neutral and cationic Ir(III) complexes in order to develop ideal nonlinear absorbing materials. Complexes **5-1** and **5-2** contain one bipyridine ligand and two substituted 2-phenylpyridine ligands instead of three 2-phenylpyridine ligands in complexes **5-3** – **5-5**. Therefore, the comparison is based on the different nature of bipyridine and 2-phenylpyridine, with the latter having much stronger ligand field. Instead of single bond connection in **5-1**, the 7-(benzothiazol-2-yl)-9,9-di(2-ethylhexyl)-9H-fluoren-2-yl unit is connected to the 2-phenylpyridine via a triple bond in **5-2**. In this way, the effect of extended π-conjugation length will be evaluated. From **5-3** to **5-5**, the number of the 7-(benzothiazol-2-yl)- 9,9-di(2-ethylhexyl)-9H-fluoren-2-yl unit increases from one in **5-3**, to two in **5-4**, and to three in **5-5**. By execution of this variation, we are expecting to have the interplay or mixing between the ligand centered $^3\pi,\pi^*$ state predominantly contributed by the 7-(benzothiazol-2-yl)-9,9-di(2-ethylhexyl)-9H-fluoren-2-yl component and the ^{3}MLCT/^{3}LLCT excited state related to the coordination core. Therefore, complexes exhibiting different emission and absorbing characteristics are anticipated. Moreover, comparison of the photophysics of **5-1** to that of **5-4** would allow us to assess the effect of ionic vs neutral complexes. Finally, reverse saturable absorption for these complexes will be investigated, aiming to develop ideal nonlinear absorbing materials.
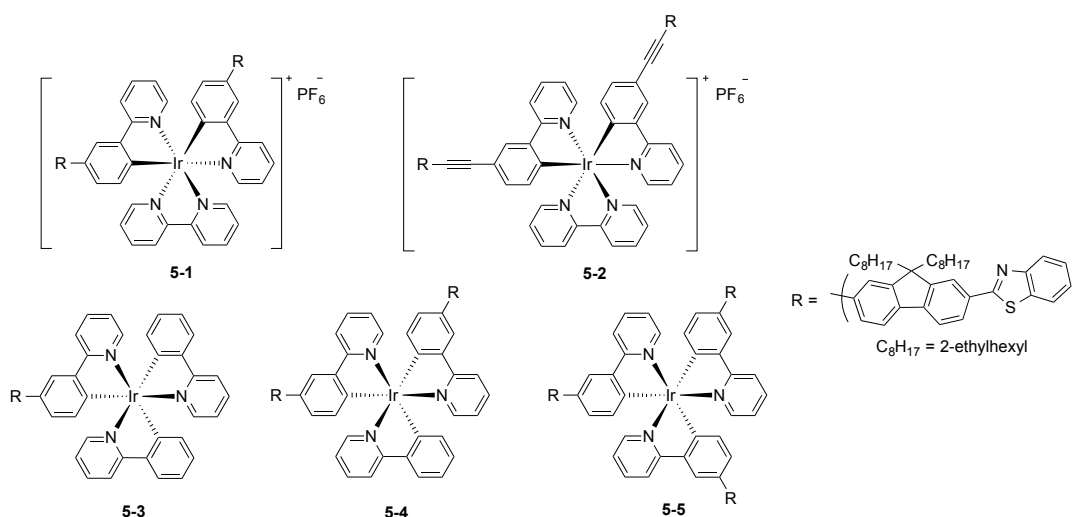
Chart 5.1. Structures of complexes **5-1 − 5-5**

5.2. Experimental Section

5.2.1. Synthesis and Characterization

The synthetic routes for **5-1 − 5-5** are illustrated in Scheme 5.1. All the chemicals and solvents were purchased from Aldrich Chemical Co. or Alfa Aesar and used as received. Silica gel for chromatography was purchased from Sorbent Technology (60 Å, 230−400 mesh, 500−600 m^2/g, pH: 6.5−7.5). Complexes **5-1 − 5-5** and ligands **5-1-L − 5-2-L** were characterized by ^{1}H NMR, electrospray ionization mass spectrometry (ESI-MS), and elemental analyses. Other intermediatex were characterized by ^{1}H NMR. ^{1}H NMR was obtained on Varian Oxford-VNMR spectrometers (400 or 500 MHz). ESI-MS analyses were performed on a Bruker BioTOF III mass spectrometer. Elemental analyses were conducted by NuMega Resonance Laboratories, Inc. in San Diego, California. Br-F8-BTZ was synthesized according to literature procedure.[18]
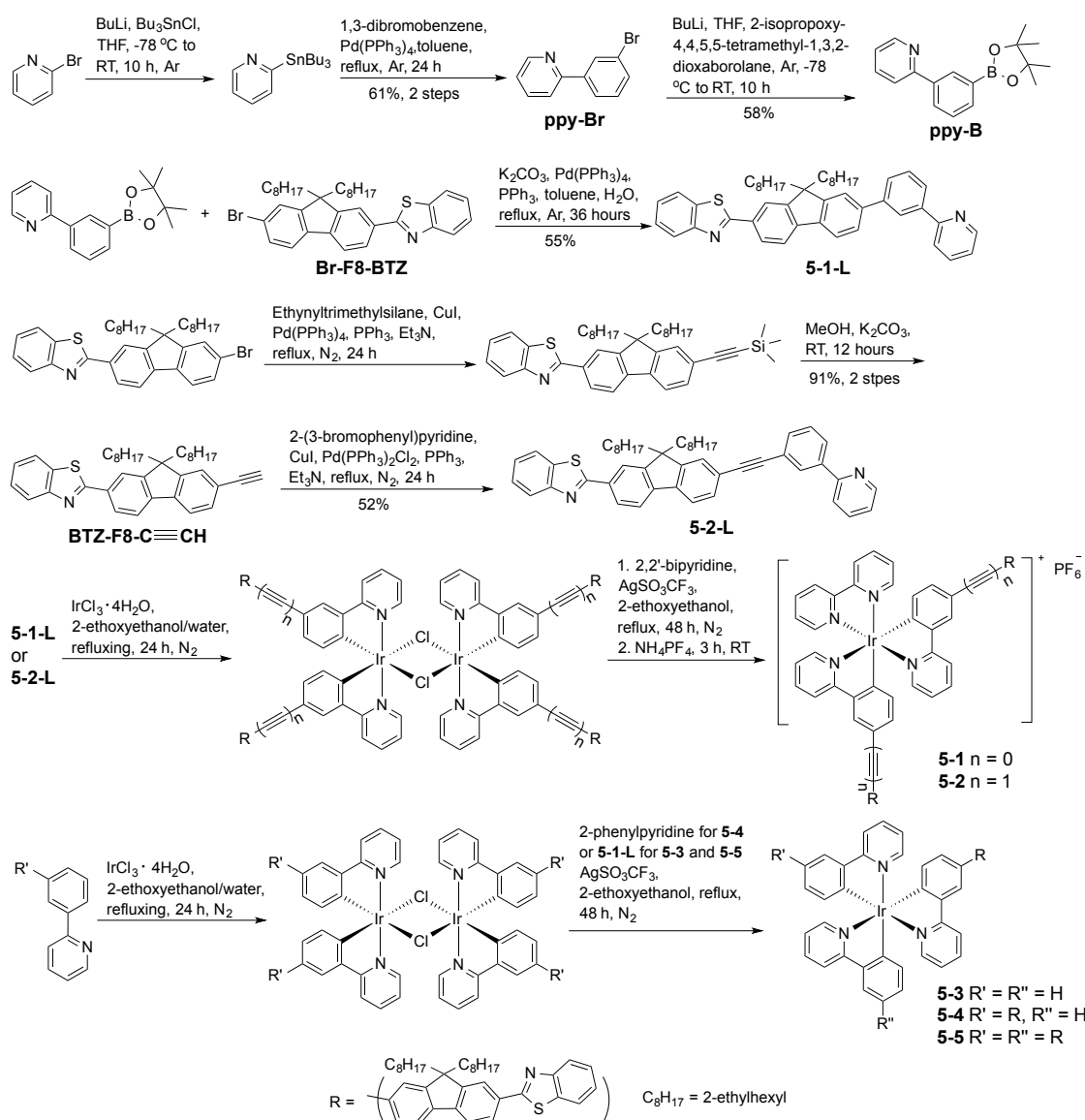
Scheme 5.1. Synthetic routes for complexes **5-1 – 5-5**

ppy-Br. To the THF (30 mL) solution of 2-bromopyridine (1 mL, 10.5 mmol) at -78 °C under argon, BuLi in hexane (6 mL, 15 mmol) was added dropwise. The solution was stirred under argon for 90 minutes. Then Bu₃SnCl (3 mL, 11 mmol) was added dropwise at -78 °C. The mixture was then allowed to gradually warm up to room temperature. After 15 hours, the reaction was stopped, and the solution was poured into saturated aqueous NH₄Cl solution (50 mL). The organic layer was collected and dried over MgSO₄. The solvent was removed and the residue was purified by a silica gel column eluted with hexane and DCM (v/v = 8/1). The dark oil collected was dried in vacuum oven for 24 hours and was used for next step reaction directly without any further purification. Then, the dried oil produced from

163

the previous step, 1,3-dibromobenzene (2.5 g, 10.5 mmol), Pd(PPh$_3$)$_4$ (30 mg), and toluene (30 mL) was added. The reaction mixture was degassed with argon and heated to reflux for 24 hours. After reaction, the precipitate was removed by filtration. The solvent of the filtrate was then removed by distillation. The resultant dark oil was purified by running a silica gel column eluted with hexane and ethyl acetate (v/v = 10/1). 1.7 g yellow oil was collected as the final product (yield: 61% from 2-bromopyridine). ^{1}H NMR (CDCl$_3$, 500 MHz): 8.69 – 8.70 (m, 1H), 8.19 (s, 1H), 7.91 (d, J = 8.4 Hz, 1H), 7.73 – 7.77 (m, 1H), 7.69 (d, J = 8.0 Hz, 1H), 7.54 (d, J = 8.0 Hz, 1H), 7.32 – 7.35 (m, 1H), 7.24 – 7.28 (m, 1H).

ppy-B. To the argon protected THF (30 mL) solution of 2-(3-bromophenyl)pyridine (1.5 g, 6.4 mmol) at -78 ^{o}C, BuLi in hexane solution (2.5 M, 4 mL, 10 mmol) was added dropwise. After stirring for 2 hours, 2-isopropoxy-4,4,5,5-tetramethyl-1,3,2-dioxaborolane (2 mL, 11.8 mmol) was added dropwise to the solution. The system was allowed to warm up to room temperature afterwards, and continued stirring for 12 hours. Then the mixture was poured into saturated aqueous NH$_4$Cl solution (100 mL). The organic phase was collected and dried over MgSO$_4$. After removal of the solvent, purification of the residue was carried out by running a silica gel column eluted with mixed solvent of hexane and ethyl acetate (v/v = 7.5/1). 1.04 g colorless oil was collected as the final product (yield: 58%). ^{1}H NMR (CDCl$_3$, 500 MHz): 8.70 – 8.71 (m, 1H), 8.41 (s, 1H), 8.14 – 8.16 (m, 1H), 7.87 – 7.89 (m, 1H), 7.79 – 7.80 (m, 1H), 7.72 – 7.75 (m, 1H), 7.49 – 7.52 (m, 1H), 7.20 – 7.23 (m, 1H), 1.37 (s, 12H).

5-1-L. The mixture of Br-F8-BTZ (1.78 g, 3.0 mmol), ppy-B (0.87 g, 3.0 mmol), K$_2$CO$_3$ (2.11 g, 15.3 mmol), Pd(PPh$_3$)$_4$ (55 mg, 0.048 mmol), PPh$_3$ (150 mg, 0.57 mmol), toluene (30 mL), and H$_2$O (15 mL) was heated to reflux under argon for 36 hours. After reaction, the organic phase was collected, washed with brine (50 mL × 2) and water (50 mL × 2), and dried over MgSO$_4$. After toluene was removed by distillation, the sticky oil was

purified by silica gel column eluted with mixed solvent of hexane and ethyl acetate (v/v = 10/1). 1.11 g colorless oil was collected as the product (yield: 55%). ^{1}H NMR (CDCl$_3$, 500 MHz): 8.76 (d, J = 4.5 Hz, 1H), 8.29 − 8.31 (m, 1H), 8.15 − 8.19 (m, 1H), 8.11 − 8.14 (m, 2H), 8.01 (d, J = 7.5 Hz, 1H), 7.93 (d, J = 8.0 Hz, 1H), 7.78 − 7.86 (m, 4H), 7.70 − 7.74 (m, 3H), 7.59 − 7.62 (m, 1H), 7.50 − 7.53 (m, 1H), 7.40 (t, J = 7.5 Hz, 1H), 7.27 − 7.30 (m, 1H), 2.11 − 2.21 (m, 4H), 0.54 − 0.99 (m, 30H). HRMS: m/z Calc. for $[C_{47}H_{52}N_2S + H]^+$: 677.3924; Found: 677.3918. Anal. Calc. for $C_{47}H_{52}N_2S \cdot 0.5H_2O \cdot 0.5C_6H_{14}$: C, 82.37; H, 8.30; N, 3.84; Found: C, 82.24; H, 8.52; N, 4.21.

BTZ-F8-C≡CH. The mixture of BTZ-F8-Br (3.2 g, 5.3 mmol), (trimethylsilyl)acetylene (1 mL, 7.1 mmol), Pd(PPh$_3$)$_2$Cl$_2$ (10 mg, 0.014 mmol), PPh$_3$ (20 mg, 0.076 mmol), CuI (2 mg, 0.01 mmol), and Et$_3$N (50 mL) was heated to reflux under argon for 24 hours. After reaction, the precipitate was removed by filtration. After being confirmed by HRMS, the yellow oil obtained after distillation of Et$_3$N was used directly for the next step without further purification. The yellow oil collected in the previous step, combined with K$_2$CO$_3$ (3.7 g, 27 mmol) and MeOH (50 mL), was stirred at room temperature for 12 hours. After reaction, water (100 mL) was added and the mixture was extracted with hexane (50 mL × 3). The combined hexane solution was then dried over MgSO$_4$. After the solvent was removed, the red oil was purified by running a silica gel column eluted first with hexane and then with the mixed solvent of hexane and dichloromethane (v/v = 3/1). 2.65 g yellow oil was collected as the final product (yield: 91% from Br-F8-BTZ). ^{1}H NMR (CDCl$_3$, 400 MHz): 8.06 − 8.13 (m, 3H), 7.88 − 7.91 (m, 1H), 7.76 − 7.78 (m, 1H), 7.67 − 7.69 (m, 1H), 7.46 − 7.54 (m, 3H), 7.35 − 7.39 (m, 1H), 3.13 (t, J = 2.4 Hz, 1H), 1.97 − 2.12 (m, 4H), 0.48 − 0.96 (m, 30H).

5-2-L. The mixture of Br-ppy (0.60 g, 2.6 mmol), BTZ-F8-C≡CH (1.4 g, 2.6 mmol), Pd(PPh$_3$)$_2$Cl$_2$ (20 mg, 0,028 mmol), PPh$_3$ (50 mg, 0.19 mmol), CuI (5 mg, 0.025), and Et$_3$N

(30 mL) was heated to reflux under argon for 24 hours. After reaction, the precipitate was removed by filtration. The solvent was removed by distillation and the resulted brown oil was purified by running a silica gel column. The column was first eluted with CH_2Cl_2/hexane (v/v = 1/1) then with ethyl acetate/hexane (v/v = 1/3). 0.95 g yellow oil was collected as the final product (yield: 52%). ^{1}H NMR (CDCl$_3$, 400 MHz): 8.70 – 8.72 (m, 1H), 8.22 – 8.23 (m, 1H), 8.07 – 8.14 (m, 3H), 7.95 – 7.98 (m, 1H), 7.88 – 7.91 (m, 1H), 7.71 – 7.79 (m, 4H), 7.54 – 7.62 (m, 3H), 7.44 – 7.50 (m, 2H), 7.34 – 7.38 (m, 1H), 7.22 – 7.25 (m, 1H), 2.03 – 2.16 (m, 4H), 0.50 – 0.96 (m, 30H). HRMS: m/z Calc. for $[C_{49}H_{52}N_2S + H]^+$: 701.3924; Found: 701.3924. Anal. Calc. for $C_{49}H_{52}N_2S \cdot 0.4H_2O \cdot 0.8C_6H_{14}$: C, 83.15; H, 8.30; N, 3.60; Found: C, 82.79; H, 8.76; N, 4.06.

5-1. The mixture of **5-1-L** (136 mg, 0.20 mmol), IrCl$_3$·4H$_2$O (37 mg, 0.1 mmol), 2-ethoxyethanol (9 mL) and water (3 mL) was heated to reflux under argon for 24 hours. After the mixture was cooled down to room temperature, 50 mL water was added and the yellow precipitate was collected and washed with hexane and water. The resultant yellow powder was dried in vacuum oven for 24 hours and used for the following reaction directly. The yellow powder collected, 2,2'-bipyridine (16 mg, 0.1 mmol), AgCF$_3$SO$_3$ (26 mg, 0.1 mmol) and 2-ethoxyethanol (10 mL) were heated to reflux under argon for 48 hours. After the mixture was cooled down to room temperature, NH$_4$PF$_6$ (17 mg, 0.1 mmol) was added and the mixture was stirred at room temperature for 3 hours. After the reaction was finished, 50 mL ethyl acetate was added. The combined organic solution was washed with brine (50 mL × 3). After drying over MgSO$_4$ and filtered, the solvent was removed by distillation. Purification was conducted by a flash silica gel column eluted with dichloromethane followed by recrystallization from dichloromethane and hexane. 69 mg orange powder was collected as the final product (yield: 37% for two steps). ^{1}H NMR (CDCl$_3$, 500 MHz): 8.70 – 8.71 (m, 2H), 8.19 – 8.23 (m, 2H), 8.07 – 8.16 (m, 10H), 7.99 – 8.00 (m, 2H), 7.79 – 7.93 (m,

8H), 7.62 – 7.65 (m, 6H), 7.48 – 7.52 (m, 4H), 7.39 (t, J = 7.5 Hz, 2H), 7.30 – 7.33 (m, 2H), 7.17 (t, J = 6.5 Hz, 2H), 6.50 – 6.53 (m, 2H), 2.07 – 2.20 (m, 8H), 0.51 – 0.99 (m, 60H). HRMS: m/z Calc. for $[C_{104}H_{110}N_6S_2Ir]^+$: 1699.7866; Found: 1699.7893; m/z Calc. for $[C_{104}H_{110}N_6S_2Ir+H]^{2+}$: 850.3969; Found: 850.3998. Anal. Calc. for $C_{104}H_{110}N_6S_2IrPF_6$: C, 67.69; H, 6.01; N, 4.55; S, 3.48; Found: C, 67.63; H, 6.32; N, 4.62; S, 3.80.

5-2. The synthesis of **5-2** followed the same procedure as for **5-1**. **5-2-L** (140 mg, 0.20 mmol) was used. 43 mg yellow powder was collected as the final product (yield: 23% for two steps). ^{1}H NMR (CDCl$_3$, 400 MHz): 8.67 – 8.69 (m, 2H), 7.69 – 8.18 (m, 24H), 7.35 – 7.56 (m, 12H), 7.10 – 7.13 (m, 2H), 6.30 – 6.32 (m, 2H), 1.98 – 2.12 (m, 8H), 0.46 – 0.90 (m, 60H). HRMS: m/z Calc. for $[C_{108}H_{110}N_6S_2Ir+H]^{2+}$: 874.3970; Found: 874.3999. Anal. Calc. for $C_{108}H_{110}N_6S_2IrPF_6 \bullet 4H_2O$: C, 66.00; H, 6.05; N, 4.28; Found: C, 65.93; H, 6.29; N, 4.03.

5-3. The mixture of 2-phenylpyridine (32 mg, 0.20 mmol), IrCl$_3$·4H$_2$O (37 mg, 0.1 mmol), 2-ethoxyethanol (9 mL) and water (3 mL) was heated to reflux under argon for 24 hours. After the mixture was cooled down to room temperature, 50 mL water was added and the yellow precipitate was collected and washed with hexane and water. The resultant yellow powder was dried in vacuum oven for 24 hours and used for the following reaction directly. The yellow powder collected, **5-1-L** (68 mg, 0.1 mmol), AgCF$_3$SO$_3$ (26 mg, 0.1 mmol) and 2-ethoxyethanol (10 mL) were heated to reflux under argon for 48 hours. After the reaction was finished, 50 mL ethyl acetate was added. The combined organic solution was washed with brine (50 mL × 3). After drying over MgSO$_4$, the solvent was removed by distillation. Purification was carried out by a flash silica gel column eluted with dichloromethane followed by recrystallization from dichloromethane and hexane. 15 mg yellow powder was collected as the final product (yield: 13% for two steps). ^{1}H NMR (CDCl$_3$, 500 MHz): 7.88 – 8.14 (m, 8H), 7.19 – 7.81 (m, 13H), 7.37 – 7.41 (m, 1H), 7.18 – 7.20 (m, 1H), 6.85 – 6.99 (m, 10H), 2.06 – 2.16 (m, 4H), 0.51 – 0.90 (m, 30H). HRMS: m/z Calc. for $[C_{69}H_{67}N_4SIr+H]^+$:

1177.4793; Found: 1177.4806. Anal. Calc. for $C_{69}H_{67}N_4SIr\bullet0.5CH_3COOC_2H_5$: C, 69.86; H, 5.86; N, 4.59; Found: C, 69.98; H, 6.22; N, 4.27.

5-4. The mixture of **5-1-L** (136 mg, 0.20 mmol), $IrCl_3\cdot4H_2O$ (37 mg, 0.1 mmol), 2-ethoxyethanol (9 mL) and water (3 mL) was heated to reflux under argon for 24 hours. After the mixture was cooled down to room temperature, 50 mL water was added and the yellow precipitate was collected and washed with hexane and water. The resultant yellow powder was dried in vacuum oven for 24 hours and used for the following reaction directly. The yellow powder collected, 2-phenylpyridine (16 mg, 0.1 mmol), $AgCF_3SO_3$ (26 mg, 0.1 mmol) and 2-ethoxyethanol (10 mL) were heated to reflux under argon for 48 hours. After the reaction was finished, 50 mL ethyl acetate was added. The combined organic solution was washed with brine (50 mL × 3). After drying over $MgSO_4$, the solvent was removed by distillation. Purification was carried out by a flash silica gel column eluted with dichloromethane followed by recrystallization from dichloromethane and hexane. 11 mg orange powder was collected as the final product (yield: 6% for two steps). ^{1}H NMR ($CDCl_3$, 400 MHz): 7.88 – 8.12 (m, 13H), 7.73 – 7.78 (m, 4H), 7.57 – 7.70 (m, 11H), 7.45 – 7.50 (m, 2H), 7.34 – 7.37 (m, 2H), 7.17 – 7.20 (m, 2H), 6.85 – 7.04 (m, 8H), 2.01 – 2.13 (m, 8H), 0.47 – 0.86 (m, 60H). HRMS: *m/z* Calc. for $[C_{105}H_{110}N_5S_2Ir+2H]^{2+}$: 849.8993; Found: 849.8991. Anal. Calc. for $C_{105}H_{110}N_5S_2Ir\bullet2.5CH_2Cl_2$: C, 67.57; H, 6.07; N, 3.67. Found: C, 67.91; H, 6.31; N, 3.26.

5-5. The mixture of **5-1-L** (136 mg, 0.20 mmol), $IrCl_3\cdot4H_2O$ (37 mg, 0.1 mmol), 2-ethoxyethanol (9 mL) and water (3 mL) was heated to reflux under argon for 24 hours. After the mixture was cooled down to room temperature, 50 mL water was added and the yellow precipitate was collected and washed with hexane and water. The resultant yellow powder was dried in vacuum oven for 24 hours and used for the following reaction directly. The yellow powder collected, **5-1-L** (68 mg, 0.10 mmol), $AgCF_3SO_3$ (26 mg, 0.1 mmol) and 2-

ethoxyethanol (10 mL) were heated to reflux under argon for 48 hours. After the reaction was finished, 50 mL ethyl acetate was added. The combined organic solution was washed with brine (50 mL × 3). After drying over MgSO$_4$, the solvent was removed by distillation. Purification was carried out by a flash silica gel column eluted with dichloromethane followed by recrystallization from dichloromethane and hexane. 9 mg orange powder was collected as the final product (yield: 4% for two steps). ^{1}H NMR (CDCl$_3$, 500 MHz): 8.07 – 8.14 (m, 12H), 7.98 (m, 3H), 7.92 (d, J = 8.0 Hz, 3H), 7.78 – 7.81 (m, 6H), 7.66 – 7.71 (m, 12H), 7.48 – 7.52 (m, 3H), 7.39 (t, J = 8.0 Hz, 3H), 7.25 – 7.31 (m, 3H), 7.10 (m, 3H), 6.98 – 7.00 (m, 3H), 2.05 – 2.19 (m, 12H), 0.51 – 0.99 (m, 90H). Anal. Calc. for C$_{141}$H$_{153}$N$_6$S$_3$Ir•3CH$_2$Cl$_2$: C, 69.88; H, 6.48; N, 3.40. Found: C, 69.98; H, 6.58; N, 3.71.

5.2.2. Photophysical and Nonlinear Absorption Studies

The solvents used for photophysical experiments were spectroscopic grade, and were purchased from VWR International and used as is without further purification. UV-vis absorption spectra were recorded on a Shimadzu UV-2501 spectrophotometer. A FluoMax-4 fluorometer/phosphorometer was used to measure the steady-state emission spectra in different solvents. The emission quantum yields were determined by the relative actinometry method[19] in degassed solutions, in which the degassed acetonitrile solution of [Ru(bpy)$_3$]Cl$_2$ (Φ_{em} = 0.097, λ_{ex} = 436 nm)[20] was used as the reference for complexes **5-1 – 5-5**.

The nanosecond transient difference absorption (TA) spectra and decays were measured in degassed toluene solutions on an Edinburgh LP920 laser flash photolysis spectrometer. The third harmonic output (355 nm) of a Nd:YAG laser (Quantel Brilliant, pulse width: 4.1 ns, repetition rate was set to 1 Hz) was used as the excitation source. Each sample was purged with argon for 30 min prior to measurement. The triplet excited-state absorption coefficient (ε_T) at the TA band maximum was determined by the singlet depletion method, and the detail has been desctibed previously.[21] After obtaining the ε_T value, the Φ_T

could be determined by the relative actinometry using SiNc in benzene as the reference (ε_{590} = 70000 M^{-1} cm^{-1}, Φ_T = 0.20).[22]

The reverse saturable absorption of complexes **5-1** – **5-5** was characterized by nonlinear transmission experiment at 532 nm using a Quantel Brilliant laser as the light source. The pulse width of the laser was 4.1 ns and the repetition rate was set to 10 Hz. The complexes were dissolved in CH_2Cl_2. The concentration of the sample solutions was adjusted to obtain a linear transmission of 90% at 532 nm in a 2-mm-thick cuvette. The experimental setup and details are similar to that reported previously.[23] A 40-cm plano-convex lens was used to focus the beam to the center of the 2-mm thick sample cuvette. The radius of the beam at the focal plane was approximately 96 μm.

5.3. Results and Discussion

5.3.1. Electronic Absorption

The electronic absorption of **5-1-L**, **5-2-L**, and **5-1** – **5-5** in toluene obey Beer's law in the concentration range of 5×10^{-6} – 1×10^{-4} mol/L, suggesting the absence of ground-state aggregation in the concentration range used. Meanwhile, the magnitude of the molar extinction coefficients for the major absorption bands below 400 nm of the complexes roughly correlate to the number of the substituted ligand **5-1-L** or **5-2-L**. The electronic absorption spectra of **5-1-L**, **5-2-L**, and **5-1** – **5-5** in toluene are shown in Figure 5.1, and their absorption band maxima and molar extinction coefficients are presented in Table 1.
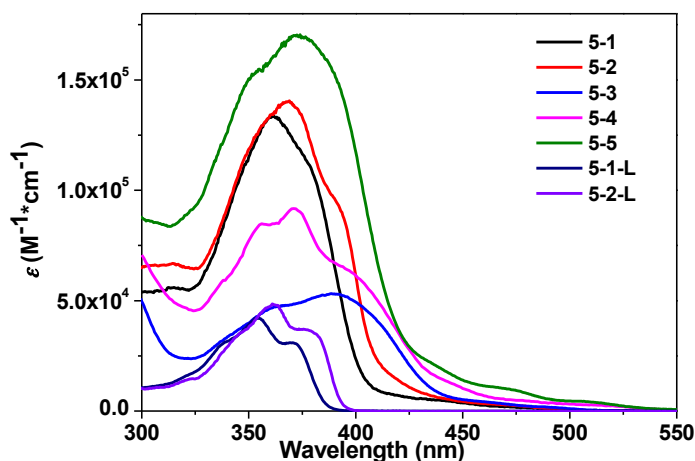
Figure 5.1. UV-vis absorption spectra of **5-1** – **5-5**, **5-1-L**, and **5-2-L** at room temperature in toluene

Table 5.1. Electronic absorption, emission (room temperature and 77 K), and excited-state absorption parameters for complexes **5-1** – **5-5** and ligands **5-1-L** and **5-2-L** in toluene

	λ_{abs}/nm ($\log\varepsilon$/Lmol^{-1}cm^{-1})	λ_{em}/nm (τ/μs); Φ_{em}[a] R.T.	λ_{em}/nm (τ/μs); 77 K	$\lambda_{T_1-T_n}$/nm (τ_T/μs; $\log\varepsilon_{T_1-T_n}$/L mol^{-1} cm^{-1}; Φ_T)[c]
5-1	350 (sh, 5.06), 361 (5.13), 380 (sh, 5.03), 420 (3.85)	583 (6.4), 633 (7.6); 0.095	546 (1447); 594 (966)	602 (0.058; 5.14; 0.042)
5-2	350 (sh, 5.07), 369 (5.15), 392 (sh, 4.97), 425 (4.03)	592 (6.3), 644 (6.0); 0.13	558 (933); 598 (-)	590 (4.2; 5.04; 0.063)
5-3	363 (sh, 4.68), 390 (4.73), 440 (3.89)	520 (6.9), 555 (5.3); 0.22	548 (857); 592 (622)	524 (44.2; 4.64; 0.25)
5-4	356 (sh, 4.93), 371 (4.96), 395 (sh, 4.81), 455 (3.93)	596 (1.9), 644 (2.0); 0.047	552 (426); 590 (-)	532 (33.7; 4.74; 0.17)
5-5	350 (sh, 5.18), 372 (5.23), 395 (5.14), 470 (4.01)	600 (2.1), 650 (2.1); 0.055	556 (502); 586 (411)	545 (15.5; 5.21; 0.021)
5-1-L	353 (4.63), 371 (4.49)	389 (-), 409 (-), 429 (-); -		510 (56.3; -; -)
5-2-L	362 (4.68), 377 (4.57)	392 (-), 415 (-), 438 (-); -		510 (58.8; -; -)

[a] At 1×10^{-5} mol/L concentration.

For ligands **5-1-L** and **5-2-L**, well-resolved vibronic structures were observed in the 300 – 400 nm region, which are attributed to the $^1\pi,\pi^*$ transitions considering their strong intensity (molar extinction coefficient in the magnitude of 10^4) and well resolved vibronic structures. The electronic absorption of **5-2-L** is red-shifted compared to that of **5-1-L**, which can be explained by the extended π-conjugation via incorporating the triple bond.

Comparing to the ligand absorption spectra, the absorption spectra of **5-1** – **5-5** are broader and somewhat red-shifted, and the molar extinction coefficients of the major absorption bands are much stronger than the corresponding C^N ligands. The bathochromic shift indicates electron delocalization induced by the interaction with the metal center. The broadening and red-shift of the ligand centered $^1\pi, \pi^*$ transitions are more significant for neutral complexes **5-3** – **5-5** comparing to the cationic complexes **5-1** and **5-2**, suggesting a stronger interaction between the ligand and the metal center in the neutral complexes than the cationic complexes. This can be explained by the stronger ligand field strength of the 2-phenylpyridine ligand than the bipyridine ligand. In addition to the ligand centered $^1\pi,\pi^*$ transitions, lower energy absorption bands are observed for all the five complexes, which can be tentatively attributed to the charge transfer transitions including ^{1,3}MLCT, ^{1,3}ILCT or ^{1,3}LLCT. Similar to the trend observed from the $^1\pi,\pi^*$ transitions, the charge-transfer absorption bands in the neutral complexes **5-3** – **5-5** are more red-shifted and stronger in comparison to the cationic complexes **5-1** and **5-2**. With the increased number of the substituted ppy ligands, the charge-transfer bands become stronger and more distinct in complexes **5-3** – **5-5**. It is also worthy noting that the ratio of the absorption band/shoulder at ca. 400 nm relative to the major band at ca. 370 nm decreases with the increased number of substituted ppy ligand, indicating the decreased contribution of the ^{1}MLCT transition with the increased contribution from the $^1\pi,\pi^*$ transitions.

The absorption spectra of the complexes **5-1** – **5-5** exhibit minor solvatochromic effect, as illustrated in Figure 5.2. This supports the assignment of the $^1\pi, \pi^*$ transitions for the major absorption bands. Note that even if the low-energy charge transfer states are also insensitive to solvents polarity, which could probably be explained by the strong mixing of the charge transfer transitions with the $^1\pi,\pi^*$ transitions in the low energy transitions.
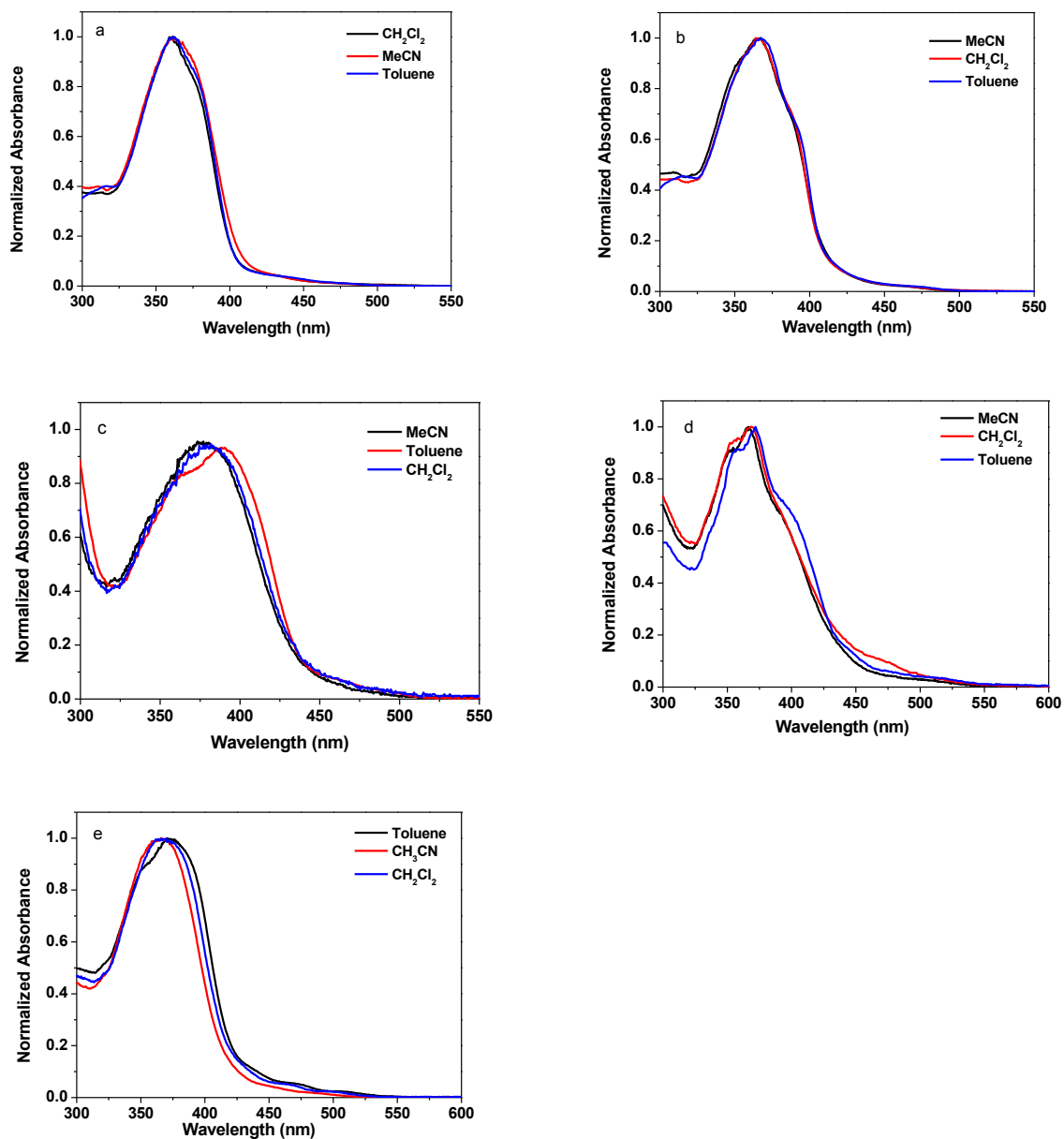
Figure 5.2. Electronic absorption of **5-1** – **5-5** at room temperature in different solvents (a: **5-1**; b: **5-2**; c: **5-3**; d: **5-4**; e: **5-5**)

5.3.2. Photoluminescence

5-1 – **5-5** all exhibit strong emission with relatively long lifetime (in the scale of several microseconds) both in room temperature solution and in butyronitrile glassy matrix at 77 K. The emission spectra of **5-1** – **5-5** at room temperature are shown in Figure 5.3(a), and the emission spectra of **5-1** – **5-5** at 77 K are shown in Figure 5.3(b). The emission spectra of

5-1-L and **5-2-L** are included in Figure 5.3(a) for comparison purpose. The emission band maxima, emission lifetimes, and quantum yields are summarized in Table 5.1.
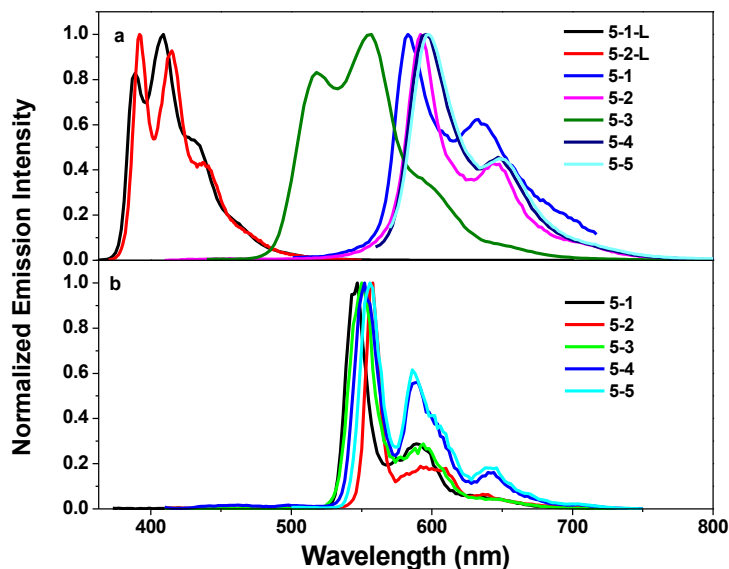
Figure 5.3. (a) Normalized emission spectra of **5-1 – 5-5**, **5-1-L**, and **5-2-L** at room temperature in toluene at the concentration of 1×10^{-5} mol/L (λ_{ex}: 353 nm for **5-1-L**, 360 nm for **5-1-L**, 363 nm for **5-1**, 400 nm for **5-2 – 5-4**, and 430 nm for **5-5**); (b) Normalized emission spectra of **5-1 – 5-5** at 77 K in butyronitrile matrix at the concentration of 1×10^{-5} mol/L (λ_{ex}: 363 nm for **5-1**, 400 nm for **5-2 – 5-4**, and 430 nm for **5-5**).

The ligands **5-1-L** and **5-2-L** show strong emission with well-resolved vibronic structures and short lifetimes (too short to be measured on our spectrometer), which can be assigned to the $^1\pi,\pi^*$ fluorescence. Similar to the electronic absorption, the fluorescence spectrum of **5-2-L** is red shifted compared to that of **5-1-L**, indicating the electron delocalization induced by the more extended π-conjugation in **5-2-L** with the triple bond.

The emission spectra of the complexes **5-1 – 5-5** are all drastically red-shifted in comparison to their corresponding ligands. They all possess well-resolved vibronic structures, with the lifetimes in several microseconds. Considering these characteristics, we assign the observed emission to predominantly ligand centered $^3\pi,\pi^*$ phosphorescence. However, contribution of the charge transfer state cannot be excluded.

The emission of **5-2** is red-shifted compared to that of **5-1**, manifesting the extended electron delocalizing by the triple bond in **5-2**. In **5-3** – **5-5**, the emission band maximum is red-shifted as the number of 7-(benzothiazol-2-yl)-9,9-di(2-ethylhexyl)-9H-fluoren-2-yl unit increases, indicating a stronger electron delocalization across the whole molecule as the conjugation extends in each ligand.

In Figure 5.4, the emission spectra of **5-1** – **5-5** in toluene at different concentrations as well as the Stern-Volmer plots for the emission decay rate at different concentration are provided. As illustrated in Figure 5.4(a-c), the emission intensity of complexes **5-1** – **5-3** reaches the maximum value at the concentration of 1×10^{-5} mol/L. Above this concentration, the intensity decreases with increased concentration. Meanwhile, the lifetime decreases with increased concentration. This clearly indicates the occurrence of self-quenching. However, considering the considerable ground-state absorption at the excitation wavelength, inner-filter effect should also play a role in the emission intensity decrease at higher concentrations. The self-quenching rate constant and the intrinsic lifetimes for **5-1** – **5-3** are calculated from the slope and intercept of the fitting line of the Stern-Volmer plot, and the values are summarized in Table 5.2. However, self-quenching is not observed in complexes **5-4** and **5-5**, probably due to the highly branched structure of the two complexes, which could substantially inhibit inter-molecular packing between the molecules.

Table 5.2. Intrinsic lifetimes and self-quenching rate constants at the emission band maximum for complexes **5-1** – **5-3** in toluene

λ_{em}/nm ($\tau_0/\mu s$; k_{sq}/L.mol^{-1}.s^{-1})		
5-1	**5-2**	**5-3**
583 (6.8; 2.3×10^8)	592 (8.5; 1.1×10^9)	555 (6.9; 4.2×10^8)
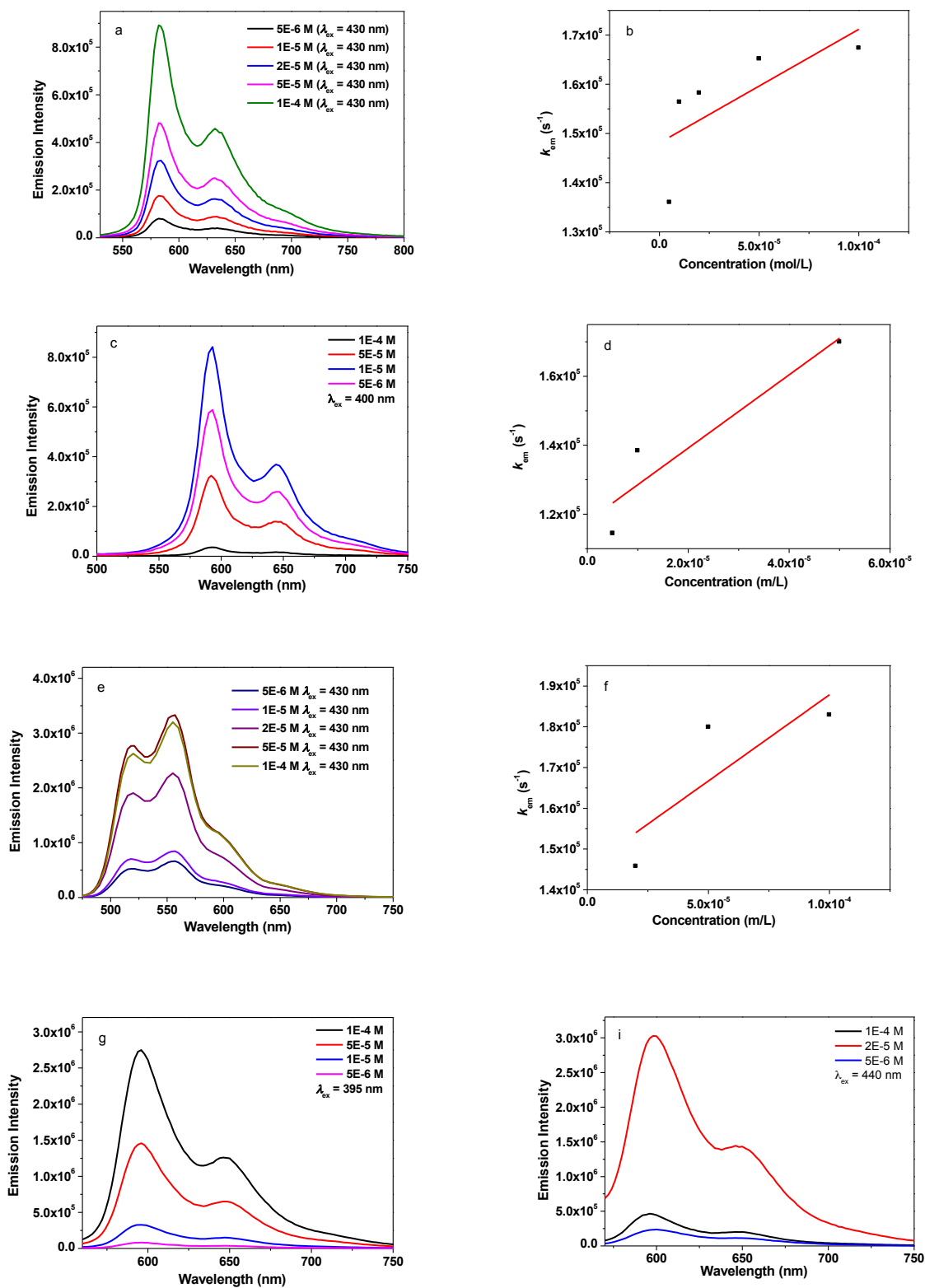
Figure 5.4. Emission spectra of **5-1** – **5-5** at room temperature at different concentrations and Stern-Volmer plots for the emission lifetime at the emission band maximum (a and b: **5-1**; c and d: **5-2**; e and f: **5-3**; g: **5-4**; i: **5-5**)

The emission spectra of complexes **5-1** – **5-5** in butyronitrile matrix at 77 K are shown in Figure 5.3(b). The well-resolved emission spectra are significantly blue-shifted and become narrower compared to the room temperature emission spectra due to rigidochromic effect in the solid matrix.[24] The lifetime of the emission at 77 K is extremely long, up to 1.4 ms. This supports the $^3\pi,\pi^*$ nature for the emitting states.
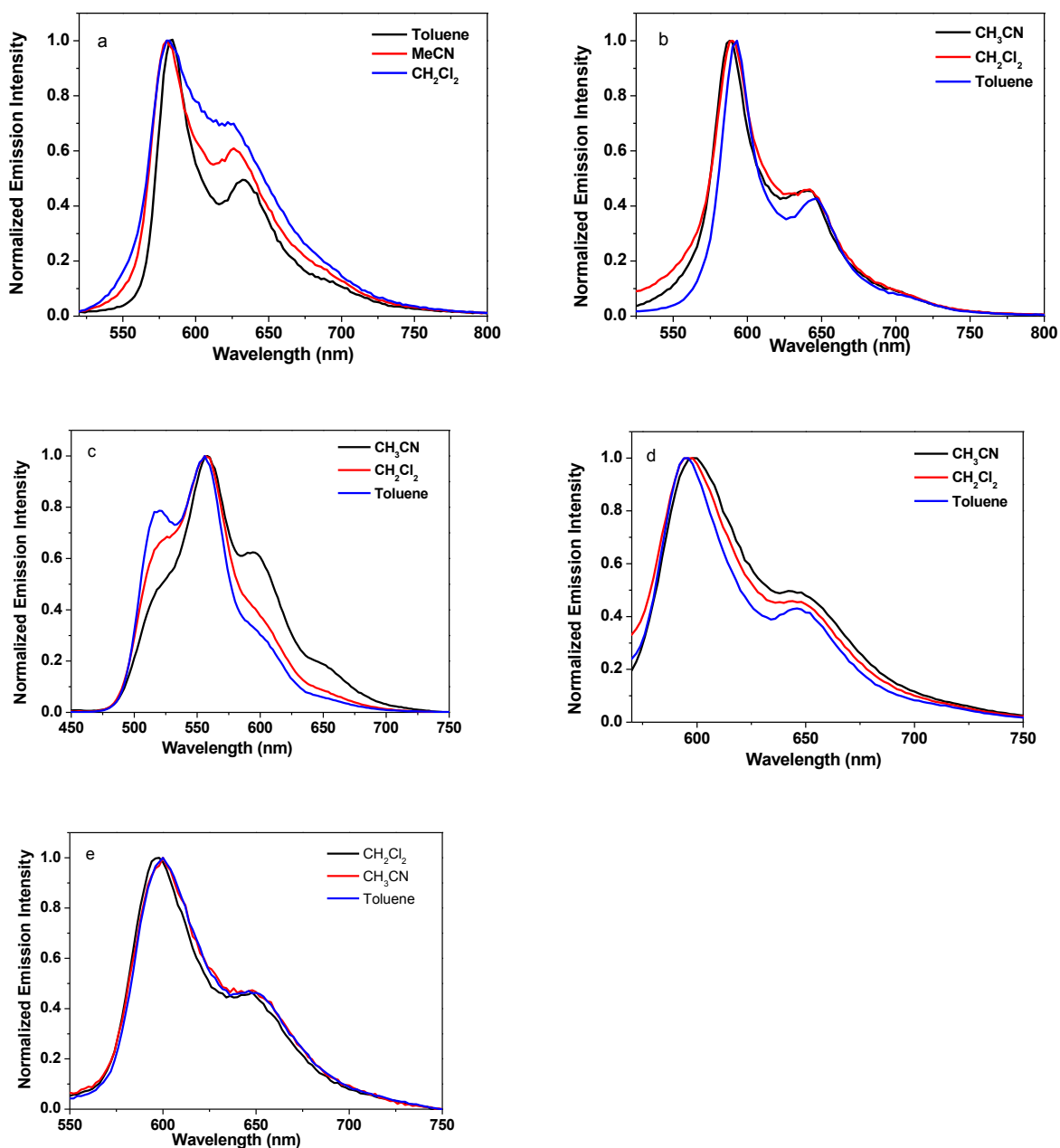
Figure 5.5. Emission spectra of **5-1** – **5-5** at room temperature in different solvents upon 436 nm excitation (a: **5-1**; b: **5-2**; c: **5-3**; d: **5-4**; e: **5-5**)

To verify the nature of the emitting state for **5-1** – **5-5**, emission in solvents with different polarities was studied and the spectra are shown in Figure 5.5. Minor solvatochromic effect for the emission was observed for all complexes, testifying the assignment of the emission state being predominantly $^3\pi, \pi^*$ state.

5.3.3. Transient Absorption

Nanosecond transient absorption (TA) of complexes **5-1** – **5-5** in toluene were investigated to understand their triplet excited-state characteristics. The spectra for **5-1** – **5-5** at zero delay after excitation are displayed in Figure 5.6. The triplet excited-state lifetimes, extinction coefficients, and quantum yields are deduced or calculated and the results are summarized in Table 5.1.
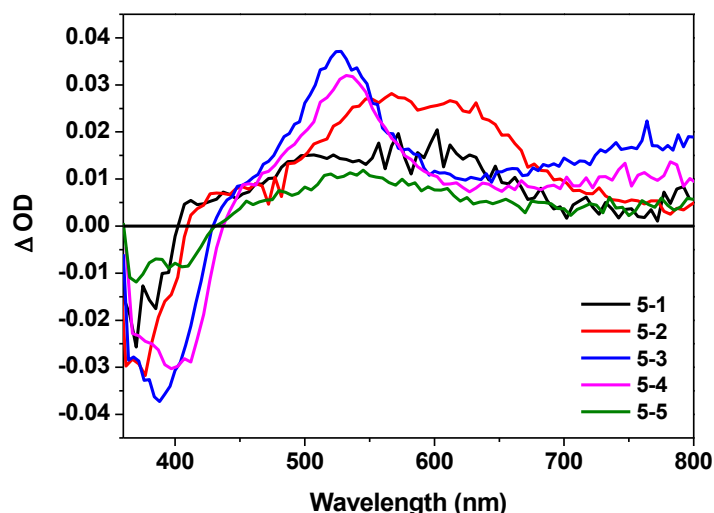
Figure 5.6. Nanosecond transient difference absorption spectra of **5-1** – **5-5** in toluene at zero time decay (λ_{ex} = 355 nm, A_{355} = 0.4 in a 1-cm cuvette).

The TA spectra of all complexes feature a bleaching band in the blue spectral region corresponding to their respective $^1\pi,\pi^*$ absorption band. Complexes **5-1** and **5-2** show moderate and broad TA band spreading the wavelength range of 400 – 700 nm, and the TA of **5-2** is red shifted in comparison to that of **5-1** due to more extended π-conjugation in the ligand. The positive TA region of **5-3** – **5-5** feature two parts: a narrow but stronger

absorption in the wavelength range of 450 – 600 nm and a wider and weaker region in the wavelength range of 600 – 800 nm. The TA spectra are red-shifted from **5-3** to **5-4** to **5-5**, indicating the stronger electron delocalization when the number of substituted C^N ligand increases. However, the intensity of the TA decreases from **5-3** to **5-4** to **5-5**.
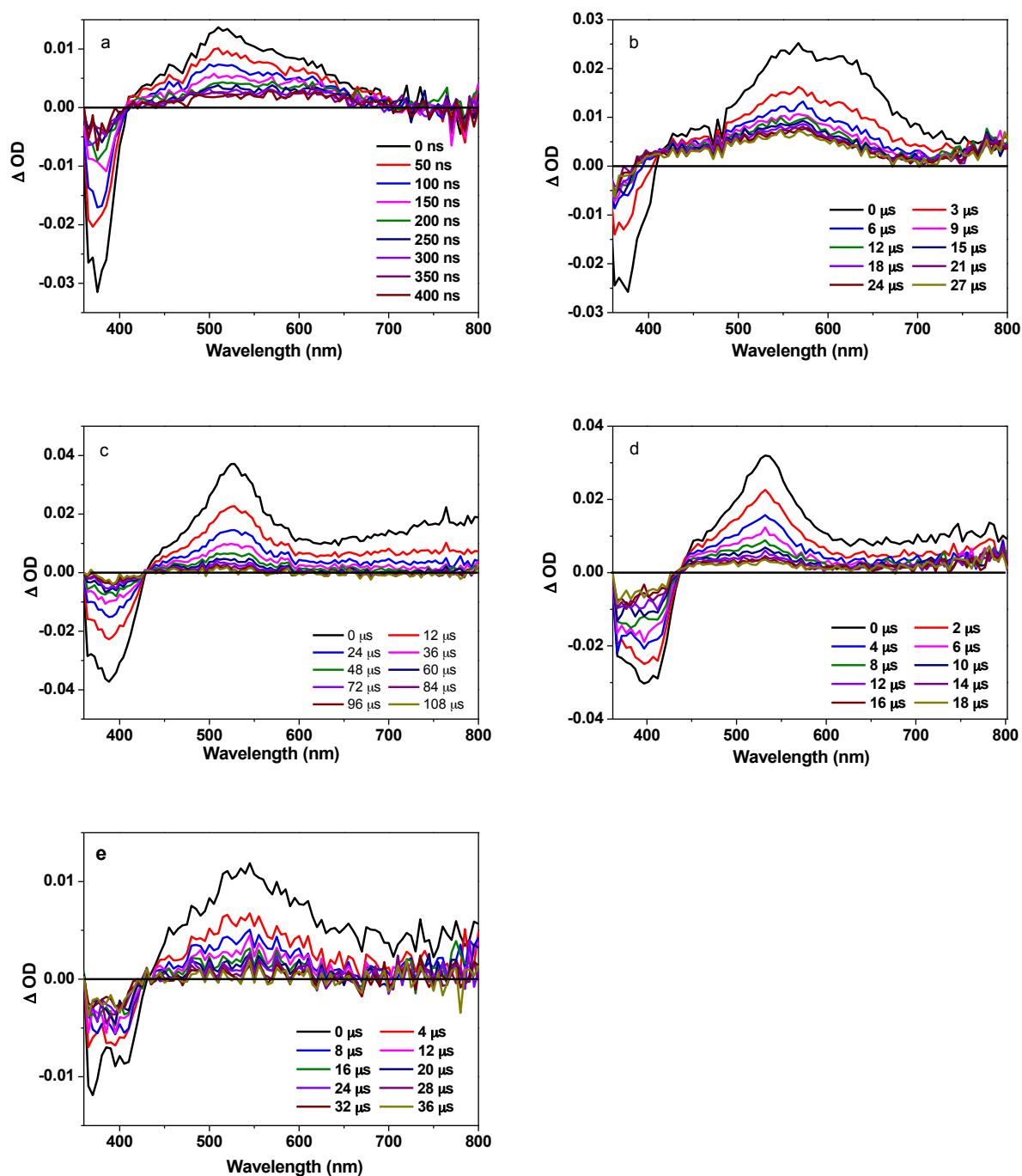
Figure 5.7. Time resolved transient difference absorption spectra of **5-1** – **5-5** in toluene (λ_{ex} = 355 nm, A_{355} = 0.4 in a 1-cm cuvette；a: **5-1**; b: **5-2**; c: **5-3**; d: **5-4**; e: **5-5**).

The time-resolved TA spectra of **5-1** – **5-5** are shown in Figure 5.7. From the decay of the TA, the triplet excited-state lifetimes can be deduced. The triple lifetime of **5-1** is 58 ns, suggesting the triplet excited-state absorption is from the short-lived ^{3}MLCT state. The triplet lifetime of **5-2** is several microseconds, which is in line with the lifetime deduced from the emission. Therefore, the observed TA for **5-2** is tentatively attributed to predominant $^3\pi, \pi^*$ state. In contrast, the lifetimes of **5-1** – **5-5** are much longer (tens of microseconds) compared to those observed from the emission decay. These long lifetimes suggest that the nature of the excited state giving rise to the observed TA could be mainly the ligand-centered $^3\pi,\pi^*$. Notably, the lifetimes of **5-3** – **5-5** decreased from 44.2 μs for **5-3** to 33.7 μs for **5-4** to 15.5 μs for **5-5**.

Comparison of the TA features of **5-4** to those of **5-1**, it is obvious that replacing the bipyridine ligand with the 2-phenylpyridine ligand results in a broadening of the TA spectrum of **5-4**, and switching the TA excited state from ^{3}MLCT in **5-1** to $^3\pi,\pi^*$ in **5-4**.

5.3.4. Reverse Satuable Absorption

Complexes **5-1** – **5-5** all manifest stronger excited-state absorption than that of the ground state at 532 nm noticing the positive absorption bands in the visible spectral region of their TA spectra. Meanwhile, the triplet-state lifetimes are significantly longer than the ns laser pulse width (4.1 ns). Therefore, it is expected that these complexes would exhibit reverse saturable absorption (RSA) for ns laser pulses at 532 nm. To verify this assumption, nonlinear transmission experiment was carried out for complexes **5-1** – **5-5** in CH_2Cl_2 solutions with a linear transmission of 90% in a 2-mm cuvette using the 532-nm ns laser pulses and the results are shown in Figure 5.8. The transmissions of all of the complexes decrease remarkably with increased incident energy, which clearly demonstrates a strong RSA from these complexes. The strength of the RSA follows this trend: **5-5**＜**5-4**＜**5-1**＜**5-3**＜**5-2**.
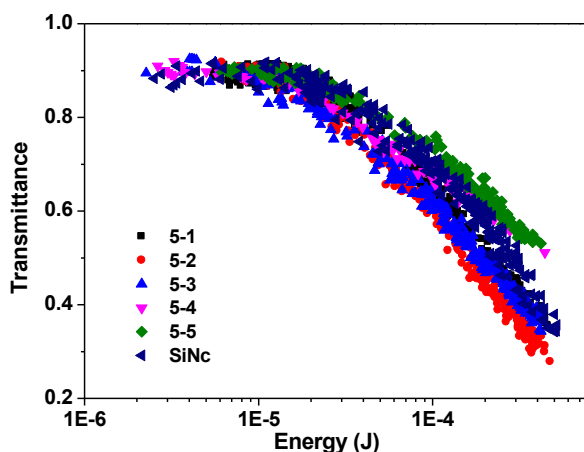
Figure 5.8. Nonlinear transmission of **5-1** – **5-5** at the linear transmission of 90% in CH_2Cl_2 solution in a 2-mm cuvette for 532 nm 4.1 ns laser. SiNc was plotted for comparison. The radius of the beam waist at the focal point was approximately 96 μm.

The ratios of the excited-state absorption cross section to that of the ground state (σ_{ex}/σ_0) at 532 nm was evaluated to rationalize the trend of RSA for these complexes. According to the ground-state absorption at 532 nm and at the wavelength of the TA band maximum, the optical density changes (ΔOD) at 532 nm and at the TA band maximum, the molar extinction coefficient at the TA band maximum (ε_{T1-Tn}), and the method described by our group previously,[25] the excited-state absorption cross sections (σ_{ex}) for **5-1** – **5-5** at 532 nm were estimated and the results are shown in Table 5.3. The trend of the calculated ratios of σ_{ex}/σ_0 matches the observed RSA trend very well.

Table 5.3. Ground-state (σ_0) and excited-state (σ_{ex}) absorption cross-sections of complexes **5-1**–**5-5** at 532 nm in toluene

	5-1	**5-2**	**5-3**	**5-4**	**5-5**
$\sigma_0/\ 10^{-18}\ cm^{2a}$	0.63	0.65	0.35	0.75	2.1
$\sigma_{ex}\ /10^{-18}\ cm^{2b}$	298	394	172	210	568
σ_{ex}/σ_0	473	606	491	280	270

5.4. Conclusion

The synthesis, photophysics, and reverse saturable absorption of five iridium(III) complexes with 7-(benzothiazol-2-yl)-9,9-di(2-ethylhexyl)-9H-fluoren-2-yl pedant attached

181

to the 2-phenylpyridine ligand was reported. The effects of the extenden of the π-conjugation in the ligand was studied by the comparison between **5-1** and **5-2**, and the effects of the number of the 7-(benzothiazol-2-yl)-9,9-di(2-ethylhexyl)-9H-fluoren-2-yl unit was compared among **5-3**, **5-4**, and **5-5**. The results show that the electronic absorption, emission, and ns transient absorption are all red shifted by extending the π-conjugation or increasing the numbers of 7-(benzothiazol-2-yl)-9,9-di(2-ethylhexyl)-9H-fluoren-2-yl unit. The emission of the complexes are dominated by ligand-centered $^3\pi,\pi^*$ excited state. All complexes possess moderate TA in the sivible spectral region, with the TA predominantly emanates form the ^{3}MLCT state for **5-1**, and from $^3\pi,\pi^*$ states for **5-2** – **5-5**. Reverse saturable absorption of these complexes at 532 nm were evaluated for nanosecond laser pulses. The results demonstrate that these complexes all exhibit strong exhibit strong RSA for ns laser pulses at 532 nm, with a trend of **5-5**＜**5-4**＜**5-1**＜**5-3**＜**5-2**. The trend is primarily determined by ratios of the excited-state absorption cross section to that of the ground state (σ_{ex}/σ_0) at 532 nm.

5.5. References

[1] Cotton, F. A.; Wilkinson, G. *Advanced Inorganic Chemistry: A Comprehensive Text*; Wiley, New York, **1980**.

[2] Wu, C.; Chen, H.-F.; Wong, K.-T.; Thompson, M. E. *J. Am. Chem. Soc.* **2010**, *132*, 3133.

[3] Bruce, D.; Richter, M. M. *Anal. Chem.* **2002**, *74*, 1340.

[4] Tordera, D.; Bünzli, A. M.; Pertegás, Antonio; Junquera-Hernández, J. M.; Constable, E. C.; Zampese, J. A.; Housecroft, C. E.; Ortí, E.; Bolink, H. J. *Chem. Eur. J.* **2013**, asap. DOI: 10.1002/chem.201300457

[5] Hu, T.; He, L.; Duan, L.; Qiu, Y. *J. Mater. Chem.* **2012**, *22*, 4206.

[6] Lo, K. K.-W.; Zhang, K. Y. *RSC Adv.* **2012**, *2*, 12069.

[7] Huynh, L.; Wang, Z.; Yang, J.; Stoeva, V.; Lough, A.; Manners, I.; Winnik, M. A. *Chem. Mater.* **2005**, *17*, 4765.

[8] Lowry, M. S.; Goldsmith, J. I.; Slinker, J. D.; Rohl, R.; Pascal Jr., R.A.; Malliaras, G. G.; Bernhard, S. *Chem. Mater.* **2005**, *17*, 5712.

[9] Lowry, M. S.; Bernhard, Stefan. *Chem. Eur. J.* **2006**, *12*, 7970.

[10] Dedeian, K.; Djurovich, P. I.; Garces, F. O.; Carlson, G.; Watts, R. J. *Inorg. Chem.* **1991**, *30*, 1685.

[11] Tamayo, A. B.; Garon, S.; Sajoto, T.; Djurovich, P. I.; Tsyba, I. M.; Bau, R.; Thompson, M. E. *Inorg. Chem.* **2005**, *44*, 8723.

[12] Hay, P. J. *J. Phys. Chem. A* **2002**, *106*, 1634.

[13] Watts, R. J.; Van Houten, J. *J. Am. Chem. Soc.* **1974**, *96*, 4334.

[14] Yan, Q.; Yue, K.; Yu, C.; Zhao, D. *Macromolecules* **2010**, *43*, 8479.

[15] Yan, Q.; Fan, Y.; Zhao, D. *Macromolecules* **2012**, *45*, 133.

[16] Kim, K.-Y.; Farley, R. T.; Schanze, K. S. *J. Phys. Chem. B* **2006**, *110*, 17302.

[17] Li, Y.; Dandu, N.; Liu, R.; Hu, L.; Kilina, S.; Sun, W. *ACS Appl. Mater. Interfaces* **2013**, *5*, 6556.

[18] Li, Z.; Ekaterina, B.; Ugrinov, A.; Killina, S.; Sun, W. *Inorg. Chem.* **2013**, *52*, 7578.

[19] Demas, J. N.; Crosby, G. A. *J. Phys. Chem.* **1971**, *75*, 991.

[20] Van Houten, J.; Watts, R. *J. Am. Chem. Soc.* **1976**, *98*, 4853.

[21] Eaton, D. F. *Pure Appl. Chem.* **1988**, *60*, 1107.

[22] Carmichael, I.; Hug, G. L. *J. Phys. Chem. Ref. Data.* **1986**, *15*, 1.

[23] Guo, F.; Sun, W.; Liu, Y.; Schanze, K. *Inorg. Chem.* **2005**, *44*, 4055.

[24] Watts, R. J.; Missimer, D. *J. Am. Chem. Soc.* **1978**, *100*, 5350.

[25] Li, Y.; Liu, R.; Badaeva, E.; Kilina, S.; Sun, W. *J. Phy. Chem. C* **2013**, *117*, 5908.

CHAPTER 6. SYNTHESIS, PHOTOPHYSICS, AND NONLINEAR ABSORPTION OF A SERIES OF BIPYRIDYL IRIDIUM(III) COMPLEXES WITH DIFFERERENT CYCLOMETALLATING ARYLPYRIDINE LIGANDS

6.1. Introduction

Ionic iridium(III) complexes, featuring d^6 transition metal center and octahedral coordination geometry, have drawn intense attention due to their intriguing photophysical and photochemical properties.[1−5] Undersranding the photophysics of the Ir(III) complexes is the key for utilizing them as electrochemical light emitters, one of the most important applications for iridium complexes.[6−10] Tremendous efforts have been engaged to tune the ground-state and excited-state properties of iridium complexes with different diimine or cyclomatallating ligands. These studies have found outstanding luminophore with lifetime in the microsecond scale or longer, and tunable colors from blue to red.

Ir(bpy)$_3^{3+}$ (bpy = 2,2′-bipyridine) complex was first reported by Martin in 1958.[11] In 1974, Demas[12,13] reported the synthesis and luminescence property of [Ir(bpy)$_3$](ClO$_4$)$_3$. It was found that the emission lifetime of this complex at 77 K was about 80 μs, thus had ligand-centered (LC) characteristic; while at room temperature, the lifetime was about 2.4 μs, showing some metal to ligand charge transfer (MLCT) character. Comparing to bipyridine ligand (bpy), 2-phenylpyridine (ppy) loses one proton during the coordination, thus forming carbon-metal bond in which the coordinating carbon atom has one negative charge. As a result, after coordination of three ppy ligands to the Ir(III) ion, neutral complexes are formed. Ir(ppy)$_3$ was first reported by Watt in 1985,[14] in which the lifetime of the complex at 77 K was found to be ~ 5 μs in ethanol/methanol glassy matrix (4/1 v/v), and at ambient temperature the lifetime was found to be up to 2 μs in toluene or acetonitrile. The luminescence was assigned as ^{3}MLCT transition.[15−18]

Although not widely investigated, nonlinear absorption of Ir(III) complexes is an important and intriguing phenomenon associated with the strong intersystem crossing induced by the heavy atom effect of iridium and the broad and relatively strong excited-state absorption.[22] Our group has long been developing platinum(II) complexes to explore their nonlinear absorption properties.[23 – 25] Due to the large spin-orbit coupling constant of iridium,[26] Ir(III) complexes are good candidates for the nonlinear absorption application.

When two cyclometallating ligands and one diimine ligand are incorporated or coordinated to the same iridium(III) ion, monocationic complexes can be obtained, which show intriguing photophysics. As a prototype example, [Ir(ppy)$_2$(bpy)]PF$_6$ was found to show intriguing interplay between the LC and the MLCT excited states.[19] The lowest-energy excited state of the complex in solution or in poly(methyl methacrylate) glasses at room temperature is dominated by the MLCT transitions. In contrast, in the host crystalline lattice of [Rh(ppy)$_2$(bpy)]PF$_6$ the lowest excited state was assigned to LC state localized on the ppy ligand. The interplay between the ligand-centered excited state and the MLCT state results in versatile and tunable photophysics, which leads to various important applications such as high efficiency light-emitting electrochemical cell.[20, 21]

Inspired by the interesting properties of the monocationic complexes, seven iridium(III) complexes **6-1 – 6-7** were designed and synthesized, and the structures are shown in Chart 6.1. These complexes all feature one bpy ligand, but the 2-arylpyridine ligand varies from **6-1** to **6-7** as following: benzo[H]isoquinoline (**6-1-L**), 1-phenylisoquinoline (**6-2-L**), 1-(2-pyridyl)naphthalene (**6-3-L**), 2-(2-pyridyl)naphthalene (**6-4-L**), 1-(2-pyridyl)pyrene (**6-5-L**), fused imidazole (**6-6-L**), and 3-(2-pyridyl)perylene (**6-7-L**). By varying different ligands with similar coordination nature with ppy, we are aiming to understand the effect of different 2-arylpyridine ligands on the photophysics and nonlinear absorption. By studying these seven complexes, the following factors will be evaluated: 1) the extent of the π-conjugation of the

aryl group from **6-3**, to **6-5**, to **6-7**; 2) the position of the fused benzene ring on the 2-phenylpyridine ligand.
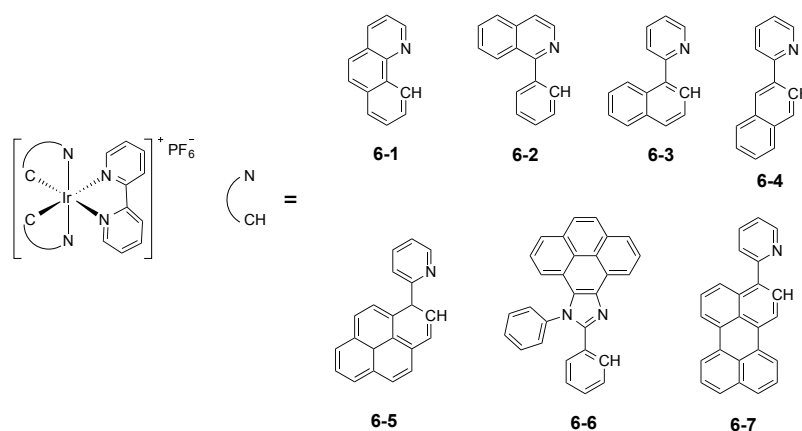
Chart 6.1. Structure of the targeted iridium(III) complexes of **6-1 – 6-7**

6.2. Experimental Section

6.2.1. Synthesis and Characterization

All the chemicals and solvents were purchased from Aldrich Chemical Co. or Alfa Aesar and used as received unless otherwise mentioned. **6-1-L** was purchased from Alfa Aesar and used as received. **6-2-L** was purchased from Aldrich Chemical Co. and used as is. **6-6-L** was synthesized from pyrene according to the literature procedure.[27, 28] **6-3-L**, **6-4-L**, **6-5-L**, and **6-7-L** were synthesized by Stille coupling exemplified by the synthesis of **6-3-L** in Scheme 6.1. 1-bromonaphthalene, 2-bromonaphthalene, ad 1-bromopyrene were purchased from Alfa Aesar. 3-bromoperylene was synthesized following the literature procedure.[29] The synthesis of **6-1 – 6-7** followed a two-step procedure exemplified by the synthesis of **6-3** in Scheme 6.1. Silica gel for chromatography was purchased from Sorbent Technology (60 Å, 230−400 mesh, 500−600 m^2/g, pH: 6.5−7.5). Complexes **6-1 – 6-7** were characterized by ^{1}H NMR and electrospray ionization mass spectrometry (ESI-MS). Each intermediate and ligand were characterized by ^{1}H NMR. ^{1}H NMR was obtained on Varian Oxford-VNMR spectrometers (400 or 500 MHz). ESI-MS analyses were performed at a Bruker BioTOF III mass spectrometer.
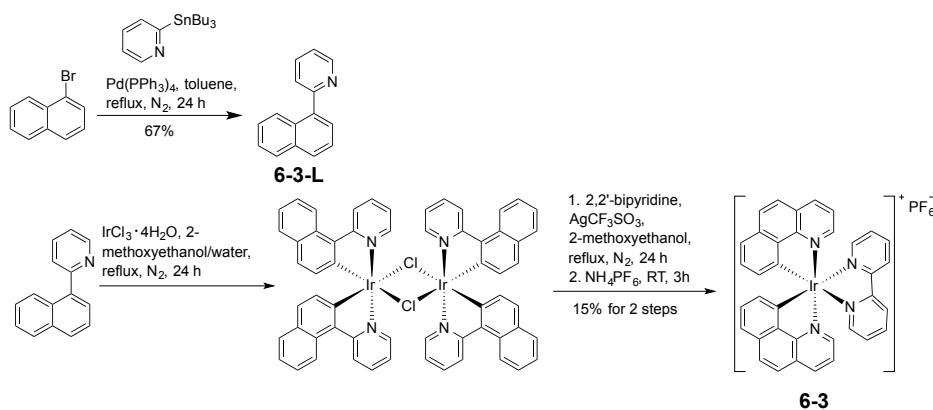
Scheme 6.1. Synthetic routes for **6-3-L** and **6-3**.

6-3-L. The synthesis follows Stille coupling procedure. The mixture of 1-bromonaphthalene (0.50 g, 2.5 mmol), 2-(tributylstannyl)pyridine (1.1 g, 3.1 mmol), Pd(PPh$_3$)$_4$ (40 mg, 0.035 mmol), and toluene (50 mL) was heated to reflux under nitrogen for 24 hours. After reaction, toluene was removed by distillation, and the resultant dark oil was purified by a silica gel column eluted with hexane/ethyl acetate (v/v = 9/1). 0.34 g colorless oil was collected as the product (yield: 67%). ^{1}H NMR (400 MHz, CDCl$_3$): 8.78 – 8.79 (m, 1H), 8.07 – 8.09 (m, 1H), 7.89 – 7.91 (m, 2H), 7.77 – 7.82 (m, 1H), 7.44 – 7.60 (m, 5H), 7.31 – 7.33 (m, 1H).

6-4-L. The procedure was similar to that of **6-3-L**, with 2-bromonaphthalene (0.53 g, 2.5 mmol) being used as the reagent. 0.28 g product was collected (yield: 55%). ^{1}H NMR (400 MHz, CDCl$_3$): 8.72 – 8.74 (m, 1H), 8.47 (s, 1 H), 8.12 (*dd*, *J* = 8.6, 1.8 Hz, 1H), 7.93 (d, J = 8.4 Hz, 2H), 7.84 – 7.87 (m, 2H), 7.74 – 7.79 (m, 1H), 7.48 – 7.51 (m, 2H), 7.22 – 7.25 (m, 1H).

6-5-L. The procedure was similar to that of **6-3-L**, with 1-bromopyrene (0.71 mg, 2.5 mmol) being used as the reagent. 0.55 g colorless oil was collected as the product (yield: 79%). ^{1}H NMR (CDCl$_3$, 500 MHz): 8.90 – 8.91 (m, 1H), 8.41 (d, *J* = 9 Hz, 1H), 8.28 (d, *J* = 8 Hz, 1H), 8.18 – 8.24 (m, 3H), 8.14 (s, 2H), 8.10 (d, *J* = 9.5 Hz, 1H), 8.04 (t, *J* = 7.5 Hz, 1H), 7.91 (td, *J* = 7.5, 2.0 Hz, 1H), 7.76 (d, *J* = 7.5 Hz, 1H), 7.39 – 7.42 (m, 1H).

6-7-L. The procedure was similar to that of **6-3-L**, with 3-bromoperylene (0.83 g, 2.5 mmol) being used as the reagent. 0.43 g bright yellow powder was collected as the product (yield: 52%). ^{1}H NMR (CDCl$_3$, 500 MHz): 8.83 (dd, J = 6.4, 0.5 Hz, 1H), 8.23 – 8.29 (m, 4H), 7.98 (d, J = 13.5 Hz, 1H), 7.84 – 7.87 (m, 1H), 7.70 – 7.73 (m, 2H), 7.62 – 7.64 (m, 2H), 7.47 – 7.53 (m, 3H), 7.35 – 7.37 (m, 1H).

6-1. The mixture of **6-1-L** (180 mg, 1 mmol), IrCl$_3$·4H$_2$O (186 mg, 0.5 mmol), 2-methoxyethanol (15 mL) and water (5 mL) was heated to reflux under nitrogen for 24 hours. After reaction the yellow precipitate was collected by filtration, washed with water and hexane, and dried in vacuum for 12 hours. Then the mixture of the yellow powder collected, bipyridine (79 mg, 0.5 mmol), AgSO$_3$CF$_3$ (129 mg, 0.5 mmol), and 2-methoxyethanol (15 mL) was heated to reflux under nitrogen for 24 hours. After the reaction mixture was cooled down to room temperature, NH$_4$PF$_6$ (82 mg, 0.5 mmol) was added and the mixture was stirred for another 3 hours. The yellow precipitate was collected by filtration and the washed with water and hexane. Separation was carried out by running a silica gel column eluted with dichloromethane and ethyl acetate (v/v = 6:1). Further purification was conducted by recrystalization from dichloromethane and hexane. 62 mg bright yellow powder was collected as the product (yield: 15% for two steps). ^{1}H NMR (CDCl$_3$, 400 MHz): 8.68 (d, J = 8.4 Hz, 2H), 8.25 (dd, J = 8.0, 1.2 Hz, 2H), 8.11 (td, J = 8.0, 1.6 Hz, 2H), 7.87 – 7.90 (m, 2H), 7.85 (d, J = 8.8 Hz, 2H), 7.66 (d, J = 8.8 Hz, 2H), 7.42 – 7.50 (m, 4H), 7.27 – 7.29 (m, 2H), 6.97 – 7.19 (m, 4H), 6.30 (dd, J = 7.2, 0.8 Hz, 2H). ESI-HRMS: m/z calc. for [C$_{36}$H$_{24}$N$_4$Ir]$^+$: 705.1627; Found: 705.1607. Anal. Calc. for C$_{36}$H$_{24}$N$_4$IrPF$_6$•0.5CH$_2$Cl$_2$: C, 49.13; H, 2.82; N, 6.28; Found: C, 49.07; H, 3.08; N, 6.27.

6-2. The procedure is the same as that described for **6-1**, with **6-2-L** (205 mg, 1 mmol) being used as the reagent. 71 mg orange powder was collected as the product (yield: 16% for two steps). ^{1}H NMR (CDCl$_3$, 400 MHz): 8.88 – 8.92 (m, 2H), 8.65 (d, J = 8.0 Hz,

2H), 8.24 (d, J = 8.0 Hz, 2H), 8.08 – 8.12 (m, 2H), 7.86 – 7.90 (m, 2H), 7.71 – 7.76 (m, 6H), 7.33 – 7.37 (m, 6H), 7.06 – 7.10 (m, 2H), 6.84 – 6.88 (m, 2H), 6.26 (dd, J = 7.6, 0.8 Hz, 2H). ESI-HRMS: m/z calc. for $[C_{40}H_{28}N_4Ir]^+$: 757.1940; Found: 757.1936. Anal. Calc. for $C_{40}H_{28}N_4IrPF_6$: C, 53.27; H, 3.13; N, 6.21; Found: C, 52.96; H, 3.33; N, 6.25.

6-3. The procedure is the same as that described for **6-1**, with **6-3-L** (205 mg, 1 mmol) being used as the reagent. 83 mg red powder was collected as the product (yield: 18% for two steps). ^{1}H NMR (CDCl$_3$, 400 MHz): 8.60 (d, J = 8.0 Hz, 2H), 8.51 – 8.56 (m, 4H), 8.06 – 8.10 (m, 2H), 7.82 – 7.86 (m, 2H), 7.77 – 7.79 (m, 2H), 7.71 (d, J = 8.0 Hz, 2H), 7.61 – 7.63 (m, 2H), 7.51 – 7.55 (m, 2H), 7.23 – 7.37 (m, 2H), 7.23 – 7.31 (m, 4H), 7.03 – 7.07 (m, 2H), 6.28 (d, J = 8.4 Hz, 2H). ESI-HRMS: m/z calc. for $[C_{40}H_{28}N_4Ir]^+$: 757.1940; Found: 757.1922. Anal. Calc. for $C_{40}H_{28}N_4IrPF_6 \cdot 0.3CH_2Cl_2$: C, 52.20; H, 3.11; N, 6.04; Found: C, 52.23; H, 3.29; N, 6.04.

6-4. The procedure is the same as that described for **6-1**, with **6-4-L** (205 mg, 1 mmol) being used as the reagent. 79 mg yellow powder was collected as the product (yield: 18% for two steps). ^{1}H NMR (CDCl$_3$, 500 MHz): 8.93 (d, J = 8.0 Hz, 1H), 8.18 – 8.23 (m, 6H), 8.02 (dd, J = 5.5, 1.0 Hz, 2H), 7.89 – 7.92 (m, 2H), 7.77 – 7.79 (m, 2H), 7.65 – 7.66 (m, 2H), 7.30 – 7.38 (m, 8H), 7.15 – 7.18 (m, 2H), 6.65 (s, 2H). ESI-HRMS: m/z calc. for $[C_{40}H_{28}N_4Ir]^+$: 757.1940; Found: 757.1944. Anal. Calc. for $C_{40}H_{28}N_4IrPF_6 \cdot 0.5CH_2Cl_2$: C, 51.51; H, 3.10; N, 5.93; Found: C, 51.42; H, 3.27; N, 5.99.

6-5. The procedure is the same as that described for **6-1**, with **6-5-L** (281 mg, 1 mmol) being used as the reagent. 101 mg yellow powder was collected as the product (yield: 19% for two steps). ^{1}H NMR (CDCl$_3$, 500 MHz): 8.88 (d, J = 9.0 Hz, 2H), 8.80 (d, J = 8.5 Hz, 2H), 8.76 (d, J = 8.0 Hz, 2H), 8.14 – 8.22 (m, 6H), 8.02 – 8.08 (m, 2H), 7.93 (t, J = 7.5 Hz, 2H), 7.88 (d, J = 9.0 Hz, 2H), 7.84 (d, J = 5.5 Hz, 2H), 7.73 (d, J = 5.0 Hz, 2H), 7.51 (d, J = 9.0 Hz, 2H), 7.26 – 7.28 (m, 2H), 7.21 – 7.24 (m, 2H), 6.87 (s, 2H). ESI-HRMS: m/z

calc. for $[C_{52}H_{32}N_4Ir]^+$: 905.2254; Found: 905.2239. Anal. Calc. for $C_{52}H_{32}N_4IrPF_6$: C, 59.48; H, 3.07; N, 5.34; Found: C, 59.08; H, 3.26; N, 5.30.

6-6. The procedure is the same as that described for **6-1**, with **6-6-L** (394 mg, 1 mmol) being used as the reagent. 111 mg yellow powder was collected as the product (yield: 17% for two steps). ^{1}H NMR (CDCl$_3$, 500 MHz): 8.60 (d, J = 6.0 Hz, 2H), 8.24 (d, J = 8.0 Hz, 2H), 8.09 (t, J = 7.5 Hz, 2H), 7.99 – 8.03 (m, 4H), 7.90 – 7.96 (m, 4H), 7.80 – 7.85 (m, 8H), 7.70 – 7.72 (m, 2H), 7.64 (t, J = 8.0 Hz, 2H), 7.43 – 7.46 (m, 2H), 7.37 (d, J = 8.0 Hz, 2H), 7.29 (m, 2H), 7.09 – 7.12 (m, 2H), 6.93 (d, J = 8.0 Hz, 2H), 6.84 – 6.87 (m, 2H), 6.78 – 6.81 (m, 2H), 6.67 (d, J = 8.0 Hz, 2H). ESI-HRMS: m/z calc. for $[C_{68}H_{42}N_6Ir]^+$: 1135.3101; Found: 1135.3151. Anal. Calc. for $C_{68}H_{42}N_6IrPF_6 \bullet 0.2C_4H_{10}O_2$ ($C_4H_{10}O_2$: 2-ethoxyethanol): C, 63.65; H, 3.42; N, 6.47; Found: C, 63.35; H, 3.78; N, 6.37.

6-7. The procedure is the same as that described for **6-1**, with **6-7-L** (329 mg, 1 mmol) being used as the reagent. 87 mg red powder was collected as the product (yield: 15% for two steps). ^{1}H NMR (CDCl$_3$, 500 MHz): 8.78 (d, J = 8.5 Hz, 2H), 8.63 (d, J = 8.0 Hz, 2H), 8.45 (d, J = 8.5 Hz, 2H), 8.19 – 8.21 (m, 6H), 8.01 – 8.06 (m, 4H), 7.77 (d, J = 5.0 Hz, 2H), 7.60 – 7.66 (m, 6H), 7.46 – 7.49 (m, 2H), 7.41 – 7.43 (m, 2H), 7.34 – 7.35 (m, 2H), 7.26 – 7.30 (m, 2H), 7.16 – 7.19 (m, 2H), 6.95 (s, 2H). ESI-HRMS: m/z calc. for $[C_{60}H_{36}N_4Ir]^+$: 1005.2568; Found: 1005.2602. Anal. Calc. for $C_{60}H_{36}N_4IrPF_6 \bullet 1.2CH_2Cl_2$: C, 58.71; H, 3.09; N, 4.47; Found: C, 58.72; H, 3.13; N, 4.74.

6.2.2. Photophysical and Nonlinear Absorption Measurements

The solvents used for photophysical experiments were spectroscopic grade, and were purchased from VWR International and used as is without further purification. UV-vis absorption spectra were recorded on a Shimadzu UV-2501 spectrophotometer. A Jobin-Yvon FluoroMax-4 fluorometer/phosphorometer was used to measure the steady-state emission spectra in different solvents. The emission quantum yields were determined by the relative

actinometry method[30] in degassed solutions, in which the degassed aqueous solution of $[Ru(bpy)_3]Cl_2$ ($\Phi_{em} = 0.097$, $\lambda_{ex} = 436$ nm)[31] was used as the reference for complexes **6-1 – 6-7**.

The nanosecond transient difference absorption (TA) spectra and decays were measured in degassed toluene or acetonitrile solutions on an Edinburgh LP920 laser flash photolysis spectrometer. The third harmonic output (355 nm) of a Nd:YAG laser (Quantel Brilliant, pulse width: 4.1 ns, repetition rate was set at 1 Hz) was used as the excitation source. Each sample was purged with argon for 30 min prior to measurement. The triplet excited-state absorption coefficient (ε_T) at the TA band maximum was determined by the singlet depletion method that was decribed previously.[32] After obtaining the ε_T value, the Φ_T could be determined by the relative actinometry using SiNc in benzene as the reference (ε_{590} = 70000 M^{-1} cm^{-1}, $\Phi_T = 0.20$).[33]

The reverse saturable absorption of complexes **6-1 – 6-7** was characterized by nonlinear transmission experiment at 532 nm using a Quantel Brilliant laser as the light source. The pulse width of the laser was 4.1 ns and the repetition rate was set at 10 Hz. The complexes were dissolved in CH_2Cl_2. The concentration of the sample solutions was adjusted to obtain a linear transmission of 90% at 532 nm in a 2-mm-thick cuvette. The experimental setup and details are similar to that reported previously.[34] A 40-cm plano-convex lens was used to focus the beam to the center of the 2-mm thick sample cuvette.

6.3. Results and Discussion

6.3.1. Electronic Absorption

The electronic absorption of **6-1-L – 6-4-L**, **6-6-L, 6-7-L** and **6-1 – 6-7** were carried out in dichloromethane and the absorption obeys Beer's law in the concentration range of 5×10^{-6} – 1×10^{-4} mol/L, suggesting the absence of ground-state aggregation in the concentration range tested. The UV-vis absorption spectra of the ligands and complexes are

shown in Figure 6.1, and their absorption band maxima and molar extinction coefficients are
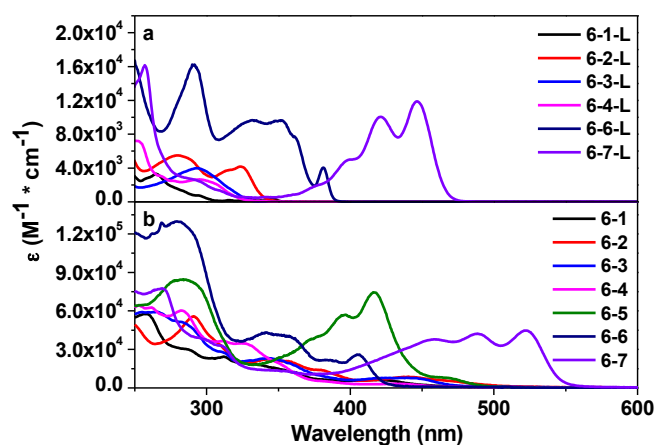
summarized in Table 6.1.

Figure 6.1. UV-vis absorption spectra of **6-1-L** – **6-4-L**, **6-6-L** and **6-7-L**
(a), **6-1** – **6-7** (b) at room temperature in dichloromethane

Table 6.1. Electronic absorption, emission (room temperature and 77 K), and excited-state absorption parameters for complexes **6-1** – **6-7** and ligands **6-1-L** – **6-4-L**.

	λ_{abs}/nm (log ε/L.mol^{-1}.cm^{-1})[a]	λ_{em}/nm (τ_0/μs; k_{sq}/10^9.L.mol^{-1}.s^{-1}); Φ_{em}[b] R. T.	λ_{em}/nm (τ_0/μs; k_{sq}/L.mol^{-1}.s^{-1})[c] 77 K
6-1	312 (4.39), 365 (4.02), 423 (3.79)	580 (0.53, 1.7), 600 (0.53, 1.6); 0.33	500 (6.9), 534 (4.6)
6-2	343 (4.35), 380 (4.15), 441 (3.93)	587 (3.5, 0.87), 622 (3.4, 0.85); 0.44	580 (-), 628 (4.4)
6-3	311 (4.45), 343 (4.37), 439 (3.90)	585 (5.7, 1.2), 615 (6.2, 1.4); 0.18	570 (13.5), 620 (12.9)
6-4	324 (4.54), 387 (3.67), 435 (3.50)	604 (0.20, 1.1), 650 (0.20, 1.6); 0.089	527 (221), 570 (163)
6-5	283 (4.93), 417 (4.87), 469 (3.88)	680 (9.5, 0.52); 0.0046	670 (17.8), 735 (-)
6-6	342 (4.64), 405 (4.41), 440 (3.15)	570 (30.3, 0.40), 585 (27.4, 0.44); 0.024	566 (44.7), 580 (-)
6-7	488 (4.62), 522 (4.65), 553 (3.43)	570 (-, -), 628 (-, -)	566 (-), 623 (-)
6-1-L	265 (3.52), 330 (2.55), 346 (2.64)	350 (-, -), 368 (-, -), 386 (-, -)	
6-2-L	280 (3.74), 324 (3.62)	-	
6-3-L	293 (3.60)	368 (-, -)	
6-4-L	251 (3.86), 295 (3.42)	346 (-, -), 364 (-, -), 382 (-, -)	
6-6-L	291 (4.21), 350 (3.98), 381 (3.61)	387 (-, -), 407 (-, -), 427 (-, -)	
6-7-L	257 (4.21), 421 (4.00), 446 (4.07)	470 (-, -), 496 (-, -)	

[a]Absorption band maxima (λ_{abs}) and molar extinction coefficient (ε_{max}) in CH$_2$Cl$_2$. [b]Emission wavelength (λ_{em}), intrinsic lifetime (τ_0), self-quenching rate constant (k_{sq}), and emission quantum yield measured in CH$_2$Cl$_2$ with Ru(bpy)$_3$Cl$_2$ as the standard for the complexes. [c]In BuCN glassy matrix.

The electronic absorptions of **6-1-L** – **6-4-L**, **6-6-L** and **6-7-L** were measured in dichloromethane. All the ligand exhibited typical ligand centered $^1\pi,\pi^*$ transitions in their electronic absorption. The electronic absorption spectra of **6-6-L** and **6-7-L** are significantly red-shifted in comparison to the other four ligands' due to extended π conjugation.

The major absorption bands of all the complexes are broadened and red-shifted in comparison to their corresponding ligands, suggesting the electron delocalization induced by interaction with the metal center. For complexes **6-1** – **6-4**, the strong absorption bands with large extinction coefficients in the region of 250 – 370 nm are from the ligand centered $^1\pi,\pi^*$ transitions by comparing to the ligand absorption. However, the tails from 380 – 500 nm are absent in the ligand absorption, which are assigned to ^{1}MLCT/^{1}LLCT transitions. Similarly, for complex **6-5**, the absorption in the region of 250 – 450 nm is from the ligand-centered $^1\pi,\pi^*$ transition and the absorption in the region of 450 – 500 nm is from the ^{1}MLCT/^{1}LLCT transitions. The observable absorption for **6-1** – **6-5** above 500 nm can be attributed to the spin forbidden transition to the lowest triplet excited state. The regions for the ligand centered $^1\pi,\pi^*$ transition and ^{1}MLCT/^{1}LLCT transitions for complex **6-7** are 350 – 550 nm and 550 – 600 nm, respectively. For complex **6-6**, the separation of the ligand centered $^1\pi,\pi^*$ transitions and ^{1}MLCT transitions is not obvious. The electronic absorption of this complex is dominated by the ligand centered $^1\pi,\pi^*$ transitions by comparing the absorption spectra of the complex and the ligand, with the ^{1,3}MLCT/^{1,3}LLCT buried in the $^1\pi,\pi^*$ bands. Comparing to those of **6-1** – **6-4**, the absorption spectra of **6-5** – **6-7** are significantly red-shifted, indicating that extending the π-conjugation of the arylpyridine ligand has significantly delocalized the electron density.
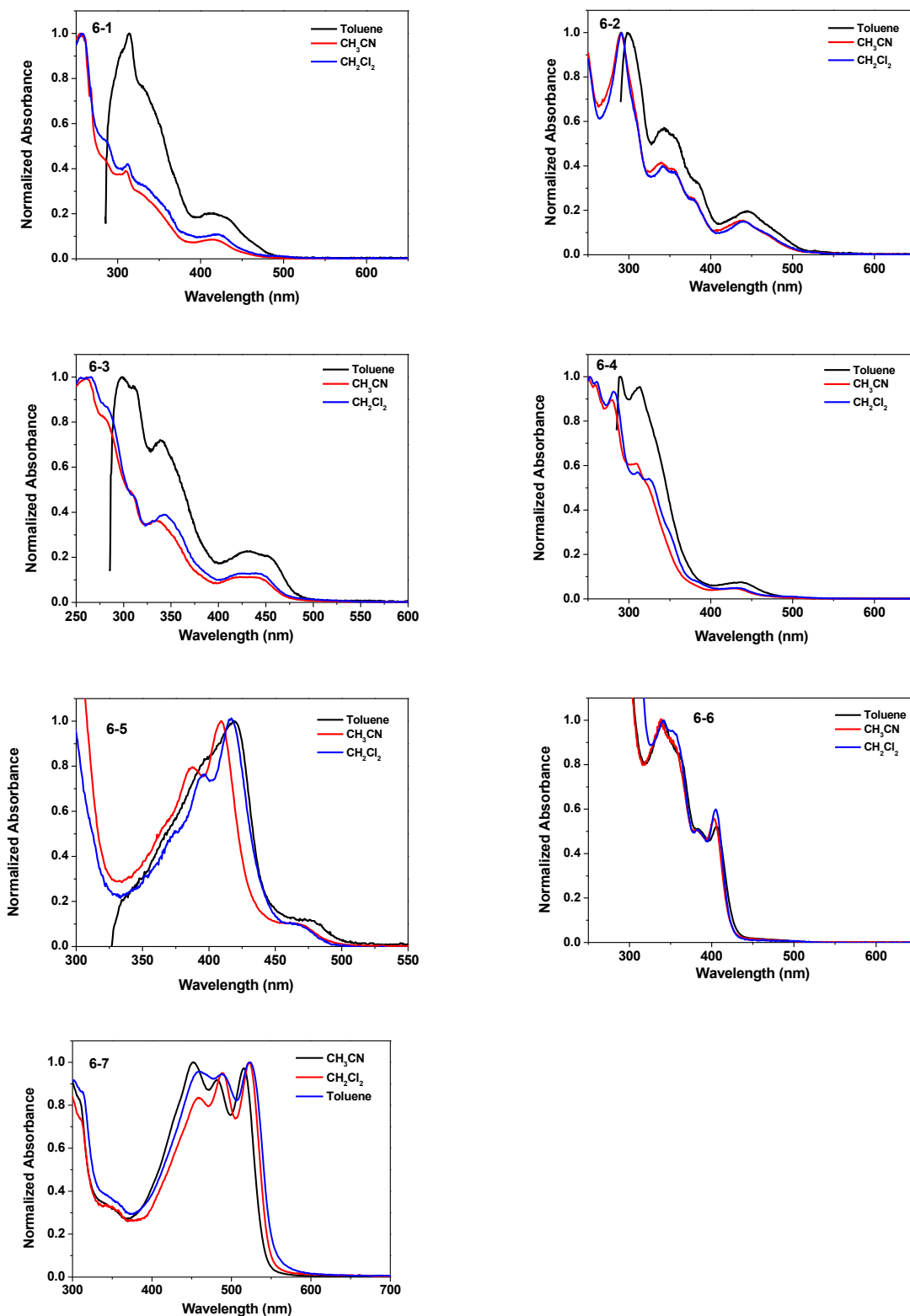
Figure 6.2. Normalized UV-vis absorption spectra of **6-1** − **6-7** at room temperature in different solvents.

The UV-vis absorption studies of the complexes **6-1** − **6-7** in different solvents support the assignments of the transitions. As shown in Figure 6.2, the less pronounced

solvatochromic effect with red-shifted absorption in less polar solvents like toluene for all the complexes except **6-6** suggests the $^1\pi,\pi*$ percentage of the major absorption bands and the charge-transfer nature of the transitions in the region of 400 – 450 nm for complexes **6-1** – **6-4**, 450 – 500 nm for complex **6-5**, and 550 – 600 nm for complex **6-7**.

6.3.2. Photoluminescence

6-1 – **6-6** all exhibit moderate to strong emission with lifetimes spanning from hundreds of nanoseconds to tens of microseconds both in solution at room temperature and in butyronitrile glassy matrix at 77 K. The emissions of **6-7** and **6-2-L** are too weak to be observed. The emission spectra of **6-1** – **6-7**, **6-1-L**, **6-3-L**, **6-4-L**, **6-6-L**, and **6-7-L** at room temperature are shown in Figure 6.3, and the emission spectra of **6-1** – **6-7** at 77 K are shown in Figure 6.4. The emission band maxima and emission lifetimes are summarized in Table 6.1.
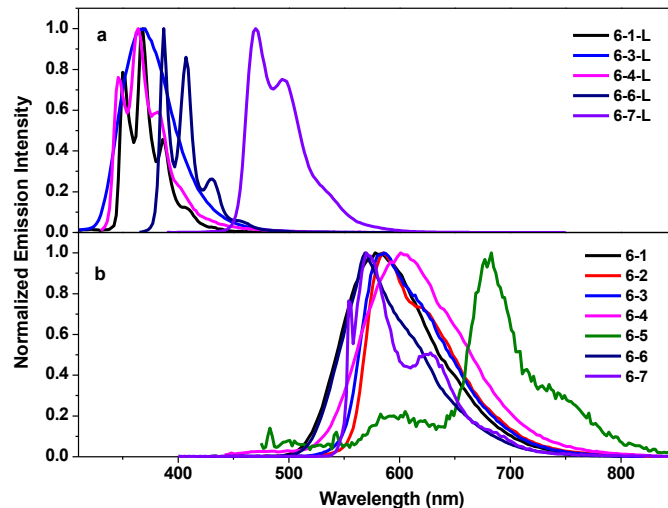
Figure 6.3. (a) Normalized emission spectra of **6-1-L** – **6-4-L**, **6-6-L** and **6-7-L** at room temperature in CH_2Cl_2 at the concentration 1×10^{-5} mol/L (λ_{ex}: 300 nm for **6-1-L** and **6-3-L**; 320 nm for **6-4-L**; 350 nm for **6-6-L**; 380 nm for **6-7-L**). (b) Normalized emission spectra of **6-1** – **6-7** at room temperature in CH_2Cl_2 at the concentration of 1×10^{-5} mol/L (λ_{ex}: 418 nm for **6-1**; 440 nm for **6-2** and **6-3**; 432 nm for **6-4**; 465 nm for **6-5**; 405 nm for **6-6**; 553 nm for **6-7**).

As shown in Figure 6.3a, all the ligands measured showed strong emissions with vibronic structures for the emission spectra. The virtue of the emissions is attributed to ligand

centered $^1\pi,\pi^*$ transitions. The emission spectra of **6-6-L** and **6-7-L** are significantly red-shifted due to extended π conjugation.

Except for **6-5**, all the complexes emit in the region of 500 – 700 nm, while **6-5** emits in the region of 550 – 800 nm. The relatively long lifetimes of the emission for complexes **6-1 – 6-6** suggest that the emitting states are triplet-excited states for these complexes. In view of the vibronic structure or the long lifetimes of **6-5 – 6-7**, the emission of these three complexes are ascribed to the $^3\pi,\pi^*$ phosphorescence. For **6-2** and **6-3**, the moderately long lifetimes suggest that the emitting states possess predominantly $^3\pi,\pi^*$ character in nature, possibly mixed with some ^{3}MLCT/^{3}LLCT characters. For **6-1** and **6-4**, the relatively short lifetimes and structureless feature imply the charge transfer nature of the emitting excited states.

Table 6.2. Emission characteristics of complexes **6-1 – 6-6** in different solvents at room temperature*

λ_{em} /nm (τ_{em}/μs); Φ_{em}			
	CH$_2$Cl$_2$	CH$_3$CN	Toluene
6-1	593 (0.22); 0.33	587 (0.26); 0.12	580 (0.51); 0.14
6-2	587 (3.6), 650 (3.6); 0.44	588 (1.6), 644 (1.5); 0.18	592 (2.5), 630 (2.6); 0.38
6-3	575 (5.3), 585 (5.3), 615 (5.3); 0.18	574 (3.8), 584 (3.8), 640 (3.8); 0.11	574 (5.0), 585 (4.9), 640 (5.4); 0.23
Table 6.2. Continued.			
6-4	590 (0.2), 604 (0.2), 650 (0.2); 0.089	575 (0.1), 609 (0.1), 660 (0.1); 0.031	623 (0.08), 650 (0.09); 0.025
6-5	680 (-); 0.0046	677 (-); 0.0045	682 (-); 0.0056
6-6	570 (23.1); 0.024	568 (11.9), 613 (12.7); 0.028	568 (12.2); 0.064
6-7	574 (-); -	576 (-); -	620 (-); -

*The emission quantum yields of **6-7** in different solvents were not obtained due to its weak emission and lack of proper reference. Ru(bpy)$_3$Cl$_3$ was used as the reference (λ_{ex} = 436 nm, Φ_{em} = 0.097) for the emission quantum yield. Signal is too weak to deduce the emission lifetime for complex **6-5**.
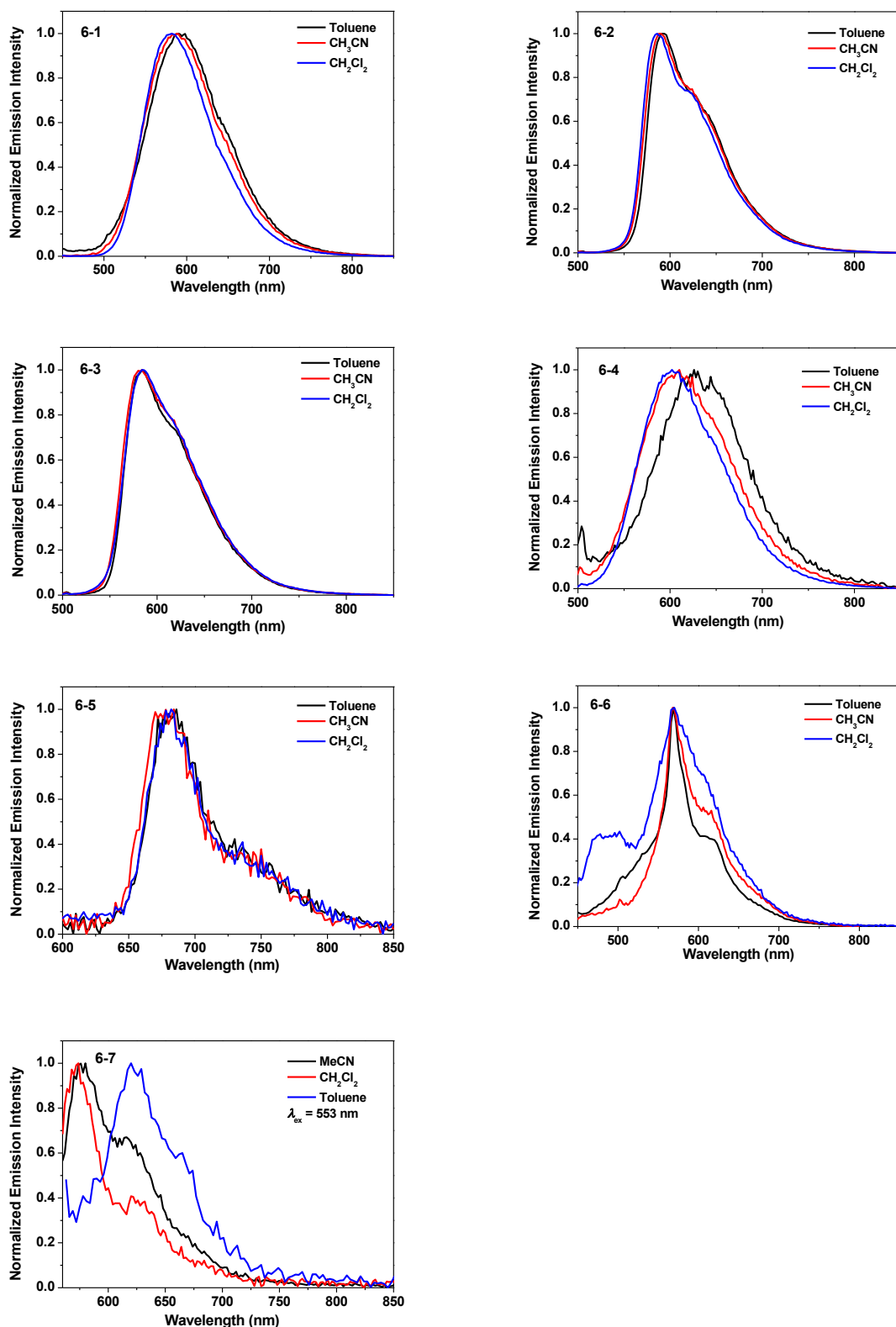
Figure 6.4. Normalized emission spectra of **6-1** – **6-7** at room temperature in different solvents

Our assignment of the emitting state is supported by the solvent-dependency emission study. As demonstrated in Figure 6.4, minor solvatochromic effect for the emission was

observed for all the complexes except **6-1** and **6-4**, suggesting that the emitting states for **6-2**, **6-3**, and **6-5** – **6-7** are predominantly $^3\pi,\pi^*$ states. For complexes **6-1** and **6-4**, negative solvatochromic effect is observed, indicating the charge-transfer nature of the emission in these two complexes. The emission maxima, emission lifetime, and quantum yields in different solvents are summarized in Table 6.2.

To evaluate whether self-quenching occurs at high concentrations for **6-1** – **6-7**, the emission intensity and the emission lifetimes were measured at different concentrations in CH_2Cl_2. The results are displayed in Figure 6.5. By plotting the observed radiative rate constant vs concentration, the self-quenching rate constant and intrinsic lifetimes for complexes **6-1** – **6-6** were deduced from the slope and intercept of the fitted linear plots, and the values are summarized in Table 6.1.

The emission of complexes **6-1** – **6-7** in butyronitrile matrix was recorded and the spectra are shown in Figure 6.6. The well-resolved emission spectra are significantly blue-shifted and narrower comparing to the room temperature emission due to rigidochromic effect in the solid matrix.[35] Considering the small thermally induced Stokes shifts of **6-2**, **6-3**, **6-5** – **6-7** (206 cm^{-1} for **6-2**, 450 cm^{-1} for **6-3**, 219 cm^{-1} for **6-5**, 124 cm^{-1} for **6-6**, and 124 cm^{-1} for **6-7**), and long lifetimes, the emission in these five complexes are verified to be predominantly $^3\pi,\pi^*$ in nature. In contrast, the thermally induced Stokes shift of **6-1** and **6-4** (2759 cm^{-1} for **6-1** and 2419 cm^{-1} for **6-4**,) are quite large, and the lifetimes are relatively short, confirming the charge-transfer nature for the emission of the two complexes.
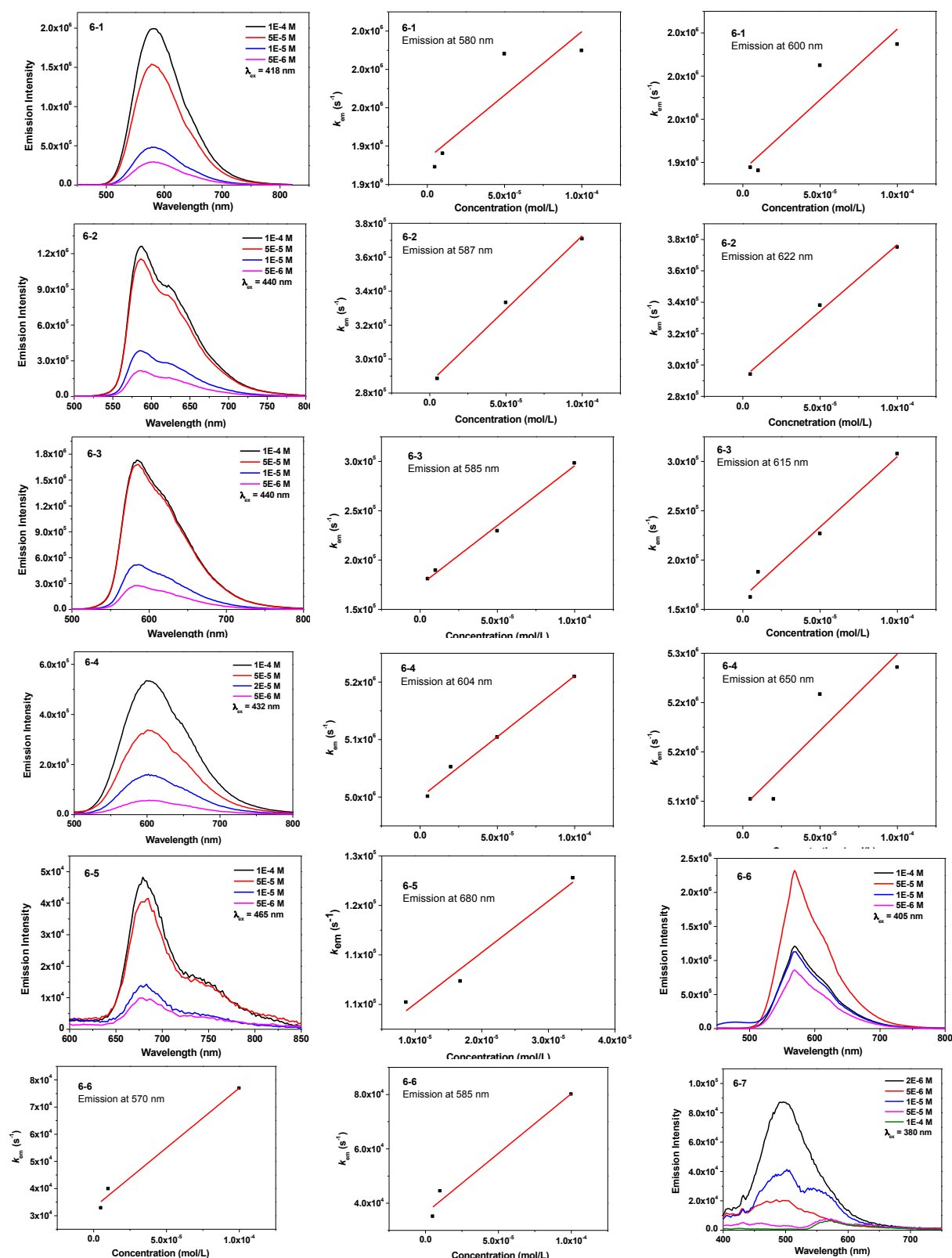
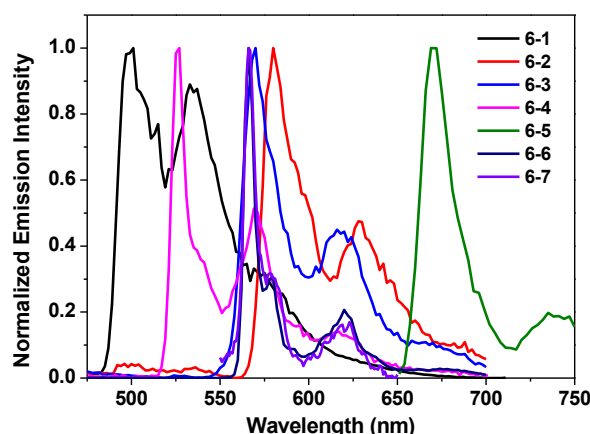**Figure 6.5.** Emission of **6-1** – **6-7** at room temperature at different concentration in dichloromethane and Stern-Volmer plots

Figure 6.6. Normalized emission spectra of **6-1** – **6-7** at 77 K in butyronitrile matrix at the concentration of 1×10^{-5} mol/L. (λ_{ex}: 355 nm for **6-1** and **6-7**; 360 nm for **6-2**, **6-3**, and **6-4**; 400 nm for **6-5**; 360 nm for **6-6**).

6.3.3. Transient Absorption

Nanosecond transient absorption (TAs) studies of complexes **6-1** – **6-7** in toluene or acetonitrile were carried out to further understand their triplet excited-state characteristics. The time-resolved spectra for **6-1** – **6-6** are shown in Figure 6.7. The TA for **6-7** was too weak to be observed. The triplet excited-state lifetimes, extinction coefficients, and quantum yields are deduced or calculated and the results are summarized in Table 6.3. The triplet excited-state lifetimes for these complexes are similar to their emission lifetimes. Therefore, we tentatively assign the transient absorption of these complexes being from the same excited-states that emit.

Table 6.3. Excited state absorption parameters for complexes **6-1** – **6-7** in CH$_3$CN

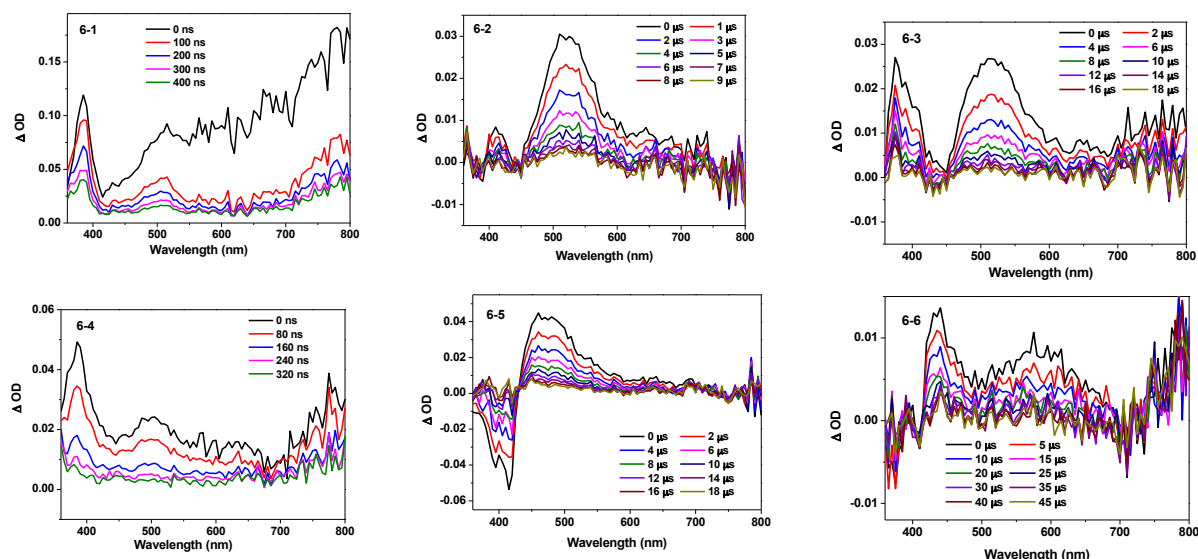|	$\lambda_{T_1-T_n}$ /nm(τ_T /μs; $\varepsilon_{T_1-T_n}$ /M^{-1} cm^{-1}; Φ_T)
6-1	590 (0.30; -; -)
6-2	590 (3.0; -; -)
6-3	590 (2.0; -; -)
6-4	590 (0.10; -; -)
6-5	460 (7.3; 41910; 0.28)
6-6	590 (29.8; -; -)
6-7	560 (0.44; -; -)

Figure 6.7. Time-resolved ns transient absorption spectra of **6-1** – **6-6**. (**6-1** and **6-4**, in toluene; **6-2**, **6-3**, **6-5**, and **6-6**, in acetonitrile; $\lambda_{ex} = 355$ nm; $A_{355} = 0.4$ in a 1-cm cuvette).

6.3.4. Reverse Satuable Absorption

Nonlinear transmission experiment was carried out for complexes **6-1** – **6-7** in CH_2Cl_2 solutions at a linear transmittance of 80% in a 2-mm cuvette using the 532-nm ns laser pulses and the results are shown in Figure 6.8. The transmission of all of the complexes decreases remarkably with increased incident energy except for **6-7**, which clearly demonstrates a strong reverse satuable absorption (RSA) from these complexes except for **6-7**. The strength of the RSA follows this trend: **6-7** $<$ **6-1** $<$ **6-4** $<$ **6-6** $<$ **6-5** $\approx$ **6-2** $\approx$ **6-3**. The very weak RSA of **6-7** should be due to the strong ground-state absorption at 532 nm, which dramatically decreases the ratio of the excited-state absorption cross-section to that of the ground state.
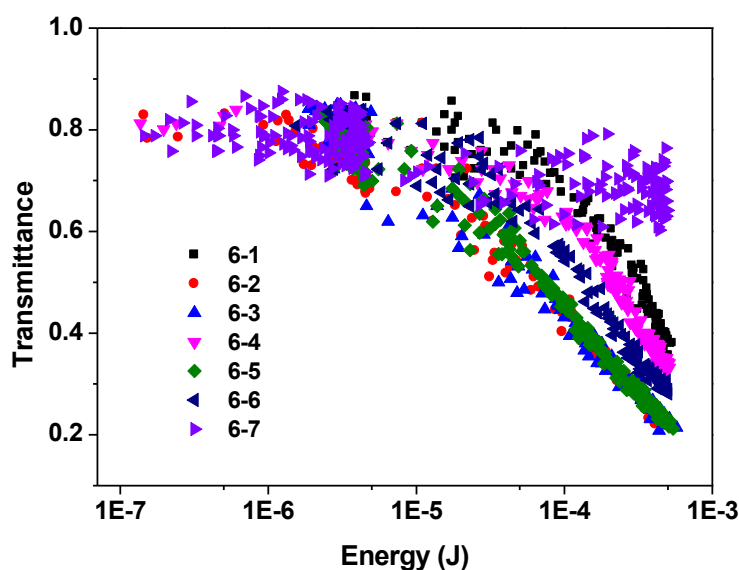
Figure 6.8. Nonlinear transmission plot of **6-1** – **6-7** at the linear transmittance of 80% in CH_2Cl_2 solution in a 2-mm cuvette for 532 nm 4.1 ns laser. The radius of the beam waist at the focal point was approximately 96 μm.

6.4. Conclusion and Future Direction

The synthesis, photophysics, and reverse saturable absorption of seven cationic iridium(III) bipyridine complexes with different cyclometallating arylpyridine ligands were discussed in this chapter. The effects of extended π-conjugation of the arylpyridine ligands were systematically investigated. With extended π-conjugation in the arylpyridine ligand, the absorption spectra are red-shifted. The emission of all the complexes is dominated by ligand-centered $^3\pi,\pi*$ transition except for complex **6-1** and **6-4**, which has predominant contribution from the ^{3}MLCT/^{3}LLCT states. Complexes **6-2**, **6-3**, and **6-5** show moderate triplet transient absorption in the visible spectral region of 450 – 600 nm while **6-6** exhibits broad and weak transient absorption in the region of 430 – 700 nm, which can be assigned to the ligand centered $^3\pi,\pi*$ state for all four complexes. The transient absorptions of 6-1 and 6-4 are broad but short lived, which implies the charge-transfer nature of the transient species.

202

The reverse saturable absorption of these complexes was evaluated at 532 nm for ns laser pulses. The results demonstrat that these complexes all exhibit strong RSA for ns laser pulses at 532 nm except for **6-7**, with a trend of **6-7**＜**6-1**＜**6-4**＜**6-6**＜**6-5** ≈ **6-2** ≈ **6-3**.

To further understand the ground-state and excited-state properties, TD-DFT calculations are necessary to help figuring out the nature of the lowest energy transitions. On the other hand, to rationalize the RSA performance of these complexes, measurement of the ratios of the excited-state absorption cross section to that of the ground state should be conducted using z-scan technique.

6.5. References

[1] Flamigni, L.; Barbieri, A.; Sabatini, C.; Ventura, B.; Barigelletti, F. *Top. Curr. Chem.* **2007**, *281*, 143.

[2] Dixon, I. M.; Collin, J.-P.; Sauvage, J.-P.; Flamigni, L.; Encinas, S.; Barigelletti, F. *Chem. Soc. Rev.* **2000**, *29*, 385.

[3] Lamansky, S.; Djurovich, P.; Murphy, D.; Abdel-Razzaq, F.; Kwong, R.; Tsyba, I.; Bortz, M.; Mui, B.; Bau, R.; Thompson, M. E. *Inorg. Chem.* **2001,** *40,* 1704.

[4] Goldsmith, J. I.; Hudson, W. R.; Lowry, M. S.; Anderson, T. H.; Bernhard, S. *J. Am. Chem. Soc.* **2005**, *127*, 7502.

[5] Yu, Z.-T.; Yuan, Y.-J.; Cai, J.-G.; Zou, Z.-G. *Chem. Eur. J.* **2013**, *19*, 1303.

[6] Yersin, H. *Highly Efficient OLEDs with Phosphorescent Materials*; WILEY-VCH Verlag GmbH & Co. KGaA. **2008**.

[7] Chen, X.; Liao, J.-L.; Liang, Y.; Ahmed, M. O.; Tseng, H.-E.; Chen, S.-A. *J. Am. Chem. Soc.* **2003**, *125*, 636.

[8] Tsuboyama, A.; Iwawaki, H.; Furugori, M.; Mukaide, T.; Kamatani, J.; Igawa, S.; Moriyama, T.; Miura, S.; Takiguchi, T.; Okada, S.; Hoshino, M.; Ueno, K. *J. Am. Chem. Soc.* **2003**, *125*, 12971.

[9] Zhou, G.; Wong, W.-Y.; Yao, B.; Xie, Z.; Wang, L. *Angew. Chem. Int. Ed.* **2007**, *46*, 1149.

[10] Sasabe, H.; Takamatsu, J.; Motoyama, T.; Watanabe, S.; Wagenblast, G.; Langer, N.; Molt, O.; Fuchs, E.; Lennartz, C.; Kido, J. *Adv. Mater.* **2010**, *22*, 5003.

[11] Martin, B.; Waind, G. M. *J. Chem. Soc.* **1958**, 4282.

[12] Flynn Jr., C. M.; Demas, J. N. *J. Am. Chem. Soc.* **1974**, *96*, 1959.

[13] Demas, N.; Harris, E. W.; Flynn Jr., C. M.; Diemente, D. *J. Am. Chem. Soc.* **1975**, *97*, 3838.

[14] King, K.A.; Spellane, P. J.; Watts, R. J. *J. Am. Chem. Soc.* **1985**, *107*, 1431.

[15] Demas, J. N.; Crosby, G. A. *J. Am. Chem. Soc.* **1970**, *92*, 7262.

[16] Demas, J. N.; Crosby, G. A. *J. Am. Chem. Soc.* **1971**, *93*, 2841.

[17] Watts, R. J.; Crosby, G. A. *J. Am. Chem. Soc.* **1972**, *94*, 2606.

[18] Watts, R. J.; Crosby, G. A.; Sansregret, J. L. *Inorg. Chem.* **1972,** *11,* 1474.

[19] Colombo, M. G.; Hauser, A.; Gudel, H. U. *Inorg. Chem.* **1993**, *32,* 3088

[20] Bolink, H. J.; Coronado, E.; Costa, R. D.; Lardiés, N.; Ortí, E. *Inorg. Chem.* **2008**, *47*, 9149.

[21] Bolink, H. J.; Coronado, E.; Costa, R. D.; Ortí, E.; Sessolo, M.; Graber, S.; Doyle, K.; Neuburger, M. *Adv. Mater.* **2008**, *20*, 3910.

[22] Kim, K.-Y.; Farley, R. T.; Schanze, K. S. *J. Phys. Chem. B* **2006**, *110,* 17302.

[23] Sun, W.; Zhang, B.; Li, Y.; Pritchett, T. M.; Li, Z.; Haley, J. E. *Chem. Mater.* **2010**, *122*, 6384.

[24] Liu, R.; Zhou, D.; Azenkeng, A.; Li, Z.; Li, Y.; Glusac, K. D.; Sun, W. *Chem. Eur. J.* **2012**, *18*, 11440.

[25] Li, Z.; Badaeva, E.; Zhou, D.; Bjorgaard, J.; Glusac, K. D.; Killina, S.; Sun, W. *J. Phys. Chem. A* **2012**, *116*, 4878.

[26] Cotton, F. A.; Wilkinson, G. *Advanced Inorganic Chemistry: A Comprehensive Text*; Wiley, New York, **1980**.

[27] Linder, T.; Badiola, E.; Baumgartner, T.; Sutherland, T. C. *Org. Lett.* **2010**, 4520.

[28] Yi, X.; Yang, P.; Huang, D.; Zhao, J. *Dyes Pigm.* **2013**, *96*, 104.

[29] Brown, K. E.; Veldkamp, B. S.; Co, D. T.; Wasielewski, M. R. *J. Phys. Chem. Lett.* **2012**, *3*, 2362.

[30] Demas, J. N.; Crosby, G. A. *J. Phys. Chem.* **1971**, *75*, 991.

[31] Van Houten, J.; Watts, R. *J. Am. Chem. Soc.* **1976**, *98*, 4853.

[32] Eaton, D. F. *Pure Appl. Chem.* **1988**, *60*, 1107.

[33] Carmichael, I.; Hug, G. L. *J. Phys. Chem. Ref. Data.* **1986**, *15*, 1.

[34] Guo, F.; Sun, W.; Liu, Y.; Schanze, K. *Inorg. Chem.* **2005**, *44*, 4055.

[35] Watts, R. J.; Missimer, D. *J. Am. Chem. Soc.* **1978**, *100*, 5350.